VOLUME 79 AUGUST 28, 1975 NUMBER 18

JPCHAx

THE JOURNAL OF PHYSICAL CHEMISTRY

PUBLISHED BIWEEKLY BY THE AMERICAN CHEMICAL SOCIETY

THE JOURNAL OF

PHYSICAL CHEMISTRY

AMERICAN CHEMICAL SOCIETY, *1155 Sixteenth St., N.W., Washington, D.C. 20036*

Books and Journals Division

D. H. MICHAEL BOWEN *Director*

CHARLES R. BERTSCH *Head, Editorial Processing Department*
BACIL GUILEY *Head, Graphics and Production Department*
SELDON W. TERRANT *Head, Research and Development Department*

 Published biweekly by the American Chemical Society at 20th and Northampton Sts., Easton, Pa. 18042. Second-class postage paid at Washington, D.C., and at additional mailing offices.

All manuscripts should be sent to *The Journal of Physical Chemistry*, Department of Chemistry, University of Minnesota, Minneapolis, Minn. 55455.

Additions and Corrections are published once yearly in the final issue. See Volume 78, Number 26 for the proper form.

Extensive or unusual alterations in an article after it has been set in type are made at the author's expense, and it is understood that by requesting such alterations the author agrees to defray the cost thereof.

The American Chemical Society and the Editor of *The Journal of Physical Chemistry* assume no responsibility for the statements and opinions advanced by contributors.

Correspondence regarding accepted copy, proofs, and reprints should be directed to Editorial Processing Department, American Chemical Society, 20th and Northampton Sts., Easton, Pa. 18042. Department Head: CHARLES R. BERTSCH. Associate Department Head: MARIANNE C. BROGAN, Assistant Editors: CELIA B. MCFARLAND, JOSEPH E. YURVATI.

Advertising Office: Centcom, Ltd., 50 W. State St., Westport, Conn. 06880.

Business and Subscription Information

Send all new and renewal subscriptions *with payment* to: Office of the Controller, 1155 16th Street, N.W., Washington, D.C. 20036. Subscriptions should be renewed promptly to avoid a break in your series. All correspondence and telephone calls regarding changes of address, claims for missing issues, subscription service, the status of records, and accounts should be directed to Manager, Membership and Subscription Services, American Chemical Society, P.O. Box 3337, Columbus, Ohio 43210. Telephone (614) 421-7230. For microfiche service, contact ACS Microfiche Service, 1155 16th St. N.W., Washington, D.C. 20036. Telephone (202) 872-4444.

On changes of address, include both old and new addresses with ZIP code numbers, accompanied by mailing label from a recent issue. Allow four weeks for change to become effective.

Claims for missing numbers will not be allowed (1) if loss was due to failure of notice of change in address to be received before the date specified, (2) if received more than sixty days from date of issue plus time normally required for postal delivery of journal and claim, or (3) if the reason for the claim is "issue missing from files."

Subscription rates (hard copy or microfiche) in 1975: $20.00 for 1 year to ACS members; $80.00 to nonmembers. Extra postage $4.50 in Canada and PUAS, $5.00 other foreign. Supplementary material (on microfiche only) available on subscription basis, 1975 rates: $15.00 in U.S., $19.00 in Canada and PUAS, $20.00 elsewhere. All microfiche airmailed to non-U.S. addresses; air freight rates for hard-copy subscriptions available on request.

Single copies for current year: $4.00. Rates for back issues from Volume 56 to date are available from the Special Issues Sales Department, 1155 Sixteenth St., N.W., Washington, D.C. 20036.

Subscriptions to this and the other ACS periodical publications are available on microfilm. For information on microfilm write Special Issues Sales Department at the address above.

Notice to Authors last printed in the issue of July 3, 1975

THE JOURNAL OF

PHYSICAL CHEMISTRY

Volume 79, Number 18 August 28, 1975

JPCHAx 79(18) 1891–1984

ISSN 0022-3654

COMMUNICATIONS TO THE EDITOR

There is no supplementary material for this issue.

* In papers with more than one author, the asterisk indicates the name of the author to whom inquiries about the paper should be addressed.

AUTHOR INDEX

THE JOURNAL OF
PHYSICAL CHEMISTRY

VOLUME 79, NUMBER 18 AUGUST 28, 1975

Reaction of Excited Oxygen Atoms, $O(^1D_2)$, with Cyclobutane[1a]

A. J. Colussi[1b] and R. J. Cvetanović*

Division of Chemistry, National Research Council of Canada, Ottawa, Canada K1A 0R9 *(Received January 6, 1975)*

Publication costs assisted by the National Research Council of Canada

Gas and liquid phase reaction of singlet oxygen atoms $O(^1D_2)$ with cyclobutane has been studied at room temperature (25 ± 2°). The effects of pressure and of O_2 on the yields of the main products show that the reaction mechanism is basically the same as found in related reactions of $O(^1D_2)$ with saturated hydrocarbons. The insertion product, excited cyclobutanol, is only partly stabilized in the gas phase at pressures below 15 atm. Its decomposition products are ethylene and acetaldehyde. From the pressure dependence of the yields of ethylene a lifetime of 8×10^{-12} sec is estimated for the excited cyclobutanol, assuming that deactivation occurs at each collision. This result is used to evaluate approximately the Arrhenius A factor for unimolecular decomposition of cyclobutanol. The calculated value is consistent with the literature value of A for pyrolysis of cyclobutanol, in agreement with the postulate that the "hot" intermediate is vibrationally excited cyclobutanol in the ground electronic state.

Introduction

Reactions of singlet oxygen atoms $O(^1D_2)$ have received much attention in recent years.[2a] Apart from their basic interest as reactions of an electronically excited atomic species of a particular multiplicity, some of the $O(^1D_2)$ reactions play also a significant role in atmospheric chemistry.[2a] A detailed understanding of their mechanisms is therefore of considerable importance.

In their reactions with saturated hydrocarbons, $O(^1D_2)$ atoms enter into three general types of elementary processes.[2b,3] The most important of these is insertion of $O(^1D_2)$ into CH bonds (but not into CC bonds), which occurs to an extent of about 65%. Somewhat less important is hydrogen atom abstraction (20 to 30%), while the third process, molecular elimination (e.g., elimination of H_2 to produce a carbonyl compound) generally occurs only to a minor extent (at best up to about 10%). Physical quenching of $O(^1D_2)$ to $O(^3P)$ by paraffins occurs to an extent not exceeding 2–3% and perhaps not at all.[3]

Insertion of $O(^1D_2)$ atoms into the CH bonds of hydrocarbons is a strongly exothermic process and the "hot" alcohols formed possess typically 140–160 kcal mol^{-1} of excess energy. This energy is probably sufficient in most cases for the electronic excitation to the first excited singlet ($n \rightarrow \sigma^*$) of the alcohols formed. However, this is perhaps not always true, e.g., in the $O(^1D_2)$ reaction with methane.[4] Furthermore, the small extinction coefficients of simple alcohols at 180–200 nm suggest some forbidden character of the $n \rightarrow \sigma^*$ transition. It seems therefore very unlikely that the extremely rapidly occurring $O(^1D_2)$ reactions with alkanes produce electronically excited alcohols. This assumption is further supported by the vastly different products of $O(^1D_2)$ reaction with cyclobutane and of direct photolysis of cyclobutanol observed in the present study.

The kinetics of decomposition and collisional stabilization of the "hot" alcohols may provide further indication whether these processes are likely to occur from a vibrationally excited ground electronic state or from an electronically excited state with much less vibrational excitation. This requires measurement of the rate constant $k(E)$ of unimolecular decomposition of the "chemically activated" alcohol and calculating from it in a suitable manner a value (A_{calcd}) of the Arrhenius A factor, i.e., of the entropy of activation, assuming that the alcohol is not electronically excited. Consistency of A_{calcd} with the expected or still better, if possible, with an experimental value (A_{expt}) of A would then provide support for the postulate that the decomposing molecule is in the ground electronic state. (It seems reasonable to assume that unimolecular decomposition of an electronically excited molecule with much less vibrational energy would lead to significantly different results, although little information is available at present on such processes.)

Previous work from this laboratory, as discussed in particular by Mintz and Cvetanović,[4] has shown that A_{calcd} for a number of "hot" alcohols formed by reaction of $O(^1D_2)$ with paraffins is of the magnitude expected for the observed fragmentation into free radicals. The fragmentation occurs with large entropy increase, i.e., with "high" A values, of the order of 10^{15} to 10^{16} sec^{-1}. The results are therefore consistent with the postulate that the decomposing molecules are highly vibrationally excited alcohols in their ground electronic state. However, in unimolecular thermal decompositions of alcohols, which occur at much smaller average energies than are available in chemical activation by $O(^1D_2)$ insertion into CH bonds, the decomposition is generally quite different, involving molecular fragmentation into H_2O and an olefin. Thus, for example, thermal decomposition of *tert*-butyl alcohol leads to dehydration to isobutene. Although its Arrhenius parameters are known,[5] they cannot be compared with those calculated for the chemical activation by $O(^1D_2)$ insertion into isobutane, which leads to fragmentation into free radicals and occurs with a large gain in entropy. For this reason, no direct comparisons of A_{calcd} with the corresponding A_{expt} were previously possible.

The present paper reports the experimental results obtained in a study of the room temperature reaction of $O(^1D_2)$ with cyclobutane. It is an extension of the earlier work on $O(^1D_2)$ reactions with saturated hydrocarbons and has been carried out primarily in order to determine the mechanism of the cyclobutane reaction and the lifetime of the "chemically activated" cyclobutanol formed by $O(^1D_2)$ insertion. It was expected that the chemically activated cyclobutanol would give the same fragmentation products, ethylene and acetaldehyde, as the thermal decomposition of cyclobutanol. Since the experimental values of the Arrhenius parameters[6] for the thermal decomposition and of the vibrational frequencies of cyclobutanol[7] are available, it was hoped that a direct comparison of A_{calcd} and A_{expt} would be possible in this case.

Experimental Section

Excited oxygen atoms, $O(^1D_2)$, were generated by direct photolysis of N_2O at 213.9 nm using emission from Zn resonance lamps (Phillips 93106E).[2b] The photolysis was carried out in a metal reaction cell, designed for pressures of up to 20 atm. It consisted of a stainless steel cylinder 2.5 cm i.d., 5.0 cm long, and had a total volume of 40.2 cc. It was fitted with 10-mm thick Suprasil quartz windows and was provided with a "cold finger" to condense the gases. The cell was made vacuum tight by means of Viton O-rings and bolted flanges and was connected to the vacuum line and the analytical system through a metal valve. Checks were made for gas leaks under conditions normally employed in the experiments.

A cylindrical quartz reaction cell, 5 cm in diameter, 10 cm long, of total volume of 191.0 cc, with two thin Suprasil windows, was eventually used in experiments at pressures below 1.5 atm. Several experiments at total pressures between about 100 and 300 Torr were carried out in a similar quartz reaction cell of total volume of 158 cc.

Liquid phase experiments were carried out in a Suprasil tube 0.5 cm i.d., 5 cm long, provided with a Hoke metal valve. Sufficient cyclobutane was introduced to maintain it in liquid state under its own vapor pressure. The partial pressure of N_2O above the liquid phase was about 300 Torr; the actual amount of N_2O dissolved in liquid cyclobutane was not known but it was sufficient for convenient photolysis. Care was taken to screen adequately the gas phase and irradiate only the liquid. A mercury free vacuum line was used to store and handle the reactant gases.

Matheson N_2O (98.0% minimum, with air as principal impurity) was introduced into the storage bulb through a cold trap at −78° and was then thoroughly degassed at −196° and finally twice distilled from a bath at −120°. Matheson Instrument Purity SF_6 (99.99% min.) was degassed and used without further purification. Merck Sharp and Dohme cyclobutane was slowly bubbled through concentrated H_2SO_4 and distilled twice from a −78° bath. The purity of the final sample was checked by gas chromatography and mass spectrometry. About 1% of *n*-butane was the only impurity detected.

After irradiation the reactants and products were frozen at −196° in the cell and the noncondensable gases (H_2, O_2, N_2, CH_4, and CO) were collected by a Toepler pump through two spiral traps at −196°. To prevent loss by occlusion, the contents of the cell were frozen over into the first spiral trap under continuous pumping and collection of the noncondensables. The latter were measured in a gas buret and analyzed on a 3 m, 0.635 cm i.d., 13X molecular sieve column, with helium as the carrier gas and a Gow Mac thermistor detector. The ratio of the response factors for H_2 and N_2 was determined using samples of known composition. Literature values[8] of response factors were used for the other compounds. Quantitative determinations were based on gas chromatographic peak areas.

The condensable products were analyzed by gas chromatography using several different columns, with helium as the carrier gas and flame ionization detectors with a Varian Aerograph TM dual electrometer. Light hydrocarbons (ethane to cyclobutene) were analyzed on a 3 m, 0.635 cm i.d., 2% squalane on activated alumina column at room temperature. This column gave excellent resolutions except for cyclobutene which was poorly resolved from the huge peak of cyclobutane. Propane was used as internal standard. Response factors proportional to the number of carbon atoms were used in the evaluation of the yields of these hydrocarbons. Ethylene, the main reaction product, was identified on this column by its retention time and seeding with a known sample. The identification was also confirmed by mass spectrometric analysis of the peaks eluted from the squalane capillary column described in the following paragraph.

The heavier hydrocarbons, in particular cyclobutylcyclobutane (CBCB), were analyzed at room temperature on a 91.5 m, 0.038 cm i.d. stainless steel capillary column coated with squalane. Benzene or cyclohexene were used as internal standards. The identification of CBCB was based on the chromatogram of a sample obtained by the mercury photosensitized decomposition of cyclobutane.[9] Hydrocarbons are separated on this column by their boiling points; the logarithms of their adjusted retention times are very nearly a linear function of their boiling points. The retention time of the peak identified as CBCB corresponded closely to its reported boiling point (133.5°).[10] Mass spectrometric analysis at 70 eV of the peak showed a spectrum with a very weak parent ion (*m/e* 110) and major fragments at *m/e* 28, 67, 54, 39, 41, and 82. Fast elimination of ethylene followed by fragmentation of a cyclohexene moiety is consistent with the observed spectrum.[11] However, the mass spectrum of CBCB does not seem to have been reported in the literature. Some other minor peaks, corre-

sponding to C_5–C_6 hydrocarbons were observed on this column but no attempt was made to identify them.

For identification and analysis of oxygenated compounds the following gas chromatographic columns were used (with benzene or cyclohexene as internal standards): (1) a 0.35% di-*n*-decylphtalate on 120–140 mesh glass beads column, 6.10 m long, 0.476 cm i.d.; (2) a 20% Carbowax 20M on 80–100 mesh AW Chromosorb P column, 2.25 m long, 0.635 cm i.d., operated at 85°; (3) a 20% silicon fluid GEXF 1150 on 80–100 mesh AW DMCS Chromosorb W column, 3.05 m long, 0.635 cm i.d.; and (4) a 91.5 m, 0.038 cm i.d. stainless steel capillary column coated with β,β'-thiodipropionitrile ($\beta\beta'$-TDPN). Acetaldehyde was also analyzed on a 20% Carbowax 400 on 80–100 mesh Chromosorb P column, 3 m long, 0.635 cm i.d.

The major oxygenated compounds and heavier hydrocarbon peaks observed on these columns were acetaldehyde, CBCB, cyclobutanone, and cyclobutanol. Propanal and 1-butanal were identified on some of the columns as minor components. A few other very small peaks were observed but not identified. Acetaldehyde, cyclobutanone, and cyclobutanol were identified by seeding with authentic samples. The identity of acetaldehyde was confirmed by mass spectrometric analysis of the peak eluted from the $\beta\beta'$TDPN column.

The yields of acetaldehyde reported in the present paper are based on measurements of the peaks obtained on the $\beta\beta'$TDPN and Carbowax 400 columns. Cyclobutanol was determined on the Carbowax 20M and $\beta\beta'$TDPN columns. Empirical response factors for these two products were measured. At the low yields of cyclobutanol, especially in the low pressure experiments, the reproducibility was rather poor and it is suspected that the recovery of cyclobutanol from the reaction mixture was very incomplete.

Water was identified using a 2 m, 0.317 cm i.d., Porapak T column at 100°. Quantitative determination of its yield was not attempted.

The brownish deposit formed in the reaction cell after several runs gave a negative chromotropic acid test for formaldehyde.

A value of the extinction coefficient of cyclobutanol at 213.9 nm was required in order to assess the likelihood of its secondary photolysis in the course of the reactions studied. Measurements were therefore carried out with dilute ($\sim 10^{-2}$ *M*) solutions of cyclobutanol (Aldrich 99+%) in very pure cyclopentane (Phillips 99.96%) and a value of $\epsilon^{25°}_{213.9nm} = 0.150 \pm 0.050$ atm^{-1} cm^{-1} (base e) was obtained. Gas phase determinations were far less precise because of the errors involved in the measurement of small pressures and optical densities due to the low volatility of cyclobutanol at room temperature.

Results

The reaction of $O(^1D_2)$ atoms with cyclobutane was studied at room temperature (25 ± 2°) and at cyclobutane conversions below 0.5%. Photolysis of N_2O at 213.9 nm generated $O(^1D_2)$ atoms with a quantum efficiency very close to unity ($O(^1D_2)/N_2 \geq 0.97$).[12] Since hydrocarbons do not quench $O(^1D_2)$ atoms physically but interact with them chemically[3] and the relative rate data indicate[13,14] that in the investigated system more than 98% of $O(^1D_2)$ reacted with cyclobutane, the product yields may be expressed as fractions of the nitrogen formed in the photolysis of N_2O. Under such conditions these fractions ($r_{product}/r_{N_2}$) are to a good approximation equal to the quantum yields (ϕ) of the products, i.e., to the number of product molecules formed per $O(^1D_2)$ atom reacting with cyclobutane.

The results of a number of experiments carried out are shown in Table I. In the gas phase experiments (Table IA) the main products of the reaction of $O(^1D_2)$ with cyclobutane are seen to be ethylene and acetaldehyde. At higher pressures cyclobutanol also becomes a major product although it is a very minor product at lower pressures. In most of these experiments SF_6 was added to increase the pressure since it is a good deactivator of vibrational excitation but does not deactivate $O(^1D_2)$ atoms.[2b,3] The increase in the yields of cyclobutanol with increasing pressure and the concurrent decrease in the yields of ethylene and acetaldehyde indicate that the cyclobutanol formed by insertion of $O(^1D_2)$ into the CH bonds of cyclobutane is highly excited and readily decomposes into C_2H_4 and CH_3CHO. Only at quite high pressures in the gas phase an appreciable stabilization of cyclobutanol takes place. In agreement with this, cyclobutanol was found to be by far the major product in liquid phase (Table IB), where ethylene yield became very small and acetaldehyde was not observed at all. It should be mentioned that ethylene and acetaldehyde are also the major products of the thermal decomposition of cyclobutanol.[6]

Of the minor products listed in Table I cyclobutylcyclobutane (CBCB) and cyclobutene (CBEN) are the products logically derived from cyclobutyl radicals, the expected primary product of H abstraction from cyclobutane by $O(^1D_2)$.[3] The comparable yields of CBCB and cyclobutene in Table I are consistent with a ratio of combination to disproportionation of cyclobutyl radicals of close to one.[15] These two compounds do not show pressure dependence, following a well-established pattern for $O(^1D_2)$ abstraction products.[3] Moreover, addition of molecular oxygen, an efficient free radical scavenger, completely suppresses the "abstraction" product CBCB (run 17, Table IA), confirming its free radical origin, while it does not affect the $O(^1D_2)$ "insertion" products (cyclobutanol and its molecular fragments, C_2H_4 and CH_3CHO). Large amounts of O_2 were consumed in this experiment ($\Delta O_2/\Delta N_2 \sim 3$) and there was an appreciable increase in the yield of cyclobutanone (CBON) and especially of CO, probably as a result of a series of reactions between O_2 and free radicals.

Cyclobutanone and H_2 are perhaps partly the products of a minor "molecular elimination" path[3] in the reaction of $O(^1D_2)$ with cyclobutane. This cannot be regarded as positively established although it is supported by the fact that O_2 does not completely suppress H_2. The residual yield of H_2 in run 17 places an upper limit of slightly more than 1% on the extent of molecular elimination into H_2 and cyclobutanone. 1-Butanal is a minor product observed both in the present reaction and in the thermal decomposition of cyclobutanol.[6] Its yield in Table IA perhaps increases slightly with increasing pressure in the gas phase and is not completely suppressed by O_2. It is possible that 1-butanal is a rearrangement product of ROH*, as will be discussed later.

Water is a product of the "abstraction" reaction; its presence was established qualitatively but the difficult quantitative determinations in the present reaction system were not attempted, as mentioned in the experimental part. A lower limit for the yield of water is given approximately by the sum of cyclobutylcyclobutane and cyclobutene. On this basis then a lower limit for the O-atom material balance in Table I is typically not better than about 80%. Systematic

TABLE I: Products of the Reaction of $O(^1D_2)$ with Cyclobutane at 25°

Run	Reactants, additives, Torr (25°)					ΔN_2, μmol	Product yields relative to nitrogen ($r_{N2} = 1$)											$(\Delta[A]/[N_2])^b$
	N_2O	CB[a]	SF_6	O_2	Total		C_2H_4	CH_3CHO	ROH[a]	CO	H_2	CH_4	CBON[a]	CBCB[a]	CBEN[a]	C_3[a]	nBA[a]	
							A. Gas Phase Experiments[e]											
15	63.5	627.7			691.2	7.14	0.511	0.420	0.015	0.051	nd	0.009	0.013	0.052	0.062	0.007	0.010	0.055
13	61.3	618.3	606.1		1,285.7	2.93	0.520	0.401	0.020	0.061	nd	0.013	0.010	0.037	nd	0.014	0.003	0.023
18	62.6	662.2	1,271.8		1,996.6	2.35	0.445	0.395	0.038	0.070	nd	0.003	0.034	0.040	0.052	0.006	0.008	0.017
25	63.2	673.8	1,284.8		2,021.8	3.44	0.475	0.370	0.042	0.060	0.035	0.004	nd	0.032	nd	nd	nd	0.024
19	61.8	664.1	2,304.2		3,030.1	1.87	0.450	nd	0.030	0.075	nd	tr	0.027	0.038	nd	nd	0.005	0.013
22	59.4	634.4	2,445.0		3,139.2	4.38	0.451	0.380	0.055	0.064	0.028	0.005	0.032	0.046	0.043	nd	nd	0.030
24	61.3	673.2	3,263.5		3,998.0	3.71	0.390	0.280	0.057	0.054	0.023	nd	nd	0.033	nd	nd	nd	0.023
11	58.4	479.8	4,292.4		4,830.4	3.48	0.392	0.280	0.085	0.062	nd	0.005	0.029	0.030	nd	nd	0.012	0.021
12	61.1	614.9	7,005.8		7,681.8	3.03	0.333	0.250	0.121	0.062	nd	0.010	0.034	0.032	nd	0.028	0.017	0.015
21	65.1	670.2	8,471.3		9,206.6	4.43	0.300	0.230	0.118	0.057	0.034	nd	nd	0.056	nd	nd	nd	0.018
23	64.6	678.9	9,962.3		10,706.0	3.42	0.290	0.230	0.181	0.077	0.020	0.005	0.038	0.052	nd	nd	0.019	0.013
20	64.0	670.8	10,589.2		11,324.0	3.22	0.285	0.190	nd	0.050	nd	nd	0.034	0.055	nd	nd	0.021	0.012
26[c]	62.5	607.8	540.4		1,210.4	5.14	0.523	0.390	0.013	0.071	0.026	0.010	nd	0.040	nd	nd	nd	0.008
17	65.6	644.4		12.6	722.6	6.94	0.571	0.501	0.015	0.321	0.012	0.009	0.070	tr	nd	0.024	0.011	0.052
							B. Liquid Phase Experiments											
27	lph[d]	lph[d]				4.07	0.030	0.000	nd	nd	0.096	tr	0.024	0.027	nd	nd	nd	
28	lph[d]	lph[d]				0.498	0.037	0.000	0.470	0.068	tr	tr	nd	nd	nd	nd	nd	

[a] CB = cyclobutane; ROH = cyclobutanol; CBON = cyclobutanone; CBCB = cyclobutylcyclobutane; CBEN = cyclobutene; C_3 = C_3 hydrocarbon products; nBA = 1-butanal. [b] Calculated loss of acetaldehyde in secondary photolysis relative to N_2 formed (as discussed later in the paper). [c] Quartz reaction cell used (191 ml). [d] Liquid phase, as described in the Experimental Section. [e] nd = not determined; tr = trace.

TABLE II: Dependence of CO Yields on Conversion[a]

Run	Reactants, Torr (25°) N_2O	CB[b]	Total	ΔN_2, μmol	CO/N_2	CH_4/N_2	C_2H_4/N_2	C_2H_6/N_2	$(\Delta[A]/[N_2])^c$
66	16.3	96.2	112.5	1.79	0.047		nd	nd	0.015
64	16.4	98.4	114.8	2.03	0.064		nd	nd	0.017
65	16.4	97.4	113.8	2.69	0.064		nd	nd	0.022
67	16.7	98.0	114.7	11.04	0.099	0.015	0.579	0.013	0.082
69	16.4	302.7	319.1	11.77	0.071	0.015	0.565	0.008	0.090
68	16.2	98.0	114.2	12.32	0.100	0.014	0.598	0.014	0.093
63	16.3	96.8	113.1	16.97	0.104	0.017	0.608	0.016	0.122

[a] 25 ± 2°; the volume of the quartz reaction cell 158 ml. nd = not determined. [b] CB = cyclobutane. [c] Calculated loss of acetaldehyde in secondary photolysis relative to N_2 formed (as discussed later in the paper).

TABLE III: Effect of Additions of CH_3CHO on the Yield of CO[a]

Run	Reactants, Torr (25°) N_2O	CB[b]	Total	CH_3CHO added, μmol	ΔN_2, μmol	CO/N_2	$(\Delta[A]/[N_2])^c$
1	71.4	752.0	823.4		4.1	0.062	0.006
2	71.4	752.0	823.4		8.4	0.064	0.013
3	71.7	752.0	823.7	2.25	4.3	0.087	0.019
4	71.7	752.0	823.7	27.2	4.2	0.158	0.154

[a] 25 ± 2°; quartz reaction cell, total volume 191 ml. [b] CB = cyclobutane. [c] Calculated loss of acetaldehyde in secondary photolysis relative to N_2 formed (as discussed later in the paper).

errors in calibrations and gas chromatographic response factors, the neglect of some minor unidentified gas chromatographic peaks, lack of directly measured water yields, the difficulty of quantitative recovery of some of the oxygenated products, and the very small amount of reaction of $O(^1D_2)$ with N_2O may collectively account for the difference. It appears, however, safe to assume that no other major reaction path has been overlooked.

Although CO is a very minor reaction product, its appreciable yield even at high pressure in the gas phase and in particular in the liquid phase appears at first glance puzzling. Secondary photolyses of cyclobutanol and acetaldehyde may present at least a partial explanation. The likelihood of such secondary photolyses at 213.9 nm and at the longer wavelengths emitted by the zinc lamps used (309.2, 330.3, and 334.5 nm) will be discussed in the following section. Some experimental support that the photolysis of acetaldehyde may occur to some extent is provided by the data in Table II, which show an increase in CO/N_2 with increasing ΔN_2. Constant relatively small partial pressures of N_2O and appreciably larger partial pressures of cyclobutane were used in these experiments. Under such conditions ΔN_2 is a measure of conversion and thus of a build up of the CH_3CHO concentration. Very little cyclobutanol is produced in these low pressure experiments and the increase in CO/N_2 cannot be ascribed to a secondary photolysis of cyclobutanol.

Table III shows that secondary photolysis of acetaldehyde to produce CO must occur at least to some extent since prior additions of small amounts of acetaldehyde to a mixture of N_2O and cyclobutane brings about an increase in CO/N_2. At the same time the data indicate that only a relatively small part of CO can be ascribed to secondary photolysis of acetaldehyde. On the other hand, it is possible that in the liquid phase experiments (Table IB), in which the reaction volume was of the order of only 1 cc, secondary photolysis may have played a more important role.

Discussion

Reaction Products and Mechanism. For the case of cyclobutane (in the nitrous oxide system) the general mechanism of interaction of $O(^1D_2)$ with paraffins can be written as follows

$$N_2O + h\nu\ (213.9\ nm) \rightarrow N_2 + O(^1D_2) \quad (1)$$

$$O(^1D_2) + N_2O \rightarrow N_2 + O_2 \quad (1a)$$

$$\rightarrow 2NO \quad (1b)$$

$$O(^1D_2) + RH \rightarrow ROH^* \quad (2a)$$

$$\rightarrow R + OH \quad (2b)$$

$$\rightarrow H_2 + \text{cyclobutanone} \quad (2c)$$

$$ROH^* \rightarrow C_2H_4 + CH_3CHO \quad (3)$$

$$ROH^* + M \rightarrow ROH + M \quad (4)$$

$$OH + RH \rightarrow H_2O + R \quad (5)$$

$$R + R \rightarrow \text{cyclobutylcyclobutane} \quad (6a)$$

$$\rightarrow RH + \text{cyclobutene} \quad (6b)$$

RH represents cyclobutane, ROH cyclobutanol, R cyclobutyl, and M is any molecule removing excess vibrational energy from ROH*.

The ratio of cyclobutane to N_2O is kept high in order to minimize loss of $O(^1D_2)$ in reactions 1a and 1b. As mentioned earlier, it has been calculated that, in the experiments listed in Table IA, more than 98% of $O(^1D_2)$ reacted with cyclobutane. A 2% reaction of $O(^1D_2)$ with N_2O will increase N_2 only by about 1% (since $k_{1a}/k_{1b} \approx 1$) and will

therefore affect adversely the material balance to that extent. Since this is only a very minor effect, no corrections were made in the tables for the extra N_2 from reaction 1a. A slightly more important effect of reaction of $O(^1D_2)$ with N_2O results from the production in reactions 1a and 1b of O_2 and NO, which may act as efficient scavengers of R and thus decrease somewhat the yields of cyclobutylcyclobutane and cyclobutene. This is therefore one of the contributing causes to the low material balance mentioned in the preceding section.

It is evident that the major products observed are entirely consistent with the above general mechanism. At lower pressures ROH* predominantly decomposes and the main products are C_2H_4 and CH_3CHO. At higher pressures increasing amounts of cyclobutanol are formed. Water, cyclobutylcyclobutane, and cyclobutene show that the abstraction reaction 2b is important.

Concerted unimolecular decomposition in reaction 3 is symmetry allowed for electronically excited ROH* but is forbidden in its ground electronic state. However, both states are allowed to decompose by splitting a single CC bond and forming intermediate 1,4 biradicals (1,4-B), i.e.

$$ROH^* \rightarrow 1,4\text{-}B^* \quad (3a)$$

$$1,4\text{-}B^* \rightarrow ROH^* \quad (3b)$$

$$\rightarrow C_2H_4 + CH_3CHO \quad (3c)$$

The intermediate biradical may be either $\dot{C}H_2CH_2CH_2\dot{C}HOH^*$ or $\dot{C}H_2CH_2CH(OH)\dot{C}H_2^*$. In either case it must contain considerable excess of vibrational energy when formed in the present experiments (as indicated by the asterisk). It can be therefore expected to decompose rapidly into C_2H_4 and vinyl alcohol (i.e., CH_3CHO), reaction 3c, with essentially no recyclization, reaction 3b. However, formation of small amounts of 1-butanal may perhaps involve rearrangement of $\dot{C}H_2CH_2CH_2\dot{C}HOH^*$ through a 1,5 H-atom migration.

In the reaction of $O(^1D_2)$ with paraffins the insertion reaction 2a typically accounts for about 65% of the overall reaction, the molecular elimination (the equivalent of reaction 2c) is usually limited to a few percent and the remainder may be ascribed to abstraction. The present reaction probably conforms to this general pattern. The extent of the insertion, reaction 2a, may probably be best estimated from the yields of C_2H_4 at low pressures where ROH* predominantly decomposes. The extrapolated values of $\phi_{C_2H_4}$ from Table IA for M = O and the values of $\phi_{C_2H_4}$ (or of $\phi_{C_2H_4} + \phi_{C_2H_6}$) in Table II indicate a quantum yield of reaction 2a of 55–65%. As discussed earlier, the extent of the molecular elimination reaction 2c is only about 1–2%. The remainder of about 35–40% should then be assigned to abstraction, reaction 2b. Unfortunately, this was not possible to verify because water could not be measured quantitatively. An approximate indirect estimate of the extent of abstraction from the sum of yields of cyclobutylcyclobutane and cyclobutene (or of the doubled yield of cyclobutylcyclobutane) gives a value of only about 20%. However, this must be regarded only as a lower limit, for reasons discussed in the preceding section in connection with the observed low material balance of oxygen atoms and partly also in the following treatment of the potential effects of secondary processes.

Secondary Processes and Minor Products. The possibility that secondary photolysis of acetaldehyde may contribute to or even be entirely responsible for the formation of the small amounts of CO has already been briefly mentioned. In fact, practically all the minor products observed are the known or potential products of photolysis of acetaldehyde and cyclobutanol. It is therefore necessary to establish whether secondary photolysis of these two products is likely under reaction conditions employed in this study.

Photolysis of CH_3CHO generates CH_3 and HCO radicals and gives CO and CH_4 as the major stable products.[16] Photolysis of cyclobutanol does not seem to have been reported. We have therefore photolyzed at 213.9 nm very small amounts (ca. 0.6 μmol) of cyclobutanol in the presence of excess SF_6 (ca. 300 Torr) and have observed large amounts of CO, H_2, and CH_4, formed in the molar ratios of 1:0.40:0.067. The quantum yield of CO formation was at least 70% and might have been perhaps substantially larger.

The secondary photolytic reactions which have to be considered are therefore

$$ROH + h\nu \rightarrow \text{products (CO, } H_2, CH_4, \ldots) \quad (7)$$

$$CH_3CHO + h\nu \rightarrow \text{products (CO, } CH_4, \ldots) \quad (8a)$$

$$CH_3CHO + h\nu^i \rightarrow \text{products (CO, } CH_4, \ldots) \quad (8b)$$

where ROH represents cyclobutanol, $h\nu$ refers to the 213.9-nm line and $h\nu^i$ to the 309.2-, 330.3-, and 334.5-nm lines from the Zn lamps employed.

Secondary Photolysis of Cyclobutanol. An estimate of the extent of reaction 7 can be obtained from a steady state treatment of reactions 1–7, which gives the following expression

$$d[ROH]/d[N_2] = f^0_{ROH} - \alpha[ROH] \quad (I)$$

with

$$f^0_{ROH} = (k_{2a}/k_2)\,(1 + k_3/k_4[M])^{-1}\delta^{-1}$$

$$\alpha = (\epsilon_{ROH}/\epsilon_{N_2O}[N_2O])/\delta'$$

$$\delta = 1 + (k_{1a} + k_1)[N_2O]/k_2[RH] \quad (Ia)$$

$$\delta' = 1 + k_{1a}[N_2O]/(k_2[RH] + k_1[N_2O])$$

ϵ_{ROH} and ϵ_{N_2O} are the extinction coefficients (at 213.9 nm) of cyclobutanol and N_2O, taken, respectively, as 0.15 (present result) and 0.084 $atm^{-1}\ cm^{-1}$ (from the literature).[17] Since [ROH] = 0 when t = 0 (i.e., when $[N_2]$ = 0), it follows that at any time (t) during the reaction

$$[ROH] = (f^0_{ROH}/\alpha)\{1 - \exp(-\alpha[N_2])\}$$

If the secondary photolysis of ROH did not occur (i.e., in the limit of zero conversion or if α = 0), the concentration of ROH at any time would be simply $[ROH]^0 = f^0_{ROH}[N_2]$. The fractional decrease of [ROH] as a result of secondary photolysis is therefore

$$[ROH]/[ROH]^0 = (1/\alpha[N_2])\{1 - \exp(-\alpha[N_2])\} \quad (II)$$

and the amount of ROH photolyzed relative to N_2 produced is then

$$(\Delta[ROH])_{phot}/[N_2] = f^0_{ROH}(1 - [ROH]/[ROH]^0) \quad (III)$$

Since[13,14] k_2/k_1 = 4.3 and[18] $k_{1a} = 0.5k_1$, δ and δ' can be evaluated. (In most of the present experiments δ and δ' are both very close to unity.) It can also be taken, from present results, as discussed later, that k_{2a}/k_2 = 0.62 and $k_4/k_3 = 1.1 \times 10^{-4}\ Torr^{-1}$.

With these values, eq II shows an average (and nearly constant) loss of 2–3% cyclobutanol in each run in Table IA

as a result of secondary photolysis and $(\Delta[ROH])_{phot}/[N_2]$ values (from eq III) vary from 0.001 to about 0.006. Secondary photolysis of cyclobutanol could have therefore contributed only very little to the CO yields in these experiments.

Secondary Photolysis of Acetaldehyde. In a similar manner as with cyclobutanol, the fractional decrease in the CH_3CHO concentration ([A]) as a result of its secondary photolysis is

$$[A]/[A]^0 = (1/\beta[N_2])\{1 - \exp(-\beta[N_2])\} \quad (IV)$$

and the amount photolyzed relative to N_2 produced is

$$(\Delta[A])_{phot}/[N_2] = f^0_A\{1 - [A]/[A]^0\} \quad (V)$$

where

$$f^0_A = (k_{2a}/k_2)(1 + k_4[M]/k_3)^{-1}\delta^{-1}$$

$$\beta = (\epsilon_A/\epsilon_{N_2O}[N_2O])\{1 + \Sigma(\epsilon_A{}^i/\epsilon_A)(I^i/I)\}(1/\delta')$$

δ and δ' are the same as in eq Ia. ϵ_A is the extinction coefficient of CH_3CHO at 213.9 nm and I is the light intensity at 213.9 nm. $\epsilon_A{}^i$ and I^i are the corresponding values at the longer wavelengths (λ_i) emitted by the Zn lamp (309.2, 330.3, and 334.5 nm) which can photolyze CH_3CHO but not N_2O. We estimate from the data in the literature that $\epsilon_A/\epsilon_{N_2O} = 0.48$ and that $\epsilon_A{}^i/\epsilon_A$ is 10.0, 2.2, and 1.2 at 309.2, 330.3, and 334.5 nm, respectively. At these wavelengths, the quantum output ratios, I^i/I, found[2b] for the same type of lamp are approximately 0.28, 0.24, and 0.26. It can therefore be taken that $\beta = 4.1/p_{N_2O}\delta'$ (where p_{N_2O} is the partial pressure of N_2O in Torr). For experiments in Table IA eq IV indicates an average loss of CH_3CHO of about 5–6% as a result of secondary photolysis. The amounts of CH_3CHO photolyzed relative to N_2 produced calculated from eq V, i.e., the $(\Delta[A])_{phot}/[N_2]$ values, are shown in the last columns of Tables IA, II, and III. For runs 3 and 4 in Table III, in which CH_3CHO was initially added, eq V was replaced by

$$\frac{([A])_{phot}}{[N_2]} = f^0_A\left[1 + \left(\frac{[A]_i}{\phi^0_A[N_2]} - \frac{1}{\beta[N_2]}\right) \times \{1 - \exp(-\beta[N_2])\}\right] \quad (VI)$$

where $\phi^0_A = f^0_A\delta$.

It can be seen that at larger conversions and lower pressures and also when larger amounts of CH_3CHO are initially added ($[A]_i$), the observed CO yields can be approximately explained by secondary photolysis of CH_3CHO. However, at smaller conversions and with smaller initial additions, of CH_3CHO, the secondary photolysis can explain only a small fraction of the CO formed. It appears therefore that there is an additional source of CO. The fact that the yield of CH_3CHO is smaller than the yield of C_2H_4 and that $[CH_3CHO] + [CO] \sim [C_2H_4]$ suggests that CO is formed at the expense of CH_3CHO. Perhaps a small fraction of the excited CH_3CHO formed in reaction 3 undergoes further fragmentation even at the high pressures used in some of the experiments. At the same time, it must be emphasized that such an approximately pressure insensitive fragmentation, if it occurs at all, is a relatively unimportant feature of the reaction of $O(^1D_2)$ with cyclobutane since, in the absence of O_2, CO is a very minor reaction product. (In the presence of O_2, CO yield substantially increases, as shown in Table IA, run 17, but it is unlikely that traces of O_2 formed in reaction 1a can be responsible for more than only a small fraction of the CO found.)

Unimolecular Decomposition of the "Chemically Activated" Cyclobutanol. The pressure dependence of the quantum yields (ϕ) of C_2H_4, CH_3CHO, and cyclobutanol (ROH) provides in principle information on the lifetime of the chemically activated cyclobutanol (ROH*) formed in reaction 2a. Steady state treatment of reactions 1–4 gives the following expressions:

$$\phi_{C_2H_4} = (r_{C_2H_4}/r_{N_2})\delta = (k_{2a}/k_2)(1 + k_4[M]/k_3)^{-1} \quad (VII)$$

$$\phi^0_{CH_3CHO} = (r_{CH_3CHO}/r_{N_2})\delta = (k_{2a}/k_2)(1 + k_4[M]/k_3)^{-1} = \phi_{C_2H_4} \quad (VIII)$$

$$\phi^0_{ROH} = (r_{ROH}/r_{N_2})\delta = (k_{2a}/k_2)(1 + k_3/k_4[M])^{-1} \quad (IX)$$

$$\phi^0_{ROH}/\phi_{C_2H_4} = k_4[M]/k_3 \quad (X)$$

where δ is as given earlier (eq Ia), r indicates the observed reaction rates, and ϕ^0 the quantum yields in the absence of secondary reactions (such as secondary photolysis or secondary attack by any active intermediates present).

The observed pressure dependence of the yields of C_2H_4, CH_3CHO, and ROH is in qualitative agreement with eq VII–X. However, as discussed in the preceding section, both cyclobutanol and CH_3CHO are susceptible to secondary reactions, perhaps especially so CH_3CHO. In addition, considerable analytical difficulty was experienced with the measurements of the very small yields of cyclobutanol in the presence of huge excess of reactants and inert gas (SF_6) which had to be used. The measured yields of cyclobutanol are therefore not quantitatively reliable. For these reasons attention has to be primarily focussed on the trend in the yields of C_2H_4. Ethylene is not expected to participate in the present reaction system to any appreciable extent in secondary reactions and its quantum yields appear to be reasonably accurate and precise. A plot of $1/\phi_{C_2H_4}$ vs. [M] should therefore be linear with the intercept (I) equal to k_2/k_{2a} and the slope to intercept ratio (S/I) equal to k_4/k_3. Such a plot for all the measured yields of C_2H_4 in the present gas phase experiments (listed in Tables IA and II) is shown in Figure 1.

The least-squares values of the slope and intercept of the plot in Figure 1 are $I = 1.62 \pm 0.02$ and $S = (5.39 \pm 0.32) \times 10^{-21}$ cc molecule^{-1}, where the indicated uncertainties represent one standard deviation. (Because of the change of variable from $\phi_{C_2H_4}$ to $1/\phi_{C_2H_4}$, a statistical weight proportional to $\phi^4_{C_2H_4}$ had to be assigned to each value of $1/\phi_{C_2H_4}$. The least-squares values of I and S thus obtained have been used to draw the solid line in Figure 1.) The least-squares value of the slope gives then $k_{2a}/k_2 = 0.62 \pm 0.01$ and the intercept to slope ratio gives $k_3/k_4 = (3.00 \pm 0.18) \times 10^{20}$ molecule cc^{-1}. We estimate that in the present reaction system $k_4 \approx 4 \times 10^{-10}$ cc molecule^{-1} sec^{-1} if it is assumed that ROH* is deactivated at each collision. Subject to this assumption, $k_3 = 1.2 \times 10^{11}$ sec^{-1} and the lifetime of the chemically activated cyclobutanol is therefore $\tau_3 = 8.3 \times 10^{-12}$ sec.

The present k_3 value of 1.2×10^{11} sec^{-1} for chemically activated cyclobutanol may be compared, for example, with the corresponding values of 5.9×10^8 sec^{-1} for cyclopentanol,[19] 3.8×10^9 sec^{-1} for *tert*-butyl alcohol,[20] and 1.3×10^{12} sec^{-1} for methanol.[21] Mintz and Cvetanović[4] have recently calculated from the k_3 values available in the literature approximate Arrhenius A factors for the unimolecular decomposition of these and some other chemically activat-

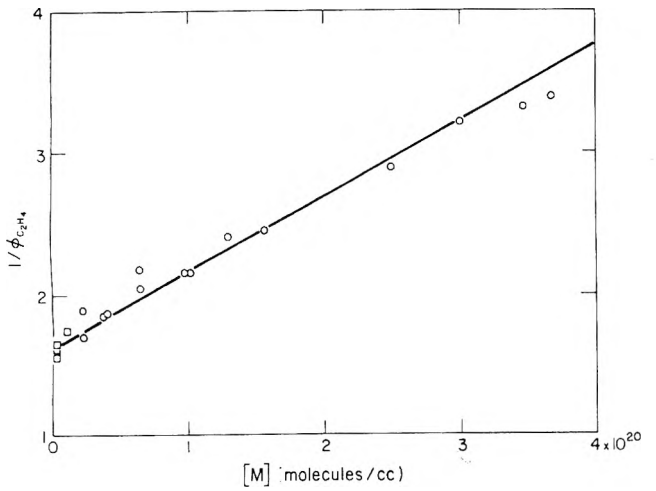

Figure 1. Plot of $1/\phi_{C_2H_4}$ vs. [M]. (O, data from Table IA; □, data from Table II. The solid line is based on the weighted least-squares estimates of the slope and intercept, as explained in the text).

ed alcohols formed by insertion of $O(^1D_2)$ into the CH bonds of alkanes. They used the theoretical expression

$$k(E) = AN(E - E_\infty)/N(E) \qquad (E > E_\infty) \qquad \text{(XI)}$$

which relates the specific rate of unimolecular decomposition, $k(E)$, to the densities of states $N(E - E_\infty)$ and $N(E)$ of the reactant molecule at energies $(E - E_\infty)$ and E, respectively, and to the Arrhenius parameters, A and E_∞.

Equation XI was derived by Forst[22] for unimolecular decomposition in thermal systems assuming that the Arrhenius parameters, A and E_∞, are temperature independent. While this assumption is not strictly valid, it may be accepted as an approximation, in particular since Arrhenius parameters are determined experimentally as temperature independent quantities and therefore represent "averaged" constant values for the temperature range employed. In fact, it was shown[4] that the curvature of the Arrhenius plot of the theoretical values of k_3 for methanol, calculated for an extensive temperature range from the transition state theory expression for k, is for all practical purposes imperceptible. The plot is therefore to a very good approximation linear (and would certainly be treated as such had it been based on experimental measurements of k) although the "preexponential" factor A (i.e., the factor dependent on the entropy of activation) varies rather rapidly with temperature. In view of this, and since E_∞ can be estimated approximately from thermochemical data, Mintz and Cvetanovic have postulated that eq XI may be used to calculate the "empirical" values of the Arrhenius A factors and thus to predict approximately the rates of the thermal decomposition of the reactant molecule using only its structural properties (to calculate the densities of states) and a single value of $k(E)$ (i.e., of the rate constant of the unimolecular decomposition of the chemically activated reactant molecule).

At the fairly high energies involved in the chemical activation experiments the densities of states can be calculated to a good approximation by the semiclassical method of Whitten and Rabinovitch[23] as modified by Forst[24] so that eq XI can be altered to

$$k(E) = A\left(\frac{E - E_\infty + a'E_z}{E + aE_z}\right)^{\upsilon - 1 + r/2} \qquad \text{(XII)}$$

where E_z is the zero-point energy of the reactant molecule, a' and a are functions of E, E_z, and the vibrational frequencies and have values between zero and unity;[24] υ is the number of vibrations excluding torsional modes and r is the number of internal rotations. Since reaction 2a has zero activation energy, the average value of the energy E available for the unimolecular decomposition of ROH* is given[4] by

$$E = -\Delta H_f^\circ{}_0(\text{ROH}) + \Delta H_f^\circ{}_0(\text{RH}) + \Delta H_f^\circ{}_0(O(^1D_2)) + E_{th} \qquad \text{(XIII)}$$

E_{th} is the average thermal energy of the reactants less $3RT$ (to allow approximately for the assumed adiabacity of the external rotations and of the translational energy of ROH* [4]).

In previous[4] evaluations of A from eq XII, E_∞ was not known and had to be estimated approximately from thermochemical data. Also, the thermal reactions of alcohols generally result in their dehydration to olefins through molecular elimination of H_2O while at the much higher energies available in the chemically activated reactions alcohols undergo fragmentation into free radicals. Thus, the two processes are basically very different, as discussed earlier,[4] and there were therefore no relevant experimental values of A to compare with those calculated from eq XII. In the case of cyclobutanol, on the other hand, both the thermal and the chemically activated reaction result in fragmentation to C_2H_4 and CH_3CHO and the Arrhenius parameters for the thermal reaction are known.[6] Furthermore the vibrational frequencies of cyclobutanol are also known[7] and do not have to be estimated by analogy, as had to be done in all cases except for methanol in the previous work.[4] Unimolecular decomposition of cyclobutanol can therefore, in principle, serve as a suitable test of the applicability of eq XII. However, as will be discussed below, appreciable quantitative uncertainties appear to be unavoidable even in this case, at least at present.

From the vibrational frequencies of cyclobutanol[7] it is found that $E_z = 69.6$ kcal mol^{-1} and from eq XIII and the relevant thermochemical data[25] $E = 145.9$ kcal mol^{-1}. With $E_\infty = 60.1$ kcal mol^{-1}, as found experimentally for the thermal reaction,[6] eq XII gives the calculated value of A, $A_{calcd} = 7.6 \times 10^{15}$. In this calculation the torsional mode of cyclobutanol was treated as a free internal rotation, so that $\upsilon = 32$, $r = 1$, and a' and a were evaluated from the appropriate expressions in the quoted literature.[24] It is found that A_{calcd} is not too sensitive to a moderate uncertainty in E. Thus, an increase in E by as much as 3 kcal mol^{-1} would decrease A_{calcd} by 23%. The value of E_z appears to be quite reliable and an effect on A_{calcd} of any slight variations in it would be quite small. On the other hand, a decrease in E_∞ by, for example, 2 kcal mol^{-1} would decrease A_{calcd} by a factor of 0.64. However, the experimental error in E_∞ appears to be much smaller.[6]

The calculated value of A, $A_{calcd} = 7.6 \times 10^{15}$ sec^{-1}, should be compared with the experimental value for the thermal decomposition, $A_{expt} = 1.3 \times 10^{15}$ sec^{-1}. However, before comparing the two values it is necessary to look into some of the finer details of this unimolecular reaction. These strongly indicate that A_{calcd} should be larger than A_{expt} perhaps by a factor of about 4, which would be very close to what is actually found. First, if the transition state for the decomposition is asymmetrical, as is very likely, the C–C bond which breaks first may be either α or β to the OH substituted carbon. β scission is likely to require a

higher activation energy and may occur to a considerably smaller extent in the thermal reaction than at high energies available in the chemical activation reaction. A_{calcd} may therefore be expected to be up to a factor of 2 larger than A_{expt} for that reason alone. In addition, as suggested by Benson and O'Neal for the unimolecular decomposition of small ring compounds,[31] the reaction in all probability proceeds reversibly via a biradical intermediate (1,4-B), i.e.

$$ROH^* \underset{-3}{\overset{3}{\rightleftharpoons}} (1,4\text{-B}) \xrightarrow{3d} C_2H_4 + CH_3CHO$$

so that the observed rate constant, k_{obsd}, is a composite quantity

$$k_{obsd} = k_3/(1 + k_{-3}/k_{3d})$$

It is clear therefore that $k_3 > k_{obsd}$, or

$$k_3/k_{obsd} = 1 + (A_{-3}/A_{3d}) \exp\{(E_{3d} - E_{-3})/RT\} \quad \text{(XIV)}$$

Since reaction −3 is a ring closure while reaction 3d is a fragmentation, it can be expected that $A_{-3} < A_{3d}$ and $E_{3d} > E_{-3}$, in line with the assigned values for the corresponding quantities in the unimolecular decomposition of cyclobutane.[32] At high energies available in the chemical activation reaction the value of k_3/k_{obsd} would be expected from eq XIV to be close to $1 + (A_{-3}/A_{3d})$, or approximately unity, while in the thermal reaction, if, as an example, a plausible value $E_{3d} - E_{-3} = 3$ kcal mol^{-1} is assumed, $k_3/k_{obsd} = 1 + 8.65(A_{-3}/A_{3d})$ at the mean experimental temperature of 700°K. Taking $A_{-3}/A_{3d} = 0.17$, as assumed for cyclobutane,[32] it is then found that A_{calcd} should be a factor of 2 larger than A_{expt} as a result of the reversible nature of decomposition and the involvement of intermediate biradicals. (An additional effect of this complexity of the process is to increase somewhat the experimental E_∞ in thermal experiments. However, this effect would be difficult to assess quantitatively.)

Strict validity of the following three assumptions implicit in the present value of A_{calcd} has also to be considered. These are: (1) "hot" cyclobutanol is deactivated by SF_6 and cyclobutane at each collision, (2) anharmonicity effects can be neglected, and (3) there is no significant contribution to the vibrational excitation of the cyclobutanol formed in reaction 2a from excess kinetic energy which $O(^1D_2)$ atoms may possess. While at the moment these assumptions appear reasonable,[33] any departures will tend to decrease further the value of A_{calcd}.

It is clear that the combination of the effects just discussed could account entirely for the observed difference between A_{calcd} and A_{expt} and, no doubt, it accounts at least for a substantial part of it. The mutual consistency of A_{calcd} and A_{expt} is therefore reasonable, in agreement with the postulate that the decomposing species is vibrationally excited cyclobutanol in its ground electronic state.

Acknowledgment. The authors are grateful to Mr. R. S. Irwin for carrying out the experiments in Table II.

References and Notes

(1) (a) NRCC No. 14838. (b) NRCC visiting research officer, supported by Consejo Nacional de Investigaciones Cientificas y Tecnicas of Argentina.
(2) (a) R. J. Cvetanović, *Can. J. Chem.* **52**, 1452 (1974), and references therein; (b) H. Yamazaki and R. J. Cvetanović, *J. Chem. Phys.*, **41**, 3703 (1964).
(3) G. Paraskevopoulos and R. J. Cvetanović, *J. Am. Chem. Soc.*, **91**, 7572 (1969).
(4) K. J. Mintz and R. J. Cvetanović, *Can. J. Chem.*, **51**, 3386 (1973).
(5) W. Tsang, *J. Chem. Phys.*, **40**, 1498 (1964).
(6) P. M. Stacy, Ph.D. Thesis, University of Rochester, 1968. [Cf. *Diss. Abstr. B*, **29**, 1632 (1968–1969)].
(7) J. R. Durig and W. H. Green, *Spectrochim. Acta, Part A*, **25**, 849 (1969).
(8) W. A. Dietz, *J. Gas Chromatogr.*, **5**, 68 (1967).
(9) D. L. Kantro and H. E. Gunning, *J. Chem. Phys.*, **21**, 1797 (1953).
(10) A. de Meijere and W. Lüttkes, *Chem. Ber.*, **99**, 2155 (1966).
(11) A. Cornu and R. Massot, "Compilation of Mass Spectral Data", Hayden, London, 1966.
(12) K. F. Preston and R. F. Barr, *J. Chem. Phys.*, **54**, 3347 (1971).
(13) P. Michaud, G. Paraskevopoulos, and R. J. Cvetanović, *J. Phys. Chem.*, **78**, 1457 (1974).
(14) G. Paraskevopoulos, V. B. Symonds, and R. J. Cvetanović, *Can. J. Chem.*, **50**, 1838 (1972).
(15) R. A. Sheldon and J. K. Kochi, *J. Am. Chem. Soc.*, **92**, 4395 (1970).
(16) J. G. Calvert and J. N. Pitts, Jr., "Photochemistry", Wiley, New York, N.Y., 1966, p 371.
(17) B. A. Thompson, P. Harteck, and R. R. Reeves, Jr., *J. Geophys. Res.*, **68**, 6431 (1963).
(18) (a) P. M. Scott, K. F. Preston, R. J. Andersen, and L. M. Quick, *Can. J. Chem.*, **49**, 1808 (1971); (b) H. A. Wiebe and G. Paraskevopoulos, *ibid.*, **52**, 2165 (1974).
(19) P. Michaud and R. J. Cvetanović, *J. Phys. Chem.*, **76**, 1375 (1972).
(20) G. Paraskevopoulos and R. J. Cvetanović, *J. Chem. Phys.*, **50**, 590 (1969).
(21) C. L. Lin and W. B. DeMore, *J. Phys. Chem.*, **77**, 863 (1973).
(22) W. Forst, *J. Phys. Chem.*, **76**, 346 (1972).
(23) G. Z. Whitten and B. S. Rabinovitch, *J. Chem. Phys.*, **38**, 2466 (1963).
(24) W. Forst, *Chem. Rev.*, **71**, 339 (1971).
(25) (a) The following values of the heats of formation ($\Delta H_f°_{298.2K}$, kcal mol^{-1}) of the different species have been used: $O(^1D_2)$ 104.9,[26] c-C_4H_8 6.3,[27] c-C_4H_7 51.1,[28] c-C_4H_7OH −33.0 (estimated from (i) assuming D_{C-O} = 93.5 kcal mol^{-1} in c-C_4H_7OH and (ii) using group additivity rules[29]), OH 9.4.[26] (b) The required corrections ($H_T° - H_0°$) have been calculated from reported values.[26] The vibrational contribution to ($H_T° - H_0°$) in the case of c-C_4H_7OH was calculated by statistical mechanics methods[30] using the reported frequencies.[7]
(26) P. R. Stull and H. Prophet, *Nat. Stand. Ref. Data Ser., Natl. Bur. Stand.*, **No. 37** (1971).
(27) S. Kaarsemaker and J. C. Coops, *Recl. Trav. Chim., Pays-Bas*, **71**, 261 (1952).
(28) D. F. McMillen, D. M. Golden, and S. W. Benson, *Int. J. Chem. Kinet.*, **4**, 487 (1972).
(29) (a) S. W. Benson, "Thermochemical Kinetics", Wiley, New York, N.Y., 1968; (b) H. K. Eigenmann, D. M. Golden, and S. W. Benson, *J. Phys. Chem.*, **77**, 1687 (1973).
(30) (a) G. Janz, "Estimation of Thermodynamic Properties of Organic Compounds", Academic Press, New York, N.Y., 1958. (b) Tables of Einstein Functions, *Natl. Bur. Stand. Monog.*, **No. 49** (1962).
(31) H. E. O'Neal and S. W. Benson, *J. Phys. Chem.*, **72**, 1866 (1968).
(32) P. C. Beadle, D. M. Golden, K. D. King, and S. W. Benson, *J. Am. Chem. Soc.*, **94**, 2943 (1972).
(33) The "strong collision" assumption is frequently made in chemical activation studies and is probably reasonably valid for such a highly vibrationally excited molecule as the "hot" cyclobutanol in the present case. Similarly, neglect of anharmonicity is likely to be relatively unimportant for a molecule as complex as cyclobutanol.[4,24] There is greater uncertainty regarding the potential effect of excess kinetic energy of $O(^1D_2)$ atoms. The amount of excess kinetic energy possessed by the $O(^1D_2)$ atoms generated in the 213.9-nm photolysis of N_2O is not known. In principle it could vary from a theoretical maximum of about 30 kcal/mol, if the whole heat of reaction (48.6 kcal/mol) is converted into kinetic energy of N_2 and $O(^1D_2)$, down to close to zero, if the heat of reaction is equilibrated as vibrational and rotational energy of N_2O prior to its unimolecular decomposition. However, even if $O(^1D_2)$ atoms possessed some excess kinetic energy, it is uncertain whether it would in fact contribute substantially to the vibrational excitation of the cyclobutanol formed or would go preferentially into rotational excitation and affect relatively little the value of $k(E)$. Boxall, Simons, and Tasker[34] and Chamberlain and Simons[35] have found no contribution from an excess of kinetic energy of $O(^1D_2)$ atoms generated by photolysis of N_2O ($\lambda \geq 170$ nm) to the vibrational excitation of NO formed in their reaction with N_2O. Lack of appropriate curvature of the plot in the present Figure 1 for a variation of the SF_6/c-C_4H_8 ratio from 0 to 15 argues also against an important contribution of excess kinetic energy of $O(^1D_2)$.
(34) C. R. Boxall, J. P. Simons, and P. W. Tasker, *Discuss. Faraday Soc.*, **53**, 182 (1972).
(35) G. A. Chamberlain and J. P. Simons, *J. Chem. Soc., Faraday Trans. 2*, **71**, 402 (1975).

Absolute Rates of Oxygen(^{3}P) Atom Reactions with Benzene and Toluene[1a]

A. J. Colussi,[1b] D. L. Singleton,[1c] R. S. Irwin, and R. J. Cvetanović*

Division of Chemistry, National Research Council of Canada, Ottawa, Ontario, Canada K1A 0R9 *(Received February 25, 1975)*

Publication costs assisted by the National Research Council of Canada

The absolute values of the rate constants, k_2, of the bimolecular reactions of ground state oxygen atoms, O(^{3}P), with benzene and toluene have been determined by a phase-shift chemiluminescence technique using modulated mercury photosensitized decomposition of nitrous oxide to generate O(^{3}P). The rate constants determined over the temperature interval 298–462°K are given by the Arrhenius expressions k_2(benzene) = (1.09 ± 0.64) × 10^{10} exp(−4.20 ± 0.43 kcal mol^{-1}/RT) and k_2(toluene) = (2.30 ± 0.11) × 10^{10} exp(−3.86 ± 0.04 kcal mol^{-1}/RT) in units of M^{-1} sec^{-1}. The uncertainties in A and E correspond to 95% confidence limits.

Introduction

While extensive information on the mechanism and the rates of the reactions of the ground state oxygen atoms, O(^{3}P), with olefins is now available, the information on the corresponding reactions with aromatic compounds is still very limited. The mechanisms of the reactions with toluene and benzene have been studied previously in this laboratory but only relative reaction rates and activation energies, determined in competitive experiments with cyclopentene, could be obtained at that time.[2] Few absolute rate measurements have been reported for benzene[3-5] or for substituted benzenes.[4] The present work deals with the determination of the absolute values of the rate constants for benzene and toluene employing a modulation technique recently developed and used in this laboratory in similar studies with olefins.[6-9] While this work was in progress, an article by Atkinson and Pitts[10] reported the rate constants for the O(^{3}P) reactions with benzene and toluene at room temperature, also obtained by the modulation technique.

Experimental Section

The experimental arrangement and the general procedure have been described in previous publications,[6-8] and only the more important points will be mentioned here. The O(^{3}P) atoms were generated by the mercury photosensitized decomposition of N_2O using a sinusoidally modulated mercury lamp. The concentration of O(^{3}P) was monitored photometrically by measuring the NO_2 chemiluminescence from their reaction with the NO added to the reactant gas mixture. The phase shift between the incident 254-nm radiation and the NO_2 chemiluminescence was measured with photomultipliers and a lock-in amplifier. The phase shift, ϕ, is related to the chemical rate processes by[6]

$$\tan \phi = 2\pi\nu(k_2[\text{aromatic}] + k_3[\text{NO}][\text{M}])^{-1}$$

where ν is the modulation frequency and k_2 and k_3 are the rate constants for reactions 2 and 3 in the sequence

$$\text{Hg}(^1\text{S}_0) \xrightarrow{254\text{ nm}} \text{Hg}(^3\text{P}_1)$$

$$\text{Hg}(^3\text{P}_1) + \text{N}_2\text{O} \rightarrow \text{Hg}(^1\text{S}_0) + \text{N}_2 + \text{O}(^3\text{P}) \quad (1)$$

$$\text{O}(^3\text{P}) + \text{aromatic} \rightarrow \text{products} \quad (2)$$

$$\text{O}(^3\text{P}) + \text{NO} + \text{M} \rightarrow \text{NO}_2^* + \text{M} \quad (3)$$

$$\text{NO}_2^* \rightarrow \text{NO}_2 + h\nu$$

$$\text{NO}_2^* + \text{M} \rightarrow \text{NO}_2 + \text{M}$$

Flow rates of N_2O and NO were determined by calibrated flow meters. The aromatics were introduced into the flow system by bubbling various fractions of the N_2O flow through the aromatic at about 19°. The flow rates of the aromatics were determined in an initial series of experiments (series A) by condensing the flowing gas mixture for a known interval and measuring the aromatic manometrically after distilling off the more volatile N_2O and NO. In a second series of experiments (series B), carried out after a number of further improvements in the phase shift apparatus,[9] the concentrations of the aromatics were determined by observing their uv absorption in a 10.0-cm cell upstream from the reaction cell with a Beckman DU-2 spectrophotometer. Benzene was monitored at 247.1 nm, and toluene at 260.3 nm. The absorbance calibrations were done by expanding mixtures, accurately made with gas burets, of the aromatic and N_2O into the absorption cell. Since the apparatus used to prepare and transfer the calibration mixture was not completely grease-free, some of the aromatic could have been lost before reaching the absorption cell. To check this possibility, a grease-free gas handling system was incorporated around the absorption cell. Mixtures were made again with a gas buret. The two procedures gave the same calibration curve. The absorbance of both aromatics was independent of the N_2O partial pressures used in the kinetic experiments.

Flow rates of the aromatics were varied by at least a factor of 4 (except for toluene at 298°K where it was varied by a factor of 3). The flow rate of NO was varied by about a factor of 2, and the total pressure was varied between 40 and 70–80 Torr. In series A experiments, the rate of the 254-nm light absorption in the reaction cell was about 2 × 10^{14} quanta cm^{-3} sec^{-1}, as determined by the amount of nitrogen formed during the mercury sensitized decomposition of N_2O. In series B experiments, the rate was about 5 × 10^{12} quanta cm^{-3} sec^{-1}, as determined by gas chromatographic analysis of the reaction products of O(^{3}P) with butene-1. In series B, less than 0.01% of the aromatics was consumed by reaction with O(^{3}P).

The temperature of the reaction cell or gas mixture was measured with thermocouples. At 470°K the difference in the two temperatures was less than 4°.

Gas chromatographic analysis showed less than 0.01%

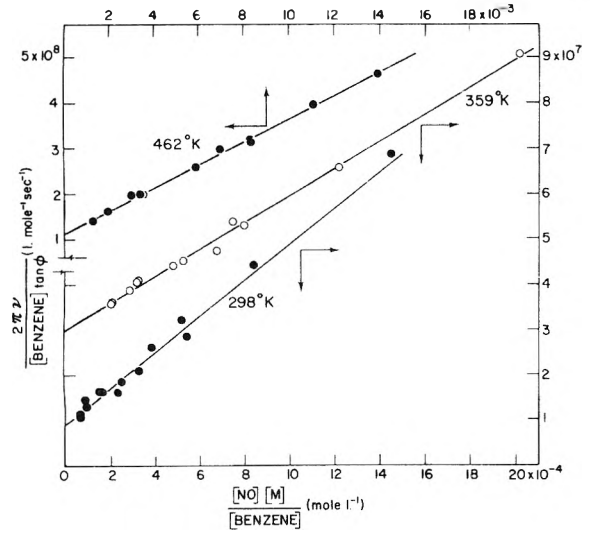

Figure 1. Plots of $2\pi\nu/[\text{benzene}]\tan\phi$ vs. $[NO][M]/[\text{benzene}]$ at three temperatures. (At 298°K 0.072 < [benzene] < 0.40, 0.013 < [NO] < 0.033, 1.5 < [N_2O] < 3.2, 700 < ν < 1250 Hz; at 359°K 0.040 < [benzene] < 0.34, 0.020 < [NO] < 0.031, 1.8 < [N_2O] < 3.1, 800 < ν < 1300 Hz; at 462°K 0.041 < [benzene] < 0.191, 0.10 < [NO] < 0.25, 1.3 < [N_2O] < 2.0, 2000 < ν < 5000 Hz. Units of concentration are m*M*.)

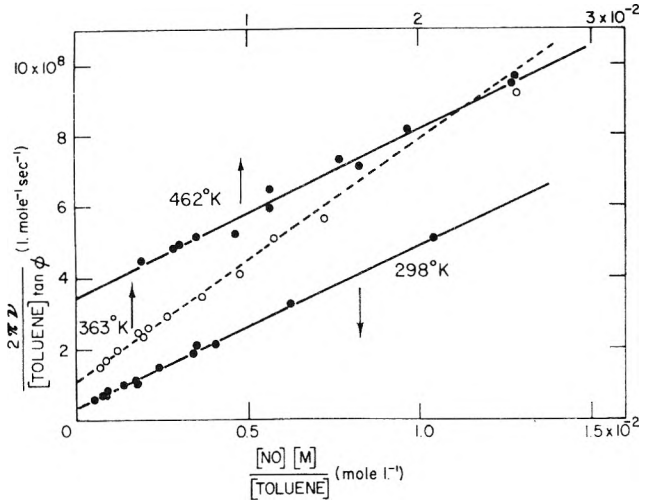

Figure 2. Plots of $2\pi\nu/[\text{toluene}]\tan\phi$ vs. $[NO][M]/[\text{toluene}]$ at three temperatures. (At 298°K 0.024 < [toluene] < 0.11, 0.013 < [NO] < 0.088, 2.0 < [N_2O] < 4.2, 800 < ν < 2000 Hz; at 363°K 0.013 < [toluene] < 0.089, 0.035 < [NO] < 0.17, 1.7 < [N_2O] < 3.5, 1250 < ν < 1400 Hz; at 462°K 0.012 < [toluene] < 0.071, 0.096 < [NO] < 0.28, 1.3 < [N_2O] < 2.5, 2000 < ν < 4000 Hz. Units of concentration are m*M*.)

toluene impurity in benzene, and less than 0.05% impurities in toluene.

Results

Rate constant measurements comprised two experimental series, extending over the temperature interval 298–498°K. The initial determinations (series A) were followed later by more accurate determinations (series B), carried out after further improvements were made in the phase shift apparatus, which substantially increased precision and accuracy of the measurements.[3] The flow rates of the aromatics were determined in the two series by different methods, as explained in the Experimental Section. Manometric measurements of the aromatics separated from other gases in the flow stream were used in series A, and continuous spectrophotometric measurements in series B. As a result of the improved experimental control and precision, series B determinations were feasible even at room temperature although the rate constants were much smaller. Thus, series B experiments covered much larger temperature intervals. Also they were carried out at substantially lower concentrations of O atoms, at which their secondary reactions with free radicals were very small or negligible. As a consequence, the random and the systematic errors of the results from the two series were quite different and therefore they could not be combined to obtain the best estimates of the Arrhenius parameters. For this purpose, the more accurate k_2 values from series B had to be used alone. Series A data do nevertheless provide relevant supporting information and will be discussed in the next section.

TABLE I: Rate Constants, k_2, of the Reactions of Ground State Oxygen Atoms with Benzene and Toluene

Aromatic	Temp, °K	$10^{-8}k_2$, M^{-1} sec^{-1}[a]	$10^{-10}k_3$, M^{-2} sec^{-1}[a]
		Series A	
Benzene	449	1.29 ± 0.05	2.30 ± 0.16
	473	1.83 ± 0.14	2.87 ± 0.38
	498	2.23 ± 0.08	2.66 ± 0.25
Toluene	373	1.54 ± 0.08	3.23 ± 0.21
	423	2.68 ± 0.11	3.43 ± 0.22
	473	4.73 ± 0.17	2.08 ± 0.17
		Series B	
Benzene	298	0.0930 ± 0.0045	3.96 ± 0.21
	359	0.300 ± 0.005	2.97 ± 0.10
	462	1.13 ± 0.03	2.56 ± 0.06
Toluene	298	0.342 ± 0.015	4.60 ± 0.09
	363	1.10 ± 0.04	3.40 ± 0.12
	462	3.45 ± 0.12	2.37 ± 0.10

[a] The indicated uncertainties are the least-squares estimates of the standard deviations.

The values of k_2 were obtained from the least-squares estimates of the intercepts of plots of $2\pi\nu/\tan\phi[\text{aromatic}]$ vs. $[NO][M]/[\text{aromatic}]$. The plots for series B determinations are shown in Figures 1 and 2, for the O(3P) reactions with benzene and toluene, respectively. The k_2 values for both series are listed in Table I, together with the corresponding k_3 values obtained from the slopes of the same plots. The uncertainties indicated in Table I are due to random errors only and are the least-squares estimates of standard deviations. The estimated overall uncertainty in $2\pi\nu/\tan\phi[\text{aromatic}]$ for the points in Figures 1 and 2 due to combined random and potential systematic errors in the phase shift, pressure, and spectrophotometric measurements was typically 10%. Series B k_3 values obtained for benzene are within 9–18% of the k_3 values determined[9] directly in separate experiments (in the absence of the aromatic), and those for toluene are within 5%. Quantitative aspects of k_3 and its temperature dependence will be discussed elsewhere.[9]

Least-squares treatment of series B k_2 values, with appropriate[11] statistical weights based on the indicated uncertainties, gives the following Arrhenius expressions: $k_2(\text{benzene}) = (1.09 \pm 0.64) \times 10^{10} \exp(-4.20 \pm 0.43 \text{ kcal mol}^{-1}/RT)$ and $k_2(\text{toluene}) = (2.30 \pm 0.11) \times 10^{10} \exp(-3.86 \pm 0.04 \text{ kcal mol}^{-1}/RT)$ in units of M^{-1} sec^{-1}.

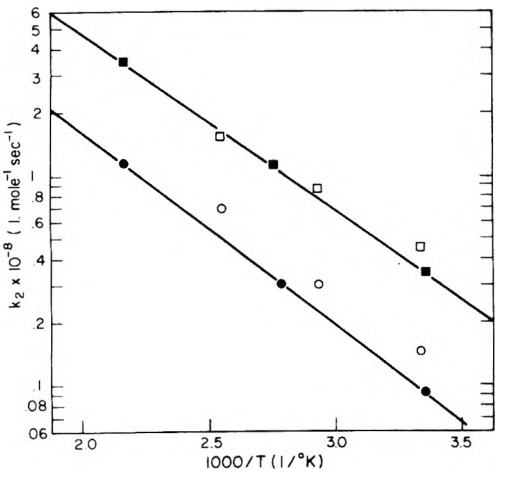

Figure 3. Arrhenius plots of the rate constants for the reaction of $O(^3P)$ with benzene (circles) and toluene (squares). (The filled symbols and the lines are this work, the open symbols are the results of Atkinson and Pitts.)[15]

The indicated uncertainties are 95% confidence limits (obtained by multiplying the standard deviations of the least-squares estimates of A and E by 12.706, i.e., by the value of Student's t distribution at the 95% confidence limit for one degree of freedom).

The Arrhenius plots are shown in Figure 3, with the solid lines corresponding to the mean A and E values in the above Arrhenius expressions.

Discussion

It is evident from Table I that the rate constants from the experimental series A are of similar magnitudes and show much the same trends with temperature as those from series B. In fact, the Arrhenius plots of the k_2 values from series A (not shown in Figure 3) are closely parallel to the series B plots, but series A lines for benzene and toluene are about 40 and 20%, respectively, higher (displaced to larger ordinate values) than the corresponding series B lines. These departures must be ascribed to systematic errors and would be consistent, for example, with systematic errors in the measured concentrations of the aromatics. Thus, if the aromatics were not completely recovered from the flow stream for the manometric determination of their concentration in series A, their concentrations would be underestimated and the calculated k_2 values would be too high. On the other hand, if in the calibration of the spectrophotometer used in series B some aromatic were lost (for example, in stopcock grease), the aromatic concentration would be overestimated and the calculated k_2 values would be too low. Corrections for either one or both of these effects would therefore tend to bring closer the results from the two experimental series.

As described earlier, the possibility of a systematic error in the calibration of the spectrophotometer used in series B was carefully checked and eliminated by employing a grease-free calibration procedure at the absorption cell itself. On the other hand, a quantitative recovery of the aromatic from NO and the huge excess of N_2O in the flow stream is difficult and it is therefore quite possible that the aromatic concentrations determined in series A by the manometric technique may have been somewhat underestimated. For this and other reasons mentioned in the preceding section and also discussed later in this article the less precise k_2 values from series A were not included with the series B values in the final least-squares evaluations of the Arrhenius expressions reported in this paper. However, even if the concentrations of the aromatics were underestimated in series A, the results obtained still provide upper limits of the absolute values of k_2 at higher temperatures and are useful as such, especially when it is desired to compare the divergent absolute values of k_2 reported in the literature.

The value of k_2 for benzene at 298°K is so small that relatively large benzene concentrations were required to give reasonable phase shifts. The benzene concentration was in this case as much as 26% of the N_2O concentration, which meant that benzene effectively competed with N_2O for $Hg(^3P_1)$ atoms. Using relative quenching rate constants[12] for benzene and N_2O of 2.7 to 1, it can be calculated that in the extreme case benzene quenched as much as 40% of the $Hg(^3P_1)$. Fortunately, the photosensitized chemical reaction of benzene involved in the $Hg(^3P_1)$ quenching process at the temperatures used in this work is essentially zero.[13] From the rate of the 254-nm light absorption and the residence time of benzene in the reaction cell, it was calculated that no more than 1×10^{-3}% of all the benzene molecules were excited as a result of quenching $Hg(^3P_1)$. Even if the rate constant for reaction of oxygen atoms with the excited benzene were as high as the collision frequency, about 1×10^{10} M^{-1} sec^{-1}, this reaction would account at most for only 1% of the total rate of reaction of oxygen atoms. Any competitive deactivation of the excited benzene by some alternative mechanism would further decrease this figure.

The present results can be compared with the previous relative determinations in this laboratory.[2] The ratio of the toluene to benzene rate constants derived from competitive experiments at 393°K is 2.7; at 493°K the ratio is 2.2. The corresponding ratios evaluated from the present Arrhenius expressions are 3.3 at 393°K and 3.0 at 493°K. The ratios from the competitive experiments are therefore about 25% smaller than those calculated from the present results. This difference, however, is not unreasonable. The competitive experiments were difficult for toluene and benzene because of the small rate constants for the aromatics compared to the rate constant for the competitive olefin, cyclopentene. Furthermore, the extent of secondary attack of oxygen atoms on the products of the initial reaction with the aromatics, although probably not too large, was not assessed in detail for the specific conditions used in the competitive experiments. In view of these factors, the agreement between the two sets of data can be considered quite reasonable.

The present results are compared in Table II with values found in the literature. The activation energy obtained for benzene by Timmons and his coworkers,[3] using discharge-flow techniques, is close to the present value, but the preexponential factor is three times larger than the present value. The room temperature rate constants reported by Mani and Sauer[4] for both aromatics are four times larger than the present values, but the ratio k_2(toluene)/k_2(benzene) is nearly the same. The experimental conditions in Mani and Sauer's experiments, however, were quite different. They determined by optical absorption the rate of formation of transient intermediates generated by the pulsed radiolysis of mixtures containing an aromatic, argon, and either CO_2 or N_2O at total pressures of 15 to 92 atm.

The results of Atkinson and Pitts[10,15] are compared with the present results in Table II and Figure 3. The values of

TABLE II: Arrhenius Parameters (E_2 and A_2) and the Absolute Values at 25° of the Rate Constants (k_2) for the Reactions of O(3P) Atoms with Benzene and Toluene

Reactant	$10^{-7}k_2$ (at 298 °K), M^{-1} sec^{-1}	E_2, kcal mol^{-1}	$10^{-10}A_2$, M^{-1} sec^{-1}
Benzene	0.930[a]	4.20[a]	1.09[a]
	1.44[b]	4.0[c]	1.11[d]
	2.8[e]	4.0[d]	3.8[e]
	3.6[f]	4.4[e]	1.7[g]
	0.63[g]	4.7[g]	
Toluene	3.42[a]	3.86[a]	2.30[a]
	4.50[b]	3.2[c]	0.82[d]
	14[f]	3.1[d]	

[a] Present values. [b] Atkinson and Pitts.[10] [c] Values calculated from competitive experiments[2] assuming zero activation energy for cyclopentene.[9,14] [d] Atkinson and Pitts.[15] [e] Bonanno et al.[3] (values were determined over the temperature range from 255 to 305°K). [f] Mani and Sauer.[4] [g] Avramenko et al.[5]

the Arrhenius parameters for benzene are in excellent agreement. However, the rate constants determined by Atkinson and Pitts are all larger than the present values, with the worst discrepancy, 55%, at room temperature. Atkinson and Pitts' values for the toluene rate constant at higher temperatures are in agreement with the present results, but their room temperature value is 30% larger, which makes their Arrhenius parameters lower. Since Atkinson and Pitts used the modulated chemiluminescence technique, better agreement might have been expected, especially since the technique yields very precise results. An examination of the experimental conditions reveals only one major difference between the present determinations and those of Atkinson and Pitts. The rate of 254-nm light absorption in the reaction cell was 2×10^{14} quanta cm^{-3} sec^{-1} in the latter (assuming full illumination of the reaction cell volume), and 5×10^{12} quanta cm^{-3} sec^{-1} in the present series B experiments. Thus the O(3P) production rate was about 40 times higher in Atkinson and Pitts' experiments. Mani and Sauer[4] reported an increase in k_2, at low benzene concentrations, as the intensity of the radiolytic pulse increased. Timmons and coworkers[3] observed a tenfold increase in k_2 when $[C_6H_6] \gg [O(^3P)]$ compared to the conditions when $[O(^3P)] \gg [C_6H_6]$. Both of these observations were interpreted in terms of a slow initial attack of O(3P) on benzene followed by rapid subsequent reactions of O(3P) with free radicals formed in the first step. Such an explanation may account for the differences between the present results and those of Atkinson and Pitts. As mentioned briefly before, it could also account for at least a part of the larger values obtained for k_2 for both benzene and toluene in the initial set of experiments (series A), carried out in this laboratory. The rate of the 254-nm light absorption in our series A experiments was about the same as in Atkinson and Pitts' experiments.

The potential importance of a consecutive attack by oxygen atoms on the primary reaction products can be estimated[8] by assuming that two free radicals are formed in the primary reaction and that two free radicals are also formed in the reaction of oxygen atoms with any free radical. The only net loss of free radicals is assumed to be by recombination. If the secondary oxygen atom reactions and the radical recombination reactions occur at nearly every collision, then it can be calculated[8] that between 0.5 and 3% of the oxygen atoms may have been consumed in secondary reactions in the present study, and 3–9% in Atkinson and Pitts' study. Thus the effect of secondary reactions may not have been entirely insignificant, although even this reaction mechanism, which probably exaggerates the loss of oxygen atoms, is not sufficient to reconcile completely the difference between the two sets of results. In this analysis, it was assumed that the rate of 254-nm light absorption was uniform throughout the illuminated volume of the reaction cell. However, the rate of light absorption, and hence the oxygen atom production rate, falls off exponentially along the length of the cell. The actinometry, of course, gives only the average rate of light absorption. In the volume near the front window of the cell, therefore, the estimated effect of secondary reactions would be larger.

For the two reactions studied, addition of the O(3P) atoms to the aromatic ring and an independent hydrogen abstraction have to be considered as the potential reaction channels. The rate constants measured in the present work are for the overall reaction, i.e. they include not only the addition of O(3P) atoms but also H atom abstraction if it occurs. However, the high value of the C–H bond dissociation energy in benzene would make direct H abstraction unlikely, in agreement with the apparent constancy of the activation energy over a wide temperature interval (255–498°K). The benzilic hydrogens in toluene, on the other hand, are much weaker and a contribution of some abstraction to the total rate cannot be ruled out. In both cases, however, the expected "abstraction" products (dibenzyl and diphenyl) were not detected at room temperature and an attack of the electrophilic O(3P) atoms on the aromatic ring appeared to be the main reaction channel.[2]

Acknowledgments. The authors are grateful to Dr. S. Furuyama for helpful discussions and to Drs. R. Atkinson and J. N. Pitts for a copy of their manuscript (ref 15) before publication.

References and Notes

(1) (a) Issued as NRCC No. 14836. (b) National Research Council of Canada visiting research officer, sponsored by Consejo Nacional de Investigaciones Cientificas y Tecnicas of Argentina. (c) National Research Council of Canada Postdoctorate Fellow (1972–1974).
(2) (a) G. Boocock and R. J. Cvetanović, *Can. J. Chem.*, **39**, 2436 (1961); (b) G. R. H. Jones and R. J. Cvetanović, *Can. J. Chem.*, **39**, 2444 (1961).
(3) R. A. Bonanno, P. Kim, J. H. Lee, and R. B. Timmons, *J. Chem. Phys.*, **57**, 1377 (1972).
(4) I. Mani and M. C. Sauer, Jr., *Adv. Chem. Ser.*, **No. 82**, 142 (1968).
(5) L. I. Avramenko, R. V. Kolesnikova, and G. I. Savinova, *Izv. Akad. Nauk. SSSR, Ser. Khim.*, 28 (1965).
(6) R. Atkinson and R. J. Cvetanović, *J. Chem. Phys.*, **55**, 659 (1971).
(7) R. Atkinson and R. J. Cvetanović, *J. Chem. Phys.*, **56**, 432 (1972).
(8) S. Furuyama, R. Atkinson, A. J. Colussi, and R. J. Cvetanović, *Int. J. Chem. Kinet.*, **6**, 741 (1974).
(9) D. L. Singleton, S. Furuyama, R. J. Cvetanović, and R. S. Irwin, *J. Chem. Phys.*, in press.
(10) R. Atkinson and J. N. Pitts, Jr., *J. Phys. Chem.*, **78**, 1780 (1974).
(11) R. J. Cvetanović, R. P. Overend, and G. Paraskevopoulos, *Int. J. Chem. Kinet.*, Supplement (Proceedings of the Symposium on Chemical Kinetics Data for the Lower and Upper Atmosphere), 1975.
(12) R. J. Cvetanović, *Prog. React. Kinet.*, **2**, 39 (1964).
(13) E. J. Y. Scott and E. W. R. Steacie, *Can. J. Chem.*, **29**, 233 (1951).
(14) R. J. Cvetanović, *Adv. Photochem.*, **1**, 115 (1963).
(15) R. Atkinson and J. N. Pitts, Jr., *J. Phys. Chem.*, **79**, 295 (1975).

Studies by the Electron Cyclotron Resonance Technique. X. Interactions of Thermal-Energy Electrons with Molecules of Chlorine, Hydrogen Chloride, and Methyl Chloride

A. A. Christodoulides, R. Schumacher, and R. N. Schindler*

Institut fur Chemie III der Kernforschungsanlage Julich GmbH, D-5170 Julich, German Federal Republic *(Received December 23, 1974; Revised Manuscript Received May 29, 1975)*

Publication costs assisted by Kernforschungsanlage Julich GmbH

Rates of electron disappearance in the presence of the molecules Cl_2, HCl, and CH_3Cl have been measured at room temperature. For Cl_2 and HCl these measurements were extended to 240° and the activation energies for the electron loss process are examined. The observed concentration dependence of the rate of electron loss for these molecules is discussed. Total scattering cross sections for HCl and CH_3Cl have been determined from changes in line width and line shape of the ECR signals.

I. Introduction

Data on the interactions of thermal electrons with the diatomic molecules Cl_2 and HCl, and the simple alkyl halide CH_3Cl, are very limited and considerable disagreement exists in their thermal capture rates.[1-8] The limited and inconsistent results are mainly due to their high chemical reactivity that causes experimental difficulties, and/or to their high polarity and low electron-capture efficiency. Little information is also available concerning the activation energies of the capture processes involved and the scattering cross sections at thermal energies.

In this study the ECR technique[9-12] has been applied in an effort to determine the thermal electron attachment rate constants, activation energies, and total scattering cross sections for the molecules Cl_2, HCl, and CH_3Cl. The observed variations in electron losses in the presence of a wide range of scavenger concentrations is discussed and related to diffusion effects. A brief description of the calculation of the capture rate constant, activation energy, and total scattering cross section is given.

II. Experimental Section

The experimental set-up for the ECR technique using Ar, He, or N_2 as a carrier gas has been previously described.[6,9-12] A quartz flow tube was designed which included five mixing chambers located at different distances from the resonance cavity. In this flow tube, the mixing chambers were surrounded by a second tube for temperature variations. Temperatures of up to 240° could be attained using an oil circulation system. With these modifications it was possible to obtain thermal electron attachment rates and activation energies from time, concentration, and temperature dependences in a much faster and more convenient way than previously.[6,9-12]

In the present work, Ar was normally used as both carrier gas and electron source.[12] In some cases, however, He or N_2 + CH_3NH_2 were used. Although in energy-dependence ECR studies it is important[12] to use He, in the present work this was not necessary since a constant low microwave power was employed throughout the experiments. The concentration of the scavengers studied is given in the text. It varied between 10^{-2} and 10^{-6} Torr. The pressure of the carrier gas was always in the range 4.5–5.5 Torr, unless a buffer gas, such as CO_2 or CH_4, was added in the flow stream. In this case $P_{total} = P_{carrier} + P_{buffer}$.

The CH_3Cl (99.9%) and Cl_2 (99.9%) gases were supplied by the J. T. Baker Co. and HCl (>99.8%) by the Messer-Griesheim Co. In our flow system with gas velocities between 40 and 50 m/sec, further purification was not necessary. A few experiments were carried out with CH_3Cl samples specially purified by use of preparative gas chromatography, as suggested elsewhere.[13] No changes in the scavenging properties were noticed.

III. Basis of Calculations

1. Electron Attachment Rate Constant k. The thermal rate constant k can be determined through the solution of the known electron-decay equation

$$d[e]/dt = -k[AB][e] = k'[e] \quad (1)$$

where [e] and [AB] are the electron and scavenger concentrations, respectively. The relation $k' \equiv k[AB]$ is valid in our experiments since [e] is $\sim 10^5$–10^6 electrons cm^{-3} and [AB] $\geq 10^{10}$ molecules cm^{-3}. From eq 1 we obtain

$$\ln([e_0]/[e_n]) = k[AB]t_n \quad (2)$$

where $[e_0]$ and $[e_n]$ are the electron concentrations without and with the scavenger AB, respectively. The scavenger was introduced from the nth mixing chamber (n = 1 to 5). In these experiments the reaction time t_n was varied from ~1.5 to ~7.5 msec.

The rate constant can be determined in two ways with the same experimental ECR set-up: (a) by varying t at constant [AB] and (b) by varying [AB] at constant t.

(a) From the proportionality[12] [e] $\propto h\Delta H_{pp}^2$, where h and ΔH_{pp} are the peak-to-peak height and line width of the ECR signal, eq 2 becomes

$$\ln(h_0/h_n) = I(\mu, [AB]) + k[AB]t_n \quad (3)$$

The slope of the plot ln (h_0/h_n) vs. t_n yields the experimental k_{expt}[AB] value. The intercept $I(\mu, [AB])$, which expresses the line width relationship with [AB] and the dipole moment μ of AB, does not alter the slope of eq 3, and hence the k value determination. Figure 1 shows such a plot of ln (h_0/h_n) as a function of t_n for different chlorine concentrations and with Ar as the carrier gas.

* Address correspondence to this author at the Universität Essen, Gesamthochschule, Fachbereich 6, West Germany.

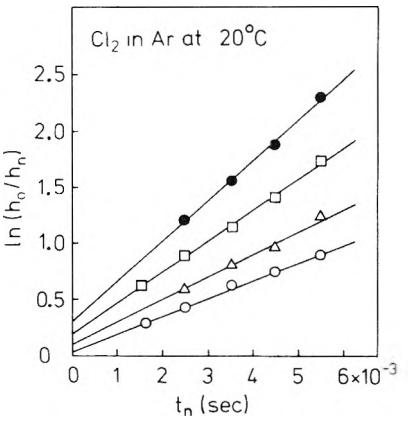

Figure 1. Time-dependence kinetic plots for the reaction of electrons with Cl_2 in Ar at various chlorine concentrations: (O) 1.6 × 10^{11}, (△) 3.0 × 10^{11}, (□) 6.2 × 10^{11}, and (●) 9.4 × 10^{11} cm^{-3}.

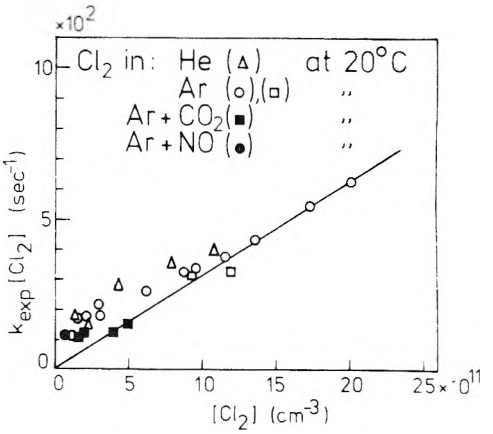

Figure 2. Concentration dependence of the electron loss frequency $k_{expt}[Cl_2]$ in He (△), Ar (O, □), Ar + CO_2 (■), and Ar + NO (●) at 20° from time-dependence measurements (see text).

(b) In calculating the k value from measurements at constant reaction time, the changes in line width upon concentration variation should be taken into account.[12] With $x = h\Delta H_{pp}^2$, eq 2 becomes

$$\ln (x_0/x_n) = kt_n[AB] \quad (4)$$

From the slope ln (x_0/x_n) vs. [AB] at constant t_n, the experimental $k_{expt}[AB]$ value can be obtained. Since the t_n is being kept constant, the index n has the meaning that anyone of the five (n = 1 to 5) inlet ports can be used for the measurements.

2. Activation Energy E_{act}. The activation energy for an electron attachment process can be defined as the energy required to thermally excite a neutral AB molecule from its ground state to a level in the vicinity of the crossing of the potential energy curves of the temporary negative ion and that for the neutral species. From the temperature dependence of the rate constant for thermal electron attachment to AB, the activation energy for this process can be determined using the Arrhenius expression

$$k = A \exp(-E_{act}/RT) \quad (5)$$

or, in practice, from the slope of an Arrhenius plot of ln k vs. $(1/T)$ when A is considered independent of temperature. Wentworth and his coworkers[4,14-16] have determined E_{act} for a large number of halogen containing compounds by applying eq 5 and using the pulse-sampling technique.

3. Total Scattering Cross Section $\langle\sigma_{sc}\rangle$. Total scattering cross sections for gas atoms or molecules in the pure form or in mixtures with a carrier gas can be determined from changes in line width and line shape of the ECR signals as a function of the gas pressure. This determination is based on the analysis[11,17] for the absorption of the microwave power by thermal electrons.

The relationship between the scattering cross section $\langle\sigma_{sc}\rangle$, the line width ΔH_{pp}, and the line shape of the ECR signal is given by the expression[11]

$$\langle\sigma_{sc}\rangle = \frac{e}{2m_e c}\left(\frac{m_e}{2kT}\right)^{1/2} K(n)\frac{\Delta H_{pp}}{[AB]} \quad (6)$$

where [AB] is the concentration of the gas atoms or molecules at a specified temperature T, and $K(n)$ is a conversion factor which considers the changes in line width and line shape and, thus, the energy dependence of the collision frequency ν_{col}.[11,17]

This method of determining $\langle\sigma_{sc}\rangle$ has several advantages when the molecule to be studied (i) is a very poor electron scavenger and (ii) has a large dipole moment. To investigate molecules with zero or very small dipole moment, their concentration has to be increased greatly. For this reason, only very poor electron scavengers can be studied by this analysis. Also, good scavengers but with large dipole moment can be investigated, because already small scavenger concentrations result in large line width and line shape changes, respectively. In ECR studies there are two methods of determining $\langle\sigma_{sc}\rangle$ for a gas atom or molecule AB mixed with a carrier gas, for example, Ar. (a) For a given Ar pressure, P_{Ar}, and by varying the pressure P_{AB} of AB, $\langle\sigma_{sc}\rangle$ can be determined from the slope of the plot ΔH_{pp} vs. [AB] and by using eq 6. The Ar contribution to the line width will show up as an intercept of this plot, but otherwise will not affect the slope. (b) For P_{Ar} = constant and P_{AB} = constant, the contribution from scattering by the carrier gas atoms has to be included. Then eq 6 is re-formed to

$$\langle\sigma_{sc}\rangle_{AB}[AB] + \langle\sigma_{sc}\rangle_{Ar}[Ar] = \frac{e}{2m_e c}\left(\frac{m_e}{2kT}\right)^{1/2} K(n)\Delta H_{pp} \quad (7)$$

This method should be used only when the product $\langle\sigma_{sc}\rangle_{AB}$ [AB] is larger than the product $\langle\sigma_{sc}\rangle_{Ar}$[Ar].

The first method is more accurate since no preconditions are required and it is not necessary that $\langle\sigma_{sc}\rangle$ of the carrier gas is known.

IV. Results and Discussion

A. Molecular Chlorine. 1. The k Value at 20°. In Figure 2 the observed variation in electron loss frequency $k_{expt}[Cl_2]$ as a function of Cl_2 concentration[40] in the range 1–20 × 10^{11} cm^{-3} is plotted. Each point given in the figure was determined from the time dependence of the electron loss process at constant scavenger concentration, as indicated in Figure 1, under the specified conditions. All measurements were carried out at 20°.

Two independent experimental set-ups were used to study the concentration dependence in Ar. One set-up included a quartz flow tube in a 9-in. magnet. In the second set-up a 12-in. system with another flow tube was employed. The results are shown in Figure 2 (points □, ■, and ● with the 9-in. magnet; points O with the 12-in. magnet). The electron loss in He was studied with the large magnet only (Figure 2, points △). In addition, a number of experi-

ments were performed in which the inert gas CO_2 was added to the carrier argon. Carbon dioxide was chosen as the additive because its electron attachment rate constant is $<10^{-16}$ cm^3 sec^{-1} [18] at room temperature and its elastic scattering cross section has a value of $\sim 300 \times 10^{-16}$ cm^2 [11,19,20] (points ■ for a partial CO_2 pressure of 0.8 Torr, Figure 2). From time-dependence measurements at $[Cl_2] = 1.0 \times 10^{11}$ cm^{-3} in Ar + NO, a k_{expt} value of 1.1×10^{-9} cm^3 sec^{-1} was obtained[21] (point ● in Figure 2).

For the three molecules described in this paper an unusual high degree of scatter in the experimental data was observed. Generally in ECR experiments scatter is around 5%. It has been noticed in a number of cases that large scatter can be connected to the occurrence of heterogeneous processes in addition to the homogeneous gas phase reaction. These heterogeneous contributions are occasionally difficult to control and show up as an increase in k_{expt} values at low scavenger concentrations.

At the surface of the flow tube wall there is a large number of adsorption sites for gas atoms or molecules. The carrier gases Ar and He are only weakly adsorbed at these sites because of their physical properties and their chemical inertness. However, molecules such as Cl_2 or HCl added to the gas flow will stick strongly to the wall from where they may act as capture centers. As the scavenger concentration is increased, the probability for reactions of the electrons with the scavenger molecules in the gas phase becomes predominant. The probability for the occurrence of heterogeneous process is independent of the scavenger concentration in the gas phase. Wall effects resulting in an increase of the electron attachment rate constant at low scavenger concentrations were observed by other workers[5,22] for CH_3Br, C_2H_5Br, and N_2O. Similar effects in a flow system were recently reported[23] to occur also in atom–molecule reactions.

If electron losses due to ambipolar diffusion and to heterogeneous reactions can be neglected, then the rate of the homogeneous attachment process follows a pseudo-first-order kinetics (eq 1) and can be derived from the slope of a straight line given by the experimental points at high scavenger concentrations and passing through the origin. From the slope in Figure 2 the rate constant for electron capture by Cl_2 in the gas phase is found to be $k = 3.1 \times 10^{-10}$ cm^3 sec^{-1}. In the absence of the buffer CO_2 a deviation from linearity at low Cl_2 concentrations is noticed. If extrapolated to $[Cl_2] = 0$, an intercept around 110 sec^{-1} is obtained.

A similar deviation at low scavenger concentrations was previously observed in a study by Biondi[24] on the dissociative attachment of electrons in iodine at room temperatures. Biondi[24] explained this deviation in terms of ambipolar diffusion and heterogeneous losses at the container walls. In an extension of this investigation[24] by Truby[25] at much higher iodine pressures, the effect of diffusion losses diminished. It is here assumed that also in the Cl_2 experiments, diffusion losses are responsible for the deviation at low Cl_2 concentrations. The rate of diffusion of electrons to the walls will depend mainly on the scattering cross sections of the gases in the flow tube. With CO_2 having a $\langle \sigma_{SC} \rangle$ value about 100 times larger than argon, the addition of 0.8 Torr of CO_2 to 4.5 Torr of argon considerably reduces the electron diffusion to the walls. Thus, even at $[Cl_2] \simeq 4$ to 5×10^{11} cm^{-3} in the presence of CO_2, the obtained data correspond to the homogeneous capture process (Figure 2).

It is of interest to point out that the buffer gas added can only be effective if the rate of the homogeneous process competes with the rate of the diffusive losses. With a limiting rate constant for the capture process of $k = 3.1 \times 10^{-10}$ cm^3 sec^{-1}, the Cl_2 concentration for which the frequency of attachment $\nu = k[Cl_2]$ for the homogeneous process becomes comparable to that for the combined diffusion losses may be estimated. With $\nu_{extr} \simeq 110$ sec^{-1} obtained under our experimental conditions, the effectiveness of the additive should start to diminish at $[Cl_2] \leq 3.5 \times 10^{11}$ cm^{-3}. Additional information on this point will be presented in the results obtained with HCl.

The mechanisms of the heterogeneous electron loss processes are complicated and difficult to deduce from these studies. For a particular flow tube, the degree of this electron loss depends on a number of factors, such as, the pressure and nature of the carrier gas, the concentration, size, polarity, and efficiency of the scavenger molecule, etc.

From mass-spectrometric studies the Cl^- resonance capture peak was observed[26] to have an onset energy at ~1.6 eV and a peak maximum at ~2.4 eV. This maximum is experimentally not accessible with the ECR technique since only capture processes occuring at electron energies ≤0.4 eV can be studied.[12] It is most probable that in the mass-spectrometric studies[26] the Cl^- ions are being produced by transitions to the highly repulsive excited Cl_2^- ($^2\Pi_g$) state[27] in a dissociative electron attachment process

$$e + Cl_2 \rightarrow Cl_2^{-*}(^2\Pi_g) \rightarrow Cl + Cl^- \qquad (8)$$

Since this process has a minimum threshold energy of 1.6 eV, Cl_2 should not be an efficient scavenger for thermal electrons. From the thermal rate constant, however, of 3.1×10^{-10} cm^3 sec^{-1} found in this work it cannot be regarded as a slow reaction. Thus, a process other than (8) should be responsible for the fast reaction at thermal energies observed in the present experiments.

From energy-dependence ECR studies of Cl_2 in Ar or He, an attachment process with a broad maximum at ~0.25 eV was found.[21] A scattering process[21] responsible for this peak can be ruled out since Cl_2 is a diatomic molecule with no dipole moment. Considering the small activation energy (see later discussion, this section) of ~0.05 eV and the potential energy diagram[21,27] for a number of negative ion states of Cl_2, the observed thermal process should be assigned to a thermal electron attachment process leading to a vibrationally excited negative parent ion Cl_2^{-*} in its electronic ground state $^2\Sigma_u^+$, i.e.

$$e_{th} + Cl_2 \rightarrow Cl_2^{-*}(^2\Sigma_u^+) \qquad (9)$$

The binding energy of Cl_2 is $D(Cl_2) = 2.514$ eV[28] and the electron affinity of the chlorine atom is EA(Cl) = 3.613 eV.[29] Thus, the dissociation asymptote of Cl_2^{-*} ($^2\Sigma_u^+$) lies ~1.1 eV below the ground state of the neutral molecule. Collisional electron detachment from the state $^2\Sigma_u^+$ can be ruled out on the above energetic grounds. Dissociation leading to Cl + Cl^- is likely to follow the formation of the intermediate temporary negative Cl_2^{-*} ion with possible stabilization of Cl_2^- at high pressures.

2. *Activation Energy.* Measurements of the rate constants for electron attachment to Cl_2 were carried out in the temperature range between 20 and 240°. The Cl_2 concentration was varied from 6×10^{10} to 2×10^{12} cm^{-3}. At higher than room temperatures, the $k_{expt}[Cl_2]$ values were found to increase linearly with $[Cl_2]$, and to pass through zero. This indicates that the wall effects observed at room temperature (Figure 2) at low $[Cl_2]$ were eliminated or at least became insignificant at higher temperatures.

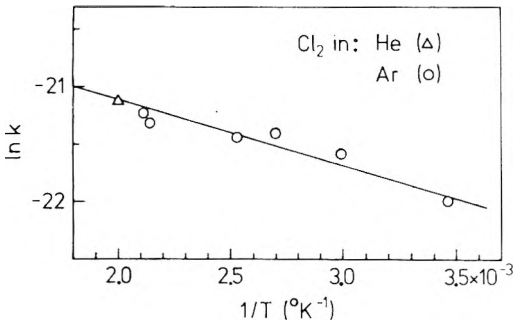

Figure 3. Arrhenius plot of the temperature-dependence of the rate constant for the electron attachment to Cl_2 in Ar (O) and in He (Δ).

In Figure 3 the Arrhenius plot of ln k vs. $(1/T)$ gave an approximate straight line. From the slope of this line, a small activation energy of 0.05 eV (1.16 kcal/mol) was obtained. The magnitude of this energy is in accord with the potential energy diagram for Cl_2 and Cl_2^- given by Gilbert and Wahl[27] and the energy dependence[21] of the electron capture process by Cl_2. The activation energy for the dissociative process leading to the excited Cl_2^- ($^2\Pi_g$) state is about 0.8 eV. Thus, in the present work, electron capture takes place in a transition from the ground state of the neutral molecule to the Cl_2^- ($^2\Sigma_u^+$) state, with subsequent dissociation of the vibrationally excited negative ion.

3. Total Scattering Cross Section. It was not possible to determine $\langle\sigma_{sc}\rangle$ for Cl_2 by the ECR technique since Cl_2 is a rather efficient electron scavenger and has no dipole moment (see section III).

B. Hydrogen Chloride. 1. The k Value at 20°. A large number of time-dependence measurements were carried out at various HCl concentrations for the determination of the rate of electron dissappearance in the presence of HCl at room temperature. If the experimental data for HCl were plotted in a similar way as for Cl_2 (see Figure 4a), only for the measurements in the large flow tube an increase in k_{expt}[HCl] values at [HCl] $\gtrsim 9 \times 10^{14}$ cm^{-3} becomes apparent. From the slope of this portion of the curve passing through the origin an upper k_{expt} value of 2×10^{-13} cm^3 sec^{-1} for the gas phase reaction can be estimated. All other points scatter strongly around 120 sec^{-1} in the [HCl] range 10^{11}–10^{14} cm^{-3}.

To illustrate the continuous decrease of the k_{expt} values with increasing [HCl] and the observation of the strong curvature toward a limiting value of $\sim 2 \times 10^{-13}$ cm^3 sec^{-1}, all data taken in different ECR studies are also plotted in Figure 4b. A log–log presentation had to be used in order to accommodate the large variation of [HCl] and k_{expt} values. Each point given in Figure 4 was again determined from the time dependence of the electron loss process at a constant HCl concentration under the specified conditions. All measurements were obtained at 20°.

In our efforts to obtain an absolute rate constant for the homogeneous gas phase capture process, different experimental methods were employed. With Ar as carrier gas, the k_{expt} value dropped from 3×10^{-10} cm^3 sec^{-1} at [HCl] = 3×10^{11} cm^{-3} to $\sim 5 \times 10^{-12}$ cm^3 sec^{-1} at $\sim 7 \times 10^{13}$ cm^{-3} (Figure 4b, points O). No change resulted in the behavior of the k_{expt} values with [HCl] when different CO_2 concentrations were introduced in the Ar flow stream after Ar has passed the discharge region. The points ●, ▲, and ■, which correspond to pressures P_{CO_2} = 0.35, 0.76, and 1.9 Torr, respectively, seem to lie on or scattered around an imaginary

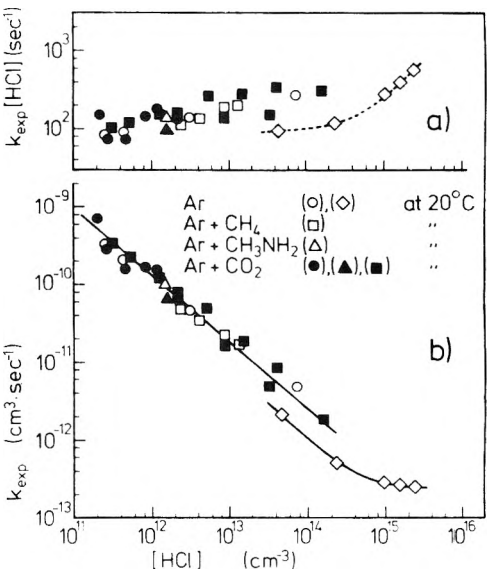

Figure 4. Concentration dependence of (a) the electron loss frequency k_{expt}[HCl] and (b) the rate of electron disappearance in the presence of HCl in Ar (O, ◇), Ar + CH_4 (□), Ar + CH_3NH_2 (Δ), and Ar + CO_2 (●, ▲, ■) at 20° from time-dependence measurements. The points ●, ▲, and ■ correspond to pressures P_{CO_2} = 0.35, 0.76, and 1.9 Torr, respectively.

line (Figure 4b). Also in measurements with CH_4 added (points □) a similar behavior was observed. In an earlier study[6] of HCl in Ar with CH_3NH_2 as the electron donor being photoionized with a Kr resonance lamp, a k_{expt} value of 1×10^{-10} cm^3 sec^{-1} was found. For the HCl concentration used[6] (1.5×10^{12} cm^{-3}) this k_{expt} value lies also on the imaginary line in Figure 4b (point Δ). The data obtained in experiments with the flow tube having a diameter a factor of 3 larger than all the others used in this work and in the past[6,9-12] are also shown in Figure 4 (points ◇). The deviation from linearity in Figure 4b at [HCl] $> 5 \times 10^{14}$ cm^{-3} might suggest that k_{expt} tends toward a plateau, with an upper limit of $k_{expt} \sim 2 \times 10^{-13}$ cm^3 sec^{-1}.

At the present time we do not offer conclusive explanations for the continuous decrease of the k_{expt} value from 10^{-9} cm^3 sec^{-1} at [HCl] = 10^{11} cm^{-3} to 10^{-13} cm^3 sec^{-1} at $>10^{15}$ cm^{-3} (Figure 4b). Some remarks, however, shall be given.

(a) Hydrogen halides, particularly HCl, are well known for their high surface activity. The adsorption of HCl at the surface of the enclosure walls causes many problems in the study of this molecule, particularly in static systems. Drastic pressure changes with time, due to adsorption to the walls, were found in earlier investigations. Barton[30] reported that most of the initially introduced HCl was adsorbed at the walls of the vacuum system. In electron beam experiments with HCl a shift in the electron energy scale, indicating a change in the surface potentials, was attributed by Fox[31] as being possibly due to surface reactions with the HCl molecules. It was found[31] necessary to stream the HCl gas through the system for about 1 hr before reproducible data could be taken. A marked decrease in pressure of HCl, HBr, and HI amounting usually from 20 up to 50% was observed in an electron-swarm study[3,32] due to the surface adsorption effect of these halides.

In our experiments a constant flow of HCl is introduced into the system from a reservoir and is pumped through the quartz tube together with the carrier gas and the additives,

if present. Thus, in contrast to static experiments, the concentration of HCl introduced into the flow tube will be identical with the concentration in the gas phase, provided stationary conditions are reached. For the higher [HCl] values stationary conditions were reached within one ECR sweep.

(b) No constancy in k value could be reached up to at least [HCl] $\simeq 10^{15}$ cm^{-3}. Also, no apparent influence from the addition of the buffer gases CO_2 and CH_4 was noticed. Hydrogen chloride is a poor electron scavenger in the gas phase. Thus the electron losses via diffusion to the walls will still dominate relative to losses due to the gas phase attachment process, at much higher HCl concentrations as compared with Cl_2. The observation that the buffer gases added showed no influence on the rate of electron disappearance serves as an additional indication of the low capture efficiency of HCl in the gas phase. As mentioned in the case of Cl_2, the effectiveness of the additives can only show up at scavenger concentrations where the electron losses due to capture in the gas phase start to compete with the rate of diffusive losses. Although there is very high scatter in the experimental k_{expt}[HCl] data where the diffusive losses prevail, the extrapolation to [HCl] = 0 yields a frequency for the electron loss of $\nu_{extr} \simeq 120$ sec^{-1}. With $k_{expt} = 2 \times 10^{-13}$ cm^3 sec^{-1}, the limiting HCl concentration for this competition is found to be $\sim 6 \times 10^{14}$ cm^{-3}. Unfortunately no experiments with buffer gases were carried out at such high [HCl] in the 2.2-cm flow tube.

Due to electron diffusion losses not corrected for in the pure gas, an upper limit of $<3.1 \times 10^{-12}$ cm^3 sec^{-1} for the thermal rate constant for HCl was also reported[7] recently. The drift–dwell–drift technique was employed[7] and N_2 was used as the carrier gas. In the early work of Bradbury,[1] a very small electron attachment to HCl in mixture with Ar was observed at very low energies, with the probability of attachment increasing rapidly from 10^2 at thermal energy to its maximum value of $\sim 5 \times 10^3$ at higher energies. A different behavior was reported[3] in an electron-swarm study of HCl mixed with the carrier gas N_2. In addition to the dissociative electron attachment with $k \simeq 2.2 \times 10^{-10}$ cm^3 sec^{-1} at higher energies ($\sim$0.8 eV),[3] another separate electron attachment process was observed[3] at lower energies with the rate constant increasing sharply with decreasing electron energy and reaching a k value of 4.3×10^{-10} cm^3 sec^{-1} at thermal energy (0.04 eV). This thermal k value is three and two orders of magnitude larger than the upper limit found in this study and in another work,[7] respectively. At this moment it is not clear as to the cause of these discrepancies in the thermal k value. It is possible that, in addition to the electron capture by HCl in the gas volume, an electron diffusion to the adsorbed HCl molecules at the walls of the collision chamber occurred. The electron loss by diffusion would be expected to become increasingly larger as the "pressure reduced electric field" (E/P) becomes smaller, thus giving an apparent very large attachment rate at thermal energies.

2. Activation Energy. In Figure 5 the k_{expt} values for HCl were plotted as a function of [HCl] at various temperatures, up to 235°. As in the case of the measurements at room temperatures (Figure 4b), the k_{expt} values showed a large decrease with increasing [HCl], ranging from $k_{expt} \simeq 8 \times 10^{-10}$ cm^3 sec^{-1} at [HCl] $\simeq 1 \times 10^{11}$ cm^{-3} to $k_{expt} \simeq 3 \times 10^{-13}$ cm^3 sec^{-1} at [HCl] $\simeq 5 \times 10^{14}$ cm^{-3}. A strong curvature, however, toward stabilization of the k_{expt} value was observed above 10^{13} cm^{-3} (Figure 5). This curvature was also seen for about the same [HCl] region at room temperature, but with the larger flow tube. The points △ and ◇ in Figure 5 correspond to measurements with the carrier gases Ar at 137° and He, respectively. Addition of CO_2 in the flow stream did not alter the k values. The points ▲, ■, and ● correspond, respectively, to measurements with Ar + CO_2 at 137°, 196°, and various other temperatures shown in Figure 5.

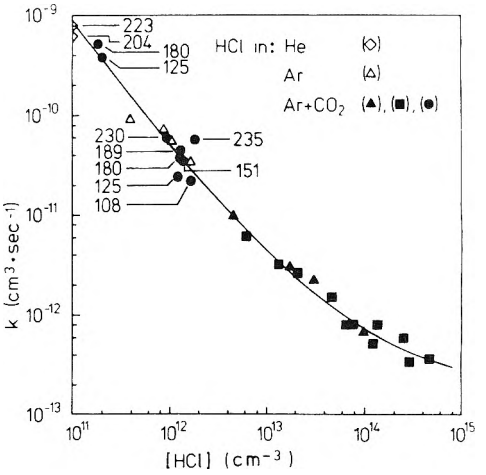

Figure 5. Concentration dependence of the rate of electron disappearance in the presence of HCl in He (◇), Ar (△), and Ar + CO_2 (▲, ■, ●) at various temperatures from time-dependence measurements. The points ▲ and ■ correspond to the temperatures 137 and 196°, respectively.

For the determination of the activation energy for the electron attachment process, it is required to work under conditions where diffusive losses become insignificant and only the homogeneous gas-phase process is present. Unfortunately these conditions could not be fulfilled in the present experiments, even at the highest [HCl] used and thus no activation energy can be given.

3. Total Scattering Cross Section. In Figure 6 the peak-to-peak line width ΔH_{pp} was plotted as a function of HCl concentration with Ar as the carrier gas at $P_{Ar} = 3.6$ Torr and $T = 20°$. The small intercept of 10 G at zero [HCl] was due to Ar scattering at the above pressure.

From the analysis[6,11] of the line widths and line shapes of the ECR signals, the exponent n was found to be about zero for the highest [HCl] used. For $n = 0$, $K(n)$ takes the value of 1.73.[6,11,17] From the slope ΔH_{pp}/[HCl] (Figure 6) and by applying eq 6, the total scattering cross section for HCl was found as $\sim$1260 Å^2. Use of eq 7, by considering the highest [HCl] and $\langle\sigma_{sc}\rangle_{Ar} = 2.8$ Å^2,[12] yielded $\langle\sigma_{sc}\rangle_{HCl} = 1230$ Å^2. These two σ values for HCl are in good agreement.

HCl is a polar molecule with an electric dipole moment $\mu = 1.08$ D[33] which is below the minimum dipole moment $\mu_{min} = 1.63$ D required to bind an electron[20,34,35] temporarily to the ground state of a stationary electric dipole. The obtained value of $\langle\sigma_{sc}\rangle_{HCl} = 1260$ Å^2 is higher than the theoretical value of Altshuler[36] who considered the point-dipole Born approximation in his calculations. This is in agreement with the findings for 21 polar molecules with $\mu < 2.4$ D studied[20,33] by the electron-swarm technique, in that, the scattering cross sections were higher than those predicted by theory.[36]

C. Methyl Chloride. 1. The k Value at 20°. As in the case of HCl, the observed rate of electron loss in the presence of CH_3Cl at 20° decreased with increasing [CH_3Cl]. Figure 7 shows this behavior. The k_{expt} value drops from 6×10^{-13}

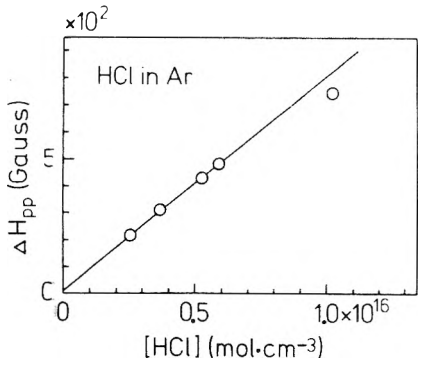

Figure 6. Concentration dependence of the ECR peak-to-peak line width ΔH_{pp} of HCl in Ar gas.

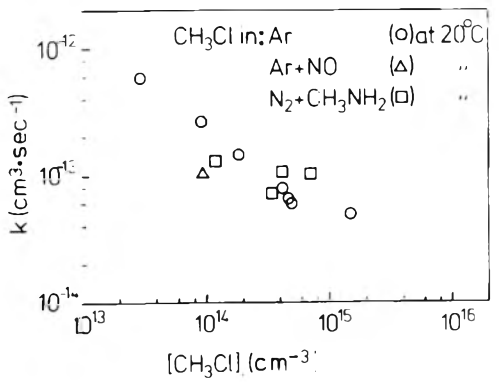

Figure 7. Concentration dependence of the rate of electron disappearance in the presence of CH_3Cl in Ar (O), Ar + NO (Δ), and N_2 + CH_3NH_2 (□) at 20° from time-dependence measurements.

$cm^3\ sec^{-1}$ at $[CH_3Cl] \simeq 3 \times 10^{13}\ cm^{-3}$ to $5 \times 10^{-14}\ cm^3\ sec^{-1}$ at $[CH_3Cl] \simeq 1.5 \times 10^{15}\ cm^{-3}$. The points O and □ in Figure 7 correspond to measurements of CH_3Cl in the carrier gases Ar and N_2, respectively. In the latter case, CH_3NH_2 was used as the electron donor being photoionized with a Kr resonance lamp. The lowest rate was measured in an experiment in the presence of CO_2. At $P_{Ar} = 5$ Torr, $P_{CO_2} = 1.4$ Torr, and $[CH_3Cl] = 5.3 \times 10^{15}\ cm^{-3}$ ($\simeq$0.16 Torr) the determined k_{expt} value was $\sim 5 \times 10^{-15}\ cm^3\ sec^{-1}$.

Considerable disagreement exists in the literature on the rate constant for electron capture by CH_3Cl. The highest value of $6.1 \times 10^{-12}\ cm^3\ sec^{-1}$ was calculated[3] from reported[2] electron swarm measurements. Lee's[2] thermal k values, however, except for the very strong electron scavengers, are generally much higher than other values existing in the literature. For example, the thermal k values for $CClF_3$ and CHF_3 from Lee's[2] results are, respectively, four and five orders of magnitude larger than recently reported data.[7,13,37] Probably an impurity of a very effective electron scavenger caused these large discrepancies in Lee's[2] work. Only an upper limit of $<1 \times 10^{-13}\ cm^3\ sec^{-1}$ could be measured[6] following the time dependence by the ECR technique with Ar as carrier gas and NO as electron donor using photoionization. From microwave conductivity measurements an upper limit of $<1.9 \times 10^{-15}\ cm^3\ sec^{-1}$ was obtained[5] in a pressure range of 9–50 Torr of CH_3Cl without any carrier gas. The temperature dependence for electron capture processes by CH_3Cl was studied[4] by the pulse-sampling method. Because this technique does not give directly absolute k values, we have related the electron capture coefficients K of SF_6[38] and CH_3Cl,[4] as well as the thermal electron attachment rate of SF_6 ($k_1 = 2.41 \times 10^{-7}\ cm^3\ sec^{-1}$)[38] in order to obtain the absolute k value for CH_3Cl. Extrapolation at 20° of the plot $\ln (KT^{3/2})$ vs. $(1/T)$ for the dissociative mechanism[4] gave a k value of $7.0 \times 10^{-16}\ cm^3\ sec^{-1}$. By considering the plateau[4] at the temperature region 60–120°, a k value of $8.5 \times 10^{-14}\ cm^3\ sec^{-1}$ was obtained for an undetermined capture process. From a competitive electron scavenging study[8] of N_2O with SF_6 and CH_3Cl in liquid neopentane, the scavenging efficiency of CH_3Cl was $\sim$0 as compared with that for SF_6 of $\sim$30. This comparison, however, gives only indications that CH_3Cl is a very poor electron scavenger, even in a nonpolar liquid.

A summary of the presented data for CH_3Cl is given in Table I. Although a definite rate constant for the thermal electron capture by CH_3Cl is difficult to obtain, the lower k values of $\lesssim 10^{-15}\ cm^3\ sec^{-1}$ are preferred.

Apparently all experimental data presented in Figure 7 were obtained under conditions where diffusive electron losses predominate. Again, a large scatter in the k_{expt} values determined from the time dependences is noticed. There is no indication for contributions from the attachment process in the gas phase up to $[CH_3Cl] = 2 \times 10^{15}\ cm^{-3}$ (0.06 Torr). It is of interest to make an estimate on the minimum methyl chloride pressure needed in the 2.2-cm flow tube in order to see the homogeneous process, assuming the rate constant for electron capture by CH_3Cl to be $\sim 5 \times 10^{-15}\ cm^{-3}\ sec^{-1}$. With the average electron loss frequency of $\nu_{extr} \simeq 50\ sec^{-1}$, obtained in these experiments, the estimate yields $[CH_3Cl] \gtrsim 1 \times 10^{16}\ cm^{-3}$ ($\simeq$0.3 Torr). However, if CH_3Cl is present in the ECR experiment at concentrations $\gtrsim 10^{16}\ cm^{-3}$, the resonance signal is strongly broadened and distorted due to the high scattering cross section of this molecule toward thermal electron energies.

2. Activation Energy. It was not possible to determine the activation energy for the thermal electron capture process by CH_3Cl. This was due to the fact that a plateau of the k_{expt} vs. $[CH_3Cl]$ plot could not be reached. The only known value of E_{act} for the dissociative attachment process was determined by the pulse-sampling method and was found as 12.5 kcal/mol.[4]

3. Total Scattering Cross Section. In the determination of $\langle \sigma_{sc} \rangle$ for CH_3Cl with N_2 as the carrier gas, eq 7 was applied. A nitrogen pressure of 3.8 Torr was used and a cross section $\langle \sigma_{sc} \rangle$ for nitrogen of 3.8 Å^2 was considered.[12] With these values the calculated total scattering cross section for CH_3Cl was found to be 1790 Å^2, using the value of -0.4 for the exponent n in eq 7.[6,11] This cross section is in good agreement with the momentum transfer cross section of 1838 Å^2 obtained[20] by the electron-swarm technique.

The dipole moment of CH_3Cl is reported to be 1.87 D,[20,33] which is just above the critical dipole moment $\mu_{min} = 1.63$ D.[24,34,35] As in the case for HCl, $\langle \sigma_{sc} \rangle$ for CH_3Cl lies above the value given by the Born approximation.[36] It was found experimentally[20] that generally the scattering cross sections for molecules with dipole moments at and around μ_{min} were higher than the predicted[36] ones while with $\mu \geq 2.4$ D the σ values were lower. Christophorou and Christodoulides[20] suggested that this deviation from the theoretical behavior could be attributed to a resonance-type contribution to the cross section, as predicted by the treatment of Takayanagi and Itikawa.[39]

The collision frequency ν_{col} is proportional[11] to the electron energy $u = (mv^2/2)$ raised to the power n, i.e.

TABLE I: Rate Constants k for the Capture of Thermal Electrons by CH_3Cl at 20°

k_{th}, cm^3 sec^{-1}	$[CH_3Cl]$, cm^{-3}	Carrier gas	Method	Ref
6.1×10^{-11}		N_2	Electron swarm	2
$<1 \times 10^{-13}$ [a]	9.3×10^{13}	Ar + NO	ECR	6
$<5 \times 10^{-14}$ [a]	1.5×10^{15}	Ar	ECR	This work
$<5 \times 10^{-15}$ [a]	5.3×10^{15}	Ar + CO_2	ECR	This work
$<1.9 \times 10^{-15}$	2.9×10^{17} to 1.6×10^{18}	None	Microwave	5
8.5×10^{-14} [b]		90% Ar + 10% CH_4	Pulse sampling	4
7.0×10^{-16} [c]		90% Ar + 10% CH_4	Pulse sampling	4

[a] The values given are k_{expt} (see text). [b] Determined from plateau of ln $(KT^{3/2})$ vs. $(1/T)$ plot (Figure 1, ref 4), using a value of $k_{th} = 2.41 \times 10^{-7}$ cm^3 sec^{-1} for SF_6.[38] [c] Determined from extrapolation of ln $(KT^{3/2})$ vs. $(1/T)$ plot (Figure 1, ref 4) at 20°, using the same k_{th} of SF_6 as in 6.

$$\nu_{col} \propto u^n \tag{10}$$

The relationship between the total scattering cross section σ_{sc}, the electron velocity v, and ν_{col} is given by

$$\sigma_{sc} = \nu_{col}/Nv \tag{11}$$

From eq 10 and 11, the velocity dependence of σ_{sc} could be obtained through the proportionality

$$\sigma_{sc} \propto 1/v^{(1-2n)} \tag{12}$$

In the case of CH_3Cl, $n = -0.4$, so that $\sigma_{sc} \propto v^{-1.8}$. This is very close to the expected theoretical proportionality $\sigma_{sc} \propto v^{-2}$ for high polar molecules.

IV. Conclusion

The total scattering cross sections for HCl and CH_3Cl were found to be 1260 and 1790 Å^2, respectively. Both values were higher than the theoretical ones based[36] on the point-dipole Born approximation, in agreement with a similar behavior for a large number of polar molecules[24,34] with $\mu < 2.4$ D.

The thermal capture process in Cl_2 can be assigned to electron attachment to form the negative ion Cl_2^{-*} in the state $^2\Sigma_u^+$. It proceeds with a rate constant $k = 3.1 \times 10^{-10}$ cm^3 sec^{-1} and has an activation energy of 0.05 eV. An approximate limiting k_{expt} value of 2×10^{-13} cm^3 sec^{-1} was obtained for HCl at $[HCl] > 10^{15}$ cm^{-3}, when it was assumed that at these concentrations a plateau region was approached. Only an upper limit of $<5 \times 10^{-15}$ cm^3 sec^{-1} at $[CH_3Cl] \simeq 5 \times 10^{15}$ cm^{-3} could be obtained for CH_3Cl in Ar + CO_2.

There exists competition between electron losses due to the homogeneous capture in the gas phase and losses due to heterogeneous processes at the walls. In general, for effective electron scavengers the wall effects are insignificant and can be neglected. For poor scavengers, however, their concentration has to be large in order to supress the wall effects. This competition is clearly shown for Cl_2 in the absence of the buffer CO_2. At $[Cl_2] > 10^{12}$ cm^{-3} the homogeneous process is observed, whereas at lower $[Cl_2]$ contributions from diffusive losses become dominant. In the case of HCl this competition is only indicated in the results using the 6.5-cm flow tube. It was not observable for CH_3Cl under the present experimental conditions in the absence of CO_2.

The results reported demonstrate how processes other than the homogeneous reaction to be investigated can dominate the kinetic behavior of the system. Thus, electron capture by inefficient scavengers might become fully overshadowed.

Acknowledgments. We wish to thank Dr. E.-P. Röth from our Institute for many helpful discussions. The financial support of one of us (A.A.C.) by the Deutsche Forschungsgemeinschaft is gratefully acknowledged.

References and Notes

(1) N. E. Bradbury, *J. Chem. Phys.*, **2**, 827 (1934).
(2) G. T. Lee, *J. Phys. Chem.*, **67**, 360 (1963).
(3) L. G. Christophorou, R. N. Compton, and H. W. Dickson, *J. Chem. Phys.*, **48**, 1949 (1968).
(4) W. E. Wentworth, R. George, and H. Keith, *J. Chem. Phys.*, **51**, 1791 (1969).
(5) K. M. Bansal and R. W. Fessenden, *Chem. Phys. Lett.*, **15**, 21 (1972).
(6) E. Schultes, Doctoral Thesis, University of Bonn, Bonn, W. Germany, 1973.
(7) F. J. Davis, R. N. Compton, and D. R. Nelson, *J. Chem. Phys.*, **59**, 2324 (1973).
(8) K. Ito and Y. Hatano, *J. Phys. Chem.*, **78**, 853 (1974).
(9) K. G. Mothes, D. Mihelcic, and R. N. Schindler, *Ber. Bunsenges. Phys. Chem.*, **75**, 9 (1971).
(10) K. G. Mothes, E. Schultes, and R. N. Schindler, *J. Phys. Chem.*, **76**, 3758 (1972).
(11) E. Schultes, R. Schumacher, and R. N. Schindler, *Z. Naturforsch.*, **29**, 239 (1973).
(12) A. A. Christodoulides, E. Schultes, R. Schumacher, and R. N. Schindler, *Z. Naturforsch.*, **29**, 389 (1973).
(13) R. W. Fessenden and K. M. Bansal, *J. Chem. Phys.*, **53**, 3468 (1970).
(14) W. E. Wentworth, R. S. Becker, and R. Tung, *J. Phys. Chem.*, **71**, 1652 (1967).
(15) W. E. Wentworth and J. C. Steelhammer, *Adv. Chem. Ser.*, **No. 82**, 75 (1968).
(16) J. C. Steelhammer and W. E. Wentworth, *J. Chem. Phys.*, **51**, 1802 (1969).
(17) F. C. Fehsenfeld, L. R. Megill, and L. K. Droppleman, *J. Chem. Phys.*, **43**, 3618 (1965).
(18) R. Schumacher, A. A. Christodoulides, and R. N. Schindler, to be submitted for publication.
(19) K. D. Bayes, D. Kivelson, and S. C. Wong, *J. Chem. Phys.*, **37**, 1217 (1962).
(20) L. G. Christophorou and A. A. Christodoulides, *J. Phys. B*, **2**, 71 (1969).
(21) E. Schultes, A. A. Christodoulides, and R. N. Schindler, *Chem. Phys.*, **8**, 354 (1975).
(22) J. M. Warman, R. W. Fessenden, and G. Bakale, *J. Chem. Phys.*, **57**, 2702 (1973).
(23) D. Mihelcic, P. Potzinger, and R. N. Schindler, *Ber. Bunsenges. Phys. Chem.*, **78**, 82 (1974).
(24) M. A. Biondi, *Phys. Rev.*, **109**, 2005 (1958).
(25) F. K. Truby, *Phys. Rev.*, **172**, 24 (1968).
(26) D. C. Frost and C. A. McDowell, *Can. J. Chem.*, **38**, 407 (1960).
(27) T. L. Gilbert and A. C. Wahl, *J. Chem. Phys.*, **55**, 5247 (1971).
(28) A. E. Douglas, C. K. Moeller, and B. P. Stoicheff, *Can. J. Phys.*, **41**, 1174 (1963).
(29) R. S. Berry and C. W. Reimann, *J. Chem. Phys.*, **38**, 1540 (1963).
(30) H. A. Barton, *Phys. Rev.*, **30**, 614 (1927).
(31) R. E. Fox, *J. Chem. Phys.*, **26**, 1281 (1957).
(32) H. W. Dickson, L. G. Christophorou, and R. N. Compton, Oak Ridge National Laboratory, Report No. ORNL-TM-1724 (1967).
(33) R. D. Nelson, D. R. Lide, and A. A. Maryott, *Natl. Stand. Ref. Data Ser., Natl. Bur. Stand.*, **No. 10** (1967).
(34) A. A. Christodoulides and L. G. Christophorou, Oak Ridge National Labo-

ratory, Report No. ORNL-TM-2257 (1968).
(35) L. G. Christophorou, "Atomic and Molecular Radiation Physics", Wiley-Interscience, New York, N.Y., 1971.
(36) S. Altshuler, *Phys. Rev.*, **107**, 114 (1957).
(37) A. A. Christodoulides, R. Schumacher, and R. N. Schindler, manuscript in preparation.
(38) E. Chen, R. D. George, and W. E. Wentworth, *J. Chem. Phys.*, **49**, 1973 (1968).
(39) K. Takayanagi and Y. Itikawa, *J. Phys. Soc.*, **24**, 160 (1968).
(40) For convenience, the units for k values and for concentrations will be given in the text as $cm^3\ sec^{-1}$ and cm^{-3} rather than cm^3 molecule^{-1} sec^{-1} and molecule cm^{-3}, respectively.

Reactivity of the Carbonate Radical toward Aromatic Compounds in Aqueous Solution[1]

Schoen-nan Chen, Morton Z. Hoffman,* and George H. Parsons, Jr.

Department of Chemistry, Boston University, Boston, Massachusetts 02215 *(Received March 14, 1975)*

The rate constants for the reaction of CO_3^- and CO_3H radicals, generated in the flash photolysis of aqueous solutions of $Co(NH_3)_4CO_3^+$, with a series of substituted benzene derivatives have been measured. The rate constants at pH 7, ranging from $3 \times 10^3\ M^{-1}\ sec^{-1}$ for benzene to $1.8 \times 10^9\ M^{-1}\ sec^{-1}$ for dimethylanaline, correlate very well with the Hammett equation using σ_{para}^+ values for electrophilic substitution yielding $\rho = -3.6$. The CO_3^- radical can be viewed as a selective electrophilic reagent.

Introduction

The carbonate radical (CO_3^-) and its conjugate acid (CO_3H; $pK_a = 9.6 \pm 0.3$)[2,3] show a wide range of reactivity with aromatic compounds with the rate constants depending upon the nature of the substituents and the aromatic ring system.[4] Thus, benzene reacts very slowly ($k < 10^4\ M^{-1}\ sec^{-1}$) while phenol reacts a factor of $\sim 10^3$ more rapidly.[4] Very high rates are shown by indole and its derivatives[5] including tryptophan-containing enzymes such as lysozyme and chymotrypsin.[6] Although the exact mode of reaction of CO_3^- [7] with aromatic compounds is not known, there is evidence[8] to indicate that radical addition to the aromatic system, similar to that shown by OH radicals,[9] is the operative mechanism. In that case, the mechanism of CO_3^- addition is analogous to electrophilic substitution and should give rise to a linear free energy correlation between the rate constant for the reaction and a substituent parameter.

The reactivity of e_{aq}^-,[10] OH radicals,[11] H atoms,[12] and, most recently, positronium atoms[13] with aromatic compounds has been successfully correlated with appropriate σ constants for electrophilic and nucleophilic substitutions by some form of the Hammett equation: $\log k = \rho\sigma + \log k_0$. For OH radicals,[11] a good agreement was seen using σ_{para} and σ_{meta} values with $\rho = -0.41$ although the range of rate constants measured varied over less than a factor of 4. The small absolute value of ρ in this case is indicative of the high reactivity of OH radicals ($k \sim 10^9\ M^{-1}\ sec^{-1}$) and resulting low selectivity. The lower reactivity of CO_3^- radicals should result in a high degree of selectivity in its reaction with benzene and its derivatives.

Experimental Section

The generation of CO_3^- radicals from the flash photolysis of $Co(NH_3)_4CO_3^+$ has already been described in detail.[14] Solutions were prepared from triply distilled water containing $5 \times 10^{-5}\ M$ $Co(NH_3)_4CO_3^+$ and $\sim 0.02\ M$ phosphate buffer. The organic solutes were of the purest grade commercially available and were used without further purification. The flash photolysis apparatus dissipated up to 250 J of energy with 1/e time of 30 μsec. The solution was contained in a 22-cm quartz optical cell and the CO_3^- absorption at 600 nm was monitored by a 75-W Osram Xe lamp, a RCA 4832 PM tube, a Hilger-Engis 0.6 M spectrometer, and associated fast detection electronics. An Oriel wedge interference monochromator, set at 600 nm (band width = 28 nm) was always in place between the analyzing lamp and the cell and an electric shutter restricted exposure of the solution to the light.

The solutions were flashed without deoxygenation inasmuch as CO_3^- radicals do not react with O_2. The pseudo-first-order rate constant for the decay of CO_3^- was determined at a single scavenger concentration; the general linear dependence of k on [scavenger] had already been established.[3,4] The values of the second-order rate constants for the reaction of the radical with the solutes were obtained from at least four individual decays and are known to an accuracy of $\pm 10\%$ with the exception of benzene. Here the decay of the radical was only modestly faster than that in the absence of benzene so that the uncertainty in k may be as high as 50–100%.

Results and Discussion

Table I gives the values of the rate constants for the reaction of CO_3^- radicals with substituted benzene derivatives at pH 7.0. Those compounds which react slowly with the radical require relatively high concentrations in order for scavenging to be observed and we recognize that the presence of an adventitious impurity in the solute, although at a low concentration, may react with the radical at relatively high rates. For example, the rate constant for cyclohexene, which may be an impurity in benzene or toluene, is $2.5 \times 10^6\ M^{-1}\ sec^{-1}$. Therefore, rate constants $<10^5\ M^{-1}\ sec^{-1}$ should be viewed as upper limits for that compound. However, the quality of the Hammett correlation suggests that the role of impurities is small.

TABLE I: Rate Constants[a] and Hammett Constants[b] for Substituted Benzene Derivatives

Substituent	k, M^{-1} sec^{-1}	σ_{meta}	σ_{para}	σ_{para}^{+}
-H	3×10^{3}	0.00	0.00	0.00
$-CH_3$	4.3×10^{4}	−0.07	−0.16	−0.31
$-NHCOCH_3$	3.2×10^{5}	0.12	−0.09	−0.60
$-OC_2H_5$	4.1×10^{5}	0.12[c]	−0.27[c]	−0.78[c]
-OH	4.9×10^{6}	0.01	−0.37	−0.92
$-NH_2$	5.4×10^{8}	0.00	−0.57	−1.40
$-N(CH_3)_2$	1.8×10^{9}	−0.15	−0.83	−1.70

[a] $k(CO_3^- + \text{compound})$ at pH 7.0. [b] Values taken from ref 15. [c] Values for $-OCH_3$.

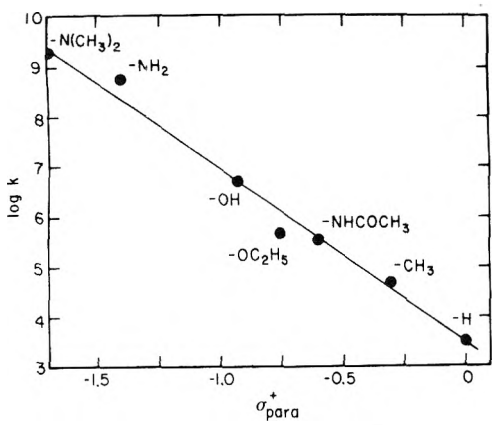

Figure 1. Hammett plot for the reaction of CO_3^- radicals with substituted benzene derivatives at pH 7.0.

Also included in Table I are values of σ_{meta}, σ_{para}, and σ_{para}^{+} Hammett substituent constants.[15] It is evident that σ_{meta} provides no correlation at all. A plot of log k vs. σ_{para} affords a poor linear graph but the best correlation arises from σ_{para}^{+} (Figure 1) which yields $\rho = -3.6$ with a correlation coefficient of 0.983 over six orders of magnitude of k.

The ρ values for the $\rho\sigma^{+}$ correlation are always negative, often with magnitudes that are in the range of the value reported here.[17] Among the reactions to which this correlation has been applied are oxidation and radical reactions as well as electrophilic aromatic substitution.[15] Inasmuch as the σ_{para}^{+} values correlate very well with the ionization potentials of the benzene derivatives,[18] and hence their oxidation potentials, the relationship shown in Figure 1 cannot be taken as a definitive indication of the mechanism of the reaction, i.e., electron transfer or radical attachment. Nevertheless, the reaction is facilitated by electron-supplying substituents and the CO_3^- radical can be viewed as a selective electrophilic reagent. The addition of CO_3^- to the aromatic system as the rate-determining (and measured) step in the overall reaction is consistent with the value and sign of ρ.

Although correlation with anionic substituents must be made with caution because of ionic strength and solvent interaction effects,[15] σ_{para} (and presumably σ_{para}^{+}) for $-O^-$ is more negative than that of -OH[19] predicting a higher reactivity of the phenoxide ion with CO_3^- compared with phenol. Figure 2 shows the dependence of $k(CO_3^- + \text{phenol})$ as a function of pH at constant ionic strength (~0.06 M) with the inflection point of the curve corresponding to the pK_a of phenol (10.0). Less than 20% of the increased reactivity

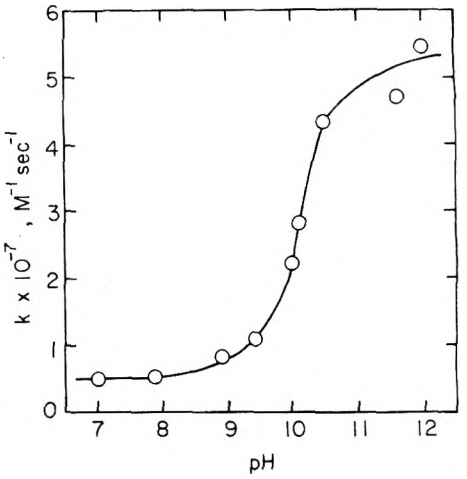

Figure 2. Dependence of k on pH for the reaction of CO_3^- radicals with phenol.

of the phenoxide ion (compared to phenol) can be attributed to the kinetic salt effect on the reaction of the negatively charged radical and compound.[3] If the reactivity of phenoxide ion can be applied to the correlation in Figure 1, a value of $\sigma_{para}^{+} \sim -1.1$ is obtained.[20] Phenoxide ion also reacts ~50% faster with OH radicals than does phenol[21] and can be seen to satisfy modestly the $\rho\sigma$ correlation[22] for that radical. Recently it has been shown[23] that O^- radicals oxidize phenoxide ions to phenoxyl radicals by means of an electron transfer mechanism; the application of this mechanism to the reaction of CO_3^- with phenoxide ions remains an interesting possibility and should be explored further.

References and Notes

(1) The support of this research by the National Science Foundation through Grant No. MPS 73-05025 is gratefully acknowledged.
(2) S.-N. Chen and M. Z. Hoffman, *J. Chem. Soc., Chem. Commun.*, 991 (1972).
(3) S.-N. Chen, V. W. Cope, and M. Z. Hoffman, *J. Phys. Chem.*, **77**, 1111 (1973).
(4) S.-N. Chen and M. Z. Hoffman, *Radiat. Res.*, **56**, 40 (1973).
(5) S.-N. Chen and M. Z. Hoffman, *J. Phys. Chem.*, **78**, 2099 (1974).
(6) S.-N. Chen and M. Z. Hoffman, *Radiat. Res.*, **62**, 18 (1975).
(7) The symbol CO_3^- will be used in this paper to designate the radical irrespective of its acidic or basic form unless the specific nature of the radical is essential for the discussion.
(8) G. E. Adams, J. E. Aldrich, R. H. Bisby, R. B. Cundall, J. L. Redpath, and R. L. Willson, *Radiat. Res.*, **49**, 278 (1972).
(9) L. M. Dorfman, I. A. Taub, and R. E. Bühler, *J. Chem. Phys.*, **36**, 3051 (1962).
(10) M. Anbar and E. J. Hart, *J. Am. Chem. Soc.*, **86**, 5633 (1964).
(11) M. Anbar, D. Meyerstein, and P. Neta, *J. Phys. Chem.*, **70**, 2660 (1966).
(12) M. Anbar, D. Meyerstein, and P. Neta, *Nature (London)*, **209**, 1348 (1966).
(13) A. L. Nichols, W. J. Madia, and H. J. Ache, *J. Phys. Chem.*, **78**, 1881 (1974).
(14) V. W. Cope, S.-N. Chen, and M. Z. Hoffman, *J. Am. Chem. Soc.*, **95**, 3116 (1973).
(15) O. Exner in "Advances in Linear Free Energy Relationships", N. B. Chapman and J. Shorter, Ed., Plenum Press, New York, N.Y., 1972, Chapter 1.
(16) H. C. Brown and Y. Okamoto, *J. Am. Chem. Soc.*, **80**, 4979 (1958).
(17) J. E. Leffler and E. Grunwald, "Rates and Equilibria of Organic Reactions", Wiley, New York, N.Y., 1963; pp 208–209.
(18) M. M. Bursey in "Advances in Linear Free Energy Relationships", N. B. Chapman and J. Shorter, Ed., Plenum Press, New York, N.Y., 1972, Chapter 10.
(19) H. H. Jaffe, *Chem. Rev.*, **53**, 191 (1953).
(20) σ_{para} for phenoxide ion is reported to be −0.52; ref 19.
(21) R. W. Matthews and D. F. Sangster, *J. Phys. Chem.*, **69**, 1938 (1965).
(22) P. Neta and L. M. Dorfman, *Adv. Chem. Ser.*, **No. 81**, 222 (1968); L. M. Dorfman and G. E. Adams, *Natl. Stand. Ref. Data Ser., Natl. Bur. Stand.*, **No. 46** (1973).
(23) P. Neta and R. H. Schuler, *J. Am. Chem. Soc.*, **97**, 912 (1975).

Radiation-Induced Homolytic Aromatic Substitution. IV. Effect of Metal Ions on the Hydroxylation of Nitrobenzene

Manfred K. Eberhardt

Puerto Rico Nuclear Center, Caparra Heights Station, San Juan, Puerto Rico 00935 *(Received March 28, 1975)*

Publication costs assisted by the Puerto Rico Nuclear Center

The effect of chromium(VI), iron(III), iron(II), and copper(II) compounds on the radiation-induced hydroxylation of nitrobenzene has been investigated. $K_2Cr_2O_7$ in unbuffered solution and $K_3Fe(CN)_6$ in acidic (pH 1.4) solution gave a high conversion of hydroxyl radicals to nitrophenols with a close to statistical isomer distribution. The isomer distribution obtained with $K_3Fe(CN)_6$ in acidic solution did not change with concentration (5×10^{-4} to 5×10^{-2} M). On the other hand with $K_2Cr_2O_7$ the G(meta) increased with concentration (5×10^{-4} to 5×10^{-3} M) approaching a close to statistical distribution at the higher concentration. In unbuffered solution $K_3Fe(CN)_6$ produced mainly m-nitrophenol. We suggest that this is due to a selective oxidation of the m-hydroxynitrocyclohexadienyl radical, and to a selective reduction of the o- and p-hydroxynitrocyclohexadienyl radicals by $Fe(CN)_6^{4-}$. Contrary to the results with $K_2Cr_2O_7$ and $K_3Fe(CN)_6$, the Fe^{3+} salts ($FeNH_4(SO_4)_2$, $Fe(ClO_4)_3$, and $Fe(NO_3)_3$) at low concentration (5×10^{-4} M) gave almost exclusively ortho and para hydroxylation in high yield. The mechanism of these oxidations is discussed. Cu^{2+} (5×10^{-4} M) does not oxidize the intermediate hydroxycyclohexadienyl radicals. In all cases ($CuSO_4$, $CuCl_2$, $Cu(ClO_4)_2$, and $Cu(OCOCH_3)_2$) only trace amounts of nitrophenols with the para isomer dominant (G(para) $\sim$ 0.1) were obtained. Depending on the metal ion, concentration, and pH, one may produce either m-nitrophenol (100%) or o- and p-nitrophenol (97.4%) or a statistical isomer distribution.

Introduction

In a previous publication[2a] we have reported on the radiation-induced hydroxylation of nitrobenzene, chlorobenzene, and toluene. In absence of oxygen the yields of the substituted phenols were much smaller than G(·OH) due to competing side reactions, such as disproportionation, dimerization, recombination of the ·OH radical adduct with the H· atom adduct,[2b] and in the case of toluene elimination of water.[3] Oxygen has been frequently used to increase the yields in homolytic aromatic substitution.[2a,4,5] Oxygen considerably increases the yields of nitrophenols, chlorophenols, and cresols, but is still much lower than G(·OH). In the hydroxylation of benzene Baxendale and Smithies[6] have been able to convert ·OH radicals quantitatively to phenol in presence of a mixture of $FeNH_4(SO_4)_2$ and $CuSO_4$. Volkert and Schulte-Frohlinde[7] in their study of the hydroxylation of benzoic acid in presence of N_2O used $K_3Fe(CN)_6$ to convert all the ·OH radicals to hydroxybenzoic acids. Most recently Bhatia and Schuler[8] have studied the effect of a variety of metal salts on the hydroxylation of benzene in N_2O-saturated aqueous solutions, and observed in some cases a G(phenol) = 6.0. In order to obtain more reliable information about the initial position of ·OH radical attack on substituted benzenes it is of course desirable to convert all the ·OH adducts to the corresponding phenols. No study on the reduction of substituted hydroxycyclohexadienyl radicals has been reported. In the present work we have studied the effects of chromium(VI), iron(III), iron(II), and copper(II) compounds and oxygen on the hydroxylation of nitrobenzene.

Experimental Section

Materials. All solutions were prepared using water which was triple distilled from an all glass still. Then it was further distilled over alkaline permanganate, acidic dichromate, and one final distillation. Nitrobenzene was reagent grade and was redistilled. All metal salts were of reagent grade quality. The aqueous solution were deoxygenated by bubbling argon through the solution as described previously.[2a]

Irradiations. Irradiations were carried out with a ^{60}Co source at a dose rate of 2.56×10^{16} eV/g min and a total dose of 1.54×10^{18} eV/g (determined by Fricke dosimetry with $G(Fe^{3+}) = 15.5$). The dosimetry was carried out by using the same bottles and volume as the irradiated solutions.

Analytical Procedure. Immediately after the irradiation the pH of the solution (1 l.) was adjusted to about 4 and then extracted once with 200 ml of ether and four times with 100 ml of ether. The ether extract was dried over 80 g of Na_2SO_4 for about 24 hr, and was then concentrated to about 20–30 ml. To this concentrate was added 20 ml of a diazomethane solution (prepared from Diazald, Aldrich Chemical Co.) and left standing for 2 days. This procedure converted all the nitrophenols quantitatively to the corresponding methoxy derivatives. Then the solution was concentrated to 10 ml and analyzed by vapor phase chromatography using a hydrogen flame detector. The column was a 6-ft DEGS (diethyleneglycol succinate 5% liquid phase on Chromosorb W-AW-DMCS (100–120 mesh)) column at 170° and a flow of about 25 ml of He/min. The isomeric nitroanisoles appeared in the following sequence: m-nitroanisole (5.0 min), o-nitroanisole (7.9 min), and p-nitroanisole (8.9 min). Standard aqueous nitrophenol solutions were prepared containing amounts of nitrophenols which were very close to the amounts present in the irradiated solutions and worked up in the same way. In this way a very accurate determination of the G values was possible. All experiments were carried out in duplicate and triplicate and were found to be reproducible within the limits of the ana-

TABLE I: Nitrophenol Yields in the Radiolysis of Aqueous Nitrobenzene Solutions[a]

Expt no.	Conditions	G(ortho)	G(meta)	G(para)	G(total)	% ortho	% meta	% para
1	$K_2Cr_2O_7$ 5×10^{-4} *M*	1.50	0.98	0.63	3.11	48.2	31.5	20.3
2	$K_2Cr_2O_7$ 5×10^{-3} *M*	1.50	1.29	0.60	3.39	44.2	38.1	17.7
3	$K_2Cr_2O_7$ 5×10^{-4} *M* pH 1.4	1.00	0.53	0.48	2.01	49.8	26.4	23.9
4	$K_3Fe(CN)_6$ 5×10^{-4} *M*	0.15	0.95	0.18	1.28	11.7	74.2	14.1
5	$K_3Fe(CN)_6$ 5×10^{-4} *M*	0.12	1.02	0.20	1.34	9.0	76.1	14.9
6	$K_3Fe(CN)_6$ 5×10^{-3} *M*	0.15	1.05	0.22	1.42	10.6	73.9	15.5
7	$K_3Fe(CN)_6$ 5×10^{-2} *M*	0.35	1.13	0.33	1.81	19.3	62.4	18.2
8	$K_3Fe(CN)_6$ 5×10^{-4} *M* + $K_4Fe(CN)_6$ 5×10^{-4} *M*	0	0.90	0	0.90	0	100	0
9	$K_3Fe(CN)_6$ 5×10^{-4} *M* pH 1.4	1.14	0.98	0.50	2.62	43.5	37.4	19.1
10	$K_3Fe(CN)_6$ 10^{-3} *M* pH 1.4	1.14	0.98	0.47	2.59	44.0	37.8	18.2
11	$K_3Fe(CN)_6$ 2×10^{-3} *M* pH 1.4	1.12	1.05	0.50	2.67	41.9	39.3	18.7
12	$K_3Fe(CN)_6$ 5×10^{-3} *M* pH 1.4	1.10	1.08	0.50	2.67	41.9	39.3	18.7
13	$K_3Fe(CN)_6$ 10^{-2} *M* pH 1.4	1.15	1.13	0.52	2.80	41.1	40.4	18.6
14	$K_3Fe(CN)_6$ 5×10^{-4} *M* + $K_4Fe(CN)_6$ 5×10^{-4} *M* pH 1.4	0.62	1.02	0.34	1.98	31.3	51.5	17.2
15	$FeNH_4(SO_4)_2$ 5×10^{-4} *M*	1.44	0.08	0.81	2.33	61.8	3.4	34.8
16	$FeNH_4(SO_4)_2$ 5×10^{-4} *M* + $Fe(NH_4)_2(SO_4)_2$ 5×10^{-4} *M*	0.47	0.08	0.70	1.25	37.6	6.4	56.0
17	$Fe(ClO_4)_3$ 5×10^{-4} *M*	1.30	0.08	0.77	2.15	60.5	3.7	35.8
18	$Fe(ClO_4)_3$ 5×10^{-3} *M*	1.46	0.24	0.80	2.50	58.4	9.6	32.0
19	$Fe(ClO_4)_3$ 5×10^{-2} *M*	1.60	0.44	0.82	2.86	55.9	15.4	28.7
20	$Fe(ClO_4)_3$ 5×10^{-4} *M* + $HClO_4$ 5×10^{-2} *M*	1.97	0.08	1.02	3.07	64.1	2.6	33.3
21	$Fe(NO_3)_3$ 5×10^{-4} *M*	1.44	0.08	0.85	2.37	60.8	3.4	33.8
22	$Fe(NO_3)_3$ 5×10^{-3} *M*	1.44	0.26	0.75	2.45	58.8	10.6	30.6
23	$Fe(NO_3)_3$ 5×10^{-2} *M*	1.11	0.25	0.55	1.91	58.1	13.1	28.8
24	$Fe(NO_3)_3$ 5×10^{-4} *M* + O_2 10^{-3} *M*	1.14	0.63	0.59	2.36	48.3	26.7	25.0
25	No additives	0.18	0.05	0.36	0.59	30.5	8.5	61.0

[a] All solutions were deoxygenated (except experiment 24) solutions (5×10^{-3} *M* nitrobenzene) irradiated at a dose rate of 2.56×10^{16} eV/g min and a total dose of 1.54×10^{18} eV/g. All solutions were unbuffered. Experiments at pH 1.4 contained H_2SO_4.

lytical technique (±5%). The smaller *G* values (<0.5) are somewhat less accurate (±8%).

Results and Discussion

The results are shown in Table I. The *G*(·OH) values at pH 7 reported in the literature vary over a wide range (2.0–3.2).[9] More recently Bielski and Allen[10] have determined $G(\cdot OH) = 2.74 \pm 0.08$ at pH 7. The results in Table I show that, under certain conditions of concentration and pH, excellent conversions of the ·OH radicals to nitrophenols are obtained. With 5×10^{-3} *M* $K_2Cr_2O_7$ in unbuffered solution we observe a *G*(total nitrophenols) of 3.29. The high *G*(total nitrophenols) may be partly due to a reaction between the reduced metal ion and H_2O_2, which would increase the *G*(·OH) by as much as the molecular peroxide yield (ca. 0.7). Evidence for this type of additional hydroxylation has also been obtained by Bhatia and Schuler[8] in the hydroxylation of benzene. A *G*(phenol) of 3.2 was reported by Baxendale and Smithies[6] in presence of 5×10^{-4} *M* Fe^{3+} + 2×10^{-3} *M* Cu^{2+}. The drastic difference in the isomer distribution obtained with $K_2Cr_2O_7$ and $K_3Fe(CN)_6$ on one hand and with the Fe^{3+} salts on the other hand is apparent. With $K_2Cr_2O_7$ and $K_3Fe(CN)_6$ we obtain much more meta substitution than with the Fe^{3+} salts, which give mainly ortho–para substitution. In order to discuss this great variation in isomer distribution we suggest the mechanism outlined in Scheme I. The ·OH radical adducts (I–III) can be oxidized by some metal ions to the corresponding nitrophenols. This oxidation will compete with the 1,2 hydroxyl radical shift II → I and II → III, and also with the reduction by the reduced metal ion. With increasing $Fe(ClO_4)_3$ and $Fe(NO_3)_3$ concentration the percentage of *m*-nitrophenol increases as expected for this competition between oxidation and rearrangement. Evidence for a 1,2 hydroxyl radical shift has been presented previously in the hydroxylation of benzoic acid[7] and anisole.[11] SCF–MO calculations of OH radical adducts of nitrobenzene, chlorobenzene, and toluene have shown that in all cases the ortho and para adducts have the lowest energies.[2a] For the mechanism of the rearrangements II → I and II → III several possibilities exist. A reversible addition possibly involving a π complex has been suggested by Volkert and Schulte-Frohlinde.[7] Recently Walling and Johnson[12] in the hydroxylation of toluene with Fenton's reagents have proposed a reversible dehydration, which could lead to isomerization. In the case of the hydroxynitrocyclohexadienyl radicals however this possible mechanism can be excluded since results of Schevchuk and Vysotskaya[13] on the hydroxylation

Scheme I

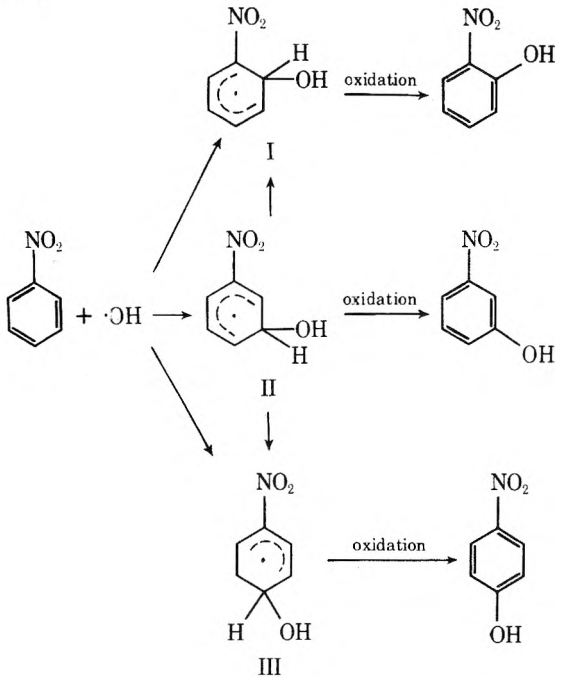

of nitrobenzene with Fenton's reagent have shown that the oxygen in the nitrophenols is solely derived from H_2O_2 and not from the water.

The anion has no effect on the isomer distribution (see experiments 15, 17, and 21). This was also observed in the oxidation of *n*-butyl radicals in water by Cu^{2+} salts,[14] and is due to the extensive hydrolysis of the salts to solvated metal ions. With $Fe(ClO_4)_3$ we find an increase and with $Fe(NO_3)_3$ we find a decrease in the total nitrophenol yield with increasing concentration. At higher NO_3^- concentration $NO_2\cdot$ is produced (through e_{aq}^- scavenging by NO_3^-) which can compete with the Fe^{3+} for the intermediate hydroxycyclohexadienyl radicals.[15] $Fe(ClO_4)_3$ shows a considerable pH effect. At 5×10^{-4} *M* $Fe(ClO_4)_3$ and 5×10^{-2} *M* $HClO_4$ we obtain almost exclusively and in quantitative yield *o*- and *p*-nitrophenol (experiment 20).

The oxidations with $K_3Fe(CN)_6$ are pH dependent. The reduction potential of $Fe(CN)_6^{3-}$ changes from +0.69 eV in 1 *N* H_2SO_4 to +0.46 eV in 0.01 *N* NaOH.[16] The oxidation with $K_3Fe(CN)_6$ in neutral solution produced mainly *m*-nitrophenol (74%) with the same *G* value as in acidic solution, where we also obtain large amounts of *o*- and *p*-nitrophenol. This indicates a selective oxidation of the *m*-hydroxynitrocyclohexadienyl radical in neutral solution. According to SCF–MO calculations[2a] (CNDO and INDO) the *m*-hydroxynitrocyclohexadienyl radical has the highest lying SOMO (singly occupied molecular orbital) of the three isomers and is, therefore, the one which is most easily oxidized. The fact that with 5×10^{-4} *M* $K_3Fe(CN)_6$ in neutral solution we observed less *o*- and *p*-nitrophenol than in absence of $K_3Fe(CN)_6$[2a] made us suspect a selective reduction of the *o*- and *p*-hydroxynitrocyclohexadienyl radicals by $Fe(CN)_6^{4-}$ which is formed during the course of the irradiation. We have to consider the following two reactions:

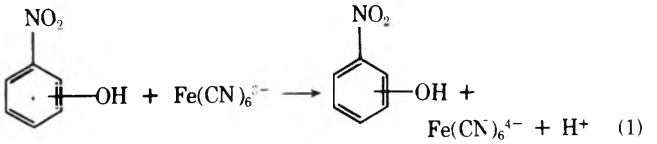

(1)

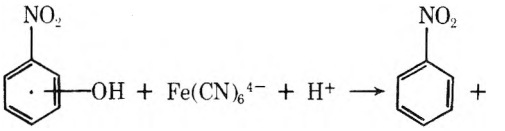

(2)

We have studied the effect of $K_4Fe(CN)_6$ (experiment 8), and observed a complete disappearance of *o*- and *p*-nitrophenol, while the *m*-nitrophenol changes very little. The small decrease in *G*(meta) is due to the competition between nitrobenzene and $Fe(CN)_6^{4-}$ for OH radicals. On the basis of the known rate constants for these reactions (4.7×10^9 and 9.3×10^9 M^{-1} sec^{-1}, respectively)[17] one would expect a decrease of 20%. The selective reduction of the *o*- and *p*-hydroxynitrocyclohexadienyl radicals is also evident from the results in acidic solutions (experiment 14). In presence of $Fe(CN)_6^{4-}$ *G*(meta) does not change, but *G*(ortho) and *G*(para) decrease considerably. In neutral solution we observe with increasing $K_3Fe(CN)_6$ concentration an increase in *G*(ortho) and *G*(para) (experiments 4–7) in agreement with the two competing reactions (reaction 1 and 2). A reduction of the *o*- and *p*-hydroxynitrocyclohexadienyl radicals was also observed with $Fe(NH_4)_2(SO_4)_2$ (experiment 16).

With $K_3Fe(CN)_6$ at low pH we obtain a statistical isomer distribution which is independent of concentration. Accepting the mechanism outlined in Scheme I we can conclude that the rate of oxidation with $K_3Fe(CN)_6$ at low pH is very much faster than the rate of oxidation with Fe^{3+}.

Another possible explanation for the big difference between the $K_3Fe(CN)_6$ experiments and the Fe^{3+} experiments is a different oxidation mechanism. The oxidation of radicals by Fe^{3+} has been discussed by Walling and coworkers,[18] who suggested a reversible electron transfer process:

$$R\cdot + Fe^{3+} \rightleftharpoons R^+ + Fe^{2+}$$

The equilibrium is determined by the stability of the carbonium ion. In our case of three isomeric hydroxynitrocyclohexadienyl radicals we expect to obtain resonance stabilized carbonium ions, which can undergo a 1,2 hydroxide anion shift to give mainly *o*- and *p*-nitrophenol. In a study on the oxidation of hydroxyl radical–anisole adducts Norman and coworkers[11] have concluded that in the oxidation with metal ions the loss of a proton is synchronous with the electron transfer. They were led to that conclusion because in the hydroxylation of *p*-deuterioanisole with Fenton's reagent they only observed a small amount of a hydride shift (the NIH shift).[19] A 1,2 hydroxide anion shift, therefore, appears unlikely. Furthermore the increase in *m*-nitrophenol with increasing concentration of $Fe(ClO_4)_3$ or $Fe(NO_3)_3$ cannot be explained by a 1,2 hydroxide anion shift, but is indicative of competition between oxidation and rearrangement.

The preferential oxidation of the meta adduct by $Fe(CN)_6^{3-}$ and the preferential reduction of the ortho and para adducts by $Fe(CN)_6^{4-}$ is in agreement with results of Walling and coworkers.[18] They find that α-hydroxyalkyl radicals are oxidized by Fe^{3+}, while radicals with strong electron-withdrawing groups in the α position are instead reduced by Fe^{2+}. The *o*- and *p*-hydroxynitrocyclohexadienyl radicals have in one of their resonance forms the NO_2 group α to the radical site. We, therefore, suggest that the mechanisms of oxidation by $K_3Fe(CN)_6$ and Fe^{3+} are the same. The only difference between these two oxidizing

metal salts is the much faster rate of oxidation by $K_3Fe(CN)_6$.

An interesting result is obtained with $Fe(NO_3)_3$ in oxygenated solution (experiment 24). Compared with the deoxygenated solution (experiment 21) G(meta) increases at the expense of G(ortho) and G(para), but G(total nitrophenols) remains the same. From this observation we conclude that k(oxidation with O_2)[20] = 2.5×10^6 M^{-1} sec^{-1} > k(oxidation with Fe^{3+}). The isomer distribution in oxygenated $Fe(NO_3)_3$ solution is almost identical with the one obtained in oxygenated nitrobenzene solutions in absence of $Fe(NO_3)_3$,[2a] but G(total nitrophenols) is higher (2.36 vs. 1.69[2a] or 1.75[21]).

The oxidation with $K_2Cr_2O_7$ has been investigated by Matthews and Sangster,[21] who obtained high conversions of the OH radicals to nitrophenols. We also find large G(nitrophenols) and we find in addition a considerable pH effect. At low pH the G values are lower than at neutral pH, probably due to further oxidation of the nitrophenols. Matthews and Sangster have suggested that all the hydroxynitrocyclohexadienyl radicals are oxidized to the corresponding nitrophenols. This, however, appears to be the case only at the higher $K_2Cr_2O_7$ concentration where we find a close to statistical isomer distribution.

Cu^{2+} salts ($CuSO_4$, $CuCl_2$, $Cu(ClO_4)_2$, and $Cu(OCOCH_3)_2$) at concentrations of 5×10^{-4} M did not oxidize the hydroxynitrocyclohexadienyl radicals. At this concentration the reaction $Cu^{2+} + OH\cdot \rightarrow Cu(III) + OH^-$ (k = 3.5×10^8 M^{-1} sec^{-1})[17] will be insignificant compared to the reaction of ·OH radicals with nitrobenzene (k = 4.7×10^9 M^{-1} sec^{-1}).[20] In all cases, only trace amounts of nitrophenols with the para isomer dominant ($G \sim 0.1$) were obtained. The oxidation of radicals with Cu^{2+} has been extensively investigated by Kochi and coworkers,[14] who have shown that the oxidation proceeds via an organocopper intermediate. Oxidation by Fe^{3+} proceeds by a different mechanism.[18] Cu^{2+} is known to oxidize the hydroxycyclohexadienyl radical[6,8] and hydroxymethylcyclohexadienyl radicals[22] to the corresponding phenols, but these radicals have much higher lying SOMO energy levels[2a] and have, therefore, lower oxidation potentials. The reduction potential of Cu^{2+} (+0.158 eV) is lower than that of Fe^{3+} (+0.770 eV). The oxidation with metal ions is competing with other radical termination processes. The reduction potential of the metal ion is, however, not the only factor which determines the rate of oxidation, since Ag^+ (+0.7996 eV) which has a higher reduction potential than Fe^{3+} or Cu^{2+} was found not to oxidize the hydroxycyclohexadienyl radical[8] whereas Fe^{3+} and Cu^{2+} did oxidize this intermediate.

The high yield of nitrophenols again confirms previous conclusions[20,23] that the ·OH radicals attack at the ring and not, or only to an insignificant extent, at the NO_2 group which is unexpected on the basis of the magnitude of orbital overlap.[2a]

The electrophilic character of ·OH radical is well documented;[2a,23-25] Eberhardt and Yoshida[2a] have shown that the ·OH radical has a very low lying SOMO (singly occupied molecular orbital) and it will, therefore, interact mainly with the HOMO (highest occupied molecular orbital) of the aromatic compounds. SCF-MO (CNDO-2 and INDO) calculations of nitrobenzene have shown that the HOMO coefficients in the aromatic ring are very small ($\leq$0.024) in agreement with the well-known resistance of nitrobenzene toward electrophilic substitution. Because of this small orbital overlap at all ring positions there may be little selectivity in the initial addition reaction and in presence of an effective oxidizing agent one may then obtain a close to statistical isomer distribution.

References and Notes

(1) This paper was prepared in connection with work under Contract No. AT(40-1) 1833 with the U.S. Atomic Energy Commission.
(2) (a) M. K. Eberhardt and M. Yoshida, *J. Phys. Chem.*, **77**, 589 (1973); (b) M. K. Eberhardt, *ibid.*, **78**, 1795 (1974).
(3) (a) H. C. Christensen and R. Gustafsson, *Acta Chem. Scand.*, **26**, 937 (1972); (b) H. C. Christensen, K. Sehested, and E. J. Hart, *J. Phys. Chem.*, **77**, 983 (1973).
(4) M. K. Eberhardt and E. L. Eliel, *J. Org. Chem.*, **27**, 2289 (1962).
(5) R. T. Morrison, J. Cazes, N. Samkoff, and C. A. Howe, *J. Am. Chem. Soc.*, **84**, 4152 (1962).
(6) J. H. Baxendale and D. Smithies, *J. Chem. Soc.*, 799 (1959).
(7) O. Volkert and D. Schulte-Frohlinde, *Tetrahedron Lett.*, **No. 17**, 2151 (1968).
(8) K. Bhatia and R. H. Schuler, *J. Phys. Chem.*, **78**, 2335 (1974). We wish to thank Drs. Bhatia and Schuler for sending us the complete manuscript prior to publication.
(9) G. V. Buxton, *Radiat. Res.*, **1**, 209 (1968).
(10) B. H. J. Bielski and A. O. Allen, *Int. J. Radiat. Phys. Chem.*, **1** (2), 153 (1969).
(11) C. R. Jefcoate, J. R. Lindsay-Smith, and R. O. C. Norman, *J. Chem. Soc. B*, 1013 (1969).
(12) C. Walling and R. A. Johnson, *J. Am. Chem. Soc.*, **97**, 363 (1975).
(13) L. G. Shevchuk and N. A. Vysotskaya, *Zh. Org. Khim.*, **4**, 1936 (1968).
(14) (a) J. K. Kochi in "Free Radicals", Vol. I, J. K. Kochi, Ed., Wiley-Interscience, New York, N.Y., 1973, pp 591-683. (b) C. L. Jenkins and J. K. Kochi, *J. Am. Chem. Soc.*, **94**, 843 (1972).
(15) M. K. Eberhardt, *J. Phys. Chem.*, **79**, 1067 (1975).
(16) J. F. Hunsberger, "Handbook of Chemistry and Physics", 51st ed, Chemical Rubber Publishing Co., Cleveland, Ohio, 1970-1971, p D-111.
(17) L. M. Dorfman and G. E. Adams, *Natl. Bur. Stand. Ref. Data Ser., Natl. Bur. Stand.*, **No. 46**, (1973).
(18) C. Walling, G. M. El-Taliawi, and R. A. Johnson, *J. Am. Chem. Soc.*, **96**, 133 (1974).
(19) For a short review on the NIH Shift see D. M. Jerina, *Chem. Tech.*, **4**, 120 (1973).
(20) K. D. Asmus, B. Cercek, M. Ebert, A. Henglein, and A. Wigger, *Trans. Faraday Soc.*, **63**, 2453 (1967).
(21) R. W. Matthews and D. F. Sangster, *J. Phys. Chem.*, **71**, 4056 (1967).
(22) M. K. Eberhardt and M. I. Martinez, *J. Phys. Chem.*, following article in this issue.
(23) P. Neta and L. M. Dorfman, *Adv. Chem. Ser.*, **No. 81**, 222 (1968).
(24) R. O. C. Norman and G. K. Radda, *Proc. Chem. Soc.*, 138 (1962).
(25) M. Anbar, K. Meyerstein, and P. Neta, *J. Phys. Chem.*, **70**, 2660 (1966).

Radiation-Induced Homolytic Aromatic Substitution. V. Effect of Metal Ions on the Hydroxylation of Toluene

Manfred K. Eberhardt* and Maria Ivelisse Martinez

Puerto Rico Nuclear Center,[1] Caparra Heights Station, San Juan, Puerto Rico 00935 *(Received March 28, 1975)*

Publication costs assisted by the Puerto Rico Nuclear Center

The radiation-induced hydroxylation of toluene was investigated in presence of $K_2Cr_2O_7$, $K_3Fe(CN)_6$, $K_4Fe(CN)_6$, $Fe(ClO_4)_3$, $Fe(NH_4)(SO_4)_2$, $CuSO_4$, $Cu(ClO_4)_2$, and $Cu(OCOCH_3)_2$. With $K_2Cr_2O_7$, $K_3Fe(CN)_6$, and the Cu^{2+} salts high conversions of the OH radicals to cresols were obtained. In all these cases the isomer distribution obtained at the highest concentration investigated (5×10^{-2} *M*) was the same (49–52% ortho, 22–24% meta, and 26–28% para). With the exception of $K_3Fe(CN)_6$ the percentage of G(*m*-cresol) increased with increasing concentration of metal salt. The pH had a marked effect on the formation of cresols due to the competing acid-catalyzed elimination of water from the initially formed hydroxymethylcyclohexadienyl radicals to give benzyl radicals. No reduction of the hydroxymethylcyclohexadienyl radicals by $Fe(CN)_6^{4-}$ was observed. For the rate of oxidation of the hydroxymethylcyclohexadienyl radicals the following sequence was established: $Fe(CN)_6^{3-} > Cu^{2+} > Fe^{3+}$.

Introduction

In the radiation-induced hydroxylation of aromatic compounds usually only a small fraction of the ·OH radicals are converted to phenols.[2,3] The radiation-induced hydroxylation of toluene has been studied previously by Christensen and Gustafsson,[4] and by Eberhardt and Yoshida.[3] Low yields of cresols were observed by both groups. Christensen and Gustafsson studied the effect of $Fe(ClO_4)_3$. They found no increase in G(cresols), but rather a decrease, however, they observed a large amount of dibenzyl which they showed to arise via an acid-catalyzed water elimination from the initially formed hydroxymethylcyclohexadienyl radicals. In a recent publication[5] we have reported on the hydroxylation of nitrobenzene in presence of a variety of metal salts and we observed a quantitative conversion of ·OH radicals to nitrophenols. In the present paper we wish to report on the effect of metal salts on the hydroxylation of toluene.

Experimental Section

Materials. All solutions were prepared using water which was doubly distilled from an all glass still. Then it was further distilled over alkaline permanganate, acidic dichromate, and one final distillation. Toluene was reagent grade and was redistilled. All metal salts were of reagent grade quality. The aqueous solutions were deoxygenated by bubbling argon through 1 l. of the solution for 1 hr. The saturation was enhanced by frequent shaking.

Irradiations. Irradiations were carried out with a ^{60}Co source at a dose rate of 2.44×10^{16} eV/g min and a total dose of 1.46×10^{18} eV/g (determined by Fricke dosimetry with $G(Fe^{3+}) = 15.5$). The dosimetry was carried out by using the same bottles and volume as the irradiated solutions.

Analytical Procedure. Immediately after the irradiation the pH of the solution (1 l.) was adjusted to about 4–4.5 and then extracted once with 200 ml of ether and four times with 100 ml of ether. The ether extract was dried over 80 g of Na_2SO_4 for about 24 hr, and was then concentrated to 10 ml and analyzed by vapor phase chromatography using a hydrogen flame detector. The column was a 6-ft DEGS (diethyleneglycol succinate 5% liquid phase on Chromosorb W-AW-DMCS (100–120 mesh)) column at 170° and a flow of about 25 ml of He/min. The products appeared in the following sequence: benzyl alcohol (2.15 min), o-cresol (2.60 min), *m*- and *p*-cresol (3.35 min), dibenzyl (3.80 min). Dimethyldiphenyls had somewhat longer retention times than dibenzyl. The *m*- and *p*-cresol were separated on a 12-ft column (xylenylphosphate 5% liquid phase on Chromosorb W-AW-DMCS (100–120 mesh)) at 150° and a flow of about 25 ml of He/min. The following retention times were observed: benzyl alcohol (13.6 min), *o*-cresol (27.2 min), *p*-cresol (34.0 min), *m*-cresol (36.5 min). Standard aqueous cresol and benzyl alcohol solutions were prepared containing amounts of cresol and benzyl alcohol which were very close to the amounts present in the irradiated solutions and worked up in the same way. The G(dibenzyl) was determined from standard ether solutions of dibenzyl. All experiments were carried out in duplicate and triplicate and were found to be reproducible within the limits of the analytical technique (±5%). The smaller G values for benzyl alcohol (<0.5) are somewhat less accurate (±10%).

In presence of $K_3Fe(CN)_6$ at low pH (see experiments 23–26) much smaller G values were observed than in neutral solutions. In order to show that this effect is partly due to secondary oxidations of the cresols we proceeded as follows: 1 l. solutions of 2.7 mg of o-cresol, 1.35 mg of *m*-cresol, and 1.35 mg of *p*-cresol and 5×10^{-4} *M* $K_3Fe(CN)_6$ at pH 1.6 in one experiment and 5×10^{-2} *M* $K_3Fe(CN)_6$ in a second experiment were left standing at room temperature for 1 hr (same time as the irradiation time) and then worked up in the usual manner. The results show that there is considerable oxidation at both concentrations and that there is a slight preference for ortho–para oxidation.

Results and Discussion

The results in Table I show that at the higher metal salt concentration (5×10^{-2} *M*) we observe a high conversion of ·OH radicals (G(·OH) = 2.74)[6] to cresols. We, therefore, feel confident that the dose was low enough to render sec-

TABLE I: Yields of Cresols, Benzyl Alcohol, and Dibenzyl in the Radiolysis of Aqueous Toluene Solutions[a]

Expt no.	Conditions	G(Ph-CH_2OH)	G(Ph-$CH_2)_2$	G(cresols) Ortho	Meta	Para	G(total cresols)	% ortho	% meta	% para
1	$Cu(OCOCH_3)_2$ $5 \times 10^{-4} M$	0.1		1.05	0.18	0.56	1.79	58.7	10.1	31.3
2	$Cu(OCOCH_3)_2$ $10^{-3} M$	Trace		1.22	0.43	0.67	2.32	52.6	18.5	28.9
3	$Cu(OCOCH_3)_2$ $5 \times 10^{-3} M$	Trace		1.20	0.58	0.67	2.45	49.0	23.7	27.3
4	$CuSO_4$ $5 \times 10^{-4} M$	0.21		0.86	0.14	0.42	1.42	60.6	9.9	29.6
5	$CuSO_4$ $10^{-3} M$	0.18		1.12	0.22	0.53	1.87	59.9	11.8	28.3
6	$CuSO_4$ $5 \times 10^{-3} M$	0.15		1.37	0.43	0.69	2.49	55.0	17.3	27.7
7	$CuSO_4$ $5 \times 10^{-2} M$	Trace		1.28	0.55	0.72	2.55	50.2	21.6	28.2
8	$Cu(ClO_4)_2$ $5 \times 10^{-4} M$	0.2		0.83	0.14	0.40	1.37	60.6	10.2	29.2
9	$Cu(ClO_4)_2$ $10^{-3} M$	0.2		1.08	0.23	0.53	1.84	58.7	12.5	28.8
10	$Cu(ClO_4)_2$ $5 \times 10^{-3} M$ nat. pH 5.0	0.12		1.20	0.36	0.58	2.14	56.1	16.8	27.1
11	$Cu(ClO_4)_2$ $5 \times 10^{-2} M$ nat. pH 4.4	Trace		1.14	0.49	0.61	2.24	50.9	21.9	27.2
12	$Cu(ClO_4)_2$ $5 \times 10^{-3} M$ + $HClO_2$ $\sim 10^{-3} M$ pH 2.6	0.52		0.78	0.14	0.32	1.24	63.0	11.2	25.8
13	$Cu(ClO_4)_2$ $5 \times 10^{-3} M$ + $HClO_2$ $\sim 5 \times 10^{-2} M$ pH 2.0	1.65		Trace	Trace	Trace				
14	$K_2Cr_2O_7$ $5 \times 10^{-4} M$	0.34		1.42	0.41	0.49	2.32	61.0	17.7	21.1
15	$K_2Cr_2O_7$ $10^{-3} M$	0.33		1.44	0.48	0.54	2.46	58.5	19.5	22.0
16	$K_2Cr_2O_7$ $5 \times 10^{-3} M$	0.2		1.44	0.55	0.67	2.66	54.1	20.7	25.2
17	$K_2Cr_2O_7$ $5 \times 10^{-2} M$	0.1		1.54	0.64	0.80	2.98	51.7	21.5	26.8
18	$K_3Fe(CN)_6$ $5 \times 10^{-4} M$			1.08	0.51	0.57	2.16	50.0	23.6	26.4
19	$K_3Fe(CN)_6$ $10^{-3} M$			1.15	0.55	0.60	2.30	50.0	23.9	26.1
20	$K_3Fe(CN)_6$ $5 \times 10^{-3} M$			1.12	0.54	0.60	2.26	49.6	23.9	26.5
21	$K_3Fe(CN)_6$ $5 \times 10^{-2} M$			1.15	0.56	0.61	2.32	49.6	24.1	26.3
22	$K_3Fe(CN)_6$ $5 \times 10^{-4} M$ + $K_4Fe(CN)_6$ $5 \times 10^{-4} M$			0.94	0.46	0.49	1.89	49.8	24.3	25.9
23	$K_3Fe(CN)_6$ $5 \times 10^{-4} M$ pH 1.6[b]	Trace		0.96	0.12	0.53	1.61	59.6	7.5	32.9
24	$K_3Fe(CN)_6$ $10^{-3} M$ pH 1.6[b]	Trace		1.14	0.17	0.63	1.94	58.8	8.8	32.4
25	$K_3Fe(CN)_6$ $5 \times 10^{-3} M$ pH 1.6[b]			0.88	0.39	0.45	1.72	51.2	22.7	26.2
26	$K_3Fe(CN)_6$ $5 \times 10^{-2} M$ pH 1.6[b]			0.36	0.30	0.21	0.87	41.4	34.5	24.1
27	$K_3Fe(CN)_6$ $10^{-3} M$ + $K_4Fe(CN)_6$ $5 \times 10^{-4} M$ pH 1.6[b]			1.06	0.16	0.60	1.82	58.2	8.8	33.0
28	$Fe(ClO_4)_3$ $5 \times 10^{-4} M$ nat. pH 3.4	0.14	1.07	Trace	Trace	Trace	Trace			
29	$Fe(ClO_4)_3$ $5 \times 10^{-3} M$ nat. pH 2.6	2.0	0.1	0.26		0.20	0.46	56.5	0	43.5
30	$Fe(ClO_4)_3$ $5 \times 10^{-2} M$ nat. pH 2.0	1.60		0.74		0.60	1.34	55.3	0	44.7
31	$Fe(NH_4)(SO_4)_2$ $5 \times 10^{-4} M$ nat. pH 3.0		1.08	Trace						
32	No additives[c]	0.02	0.02	0.22	0.09	0.14	0.45	48.9	20.0	31.1

[a] All solutions were deoxygenated solutions ($5 \times 10^{-3} M$ toluene) irradiated at a dose rate of 2.44×10^{16} eV/g min, and a total dose of 1.46×10^{18} eV/g. [b] The pH was adjusted with H_2SO_4. [c] Results taken from ref 4.

TABLE II: Dose Dependence of G(Cresols) at Low Cu^{2+} Salt Concentration ($5 \times 10^{-4} M$)[a]

Conditions	Total dose, eV/l.	G(ortho)	G(meta)	G(para)	Total G(cresols)	% ortho	% meta	% para
$Cu(OCOCH_3)_2$	4.9×10^{20}	1.28	0.22	0.68	2.18	58.6	10.2	31.2
$Cu(OCOCH_3)_2$	1.46×10^{21}	1.05	0.18	0.56	1.79	58.6	10.1	31.3
$CuSO_4$	4.9×10^{20}	1.24	0.19	0.58	2.01	61.8	9.3	28.9
$CuSO_4$	1.46×10^{21}	0.86	0.14	0.42	1.42	60.5	9.9	29.6
$Cu(ClO_4)_2$	4.9×10^{20}	1.08	0.17	0.49	1.74	62.0	9.8	28.2
$Cu(ClO_4)_2$	1.46×10^{21}	0.83	0.14	0.40	1.37	60.7	10.1	29.2

[a] All solutions were deoxygenated solutions ($5 \times 10^{-3} M$ toluene) irradiated at a dose rate of 2.44×10^{16} eV/g min.

Scheme I

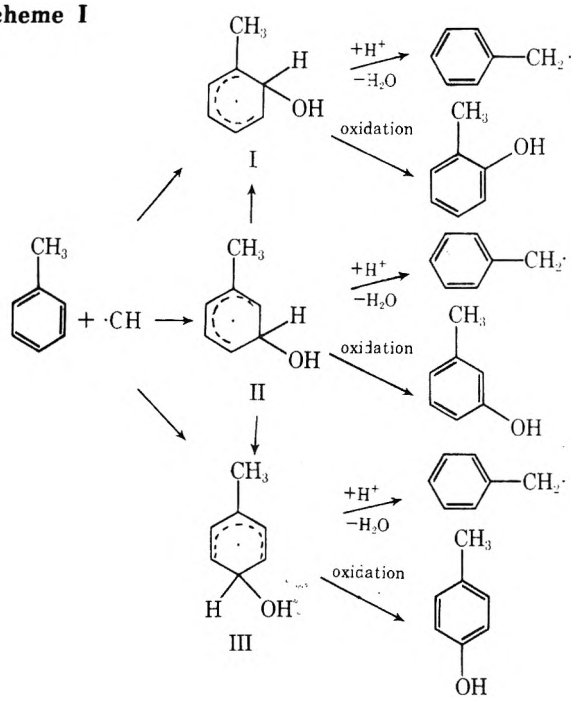

ondary reactions insignificant. At the lowest Cu^{2+} concentration (5×10^{-4} M) we have investigated a lower dose (4.98×10^{17} eV/g) and we found an increase in G(total cresols) but the percentage composition of the cresols did not change (see Table II). The high G(cresols) at the higher metal salt concentrations confirms previous conclusions[7] that the initial step in the reaction of ·OH radicals with toluene is addition at the ring positions rather than abstraction from the methyl group (Scheme I). The fate of the metal ions was not investigated quantitatively, but in the case of Cu^{2+} salts the formation of metallic copper was observed. The oxidation of the hydroxymethylcyclohexadienyl radicals I–III competes with the acid-catalyzed dehydration and the radical shifts (II → I and II → III). The acid-catalyzed formation of benzyl radicals from hydroxymethylcyclohexadienyl radicals was first reported by Norman and coworkers[8] in the hydroxylation of toluene by Fenton's reagent. Subsequently, the kinetics of this reaction was studied by pulse radiolysis[7] and it was shown that the rate of benzyl radical formation is proportional to the proton concentration, and the pseudo-first-order rate constant was found to be $1.1 \pm 0.04 \times 10^6$ M^{-1} sec^{-1}. One may speculate that the mechanism of this water elimination proceeds via protonation of the hydroxyl and formation of a radical cation, followed by a rapid deprotonation from the methyl group:

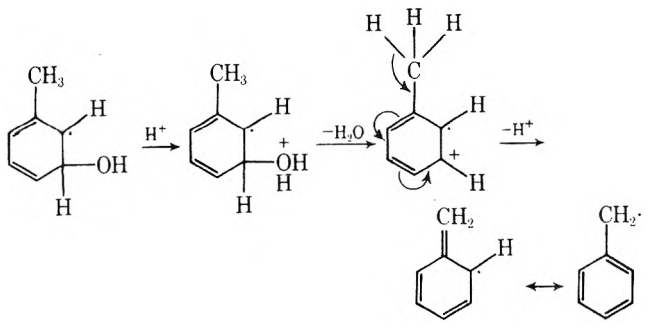

The elimination of water and the deprotonation may proceed synchronously as was suggested by Norman and coworkers.[8] Recently Walling and Johnson[9] have postulated the radical cation as a distinct intermediate. The above shown water elimination is particularly favorable from the meta hydroxyl radical adduct since the developing positive charge is stabilized by the hyperconjugating methyl group. The competition between oxidation and dehydration can be seen from the result with $Fe(ClO_4)_3$. With increasing $Fe(ClO_4)_3$ concentration the ratio Fe^{3+}/H^+ is increasing and so is the yield of cresols while the yields of benzyl radical derived products is decreasing. The same effect was observed with $Cu(ClO_4)_2$ (experiments 10, 12, 13). The cresol isomer distributions in our experiments with $Fe(ClO_4)_3$ are in excellent agreement with the isomer distribution obtained recently by Walling and Johnson[9] in the hydroxylyation with Fenton's reagent. However we observe a quantitative conversion of OH radicals to products.

While the pH has a marked effect on the product distribution if $Fe(ClO_4)_3$, $Fe(NH_4)(SO_4)_2$, or $Cu(ClO_4)_2$ are used as oxidizing agents, the pH effect is rather small at the lower concentrations of $K_3Fe(CN)_6$. The G(o-cresol) and G(p-cresol) does not change much, whereas the G(m-cresol) is decreasing substantially. (Compare experiments 18 and 19 with 23 and 24.) This decrease in G(meta) at low pH can be due to several factors: (1) a selective oxidation of m-cresol; (2) a selective reduction of the meta adduct (II) by $Fe(CN)_6^{4-}$; (3) a slower rate of oxidation of the meta adduct (II); (4) a faster rate of dehydration of the meta adduct (II). We studied the reaction of $K_3Fe(CN)_6$ (5×10^{-4} M) in acidic solutions (pH 1.6) with cresols (5×10^{-4} M) and we find no selective oxidation of m-cresol, but rather a slight preference for ortho–para oxidation. (See Experimental Section.) The experiments in presence of $K_4Fe(CN)_6$ at pH 1.6 and neutral solutions (experiments 27 and 22) show that there is no reduction of any of the isomeric hydroxymethylcyclohexadienyl radicals. A slower rate of oxidation of the m-hydroxymethylcyclohexadienyl radical at low pH compared to neutral solution appears unlikely in view of previous results[5] on the hydroxylation of nitrobenzene with $K_3Fe(CN)_6$ at low pH. A faster rate of acid-catalyzed dehydration from the meta adduct (II) compared to the ortho and para adducts (I and III) appears a reasonable assumption considering the arguments concerning the mechanism presented above.

The considerable difference in isomer distribution between the Cu^{2+} and Fe^{3+} experiments was explained by Walling and Johnson[9] on the basis of the different oxidation mechanisms by these two metal ions. The oxidation with Fe^{3+} involves the formation of a carbonium ion intermediate which can undergo 1,2 hydroxyl anion shifts to produce mainly o- and p-cresol. Norman and coworkers[8] on the other hand have concluded that the electron transfer and the deprotonation proceed synchronously. The percentage of m-cresol increases with increasing metal ion concentration with the exception of $K_3Fe(CN)_6$. This increase in G(meta) with increasing metal salt concentration was observed previously in the hydroxylation of nitrobenzene[5] and benzoic acid.[10] Radical rearrangements have been suggested as explanation for this observation. In the case of hydroxymethylcyclohexadienyl radicals analogous rearrangements may take place to give the more stable ortho and para hydroxyl radical adducts[3] (II → I, and II → III). In the case of the hydroxymethylcyclohexadienyl radicals the rearrangement may proceed via a reversible water elimination. Strong evidence for this reaction was presented by Walling and Camaioni[11] in the hydroxylation of ben-

zene and toluene by $SO_4\cdot^-$. This reversible water elimination however was not observed in the hydroxylation of phenol, chlorobenzene, and nitrobenzene.[12] The increase in G(meta) with increasing metal salt concentration, may, however be solely due to a competition between oxidation and dehydration, assuming a greater rate constant for dehydration of the meta radical (II) than of the ortho and para isomer (I and III).

Contrary to the hydroxynitrocyclohexadienyl radicals where the ortho and para isomers are selectively reduced by $Fe(CN)_6^{4-}$ no reduction of the three isomeric hydroxymethylcyclohexadienyl radicals by $Fe(CN)_6^{4-}$ was observed (experiments 21 and 27). Only those radicals which have an electron-withdrawing substituent α to the radical site undergo reduction. This observation is in agreement with results of Walling and coworkers[13] on the redox reactions of α-hydroxyalkyl radicals with Fe^{3+}–Fe^{2+}.

With $K_3Fe(CN)_6$ in neutral solutions we do not find any change in G(cresols) nor in the isomer distribution with increasing concentration (experiments 18–21). This observation together with the minor change at low pH indicates that the oxidation by $K_3Fe(CN)_6$ must be a fast process. This fast oxidation by $K_3Fe(CN)_6$ was also observed in the hydroxylation of nitrobenzene at low pH. We, therefore, suggest that the cresol isomer distribution obtained with $K_3Fe(CN)_6$ represents the relative reactivity of ·OH radicals toward the different positions in the toluene molecule. At the higher metal ion concentration (5×10^{-2} M) of the Cu^{2+} salts and $K_2Cr_2O_7$ we observed almost the same isomer distribution as with $K_3Fe(CN)_6$. From these results the relative reactivity appears to be approximately 2:1:1. This preference for ortho–para substitution is to be expected on the basis of the well-known electrophilic character of the ·OH radical.[3,14] From the results in Table I we can see that $Cu(ClO_4)_2$ at a concentration of 5×10^{-3} M and a pH of 2.6 gives more G(cresols) and less G(benzyl alcohol) than $Fe(ClO_4)_3$ at the same concentration and pH. From this we conclude that Cu^{2+} oxidizes the hydroxymethylcyclohexadienyl radicals faster than does Fe^{3+}. We have, therefore, the following reactivity sequence for oxidation: $Fe(CN)_6^{3-} > Cu^{2+} > Fe^{3+}$.

References and Notes

(1) This paper was prepared in connection with work under Contract No. AT(40-1)-1833 with The U S. Atomic Energy Commission.
(2) E. J. Fendler and J. H. Fendler, *Prog. Phys. Org. Chem.*, **8**, 229 (1970).
(3) M. K. Eberhardt and M. Yoshida, *J. Phys. Chem.*, **77**, 589 (1973).
(4) H. C. Christensen and R. Gustafsson, *Acta Chem. Scand.*, **26**, 937 (1972).
(5) M. K. Eberhardt, *J. Phys. Chem.*, preceding article in this issue.
(6) B. H. J. Bielski and A. O. Allen, *Int. J. Radiat. Phys. Chem.*, **1**(2), 153 (1969).
(7) H. C. Christensen, K. Sehested, and E. J. Hart, *J. Phys. Chem.*, **77**, 983 (1973).
(8) C. R. E. Jefcoate, J. R. Lindsay Smith, and R. O. C. Norman, *J. Chem. Soc. B*, 1013 (1969).
(9) C. Walling and R. A. Johnson, *J. Am. Chem. Soc.*, **97**, 363 (1975).
(10) O. Volkert and D. Schulte-Frohlinde, *Tetrahedron Lett.*, **No. 17**, 2151 (1968).
(11) C. Walling and D. M. Camaioni, *J. Am. Chem. Soc.*, **97**, 1603 (1975).
(12) L. G. Shevchuck and N. A. Vysotskaya, *Zh. Org. Khim.*, **4**, 1936 (1968).
(13) C. Walling and G. M. El-Taliawi, *J. Am. Chem. Soc.*, **95**, 844 (1973); C. Walling, G. M. El-Taliawi, and R. A. Johnson, *ibid.*, **96**, 133 (1974).
(14) M. Anbar, K. Meyerstein, and P. Neta, *J. Phys. Chem.*, **70**, 2660 (1966).

Kinetics and Mechanism of the Osmium Tetroxide Catalyzed Oxidation of 2-Propanol and 1-Propanol by the Hexacyanoferrate(III) Ion in Aqueous Alkaline Medium

H. S. Singh,* S. P. Singh, S. M. Singh, R. K. Singh, and A. K. Sisodia

Department of Chemistry, University of Allahabad, Allahabad, India

(Received April 25, 1974; Revised Manuscript Received June 4, 1975)

A study is reported of the hexacyanoferrate(III) oxidations of 2-propanol and 1-propanol in the presence of osmium tetroxide as catalyst. The kinetic data suggest that the oxidation of these alcohols proceeds via the formation of an activated complex between the alcohol molecule and osmium tetroxide which rapidly decomposes to an intermediate product and osmium(VI) species. The osmium(VI) thus produced is rapidly oxidized to osmium(VIII) with hexacyanoferrate(III) ion. The oxidation products are determined and a possible set of reactions for their formation is presented.

Introduction

Sussela[1] and Solymosi[2] have studied, from an analytical point of view, the oxidation of a number of organic compounds with hexacyanoferrate(III) in aqueous alkaline medium using osmium tetroxide as a homogeneous catalyst. We were the first to examine the kinetic features of the osmium tetroxide catalyzed oxidation of methanol and ethanol[3] by hexacyanoferrate(III) ion in aqueous alkaline medium. Recently, we have also studied the kinetic features of osmium tetroxide catalyzed oxidation of ketones,[4] aldehydes,[5] α-hydroxy acids,[6] and diols[7] with hexacyanoferrate(III) in aqueous alkaline medium. However, the mechanism of oxidation of monohydric alcohols has yet not been studied and in the present study we have carried out the oxidation of 2-propanol and 1-propanol by aqueous alkaline hexacyanoferrate(III) ion using osmium tetroxide as a

homogeneous catalyst. The details of the results are presented and accordingly a reaction mechanism has been proposed.

Experimental Section

Materials. (i) An aqueous solution of potassium hexacyanoferrate(III) was always prepared from an Analar (BDH) grade sample. (ii) An aqueous solution of 1-propanol and 2-propanol was prepared daily from the Merck sample of G.R. grade. The alcohols were redistilled and the fractions boiling at 97.5 and 82.0° for 1-propanol and 2-propanol, respectively, were collected for the kinetic measurements. The solution of osmium tetroxide was prepared by dissolving the sample (Johnson Mattey & Co. Ltd.) in a solution of potassium hydroxide. The final strengths of KOH and that of OsO_4 were kept 5.00×10^{-2} and 3.93×10^{-3} M, respectively. The samples of sodium hydroxide and potassium chloride were of G.R. (S. Merck) grade.

The kinetic experiments were followed by adding the required quantity of the alcohol solutions maintained at a constant temperature to the solution of $K_3Fe(CN)_6$, NaOH, and OsO_4 kept in a reaction bottle at the same temperature. The temperature of the reaction mixture was kept constant with an electrically operated thermostat with an accuracy of ±0.1°.

The progress of the reaction was measured by estimating the amount of hexacyanoferrate(II) ion produced after a definite time interval with a standard solution of ceric(IV) sulfate, using ferroin as a redox indicator. This method always gave reproducible results. The final oxidation products were confirmed with paper chromatographic[8] studies.

Results and Discussion

Details of the kinetic data for the rate of osmium tetroxide catalyzed oxidation of 2-propanol and 1-propanal are presented in the Table I and Figures 1–5. The ionic strength of the medium was kept constant with potassium chloride.

Figure 1 shows a zero-order plot for the rate of oxidation of 2-propanol and 1-propanol. It is obvious from these plots that the zero-order velocity constants begin to increase after a certain stage of the reaction. From these data we may conclude that these increases in the zero-order rate constant values are due to further oxidation of the intermediate product. In order to avoid the possible intervention of the products, the initial reaction velocity $-(dc/dt)$ was calculated by plotting the remaining hexacyanoferrate(III) vs. time. The initial $-dc/dt$ values at different initial hexacyanoferrate(III) ion concentrations are listed in Table I and show the reaction rate to be independent of hexacyanoferrate(III) ion concentration.

The exact dependence of the reaction rate on hydroxyl ion concentration is shown graphically in Figure 2, which shows that at low $[OH^-]$ levels the reaction rate follows first-order dependence and become independent at higher concentration.

It has been observed that the order of the reaction is one with respect to both alcohol and osmium tetroxide (Figures 3 and 4). This gives rise to a rate law equation at very low hydroxyl ion concentration as

$$-d[Fey]/dt = k[S][OH^-][OsO_4] \quad (1)$$

where $[Fey] = [Fe(CN)_6]^{3-}$ and $[S] = [\text{alcohol}]$.

The value of k is calculated as 4.36×10^2 and 5.15×10^2 M^{-2} min^{-1} for 2-propanol and 1-propanol, respectively.

TABLE I[a]

A: [1-Propanol] = 0.05 M, [NaOH] = 0.05 M, [OsO_4] = 1.94×10^{-5} M		B: [2-Propanol] = 0.10 M, [NaOH] = 0.05 M, [OsO_4] = 1.83×10^{-5} M	
$[K_3Fe(CN)_6]$, $M \times 10^3$	$[-dc/dt] \times 10^5$, M min^{-1}	$[K_3Fe(CN)_6]$, $M \times 10^3$	$[-dc/dt] \times 10^5$, M min^{-1}
1.0	2.20	1.0	1.60
1.5	2.24	2.0	1.70
2.0	2.15	3.0	2.00
3.0	2.20	4.0	2.00
4.0	2.20	5.0	1.94
5.0	2.20	6.0	1.94
6.0	2.20	8.0	1.90
8.0	2.20	10.0	1.94
10.0	2.20		

[a] Temp = 30°, μ = 0.5 M.

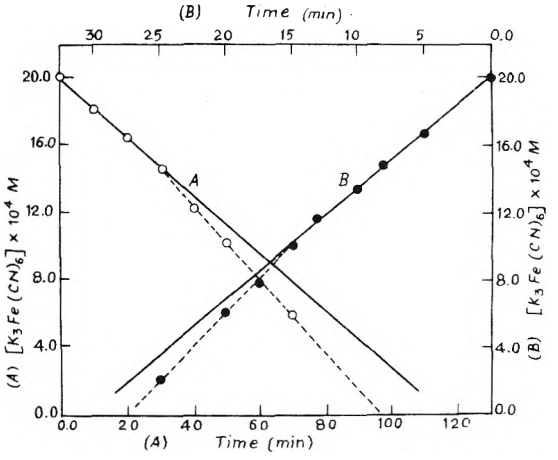

Figure 1. Reaction feature with respect to ferricyanide: (A) $K_3Fe(CN)_6$ 2.00×10^{-3} M, 1-propanol 0.10 M, NaOH 1.0×10^{-2} M, OsO_4 1.04×10^{-5} M, μ = 0.5 M, temp = 30°; (b) $K_3Fe(CN)_6$ 2.00×10^{-3} M, 2-propanol 0.3 M, NaOH 0.11 M, OsO_4 1.830×10^{-5} M μ = 0.5 M, temp = 30°.

The osmium tetroxide in alkaline medium has been reported to exist as octahedral complexes of the form[9] trans $[OsO_4(OH)(H_2O)]^{1-}$ and $[OsO_4(OH)_2]^{2-}$. The existence of these species might be considered via equilibrium step I of the proposed reaction scheme. It is also observed that the $OsO_4(OH)_2^{2-}$ is the only reacting species of the osmium tetroxide.[10]

On the basis of the above-mentioned experimental results, the following probable oxidation scheme of these alcohols can be proposed:

$$\underset{(C)}{OsO_4(H_2O)(OH)^{1-}} + [OH^-] \overset{K_1}{\rightleftharpoons} \underset{(C_1)}{OsO_4(OH)_2^{2-}} + H_2O \quad (I)$$

$$\underset{(C_1)}{OsO_4(OH)_2^{2-}} + S \overset{K_2}{\rightleftharpoons} \text{complex } (C_2) \quad (II)$$

$$C_2 \xrightarrow[\text{(slow)}]{k_1} Os(VI) + \text{intermediate products} \quad (III)$$

This scheme shows that osmium tetroxide forms an activated complex (C_2) which disproportionates slowly into a

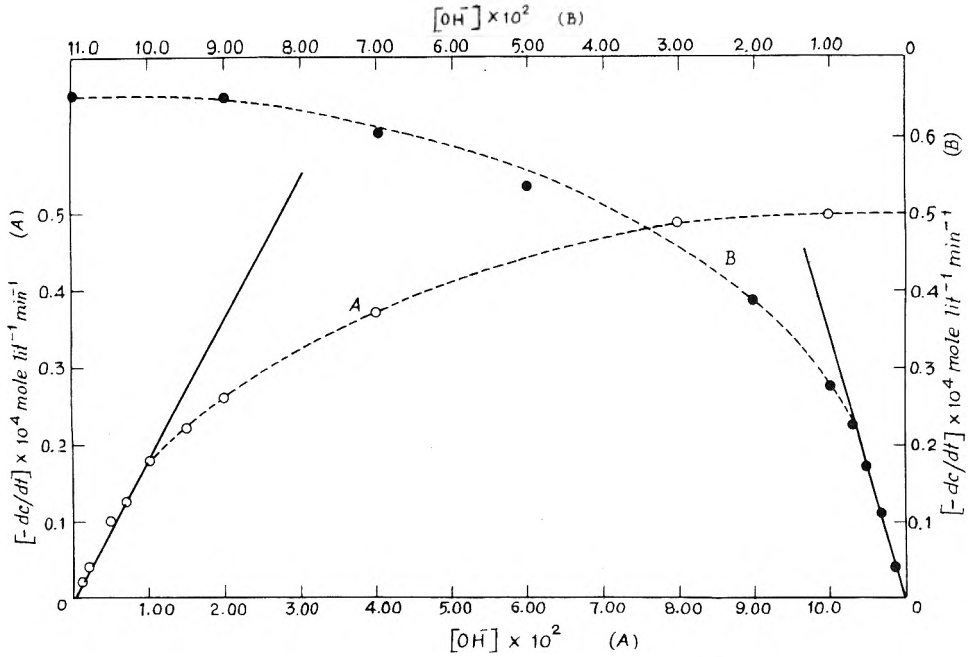

Figure 2. Effect of hydroxide ion concentration on the reaction rate: (A) $K_3Fe(CN)_6$ 2.00 × 10^{-3} *M*, 1-propanol 0.10 *M*, OsO_4 1.94 × 10^{-5} *M*, μ = 0.5 *M*, temp = 30°; (B) $K_3Fe(CN)_6$ 2.00 × 10^{-3} *M*, 2-propanol 0.3 *M*, OsO_4 1.83 × 10^{-5} *M*, μ = 0.5 *M*, temp = 30°.

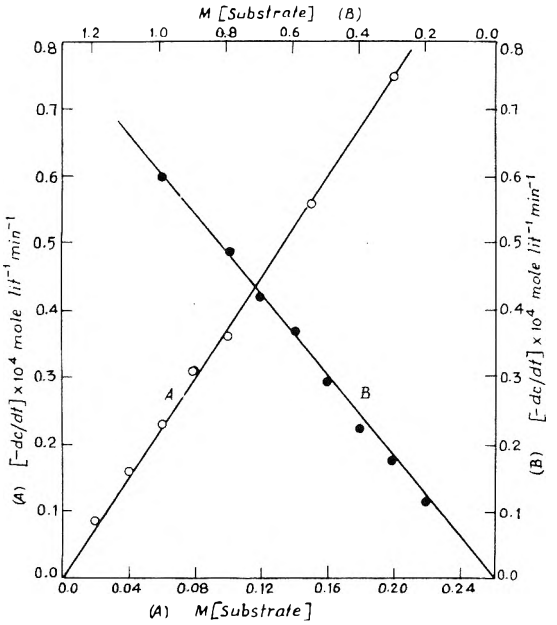

Figure 3. Effect of variation of substrate on the reaction rate: (A) (1-propanol) $K_3Fe(CN)_6$ 2.00 × 10^{-3} *M*, NaOH 5.0 × 10^{-2} *M*, OsO_4 1.94 × 10^{-5} *M*, μ = 0.5 *M*, temp = 30°; (B) (2-propanol) $K_3Fe(CN)_6$ 2.00 × 10^{-3} *M*, NaOH 5.0 × 10^{-3} *M*, OsO_4 1.83 × 10^{-5} *M*, μ = 0.5 *M*, temp = 30°.

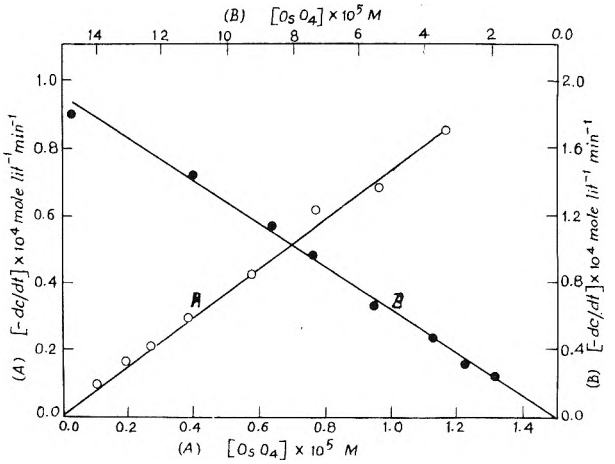

Figure 4. Effect of variation of OsO_4 on the reaction rate: (A) $K_3Fe(CN)_6$ 2.00 × 10^{-3} *M*, 1-propanol 0.05 *M*, NaOH 0.02 *M*, μ = 0.5 *M*, temp = 30°; (B) $K_3Fe(CN)_6$ 2.00 × 10^{-3}, 2-propanol 0.30 *M*, NaOH 7.0 × 10^{-3} *M*, μ = 0.5 *M*, temp = 30°.

first intermediate product and the hexavalent osmium, which in turn is reoxidized to its original oxidation state in two fast steps by the hexacyanoferrate(III) ion. The first product undergoes fast oxidation taking more of Os(VIII) and $Fe(CN)_6^{3-}$. Under such conditions, it is better to express the final rate law in terms of the total osmium(VIII) concentration.

$$[\mathrm{Os(VIII)}]_T = C + C_1 + C_2 \qquad (2)$$

Now considering eq 2 the final rate law in terms of the decreasing concentration of the hexacyanoferrate(III) would be

$$\frac{-\mathrm{d[Fey]}}{dt} = \frac{2k_1K_1K_2[\mathrm{S}][\mathrm{OH^-}][\mathrm{Os(VIII)}]_T}{1 + K_1[\mathrm{OH^-}][1 + K_2[\mathrm{S}]]} \qquad (3)$$

Since first-order kinetics was obtained with respect to alcohol concentration, the inequality $1 \gg K_2[\mathrm{S}]$ will evidently exist and rate eq 3 is reduced to

$$\frac{-\mathrm{d[Fey]}}{dt} = \frac{2k_1K_1K_2[\mathrm{S}][\mathrm{OH^-}][\mathrm{Os(VIII)}]_T}{1 + K_1[\mathrm{OH^-}]} \qquad (4)$$

The derived rate eq 4 exhibits the observed kinetics. At very low hydroxide ion concentration the inequality $1 \gg K_1[\mathrm{OH^-}]$ is evident and rate eq 4 is reduced to

$$-\frac{\mathrm{d[Fey]}}{dt} = 2k_1K_1K_2[\mathrm{S}][\mathrm{OH^-}][\mathrm{Os(VIII)}]_T \qquad (5)$$

This explains the first-order kinetics of the reaction rate with respect to alcohol, hydroxyl ion, and osmium tetroxide concentration as well as the zero-order kinetics of the reac-

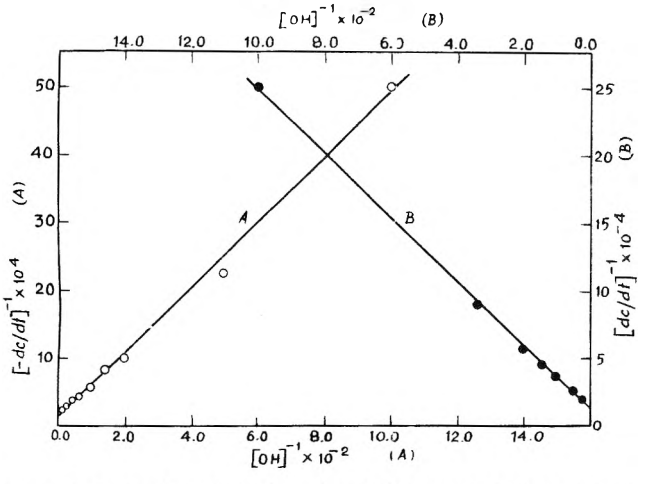

Figure 5. Plot of $[-dc/dt]^{-1}$ vs. $[OH^-]^{-1}$ for (a) $K_3Fe(CN)_6$ 2.00 × 10^{-3} *M*, 1-propanol 0.10 *M*, OsO_4 1.94 × 10^{-5} *M*, μ = 0.5 *M*, temp 30°; (B) $K_3Fe(CN)_6$ 2.00 × 10^{-3} *M*, 2-propanol 0.3 *M*, OsO_4 1.83 × 10^{-5} *M*, μ = 0.5 *M*, temp 30°.

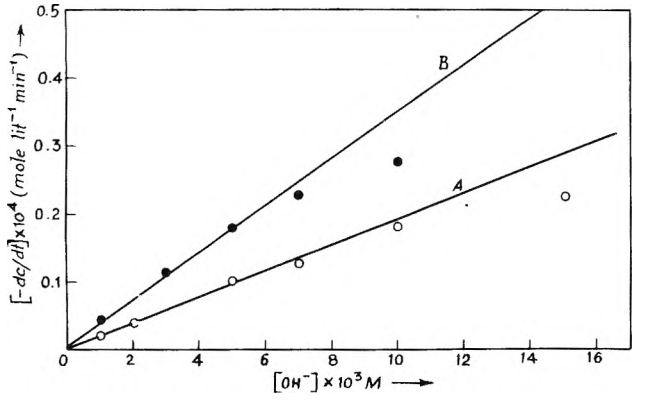

Figure 6. Effect of low hydroxide ion concentration on the reaction rate. Caption same as Figure 2.

tion with respect to the concentration of the hexacyanoferrate(III) ion. The values of $k_1K_1K_2$ were calculated and these are 4.36 × 10^2 and 5.15 × 10^2 at 30° for 2-propanol and 1-propanol, respectively.

At higher concentration of hydroxide ion the value of K_1 will be quite large and the inequality $K_1[OH^-] \gg 1$ would dominate and rate eq 4 is reduced to

$$-\frac{d[Fey]}{dt} = 2k_1K_2[S][Os(VIII)]_T \quad (6)$$

This clearly explains the zero-order kinetics with respect to hydroxide ion concentration. Under such conditions the values of k_1K_2 obtained are 5.90 and 1.3 × 10^1 for 2-propanol and 1-propanol, respectively, at 30°.

Again rate eq 4 might be written as

$$\frac{1}{-d[Fey]/dt} = \frac{1}{2k_1K_1K_2[S][OH^-][Os(VIII)]_T} + \frac{1}{2k_1K_2[S][Os(VIII)]_T} \quad (7)$$

which shows that a plot of 1/[reaction velocity] vs. 1/[hydroxide ion], should give a straight line with a positive intercept at the *y* axis. Such plots are shown in Figure 5. This again shows the validity of the rate eq 4. The values of $k_1K_1K_2$ and k_1K_2 obtained from the slope and intercept of the plots (Figure 5) are as follows:

$k_1K_1K_2$	k_1K_2	
4.24 × 10^2	6.49 × 10^1	2-propanol
5.72 × 10^2	1.51 × 10^1	1-propanol

The close agreement in $k_1K_1K_2$ values obtained by the different methods (from eq 5 and 7) substantiates the validity of rate eq 4. Similarly, the values of k_1K_2 obtained by two different methods (from eq 6 and 7) further indicate the validity of rate eq 4, and hence confirm the proposed reaction mechanism.

In the oxidation of these alcohols the chromatographic study confirms the formation of oxidation products of oxalic acid and acetic acid in 2-propanol and propionic acid in 1-propanol. On the basis of these experimental results the full sequence of the steps would be

$$OsO_4(OH)_2^{2-} + CH_3CH_2CH_2OH \overset{K_2}{\rightleftharpoons}$$

1-propanol

$$[CH_3CH_2CH_2{-}O{-}OsO_3(OH)_3]^{2-} \quad (II)$$

(C_2)

$$[CH_3CH_2CH_2{-}O{-}OsO_3(OH)_3]^{2-} \xrightarrow[\text{slow}]{k_1}$$

(C_2)

$$CH_3CH_2CHO + OsO_2(OH)_4^{2-} \quad (III)$$

$$OsO_2(OH)_4^{2-} + 2OH^- + 2Fe(CN)_6^{3-} \xrightarrow{\text{fast}}$$

$$OsO_4(OH)_2^{2-} + 2Fe(CN)_6^{4-} + 2H_2O$$

$$CH_3CH_2CHO \xrightarrow[\text{fast}]{(O)} CH_3CH_2COOH$$

propion-aldehyde — propionic acid

Similarly with 2-propanol the following steps might again be proposed

$$OsO_4(OH)_2^{2-} + \begin{matrix}H_3C\\H_3C\end{matrix}\!\!>\!CHOH \overset{K_2}{\rightleftharpoons}$$

$$\left[\begin{matrix}H_3C\\H_3C\end{matrix}\!\!>\!CH{-}O{-}OsO_3(OH)_3\right]^{2-} \quad (II)$$

complex (C_2)

$$\left[\begin{matrix}H_3C\\H_3C\end{matrix}\!\!>\!CH{-}O{-}OsO_3(OH)_3\right]^{2-} \xrightarrow[\text{slow}]{k_1}$$

(C_2)

$$\begin{matrix}H_3C\\H_3C\end{matrix}\!\!>\!C{=}O + OsO_2(OH)_4^{2-} \quad (III)$$

(acetone)

$$\begin{matrix}H_3C\\H_3C\end{matrix}\!\!>\!C{=}O \xrightarrow[\text{fast}]{O} \begin{matrix}H_3C\\HOH_2C\end{matrix}\!\!>\!C{=}O \xrightarrow[\text{fast}]{O} CH_3{-}\overset{O}{\overset{\|}{C}}{-}CHO \xrightarrow[\text{fast}]{O}$$

$$CH_3{-}\overset{O}{\overset{\|}{C}}{-}COO^- \xrightarrow[\text{fast}]{O} \begin{cases} CH_3COO^- & \text{(acetic acid)} \\ COO^- \\ | \\ COO^- & \text{(oxalic acid)} \end{cases}$$

The oxidation products for acetone are reported to be oxalic acid (80%) and acetic acid (20%) with alkaline permanganate.[11] With hexacyanoferrate(III) in the carbonate–bicarbonate buffer these oxidation products were also confirmed chromatographically.[4] Therefore, in the osmium tetroxide catalyzed oxidation of 2-propanol by hexacyanoferrate(III) the oxalic acid and acetic acid will be approximately in the same ratio.

In the proposed complex (C_2), the osmium will be in the eight coordination number, but the water molecule is not included in the complex (C_2) only due to the simple structure of the molecule. The osmium(VI) species,[10b] $OsO_2(OH)_4^{2-}$, obtained after disproportionation of the complex (C_2) is shown to be oxidized fast with the hexacyanoferrate(III) in the next step in order to regenerate the osmium(VIII) species.

If we compare the $k_1K_1K_2$ and k_1K_2 values in both cases, it can be shown that the rate of oxidation is in the order 1-propanol > 2-propanol, due to steric and inductive effect the rate of complex formation in 2-propanol and its decomposition will be slow when compared to 1-propanol.

The abnormal increase in the velocity constant after a certain fraction of the reaction might be explained as due to fast oxidation of acetone and propionaldehyde obtained as the intermediate product from 2-propanol and 1-propanol, respectively (Figure 1). Thus, in order to determine the actual nature of the reaction the initial reaction velocity was determined and the results are explained accordingly.

Acknowledgment. Authors are thankful to the S.C.S.I.R., Lucknow (India) for financial assistance.

References and Notes

(1) N. Sussela, *Z. Anal. Chem.*, **145**, 175 (1955).
(2) F. A. Solymosi, et al, *Magy. Kem. Foly.*, **62**, 318 (1957).
(3) B. Krishna and H. S. Singh, *Z. Phys. Chem.*, **231**, 399 (1966).
(4) V. N. Singh, H. S. Singh, and B. B. L. Saxena, *J. Am. Chem. Soc.*, **91**, 2643 (1969).
(5) P. C. Pandey, V. N. Singh, and M. P. Singh, *Indian J. Chem.*, **9**, 430 (1971).
(6) N. P. Singh, V. N. Singh, and M. P. Singh, *Aust. J. Chem.*, **21**, 2913 (1968); N. P. Singh, V. N. Singh, H. S. Singh, and M. P. Singh, *Aust. J. Chem.*, **23**, 921 (1970).
(7) H. S. Singh and V. P. Singh, unpublished work.
(8) R. D. Hartly and G. J. Lawson, *J. Chromatogr.*, **4**, 410 (1960).
(9) J. S. Mayell, *Ind. Eng. Chem.*, **7**, 129 (1968).
(10) (a) W. P. Griffith, *Quart. Rev.*, **19**, 254 (1965). (b) F. A. Cotton and G. Wilkinson, "Advanced Inorganic Chemistry", 2nd ed. Wiley, New York, N.Y., pp 1007 and 993.
(11) W. L. Evans and E. J. Wilzemann, *J. Am. Chem. Soc.*, **34**, 1096 (1912).

Thermochemical Properties of Ammonium Exchanged Type L Zeolite

Thomas J. Weeks, Jr.,* and A. P. Bolton

Linde Division, Union Carbide Corporation, Tarrytown Technical Center, Tarrytown, New York 10591 *(Received March 7, 1975)*

Publication costs assisted by Union Carbide Corporation

The thermochemical properties of ammonium exchanged type L zeolite (NH_4KL) have been examined by infrared spectroscopy, thermal analysis, and high-temperature X-ray diffractometry. Differential thermal analysis of NH_4KL in air shows an ammonia oxidation exotherm at 515°. Thermogravimetric analysis indicates that deammoniation and dehydroxylation overlap between 300 and 700°. Infrared spectra show that water can be removed by evacuation at room temperature and that a single weak zeolitic hydroxyl band occurs at 3630 cm^{-1}; major changes occur in the framework region upon deammoniation. High-temperature X-ray diffractometry indicates that thermal stability of NH_4KL is very dependent on bed configuration during firing. A sample fired in a thin bed loses crystallinity at 500° while one fired in a thick bed retains crystallinity until 800°. Cell constants are relatively invariant with temperature.

Introduction

Type L is a large pore (~8 Å) synthetic zeolite with a high silica content ($SiO_2/Al_2O_3 \sim 6$).[1] It possesses an hexagonal crystal structure and is composed of alternating cancrinite cages and double six rings arranged in connected columns. This gives rise to a large channel along the crystallographic c axis and a pore volume of 0.21 g of H_2O/g of zeolite.

Typical unit cell composition is $K_9[(AlO_2)_9(SiO_2)_{27}]\cdot 22H_2O$; approximately 20% of the potassium is not exchangeable. There have been a few investigations on the adsorption properties of cation exchanged[2] and acid extracted type L,[3,4] but little has been published on its catalytic activity. This may be due partly to the fact that the thermochemical properties of the ammonium exchanged form (a common catalyst precursor) have not been investigated. This is a study of those changes which occur upon thermal treatment of NH_4KL as determined by thermal analysis, infrared spectroscopy, and X-ray diffractometry. The effect of bed configuration during calcination is also discussed.

Experimental Section

Materials. Synthetic KNaL (obtained as SK-45 from the Linde Division, Union Carbide Corp.) was exchanged four times with 10% aqueous NH_4Cl at reflux temperature. Deep bed calcined material was prepared by placing NH_4KL in a preheated nonpurged muffle furnace at 800° for 1 hr; the zeolite was in an uncovered porcelain crucible and had a depth to diameter ratio of 3 to 1. This material was subjected to a single exchange with 10% aqueous NH_4Cl at reflux. Analyses of the starting KNaL (1), NH_4KL (2), and the ammonium exchanged deep bed calcined NH_4KL (3) are presented below. Oxygen capacity was determined at −183° and 100 mmHg following vacuum activation of 5-g pellets at 400° for 4 hr.

Wt %	(1)	(2)	(3)
SiO_2	64.3	68.4	74.3
Al_2O_3	18.1	19.2	20.5
Na_2O	0.8		
K_2O	16.0	3.6	2.3
$(NH_4)_2O$		7.1	1.3
Mole ratio			
SiO_2/Al_2O_3	6.03	6.04	6.15
K_2O/Al_2O_3	0.96	0.20	0.12
Na_2O/Al_2O_3	0.07		
$(NH_4)_2O/Al_2O_3$		0.73	0.12
O_2 capacity (g/g)	0.173	0.175	0.125

Procedure. Thermal Analysis. DTA were obtained on a Stone Tracor Model 202 differential thermal analyzer with a dynamic gas flow sample holder. When dry air or helium were used as purges, the following instrument conditions applied: heating rate = 10 deg/min, flow rate = 23.6 ml/min, gain = 2400 μV (air) 500 μV (He), sample wt. = 250 mg, reference = 400 mg of Al_2O_3, differential thermocouple = Platinel II. In this equipment the purge passes directly through the sample and reference cells. Use of an instrument with a different flow configuration may result in an entirely different thermogram.[5]

A DuPont Model 950 thermogravimetric analyzer was operated under the following conditions: dry air purge = 37.6 ml/min, heating rate = 10 deg/min, sample weight = 26.48 mg.

Infrared Analyses. Spectra were recorded on 0.5-in. diameter self-supporting wafers in a cell similar to that previously described.[6] Samples were heated in the cell in flowing dry air at 100° increments following evacuation to 10^{-5} Torr at room temperature. All spectra were recorded at room temperature on one thermally cycled sample. The hydroxyl stretching region was scanned with a Perkin-Elmer Model 112 single-beam spectrophotometer on a 15-mg wafer. The mid-frequency and framework regions were obtained with a Perkin-Elmer Model 225 double-beam spectrophotometer on 25- and 5-mg pellets, respectively.

X-Ray Diffraction. A Materials Research Corporation high-temperature diffractometer employing Cu Kα radiation was used over a 2θ range of 4 to 44° at a scan rate of 1 deg/min. The sample was deposited as an aqueous slurry on the platinum sample stage and vacuum dried. An internal standard was not employed. Temperature control was achieved with the heated sample stage and auxiliary side heaters; molecular sieve dried air was passed over the sample stage at 25 ml/min. Samples in the MRC diffractometer and infrared cell may be considered to have a thin bed configuration. Deep bed calcined samples were hydrated and scanned on a Norelco diffractometer with a graphite monochromator. In several instances samples were removed from the TGA apparatus at selected temperatures and scanned on the Norelco instrument.

The following 12 reflections (with approximate 2θ values at room temperature) were used to calculate cell constant data for the thin bed samples: (*hkl*), 2θ in degrees: (210) 14.60, (111) 15.10, (201) 16.08, (220) 19.15, (310) 20.00, (301) 20.35, (221) 22.52, (321) 27.00, (222) 30.55, (302) 28.95, (102) 24.18, (112) 25.45. The following eight indices were used in calculating the cell constants of the deep bed calcined material: (210), (111), (201), (220), (102), (112), (321), (330), 29.55. The computer program used in calculating the cell constants from the 2θ data is essentially an extrapolation procedure based on Cohen's least-squares method; precision is estimated at ±0.04 Å.

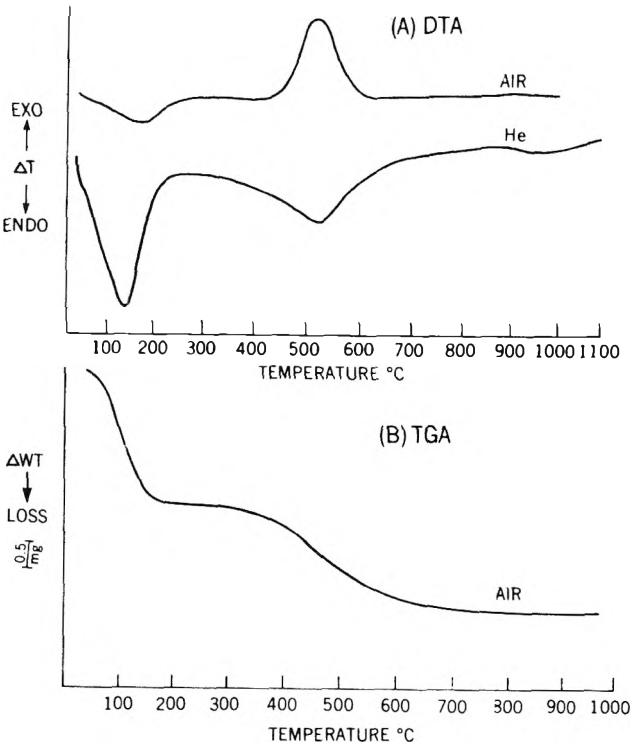

Figure 1. Thermograms of NH_4KL in air and helium.

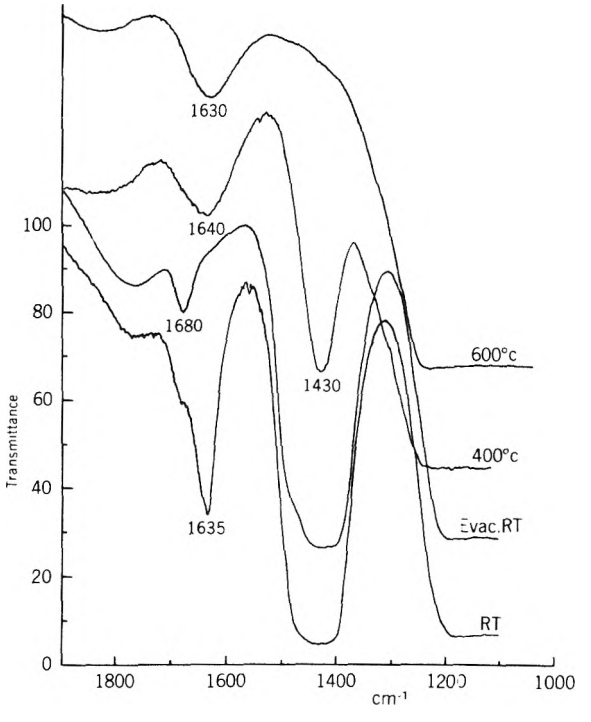

Figure 2. Mid-frequency infrared region of air calcined NH_4KL.

Results and Discussion

Thermal Analyses. Thermograms of NH_4KL are presented in Figure 1 both for air and helium atmospheres. Differential thermal analysis in air shows an endotherm at 175° due to water desorption and a sharp exotherm at 515° due to ammonia oxidation. While no evidence for a dehy-

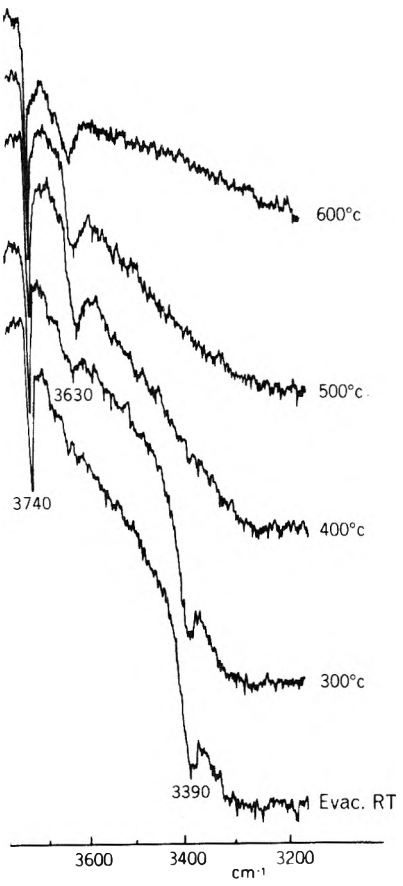

Figure 3. Infrared spectra of hydroxyl stretching region of air calcined NH_4KL.

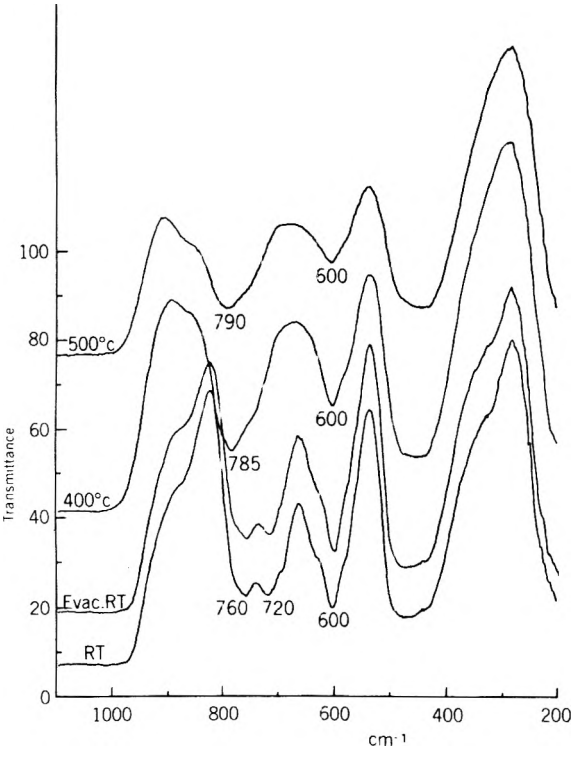

Figure 4. Infrared spectra of framework region of air calcined NH_4KL.

TABLE I: Cell Constants at Temperature of NH_4KL Thin Bed Dry Air

Conditions	a_0, Å	c_0, Å
Room temp	18.45	7.56
300° 2 hr	18.34	7.56
Room temp 1 hr	18.40	7.53
400° 2 hr	18.27	7.54
Room temp 20 min	18.25	7.51
500° 2 hr	17.8	7.3

TABLE II: Room Temperature Hydrated Cell Constants and O_2 Capacity of Deep Bed Calcined NH_4KL

Treatment	a_0, Å	c_0, Å	O_2 cap., g/g
Starting material	18.47	7.56	0.173
1 hr 700°	18.17	7.53	
3 hr 700°	18.22	7.54	0.172
6 hr 700°	18.14	7.50	
1 hr 800°	18.18	7.54	0.098
NH_4^+ exchange above	18.22	7.58	0.124
1 hr 900°			0.013

droxylation endotherm can be observed, an ill-defined exotherm can be seen at 910°. Instrument sensitivity was increased fivefold when using a helium purge. Water desorbs at 140° and a sharp endotherm is observed at 525° due to ammonia desorption. The TGA in air shows two distinct steps; thus it is more similar to that of ammonium exchanged Y[7] than ammonium exchanged mordenite.[5] Loss of physically adsorbed water occurs between room temperature and 200° while deammoniation and dehydroxylation overlap between 300 and 700°. The X-ray diffraction pattern of a sample taken at 600° is similar to that of an isothermal sample heated at 500° in that the product is almost amorphous.

The DTA of the ammonium exchanged deep bed calcined NH_4KL is similar to that shown in Figure 1. Major differences are a less intense oxidation exotherm and a high-temperature exotherm at 990°. The high-temperature exotherm may be related to the greater thermal stability of this material. The TGA is also similar to that of the noncalcined material, except as expected from the lower ammonia content, the weight loss due to deammoniation is less.

Infrared Analyses. The infrared region between 1800 and 1000 cm^{-1} of NH_4KL as a function of temperature is shown in Figure 2. Physically adsorbed water (1635 cm^{-1}) is removed after evacuation for 1 hr at room temperature; this allows a framework overtone vibration at 1680 cm^{-1} to become visible. At 400°, there is a significant decrease in the ammonium band at 1430 cm^{-1} and a shift in the framework band to 1640 cm^{-1}. The ammonium band is very small at 500° and has disappeared at 600°. The accompanying changes in the hydroxyl stretching region are shown in Figure 3. Room temperature evacuation reveals the ubiquitous band at 3740 cm^{-1} which is due to amorphous material in the zeolite. (Ammonium cation can be seen at 3390 cm^{-1}.) A zeolitic hydroxyl band at 3630 cm^{-1} does not become apparent until 300° and achieves maximum intensity between 400 and 600°; the frequency does not change with temperature. No zeolitic hydroxyl band is present at 700°. The intensity of the hydroxyl band is considerably

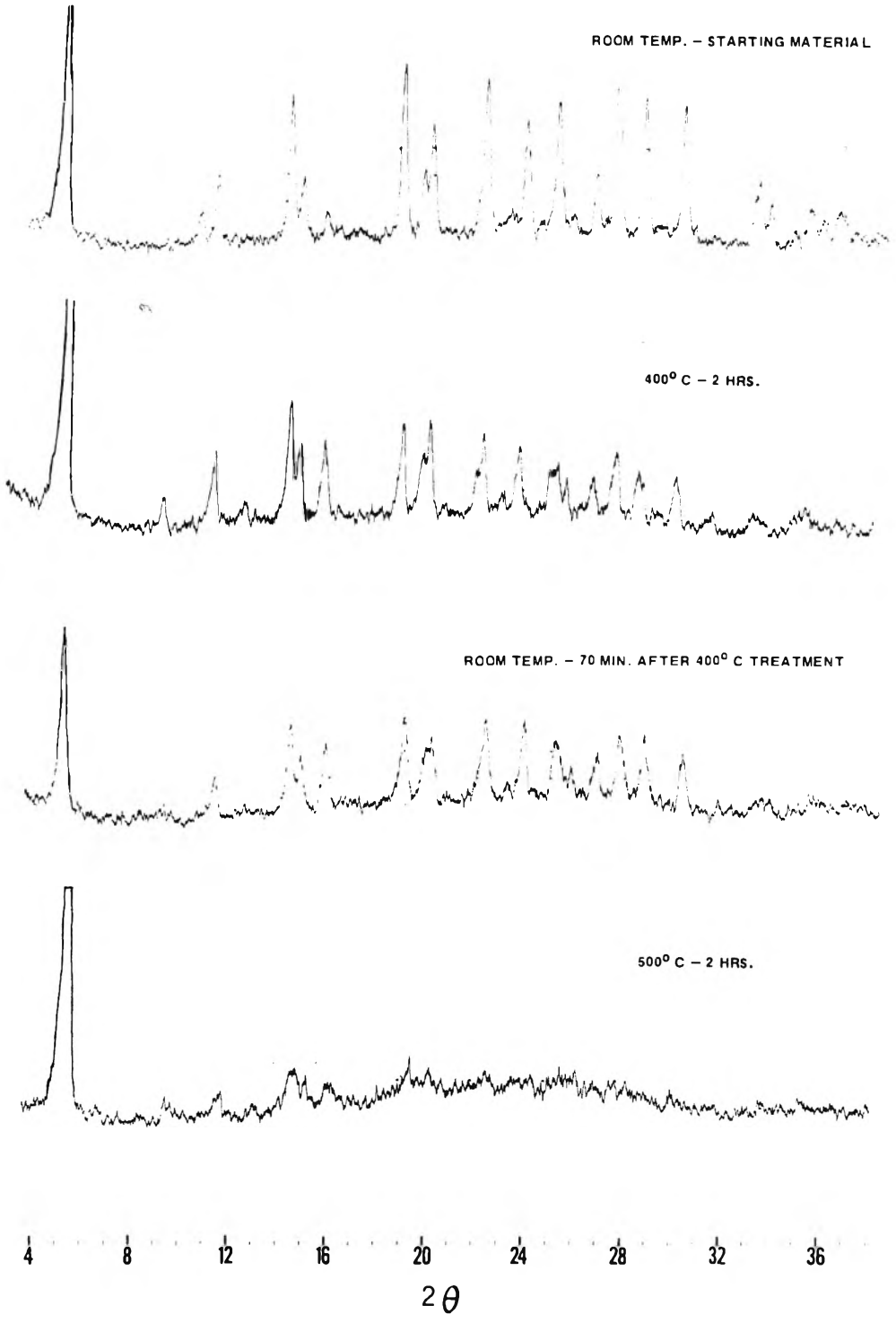

Figure 5. X-Ray diffraction patterns taken at temperature of thin bed fired NH_4KL.

less than that seen in other calcined ammonium zeolites. This might indicate that either the hydroxyl concentration is lower or the extinction coefficient is lower. X-Ray diffraction data indicate that the zeolite is substantially degraded at 500°. Thus it is difficult to determine if the 3630-cm^{-1} band is caused by a structural hydroxyl or a hydroxylated decomposition product. The high oxygen capacity of the NH_4KL (0.173 g/g cf. 0.196 g/g theoretical) indicates that it is quite crystalline and that the amount of amorphous material indicated by the 3740-cm^{-1} band is not unusually large.

Framework spectra of NH_4KL as a function of temperature are presented in Figure 4. The spectrum of the hydrated starting material is unchanged following evacuation and heating to 300°. At 400°, corresponding to loss of ammonia, the 760-cm^{-1} band shifts to 785 cm^{-1}, the 720-cm^{-1} band disappears, and the 600-cm^{-1} band remains unchanged. This poorly resolved spectrum indicates that the zeolite has lost crystallinity upon removal of the ammonium cation. Heating to 500 and 600° does not produce any other major changes. The X-ray diffraction pattern of a pellet heated to 550° shows it to be essentially amorphous in

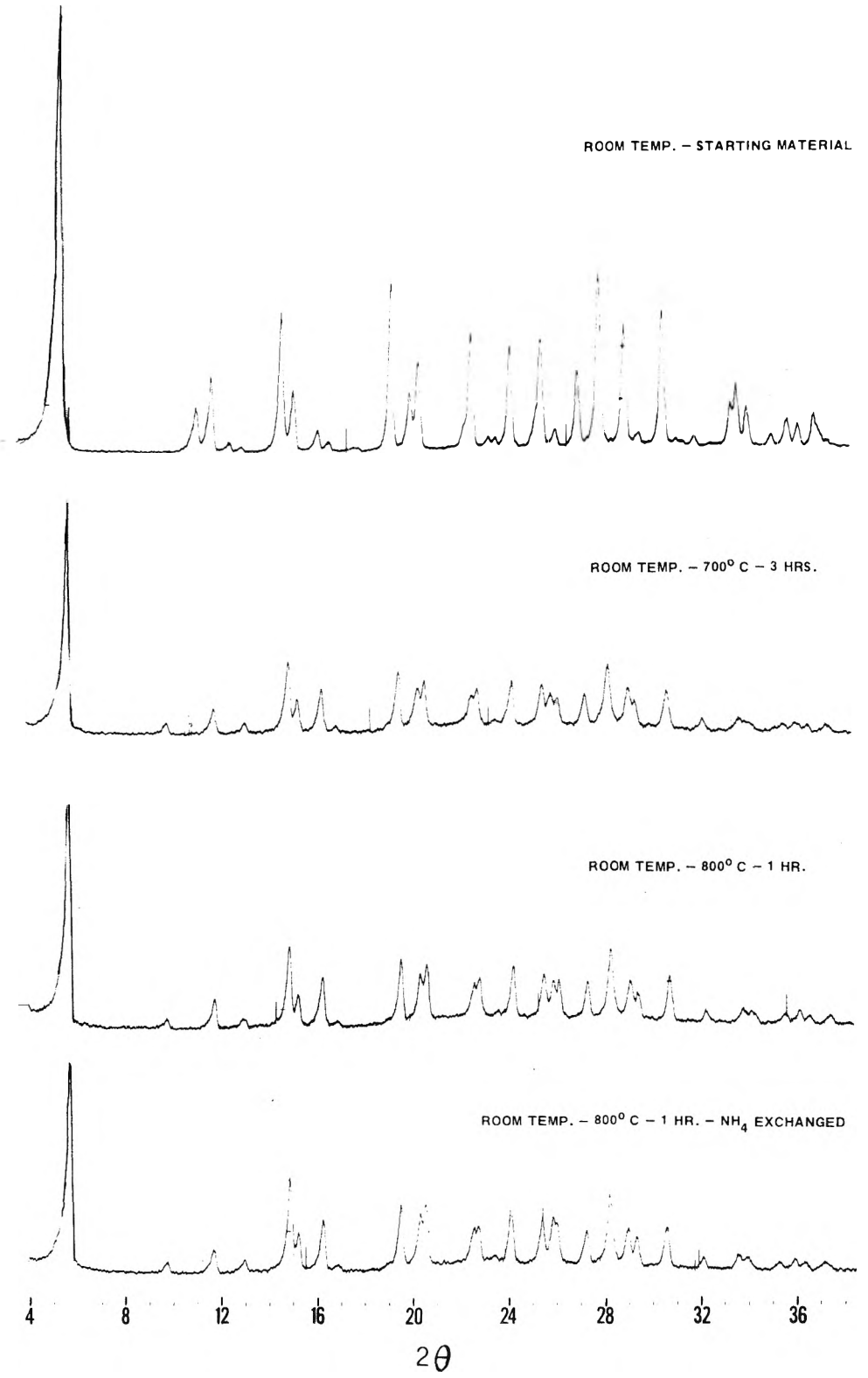

Figure 6. Room temperature X-ray diffraction patterns of deep bed calcined NH_4KL.

agreement with the infrared data. The framework spectrum of NaKL heated to 500° is identical with the starting material which shows that the changes observed are due to loss of ammonium cation. It has been suggested that an increase in the silica-alumina molar ratio of a zeolite results in a shift to higher wave numbers for specific vibrations in the framework region of the infrared spectrum.[8]

The infrared spectra of the ammonium exchanged deep bed calcined NH_4KL were also examined. The zeolite was activated at 500° in air as a self-supporting wafer. No zeolite hydroxyl band is noted other than the 3740 cm^{-1}. Chemical analysis shows that deep bed calcination reduces the cation exchange capacity of NH_4KL. Since an additional ammonium ion exchange results in a drastically lower

ammonium ion content, it should not be considered surprising that zeolite hydroxyl groups cannot be observed. The framework pattern is similar to that shown in Figure 4 at 400° (i.e., after deammoniation) but the two bands on scale occur at frequencies of 820 and 638 cm^{-1}. This indicates very substantial dealumination when compared to the 760- and 600-cm^{-1} bands in the starting material. Shoulders are noted at 590 and 870 cm^{-1}. The spectrum is unchanged after room temperature evacuation and heating to 500°. The X-ray diffraction pattern of this material indicated substantial retention of crystallinity.

X-Ray Diffraction. The X-ray diffraction pattern of a single sample of NH_4KL at various temperatures is shown in Figure 5. The geometry of the MCR instrument is such that the X-ray beam passes through a smaller sample area at low angles than at high angles. Hence, the intensity of the low angle peak at 5.6° (100) is less than would be observed in a standard instrument. No changes are observed until 300°. At 400° pronounced differences in the pattern can be noted, such as the appearance of a new peak at 9.6° (110), the disappearance of one at 11° (200), and the relative intensity increase of the low angle peaks. These changes are partially reversible after cooling to room temperature; thus, it is unlikely that they are due solely to hydration phenomena. Upon reheating to 500°, the crystal is essentially destroyed. The cell constant changes accompanying this heating sequence on a single sample are given in Table I. Typical cell constants for NaKL are a_0 = 18.40 Å and c_0 = 7.52 Å.[9] A slight decrease in a_0 can be noted at 300° and a further decrease at 400° can be seen. This may be due to loss of ammonium cation. At 500°, the temperature of crystal collapse, both a_0 and c_0 decrease substantially. The temperature of crystal collapse is not affected by thermal cycling since a sample heated directly to 500° is also essentially amorphous. It has been reported that HKL, prepared by calcination of NH_4KL in oxygen at 350°, undergoes an increase in a_0 followed by a decrease to 18.24 Å when heated incrementally from 100 to 500°, and that c_0 decreases to 7.54 Å at 500°.[2] These values are very similar to those reported here for 400°.

Figure 6 shows the diffraction patterns of several deep bed calcined materials. The patterns were run at room temperatures on hydrated samples. It is obvious that deep bed calcination results in a very thermally stable material. The bottom pattern in Figure 6 is that of the ammonium exchanged deep bed fired material described in the Materials section. The cell constants and oxygen capacities of the deep bed calcined zeolites are given in Table II. The cell constants are similar to those observed for a thin bed configuration at 400°. Thus, it appears that the crystal was stabilized just before collapse. The oxygen capacity data shows that at 700° there is no loss in crystallinity, but that degradation does begin to occur at 800°. A subsequent ammonium exchange appears to remove some amorphous material. The chemical analysis of this zeolite suggests that loss in crystallinity is related to removal of potassium. It has been claimed, however, that it is possible to remove potassium from L without crystal collapse.[10] An increase in thermal stability upon calcination of NH_4Y in a deep bed configuration is a well-known phenomenon.[11] It has been shown, however, to occur also with ammonium exchanged L and mordenite,[5] thus indicating a general reaction of siliceous zeolites.[12]

Acknowledgment. We wish to thank the following individuals for their experimental work and most helpful advice: Dr. C. L. Angell, Mr. H. F. Hillery, Mr. R. L. Bujalski, Miss D. G. Kimak, and Mr. L. G. Dowell.

References and Notes

(1) D. W. Breck, "Zeolite Molecular Sieves", Wiley, New York, N.Y., 1974.
(2) R. M. Barrer and I. M. Galabova, *Adv. Chem. Ser.*, **No. 121**, 356 (1973).
(3) G. V. Tsitsishvili, *Adv. Chem. Ser.*, **No. 121**, 291 (1973).
(4) V. Ya. Nikolina, E. B. Krasnyi, T. G. Musin, and L. I Kirkach, *Colloid J. (Russ.)*, **33** 693 (1971).
(5) T. J. Weeks, Jr., H. F/ Hillery, and A. P. Bolton, *J. Chem. Soc., Faraday Trans. 1*, in press.
(6) C. L. Angell and P. C. Shaffer, *J. Phys. Chem.*, **69**, 3463 (1965).
(7) A. P. Bolton and M. A. Lanewala, *J. Catal.*, **18**, 154 (1970).
(8) E. M. Flanigan, H. Khatami, and H. A. Szymanski, *Adv. Chem. Ser.*, **No. 101**, 201 (1971).
(9) R. M. Barrer and H. Villiger, *Z. Kristallogr.*, **128**, 352 (1969).
(10) H. U. Schutt, U.S. Patent 3,794,600 (1974).
(11) G. T. Kerr, *Adv. Chem. Ser.*, **No. 121**, 219 (1973).
(12) NOTE ADDED IN PROOF: A detailed study on the framework infrared spectra of type L zeolites has recently appeared: P. Pichat, C. Franco-para, and D. Barthomeuf, *J. Chem. Soc., Faraday Trans. 1*, **71**, 991 (1975).

Structure–Volume Relationships. Volume Effects Produced by Copper(II) Complexing with Organic Acids

Sam Katz,* Michael Patrick Donovan, and Linda Carol Roberson

West Virginia University, School of Medicine, Department of Biochemistry, Morgantown, West Virginia 26506 *(Received January 9, 1975)*

Publication costs assisted by the National Heart and Lung Institute

The volume effects produced by the formation of 1:1 complexes of Cu(II) with organic acids are a function of the structure and the protonation state of the organic compound. For the following monodentate carboxylates, volume increases of 7 ml/mol for formate and 13 ml/mol for acetate and propionate were produced upon coordination with the copper ion. The several dicarboxylate anions studied produced volume changes of about 28 ml/mol of ligand. The addition of Cu(II) to the protonated forms of these acids produced negligible volume changes, about 1–3 ml/mol of ligand; this is indicative of minimal complex formation and/or volume effect upon complex formation. The use of 8 *M* urea as solvent reduced the magnitude of the volume effects produced by the reaction of Cu(II) with carboxylates by 23% relative to that observed in water. This reduction is similar to the attenuation of the volume effects resulting from the protonation of carboxylates in this medium. The addition of Cu(II) to protonated amines caused virtually no demonstrable volume effects. The reaction of this cation with the nitrogen donor atoms in imidazole and simple amino acidates produced small volume effects, 1–3 ml/mol. The incremental increase of volume with the increase of electrostatic charge of the ligand is explicable by a model involving Cu(II) forming a chelate with bidentate ligands and the application of the Drude–Nernst equation for electrostriction. Both of these mechanisms can be considered as being operative.

Introduction

There has been a recent surge of activity dealing with the volume effects produced by the reaction of metal cations with synthetic polyfunctional compounds[1-4] and with proteins.[5] In order to resolve the contributions ascribable to cation–functional group interaction from those due to the alteration of the polyampholyte structure, it is essential to know the magnitude of the volume effects evoked when these cations react with the appropriate ligands. At present, the literature dealing with this type of reaction is limited; e.g., the paper of Spiro and associates dealing with volume changes produced by the reaction of Ce(III) with sulfate, chloride, nitrate, and propionate ions.[6]

This study is designed to determine the volume changes produced when Cu(II) complexes with organic compounds incorporating one to three ligands and also the effect of varying the concentration and ionic state of the ligand. A comparison of these reactions in water and in 8 *M* urea may provide information pertinent to the influence of a nonpolar solute, urea, on the structure of water. In addition, these data will provide a frame of reference for studying the binding of metal cations to conformationally altered proteins in a denaturing environment.

Experimental Section

Apparatus and Procedures. The volume changes were determined with Teflon-sheathed Carlsberg type dilatometers which can be read to 0.01 μl; the dilatometric procedure has been described in detail.[7,8] The 8:2 protocol employed involved mixing 8.00 ml of $Cu(NO_3)_2$ with 2.00 ml of organic reactants. The concentration of the Cu(II) after mixing was 0.050 *M* and the values for the organic compounds after mixing were 0.025 and 0.0125 *M*. The experiments were performed at 30.0 ± 0.001°. Each datum is the mean of two or more experiments so that the standard deviation is ≤0.03 μl or 4% whichever is the highest. No correction was made for the ΔV of dilution of 0.0625 *M* Cu(II) which was −0.04 μl.

pH was measured with a Radiometer pH meter, Model 26, employing a semimicro combination electrode GK 2321C; the unit was standardized against Harleco buffers at pH 6.86 and 4.01 at 25°. The reproducibility of these measurements was about 0.2 units; this variation reflects the low buffering capacity of these solutions. Conductivity measurements were made with a Radiometer conductivity meter CDM3 with CDC 314 cell.

Materials. $Cu(NO_3)_2 \cdot 3H_2O$, analytical reagent grade, was purchased from Mallinckrodt. The organic compounds, highest purity available, were from either Mallinckrodt or Sigma Chemical Co. Urea, Mallinckrodt, was purified according to our standard procedure.[9]

Results and Discussion

In the absence of information which would provide guidelines respective to volume changes produced by the reaction of Cu(II) with simple organic ligands, these experiments were designed to ascertain whether demonstrable volume effects were produced by complex formation. Another objective was to establish a frame of reference which would facilitate comparison of the effects produced by the reaction of Cu(II) with mono- and polyfunctional carboxyl compounds as a function of structure, concentration, pH, and medium. The processes involved in complex formation, but not including water per se, can be represented by the following set of equations:

$$Cu + L \rightleftharpoons CuL \qquad K_1 = (CuL)/(Cu)(L) \qquad (1)$$

$$CuL + L \rightleftharpoons CuL_2 \qquad K_2 = (CuL_2)/(CuL)(L) \qquad (2)$$

$$CuL_{j-1} + L \rightleftharpoons CuL_j \qquad K_j = (CuL_j)/(CuL_{j-1})(L) \qquad (3)$$

$$H^+ + L \rightleftharpoons HL \qquad K_a = (HL)/(H^+)(L) \qquad (4)$$

$$Cu + HL \rightleftharpoons CuL + H^+ \quad K_{H1} = (CuL)(H^+)/(Cu)(HL) \tag{5}$$

The terminology is conventional: the term L indicates the ligand; the brackets indicate concentration of the ligand; the various K's are stoichiometric stability constants. The following conservation equations are applicable to these systems:

$$L_t = (L)[1 + (H^+) + K_1(Cu) + 2K_1K_2Cu(L) + \dots] \tag{6}$$

$$Cu_t = (Cu)[1 + K_1(L) + K_1K_2(L)^2 + \dots] \tag{7}$$

The terms L_t and Cu_t indicate the total concentration of ligand and of Cu(II).

It is essential to consider the influence of pH on the volume effects. Before discussing the primary pH effect, i.e., as it determines the protonation state of the acid and thus its electrostatic charge, we will discuss the influence of pH on several other facets of these systems. The pH of the Cu(II) solution ranges from 4 to 4.5, thereby constituting a 10^{-4} M solution of hydrogen ions. The volume change attributable to the protonation of the carboxylates, assuming the absence of competitive Cu(II) binding, would be small, i.e., $\leq$0.03 μl. A more significant factor is the influence of the pH of the system after mixing since this will determine the ratio of acid to base forms of the unbound ligand. In systems containing 0.0125 M ligand and if log K_1 is 2.7, the amount of unbound ligand will be about 5%. If the value of the pH of the system is equal to or greater than the pK_a of the ligand, there can be a volume effect due to the protonation of the ligand which may amount to 5%. Consequently when the log k_1 is $\leq$2.7 and the equilibrium pH–pK relationship is such that both the acid and base forms of the ligand exist, then the appropriate correction must be made (see eq 6). In systems where the ligand exists in an alkaline environment, volume effects attributable to copper hydroxide formation must be anticipated. The addition of 0.05 M Cu(II) to 0.001 N NaOH, pH 11.2, caused a volume change of -0.03 μl. At higher alkali concentrations the volume changes were large and accompanied by precipitation. For the systems reported, the final pH never exceeded 7; thus this factor was unimportant.

The initial pH of the ligand is important since it determines the degree of protonation and the electrostatic charge of the ligand; this has a profound influence on the magnitude of volume effects produced. Illustrative of this are the small volume changes produced when Cu(II) is added to mono-, di-, or tricarboxylic acids, see Table I. The pH of the acids prior to mixing was at least one pH unit more acid than the appropriate pK_A with the exception of maleic acid where the initial pH was 1.8. The volume changes were extremely small ranging from -0.16 to 0.38 μl for maleic to tartaric acid, 0.0125 M, respectively. These values may be explained by the existence of a small ΔV for the formation of copper–organic acid complexes or, more probably, because only a small amount of complex is formed. By reference to eq 5 one notes that the equilibrium constant, K_{H1}, is given by the product, $K_1K_a^{-1}$. Consequently, when these two equilibrium constants are of similar magnitudes the amount of copper–ligand complex formed is small.[12]

Before discussing the data in Table II it is necessary to consider the basis for defining the parameter, ΔV_c. This term designates the volume change resulting from the formation of a 1:1 copper–ligand complex. The rationale for this is as follows. The value for the experimental volume change is given by the following expression:

$$V_{expt} = (n_1 + n_2)\Delta V_1 + n_2\Delta V_2 \tag{8}$$

where n_1 and n_2 are the moles of the mono- and disubstituted copper complexes formed and ΔV_1 and ΔV_2 are the molar volume changes associated with processes 1 and 2. The ratio of the concentrations of CuL to CuL_2 can be determined from the following relationship:

$$(CuL)/(CuL_2) = K_1(Cu)/K_2(CuL) \tag{9}$$

It can be shown that the amount of disubstituted copper complex formed under these experimental conditions is small; therefore, ΔV_c is a valid approximation for ΔV_1 in the systems which contain 0.0125 M ligand. The most demanding situation is exemplified by acetate, since K_1 and K_2 are 1.88 and 1.24, respectively. By substitution in eq 9 one obtains the value for the ratio of n_1:n_2 of 15:1. If one assumes that $\Delta V_2 \leq V_1$, the maximum possible contribution attributable to the formation of the CuL_2 complex is $\leq$7%. The dominant error in these calculations is that due to the selection of the values for the stoichiometric affinity constants. In this report, except for the protonated acids and the monocarboxylate compounds, the stoichiometric affinity constants exceed log 2.8; consequently, at least 95% of the ligand is combined with copper. These comments apply to the systems employing water as solvent; however, there is substantial evidence that the association constants in 8 M urea are not markedly altered by this medium (refer to subsequent discussion).

The concentration of the ligand has a large effect on the magnitude of the volume changes as seen by inspection of the ratio of volume changes at 0.025 to 0.0125 M; this ratio is 1.92, standard deviation 0.03, Table II. The influences of solute concentration are (i) the depressant effect of salts on volume changes and (ii) the salt effect on the stoichiometric affinity constants. The dependence of partial molal volumes on concentration is well established.[15] Masson[16] proposed the existence of a relationship between the apparent molal volume and the square root of the concentration of electrolytes. This relationship between molal volumes and salt concentration is the basis for the attenuation of volume effects produced by the protonation of carboxylates and neutralization reactions.[7,17] For example, Kauzmann et

TABLE I: Volume Changes Resulting from Cu(II)–Carboxyl Interaction

Ligand	Initial concn, M	Equilibrium pH	ΔV_{expt}[a] H_2O, μl	ΔV_{expt}[a] Urea, μl	pK (25°)
Acetic	0.0125	3.8	−0.03	0.01	4.76[b]
acid	0.0250	3.7	−0.02	0	
Malonic	0.0125	2.7	0.12	0.13	2.83 (1)[c]
acid	0.0250	2.6	0.04	0.12	5.69 (2)
Tartaric	0.0125	2.9	0.38		2.98 (1)[c]
acid	0.0250	2.7	0.55		4.34 (2)
Maleic	0.0125	2.5	−0.16	0	1.83 (1)[c]
acid	0.0250	2.2	−0.26	−0.02	7.07 (2)
Citric	0.0125	2.0	0.33	0.69	3.14 (1)[b]
acid	0.0250	1.9	0.50	0.94	4.77 (2)
					6.39 (3)

[a] Experimentally determined volume change. [b] Reference 10. [c] Reference 11.

TABLE II: Volume Changes Resulting from Cu(II) Complexing with Carboxylates

Ligand	Initial concn, M	Equilibrium pH	H_2O ΔV_{expt}, μl	H_2O ΔV_c, ml/mol	8 M urea ΔV_{expt}, μl	8 M urea ΔV_c, ml/mol	pK	Log K[a]
Sodium formate	0.0125	4.9	0.68	7	0.52	5	3.75[b]	2.0 (1)[d]
	0.0250	5.0	1.29		0.91			
Sodium acetate	0.0125	5.8	1.20	13	0.97	10.5	4.76[b]	1.88 (1)[e]
	0.0250	5.9	2.32		1.75			
Sodium propionate	0.0125	5.0	1.30	13	1.14	11	4.87[b]	2.0 (1)[d]
	0.0250	5.1	2.51		2.07			1.0 (2)
Sodium trichloro-acetate	0.0125	4.5	0.02		0.10		0.70[c]	
	0.0250	4.5	0.13		0.17			
Sodium *N*-acetyl-glycinate	0.0125	5.0	0.96				3.60[b]	
	0.0250	5.0	1.85					
Disodium malo-nate	0.0125	4.4	3.40	27	2.50	20	2.83 (1)[c]	5.8 (1)[d]
	0.0250	4.7	6.63		4.77		5.69 (2)[c]	1.9 (2)
Sodium hydrogen tartrate	0.0125	3.3	2.17				2.98 (1)	3.2 (1)[d]
	0.0250	3.2	4.10				4.34 (2)	1.9 2)
Disodium tartrate	0.0125	4.05	3.61	29				
	0.0250	4.02	6.91					
Disodium maleate	0.0125	5.0	3.50	28	2.70	22	1.83 (1)	3.9 (1)[d]
	0.0250	5.6	6.63		4.73		6.07 (2)	
Trisodium citrate	0.0125	2.9	6.72					
	0.025	3.0	6.22[f]				3.14 (1)	
							4.77 (2)	
							6.39 (3)	

[a] The logarithm of the stoichiometric stability constants for eq 1 and 2, see text. [b] Reference 10. [c] Reference 11. [d] Reference 13. [e] Reference 14. [f] 1:4 protocol: 1 ml of Cu(II) added to 4 ml of ligand.

al.[17] reported that the ΔV for the protonation of acetate ion decreased from 10.9 ml/mol at 0.17 ionic strength to 9.7 ml/mol at 0 3 ionic strength. Another salt effect is the reduction of the value of the stoichiometric affinity constants with increase of salt, e.g., the constant for the chelation of Cu(II) with phthalate ion decreased from 1.83×10^3 at 0.03 ionic strength to 1.4×10^3 at 0.06 ionic strength.[12] In this study, except for the monodentate ligands, the affinity constants are $\geq 10^3$; consequently a 50% reduction of the equilibrium constants would not substantially alter the amount of complex formed. Thus the depressant effects of solutes on these volume changes must be the factor primarily responsible for the depressed volume effects at 0.025 M ligand concentration.

The volume effects produced by Cu(II) complexing with carboxylate-containing compounds are a function of the number of carboxylates and their ionic charge. The validity of the values for ΔV_c reported for the monocarboxylate ligands is determined primarily by the reliability of the stoichiometric affinity constants employed; the association constants cited in Table II represent the "best" values, i.e., from systems which tend to simulate this experimental design. The amount of copper–ligand complex formed from formate, acetate, and propionate is calculated as 80, 75, and 80% of the total ligand present yielding values for ΔV_c of 7, 13, and 13 ml/mol of ligand. The nature of substituents incorporated in a ligand influences the affinity constants and thus the magnitude of the experimental volume change. For example, the addition of the trichloroacetate anion to Cu(II) produced volume changes of 0.02 and 0.13 μl at 0.0125 and 0.025 M ligand concentrations, respectively. These values are at least an order of magnitude smaller than the other monodentate ligands studied. Protonation of formate, acetate, and propionate resulted in volume changes of 7.8, 10.9, and 12.6 ml/mol at 0.08 ionic strength, respectively.[17] The parallel between these data and the results of the corresponding copper systems is indicative that similar mechanisms are operational. This finding is in accord with the hypothesis that the basicity of the Lewis base ligand is a primary factor in determining the affinity with which a proton or metal cation complexes with the ligand.[12]

The study of the dicarboxylate compounds was designed to establish the influence of structure on volume effects, i.e., to ascertain whether the formation of five-, six-, and seven-member chelates would produce volume effects of different magnitudes. It is an axiom in coordination chemistry that the stability constants of chelate complexes decrease as the ring size increases from a five-membered ring to higher values, i.e., oxalate forms chelates with the largest affinity constants. However, the volume effects produced by the reaction of Cu(II) with oxalate are not included because precipitation occurred upon mixing. The addition of Cu(II) to malonate to form a six-membered chelate resulted in a ΔV_c of 27.2 ml/mol of ligand. This is double the volume effect produced by the formation of 1:1 copper–carboxylate complexes and is the quantity anticipated for the formation of a bidentate structure. Maleate, a compound in which the carboxylates are cis with respect to the double bonded carbon chain, forms a seven atom ring with Cu(II). The value for ΔV_c was 28 ml/mol of ligand. Comparison with the trans isomer, fumarate, was not possible since precipitation occurred. The dianionic form of tartrate, which forms a seven atom chelate, yields a ΔV_c of 29 ml/mol of ligand; a result which is similar to the other bidentate ligands. To establish the influence of the protonation state on dicarboxylic acids, a similar exercise was performed with sodium hydrogen tartrate, initial pH 3.7; the experimental volume change at 0.0125 M ligand concentration

TABLE III: Volume Changes Resulting from Cu(II) Interaction with Ligands Containing Nitrogen Donor Atom

Ligands	Initial concn, M	Equilibrium pH	H_2O		pK	Log K^a
			ΔV_{expt}, μl	ΔV_c, ml/mol		
Imidazole	0.0125	5.5	0.21	1.7	6.95[b]	4.2 (1)[c]
	0.0250	5.7	0.54			3.4 (2)
Glycine (dipolar)	0.0125	2.7	0.94		2.35 (1)[b]	
	0.0250	2.6	1.80		9.78 (2)	
Sodium glycinate	0.0125	4.1	1.77	14		8.6 (1)[d]
	0.025	4.1	3.63			7.1 (2)
Sodium alaninate	0.0125	3.9	1.84	15	2.35 (1)[b]	8.54 (1)[d]
	0.0250	4.0	3.60		9.87 (2)	6.98 (2)

[a] The logarithm of the stoichiometric stability constant. [b] Reference 19. [c] Reference 20. [d] Reference 14.

was 2.17 μl. At this pH, the ratio of the mono- to dianionic forms of the ligand was 3:1 which yields a calculated value for ΔV_1 of 12 to 13 ml/mol of ligand. This is similar to the results determined for the monocarboxylate compounds. The volume effects resulting from the interaction of Cu(II) with the triply charged citrate produced volume changes nearly double that of the dicarboxylate compounds. Analysis of the data is complicated because of the occurrence of several parallel reactions; e.g., the logarithm of K_1 is 3.5 and the logarithm of the equilibrium constant for the formation of the dicupric–dicitrate complex is about 12 (ref 13). Thus several complexes may be formed under these experimental conditions and thus the data cannot be explained in terms of a simple model. The addition of Cu(II) to succinate resulted in precipitate formation; therefore, the data are not reported.

The volume effects resulting from the reaction of Cu(II) with ligands incorporating nitrogen donor atoms do not fall under the purview of this article, yet a few comments are necessary in order to interpret the volume effects resulting from the addition of cupric ions to amino acids. The addition of Cu(II) to 0.0125 M imidazolium hydrochloride, diethylammonium hydrochloride, and tris(hydroxylmethyl)ammoniummethane hydrochloride gave volume changes of ≤0.08 μl. This low value indicates a low degree of complex formation as anticipated in view of the substantial coulombic repulsion energy associated with the two cationic reactants. The reaction of Cu(II) with 0.0125 M imidazole produced a ΔV_c of 1.7 ml/mol of ligand, Table III. Since the imidazole quantitatively complexes to the metal, the logarithms of K_1 and K_2 being 4.2 and 3.4, respectively,[20] the obvious conclusion is that the volume change for this reaction is small. The addition of copper to 0.0125 M glycine, in the dipolar state, produced a volume change of 0.94 μl, about half that observed for the anionic form of this reactant, Table III. Since the value for affinity constant for the dipolar form is unavailable, the ΔV_c was not calculated. The formation of five atom chelate rings by Cu(II) with the anionic forms of glycinate and alaninate generated values for ΔV_c of 14 and 15 ml/mol of ligand, respectively. These volume effects are only 1–3 ml/mol larger than those produced by the normal monodentate carboxylates. This indicates that the complexing of Cu(II) to an amine radical produces a modest volume change; i.e., the amount of water of electrostriction released from both the copper ion and nitrogen atom is small.

The magnitudes of the volume effects resulting from the interaction of Cu(II) with carboxylate ligands and with nitrogen donor atom ligands are in accord with the thermodynamic properties of these systems. The formation of metal–carboxylate complexes is characterized by large positive values for entropy change and the enthalpy contribution is zero or slightly positive. When metal ions complex to amino donor ligands the converse is the case.[12] Generally, in coordination reactions the determinant primarily responsible for the entropic contribution is the amount of water of electrostriction released from the reactants. A detailed analysis is not possible because of the limited amount of thermodynamic data available, yet the values existing at present tend to substantiate this hypothesis. The enthalpy and entropy change for Cu(II) forming a 1:1 complex with imidazole are −7.2 kcal/mol and −4 gibbs/mol, respectively;[14] the value for ΔV_1 was 1.7 ml/mol. For acetate, the corresponding values were 1 kcal/mol, 12 gibbs/mol, and 13 ml/mol; similarly for malonate, the values were 3 kcal/mol, 35 gibbs/mol,[14] and 27 ml/mol. For the anionic forms of glycine and alanine the data were strikingly similar; i.e., the enthalpy change was about −5 kcal/mol, entropy change, 22 ml gibbs/mol, and the volume change about 15 ml/mol. Thus, there is a reasonable correlation between the magnitude of the volume effects and of the entropy changes for these systems.

One approach to explain the incremental change of volume as a function of the charge of the ligand is by considering the electrostrictive structuring of water[21] as a function of the electrostatic charge of the reactants involved in complex formation. The Drude–Nernst relationship[22] provides a qualitative statement of the compression of water in the immediate vicinity of a spherical particle of radius, r, with an electrostatic charge, ez, upon immersion in a medium of dielectric, D. The expression for the ensuing electrostrictive volume contraction, V_e, is as follows:

$$V_e = -\frac{\beta c^2 Z^2 V \, dD}{2rD^2 \, dV} \qquad (10)$$

where β and V are the compressibility and volume of the system, respectively. One can rewrite eq 1 as follows:

$$M^{Z_1} + L^{Z_2} \rightleftharpoons ML^{(Z_1+Z_2)} \qquad (1a)$$

where Z_1 represents the charge of the respective species. Then by adopting an analysis similar to Kauzmann et al.[17] the volume change for process 1a may be written as

$$\Delta V = -Q\left[\frac{(Z_1 + Z_2)^2}{r_{ML}} - \left\{\frac{Z_2^2}{r_L} + \frac{Z_1^2}{r_{Cu}}\right\}\right] \qquad (11)$$

where

$$Q = \frac{\beta c V \, dD}{2D^2 \, dV}$$

and r_{ML}, r_L, and r_{Cu} are the radii of the constituents. Even though the values for the radii of the copper–ligand com-

plexes are unavailable, considerable information can be derived from eq 11. If one considers the 1:1 complexes formed by Cu(II) reacting with mono-, di-, and tricarboxylate compounds, it is apparent that the contribution of the $(Z_1 + Z_2)^2/r_{ML}$ term is small compared to the sum of the other two terms. For all of these systems the contribution of the cupric ion is constant, $4/r_{Cu}$, whereas, the contribution of the ligand varies exponentially with increasing charge thus causing a nonlinear increase of volume effects for the several types of carboxylates investigated.

The use of 8 *M* urea depressed the volume effects resulting from the formation of Cu(II)–carboxylate complexes by about 23% relative to that in water. The ratio of the volume effects produced by 0.025 *M* ligand to that of 0.0125 *M* ligand is 1.8 in 8 *M* urea compared to the ratio of 1.9 determined in water. The constancy of these ratios indicates that the affinity constants are not altered substantially by 8 *M* urea. The 23% reduction of the volume effect due to 8 *M* urea is similar to the 22% reduction caused by this agent on the volume effects produced by the protonation of the same compounds.[18] This provides evidence that similar mechanisms are operational for these two categories of coordination processes. The attenuation of the volume effects by 8 *M* urea may be explained in terms of the reduction of the activity of water by the presence of a large amount of nonelectrolyte and by the increase of the dielectric constant of the system. By reference to eq 10, one notes that the electrostrictive contraction of water varies inversely as the square of the dielectric constant of the medium; therefore, an increase of the dielectric constant will diminish the electrostrictive effect (see ref 18 for detailed discussion).

By determining and classifying the magnitude of volume effects produced by metal–ligand complex formation in water and 8 *M* urea one establishes the frame of reference required for comparative studies of metal ion binding to proteins in water and 8 *M* urea. With this background one can delineate the geometrical contribution of the secondary and tertiary structure of the protein as it influences the combination of metal ions to native and denatured proteins.

Acknowledgments. We wish to thank Dr. Jack McCormick, Chemistry Department, for his helpful discussions during the initial portion of this study. We thank Lynn R. Chrin for repeating some of the dilatometric measurements. This research was supported in part by United States Public Health Service, National Heart and Lung Institute Grant No. HL 12955, and National Science Foundation Grant No. GB 37031.

References and Notes

(1) A. J. Begala and U. P. Strauss, *J. Phys. Chem.*, **76**, 254 (1972).
(2) G. E. Boyd and K. Bunzl, *J. Am. Chem. Soc.*, **96**, 2054 (1974).
(3) U. Crescenzi, F. Delben, S. Paoletti, and S. Skerjanc, *J. Phys. Chem.*, **78**, 607 (1974).
(4) F. Delben and S. Paoletti, *J. Phys. Chem.*, **78**, 1486 (1974).
(5) S. Katz, *Biochemistry*, in press.
(6) T. G. Spiro, A. Revesz, and J. Lee, *J. Am. Chem. Soc.*, **90**, 4000 (1968).
(7) S. Katz and J. E. Miller, *J. Phys. Chem.*, **75**, 1120 (1971).
(8) S. Katz in "Methods in Enzymology, Enzyme Structure", Vol. 26, C. H. W. Hirs and S. N. Timasheff, Ed., Academic Press, New York, N.Y., 1972, p 397.
(9) S. Katz and T. G. Ferris, *Biochemistry*, **5**, 3246 (1966).
(10) J. T. Edsall and J. Wyman, "Biophysical Chemistry", Academic Press, New York, N.Y., 1958.
(11) R. C. Weast, "Handbook of Chemistry and Physics", 54th ed, Chemical Rubber Company Press, Cleveland, Ohio, 1973.
(12) J. R. Angelici, "Inorganic Biochemistry", G. L. Eichhorn, Ed., Vol. 1, Elsevier, New York, N.Y., 1973, p 63.
(13) L. G. Sillen and A. E. Martell, *Chem. Soc., Spec. Publ.*, **No. 17**, (1964).
(14) J. J. Christensen and R. M. Izatt, "Handbook of Metal Ligand Heats", Marcel Dekker, New York, N.Y., 1970.
(15) H. S. Harned and B. B. Owen, *ACS Monogr.*, **No. 137**, 358 (1958).
(16) D. O. Masson, *Phil. Mag.*, **8**, 218 (1929).
(17) W. Kauzmann, A. Bodanszky, and J. Rasper, *J. Am. Chem. Soc.*, **84**, 1777 (1962).
(18) S. Katz and J. E. Miller, *J. Phys. Chem.*, **76**, 2778 (1972).
(19) E. J. Cohn and J. T. Edsall, *ACS Monogr.*, **No. 90**, 84 (1943).
(20) R. J. Sundberg and R. B. Martin, *Chem. Rev.*, **74**, 471 (1974).
(21) R. W. Gurney, "Ionic Processes in Solution", McGraw-Hill, New York, N.Y., 1953, p 188.
(22) P. Drude and W. Nernst, *Z. Phys. Chem.*, **15**, 80 (1894).

Interaction of Sodium Dodecyl Sulfate with the Hydrophobic Fluorescent Probe, 2-*p*-Toluidinylnaphthalene-6-sulfonate

Hsin-Chou Chiang and Aaron Lukton*

Department of Chemistry, Brooklyn College, The City University of New York, Brooklyn, New York 11210 *(Received February 18, 1975)*

Publication costs assisted by The City University of New York

The critical concentration (cmc) of sodium dodecyl sulfate at various NaCl concentrations can be followed by the increasing fluorescent intensity of 2-*p*-toluidinylnaphthalene-6-sulfonate (TNS). The thermodynamic parameters of the interaction of TNS and the SDS micelle have been obtained. Binding is exothermic and involves a positive entropy change. The negative value of enthalpy predominately contributes to the negative free energy of binding between TNS and the SDS micelle. The salt (NaCl) increases the association constant between TNS and micelle of SDS by increasing the positive entropy change. The results suggest that the binding force between TNS and the micelle of SDS is hydrophobic. The nature of hydrophobic fluorescent probe binding with proteins is discussed.

Introduction

It is well known that the quantum yield of fluorescence of 2-*p*-toluidinylnaphthalene-6-sulfonate (TNS) and related compounds, such as 1-anilino-8-naphthalenesulfonate (ANS), is very much higher in a nonpolar than in a polar solvent. Also the emission spectrum in a nonpolar solvent is blue shifted relative to the spectrum in polar solvents.[1-3] This characteristic is, therefore, widely used to detect protein conformational change assuming that the environments of dye binding sites change as protein conformation changes. This kind of research using fluorescent probes to follow protein conformation changes and to study cell membrane phenomena is leading to a better understanding of the hydrophobic characteristic of proteins and membranes with respect to the binding of substrate and inhibitors.[2,4]

Although such fluorescent probe research has been extensive, the actual probe binding environment is still obscure, and the nature of the binding forces are not well defined. In 1972, Beyer et al. suggested that, although a hydrophobic environment is essential for enhancing the fluorescence of TNS, charge neutralization is required to provide binding between peptide and TNS.[5] The studies on the interaction of polylysine and TNS show that only the β-sheet conformation of polylysine, the form which exists without charges, results in TNS fluorescence.[6,7] The negative charge repulsion between anionic ANS and negative phosphate or carboxylate groups of phosphatide[8] or of submitochondrial particles[9] is considered to be critically important for the binding of a dye to a phospholipid or a biomembrane. The same finding, namely, that charge repulsion but not charge neutralization is important, has been revealed in studies of the binding between TNS and collagen.[10]

There is extensive evidence indicating that hydrophobic interactions, not charge neutralization, provide the binding force, including the following. A positively charged derivative of ANS, *N*-(1-anilinonaphthalene-4-sulfonyl)-1,6-diaminohexane, has been observed to bind as well as ANS itself to heavy chains of human γG immunoglobulin;[11] *N*-phenyl-1-naphthalene (NPN) without a charge was found to bind more tightly to *Escherichia coli* cell envelope than negatively charged ANS;[12] Brand et al.[13] showed that 1,5-ANS but not *N,N*-dimethyl-1-aminonaphthalene-5-sufonate (DNS) could bind to alcohol dehydrogenase indicating that the hydrophobic interaction between the aromatic moiety of the fluorescent probe and the hydrophobic site of the protein plays an important role in binding; Flanagan and Ainsworth[14] showed that a negative dye can adsorb to neutral micelles if the nonpolar moiety of the probe is sufficiently large, thus ANS, but not DNS or 1-naphthylamine-5-sulfonate, was adsorbed by polyoxyethylene lauryl ether micelle. These data indicate that the hydrophobic characteristic of the nonpolar moiety determines the binding.

Sodium dodecyl sulfate (SDS) micelles, like proteins, provide hydrophobic and charged regions for interaction with amphiphilic molecules such as TNS. The formation of the SDS micelle in aqueous solution is caused by hydrophobic interactions.[15] TNS molecules could be incorporated into the SDS micelle if the hydrophobic interactions are not disrupted by negative charge repulsions between TNS and SDS. Thus, the study of SDS micelles binding with negatively charged TNS should contribute to an understanding of the TNS–protein binding parameters.

In this report, the use of TNS as a probe for detecting SDS micelle formation is presented. The thermodynamic parameters of the SDS micelle–TNS interaction at various NaCl concentrations suggest that hydrophobic forces are principal contributors to the binding.

Experimental Section

Materials. The potassium salt of 2-*p*-toluidinylnaphthalene-6-sulfonate was a product of Sigma Chemical Co. (log no. 80C-5130) and it was stored in the dark at 5°. The compound was found pure according to the results of TLC.[5] Sodium dodecyl sulfate was purchased from Bio-Rad Laboratories, Richmond, Calif., and it was used without further purification.

Fluorescence Measurements. Fluorescence measurements were done on a Perkin-Elmer fluorescence spectrophotometer MPF-2A equipped with a thermostated cell holder. Both emission and excitation slits were set at 4 nm. The emission spectra were obtained by exciting at 370 nm. The mixtures of SDS and TNS were at first incubated in a thermostat at the desired temperature for at least 0.5 hr.

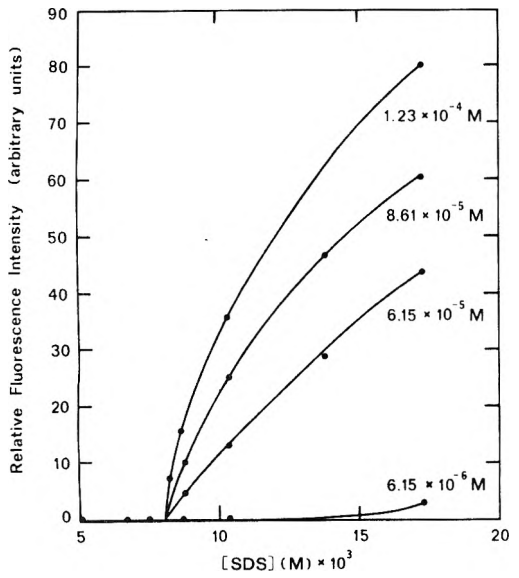

Figure 1. Critical micelle formation in water. The TNS concentration ranged from 6.15×10^{-6} to 1.23×10^{-4} *M*.

The samples were then transferred to the cell holder controlled at the same temperature.

Thermodynamic Parameters. The association constant of TNS and micelles of SDS was calculated according to eq 7, derived as follows:

$$\text{Mn} + \text{TNS} \rightleftarrows \text{Mn–TNS} \tag{1}$$

where Mn is the micelle of SDS (M is the SDS monomer). K_T is the association constant at temperature T. Then

$$K_T = \frac{[\text{Mn–TNS}]}{[\text{Mn}][\text{TNS}]} \tag{2}$$

If [Mn] ≫ [Mn–TNS], eq 3 can be obtained where $[\text{TNS}_{\text{total}}] = [\text{TNS}] + [\text{Mn–TNS}]$ and $[\text{Mn}_{\text{total}}] = [\text{Mn}] + [\text{Mn–TNS}]$.

$$\frac{1}{[\text{Mn–TNS}]} = \frac{1 + K_T[\text{Mn}_{\text{total}}]}{K_T[\text{Mn}_{\text{total}}][\text{TNS}_{\text{total}}]} \tag{3}$$

At [M] > cmc (critical micelle concentration)

$$[\text{Mn}_{\text{total}}] = \frac{1}{n}[\text{M}]_{\text{total}} \tag{4}$$

substituting (4) into (3) gives

$$\frac{1}{[\text{Mn–TNS}]} = \frac{1}{[\text{TNS}_{\text{total}}]} + \frac{n}{K_T[\text{M}]_{\text{total}}[\text{TNS}_{\text{total}}]} \tag{5}$$

Assume

$$I = \alpha_T[\text{Mn–TNS}] \tag{6}$$

where I is the fluorescence intensity and α_T is a coefficient which is temperature dependent. Then

$$\frac{1}{I} = \frac{1}{\alpha_T[\text{TNS}_{\text{total}}]} + \frac{n}{\alpha_T K_T[\text{M}]_{\text{total}}[\text{TNS}_{\text{total}}]} \tag{7}$$

The enthalpy of the binding was calculated to the following equation:

$$\Delta H = -R\frac{\mathrm{d} \ln K_T}{\mathrm{d}(1/T)} \tag{8}$$

TABLE I: Comparison of Critical Micelle Concentrations Obtained with Literature Values at 25°

Ionic strength	cmc, *M* × 10^3 (lit. values)	cmc, *M* × 10^3 (obsd)
Water	8.0,[a] 8.13,[b] 8.1[c]	8.0
0.033	2.15,[d] 3.09[c]	2.25
0.050	2.3[a]	1.55
0.10	1.39[c]	0.85
0.20	0.94,[a] 0.83[c]	0.61
0.40	0.52[c]	0.50
0.50	0.51[a]	

[a] Reference 16. [b] Reference 17. [c] Reference 18. [d] Reference 19.

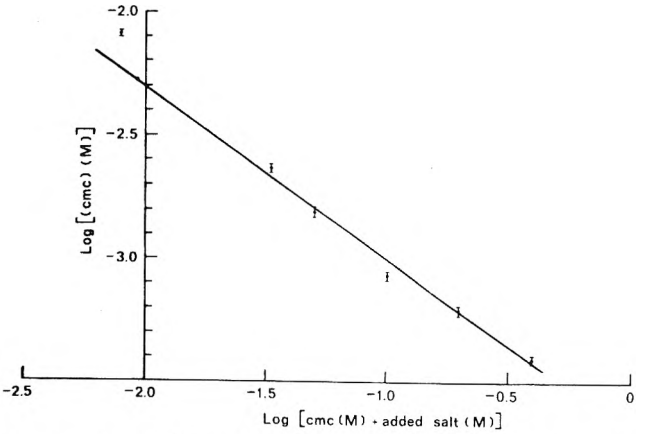

Figure 2. The plot of log [cmc (*M*)] vs. log [cmc (*M*) + added salt (*M*)] at 25°.

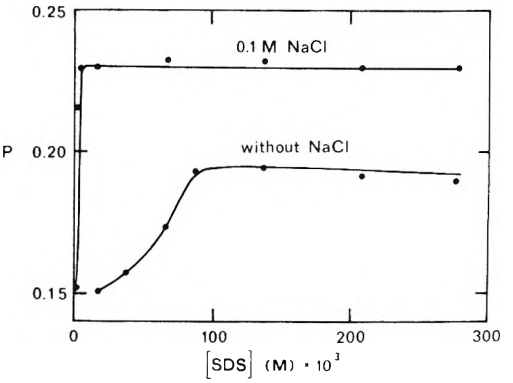

Figure 3. Polarization of fluorescence emission spectrum in water and in 0.1 *M* NaCl at 25°. [TNS] = 8.61×10^{-5} *M*.

Results

Critical Micelle Concentration (cmc). The micelle formation at SDS concentrations larger than the cmc was accompanied by a sharp increase in the fluorescence of the added TNS. Figure 1 shows how fluorescence changes with SDS micelle formation in water. In agreement with the cmc value obtained by other methods[16-18] without added salt, it was found that the cmc obtained by this method occurred at an SDS concentration of 8.0×10^{-3} *M*. This value was independent of added TNS concentrations. However, at or below a TNS concentration of 6×10^{-6} *M*, micelle formation could not be accurately detected by this method (Figure 1). The cmc at various concentrations of added salt (NaCl) compared with literature values are listed in Table

I. It has been established that there is a linear relation between log cmc and log (cmc + molarity of added salt).[16] Such a linear relationship is exhibited by a plot (Figure 2) of our values of log cmc vs. log (cmc + molarity of added salt). The formation of micelles from SDS monomers also causes an increase of polarization of fluorescence as shown in Figure 3. Salt increases the polarization of fluorescence of TNS (Figure 3). This suggests that salt may increase the rotational relaxation time[20] of TNS due to the salt-induced rigidity of the binding site of TNS in the micelle of SDS.

The Binding between TNS and the Micelle of SDS. Salt Effect and Temperature Effect. Figure 4a shows the relative fluorescence enhancement at three different TNS concentrations and varying SDS concentrations in water at 25°. Figure 4b shows a linear relation for the reciprocal plot of the intensity and [SDS] values of Figure 4a at [SDS] above 0.0694 M (see eq 7). Below this [SDS] value, the relation is nonlinear and eq 7 cannot be fitted to the data (Figure 4b). The reason may be that cooperative formation of micelles at [SDS] below 0.0694 M makes the assumption of independent formation of micelles, an assumption which was used to derive the equation, not valid (see later).

By extrapolating [SDS] to infinity, an I_{max} value of each TNS concentration in Figure 4a is obtained. The results in Figure 4c show that a linear relationship exists between I_{max} and [TNS_{total}] (eq 7). It should be noted here that one micelle of SDS consists of about 100 monomers[16] and micelle size is roughly independent of SDS concentrations up to 0.25 M.[21]

Since a high solution viscosity may enhance TNS fluorescence,[1] viscosity measurements at various SDS concentrations were made and the results are shown in Figure 4a. The viscosity contribution to fluorescence enhancement was determined by measuring the TNS fluorescence enhancement in sucrose solutions. The result in Figure 4d indicates that in the concentration range of SDS used, the viscosity contributed insignificantly to the fluorescent enhancement of TNS.

The plots of 1/[SDS] vs. $1/I$ at three different salt concentrations 0, 0.05, and 0.1 M are given in Figure 5. Figure 5a–c was obtained at 15, 25, and 35°, respectively. The line intercept is independent of salt concentration for each temperature, but the slopes are dependent on both salt concentration and temperature. The α_T values are calculated to be 58.14 × 10^5 M^{-1} at 15°, 47.7 × 10^5 M^{-1} at 25°, and 41.9 × 10^5 M^{-1} at 35° and the plot is shown in Figure 6. Temperature dependent quenching is a general phenomenon which is caused by greater collisional quenching at higher temperature.[22] No significant wavelength shift of the emission spectra can be noted in the test of temperature dependent frequency. The wavelength of maximum emission is about 455 nm.

The association constant K_T can be obtained from the slope of Figure 5. In the calculation of K_T, according to eq 7, n = 100 is assumed and the α_T values at different temperatures as obtained from the data in Figure 6 are used. As indicated in Table II, the association constant increases as the salt concentration increases for each temperature. The ΔH of binding was determined from the van't Hoff plot of association constant vs. $1/T$ (Figure 7). They are listed in Table II and three main conclusions can be drawn. First, no significant difference in enthalpy can be seen at different temperatures and salt concentrations. The negative value of enthalpy predominately contributed to the negative free energy of binding between TNS and micelles of

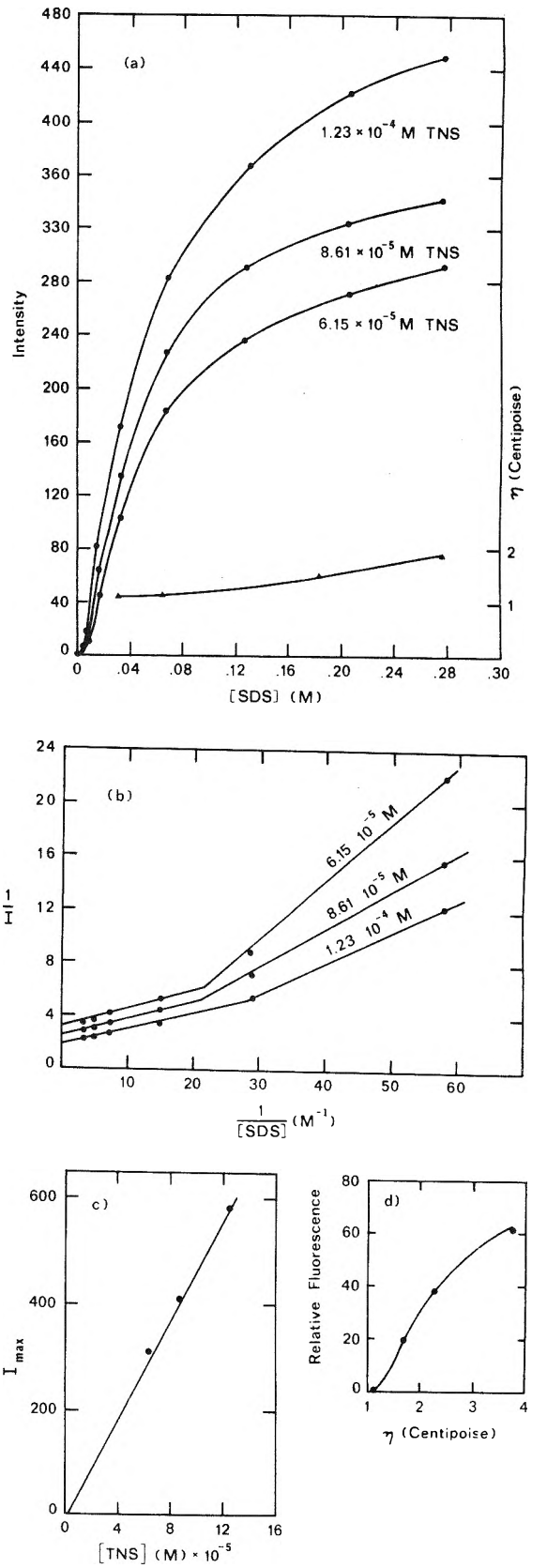

Figure 4. (a) Fluorescence titration (●) and viscosity measurement (▲) at various SDS and TNS concentrations, temperature 25°. (b) The reciprocal plot of Figure 4a (see eq 7). (c) The I_{max} vs. TNS concentration. The I_{max}'s at various TNS concentrations were obtained by extrapolating the 1/I vs. 1/[SDS] lines in Figure 4b to infinite SDS concentration. (d) Fluorescent enhancement vs. viscosity. Sucrose solutions were used. [TNS] = 1.23 × 10^{-4} M.

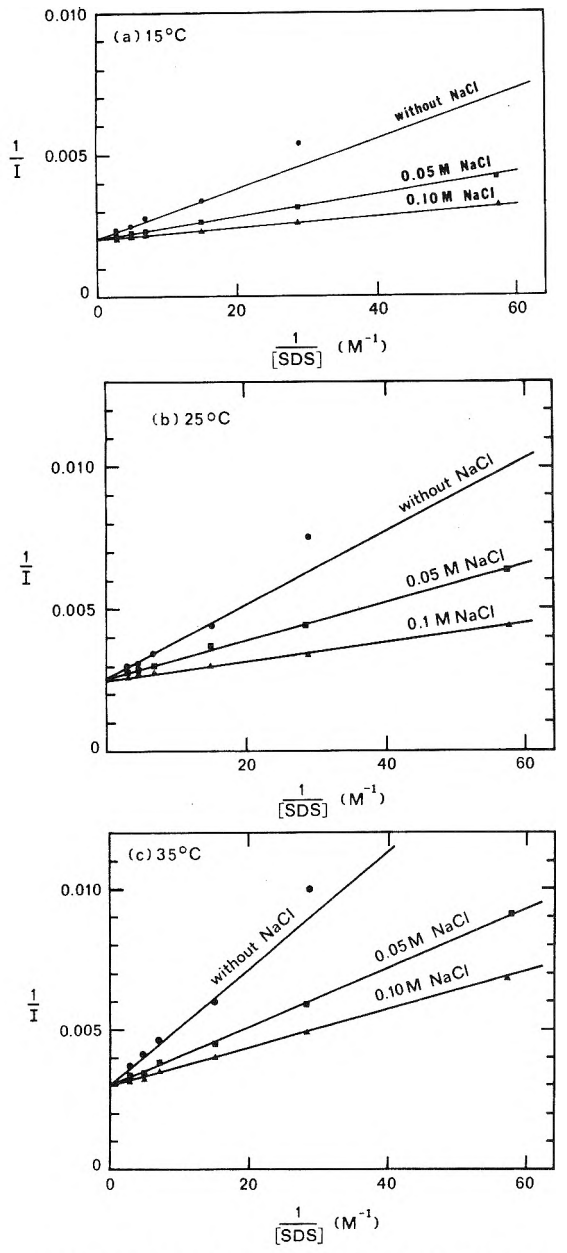

Figure 5. (a–c) The plot of $1/I$ vs. $1/[SDS]$ at 15, 25, and 35°.

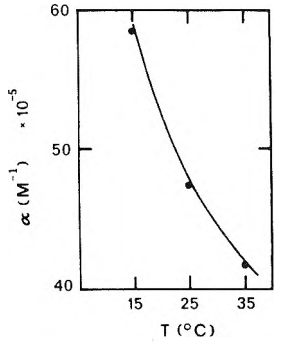

Figure 6. The plot of α_T vs. temperature (see eq 6).

SDS. Second, salt increases the association constant by increasing the entropy. The increase in the magnitude of the association constant in salt solution is a general phenomenon if the binding force is hydrophobic.[23] Third, although micelle formation may be accompanied by a positive, a negative, or a zero change of enthalpy, the entropy is always increased, i.e., the entropy gain is a general phenomenon encountered in hydrophobic interaction.[15,24] Our entropy data indicate that the interaction of TNS with SDS micelles has a strong hydrophobic contribution.

TABLE II: Thermodynamic Parameters of Binding between SDS and TNS at Different Ionic Strengths and Temperatures

Temp, °C		Ionic strength of added salt		
		0	0.05	0.10
15	ΔG^a	−4.565	−4.867	−5.240
	ΔH^a	−3.245	−3.245	−3.245
	ΔS^b	4.583	5.632	6.927
25	ΔG^a	−4.462	−4.802	−5.237
	ΔH^a	−3.245	−3.245	−3.245
	ΔS^b	4.084	5.225	6.685
35	ΔG^a	−4.407	−4.734	−5.106
	ΔH^a	−3.245	−3.245	−3.245
	ΔS^b	3.773	4.834	6.142

[a] The unit of ΔG and ΔH is kcal/mol. [b] The unit of ΔS is eu.

It is well established that micelle formation at the cmc is cooperative.[15] In Figure 8, the Hill plot[25,26] of binding between TNS and the micelle of SDS at 0, 0.05, and 0.1 *M* NaCl is given. In all cases a biphasic property is observed. The Hill coefficients near the critical micelle concentrations are greater than 1; the Hill coefficient at SDS concentration higher than the cmc is about 1. The results suggest that there is cooperative formation of micelles at an SDS concentration near the cmc. Moreover, the higher the concentration of added salt, the greater cooperativity is observed. At SDS concentrations higher than the cmc, the micelle seems to act independently. The salt also increased the polarization of the TNS fluorescence (Figure 3) indicating a salt-induced micelle rigidity.

Discussion

Evidence presented here supports the view that hydrophobic interactions contribute to the binding between TNS and the SDS micelle. It is based on the findings that binding involves a positive entropy change and that salt increases the association constant only by increasing the entropy gain. The entropy gain caused by the added NaCl was about 2.5 eu when its concentration was increased from 0 to 0.1 *M* at each temperature. The entropy increase, being caused by a hydrophobic effect, results from the freeing of water molecules from the solvent shell of the nonpolar moiety of TNS and their transfer into the bulk water phase which is less ordered than the solvent shell. It is known that hydrophobic bonds are strengthened by addition of electrolytes.[23] In other words, the increase of binding entropy may have resulted from the fact that the entropy gain caused by the loss of so-called "icebergs"[27] around the aromatic residue of TNS is greater than the entropy loss caused by the salt-induced rigidity of the SDS micelle–TNS complex (Figure 3).

The thermodynamic data obtained for the interaction of ANS and apomyoglobin were $\Delta F° = -7.32$ kcal/mol, $\Delta H° = -5.06$ kcal/mol, and $\Delta S° = 7.71$ eu.[28] The values obtained for the interaction of TNS and collagen were $\Delta G = -5.7$ kcal/mol, $\Delta H = -4.0$ kcal/mol, and $\Delta S = 6.0$ eu.[10] In these two cases, the enthalpy contributes predominantly to

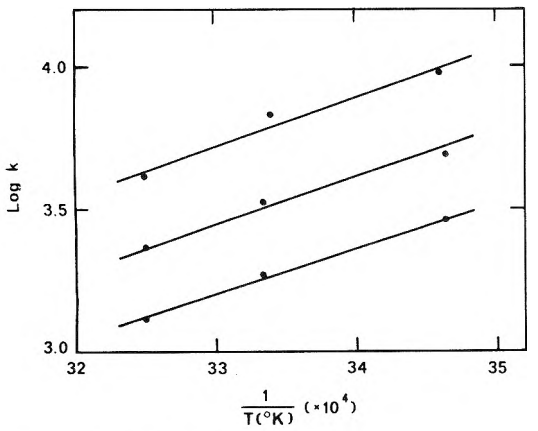

Figure 7. The plot of log K vs. $1/T$ (°K).

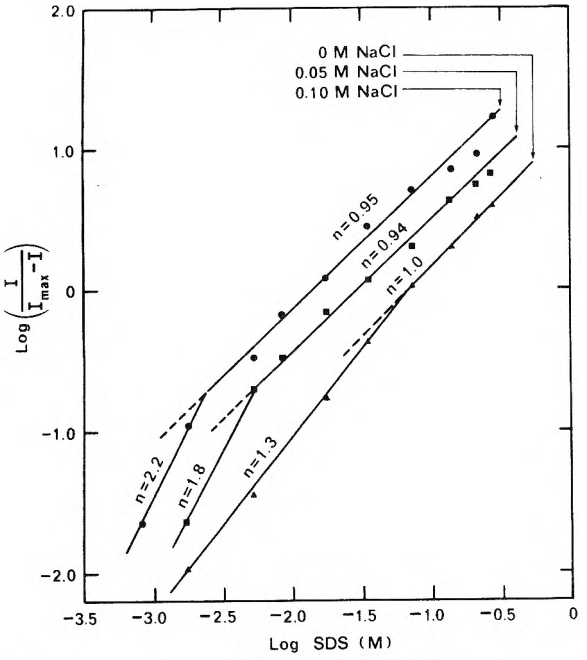

Figure 8. Hill plot of the interaction of TNS with SDS at various salt concentrations, at 25°.

the binding force, and an entropy gain is observed. These values are in good agreement with the thermodynamic data which we have obtained for the interaction of TNS and the SDS micelle. The main contribution of ΔH to the binding force may be the result of London dispersion forces for the binding of TNS to the SDS micelle. However, the possibility exists that when the TNS molecule binds to the SDS molecule, a weak, distorted hydrogen bond, formed between a water molecule in the iceberg and the TNS anilino group, breaks and becomes a stronger hydrogen bonded H_2O molecule in the bulk water. Camerman and Jensen mentioned the possible existence of hydrogen bonding in the hydrated crystal of TNS.[29]

The charge repulsion of a negatively charged fluorescent probe at the binding site of a macromolecule may be critical for the binding if the hydrophobic characteristic of the binding site is not sufficiently large or if steric hindrance, created by negatively charged groups, exists in the binding site. In the interaction of TNS with the SDS micelle, however, charge repulsion is overcome since there is a suitable hydrophobic binding environment for TNS. Tanford[15] has described the possible formation of these kinds of mixed micelles.

It has been demonstrated that a fluorescent probe–protein complex[10,30-32] or a fluorescent probe–membrane complex[8,33] shows substantial fluorescence enhancement in acidic solution. Two aspects of this have been given in the literature. First, when proteins are denatured in acidic medium, there is an increase in the value of the dissociation constants and there are a greater number of binding sites and/or there is an increase in fluorescent quantum yield of the bound probe. For example, the ANS–haptoglobin[32] or TNS–chymotrypsin[30] complex show these effects. Second, the decreased charge repulsion between negatively charged fluorescent probes with collagen[10] and with phospholipid[8] resulted in fluorescence enhancement when the pH was changed from pH 6 to 3. Neither observation requires charge neutralization for the binding of negatively charged fluorescence probes with macromolecules.

Salt-induced rigidity of a SDS micelle may be due to decreasing the charge repulsion of SDS monomers in the micelle. This may cause more efficient packing of SDS monomers in the micelle.

Flanagan and Ainsworth[14] concluded that anionic ANS could not bind to the SDS micelle because of charge repulsion. We find that the ANS concentrations used in their experiments are too low (1×10^{-6} M) to detect micelle formation. Also, ionic strength is a critical variable for the cmc value. We were not able to confirm their observation that 0.05% w/v SDS, in a solution to which no salt had been added, was the critical micelle concentration.

Acknowledgment. The authors thank Professor Paul Haberfield for helpful discussions.

References and Notes

(1) W. C. McClure and G. M. Edelman, *Biochemistry*, **5**, 1908 (1966).
(2) L. Brand and J. R. Guhlke, *Ann. Rev. Biochem.*, **41**, 843 (1972).
(3) L. Stryer, *Science*, **162**, 526 (1968).
(4) T. Takagi, *Tampakushitsu Kakusan Koso, Bessatzu*, 143 (1974).
(5) C. F. Beyer, L. C. Craig, and W. A. Gibbons, *Biochemistry*, **11**, 4920 (1972).
(6) J. Lynn and C. D. Fasman, *Biochem. Biophys. Res. Commun.*, **33**, 327 (1968).
(7) G. Witz and B. L. van Duurren, *J. Phys. Chem.*, **77**, 648 (1973).
(8) M. T. Flanagan and T. R. Hesketh, *Biochim. Biophys. Acta*, **298**, 535 (1973).
(9) G. K. Radda, *Biochem. J.*, **122**, 385 (1971).
(10) H.-C. Chiang and A. Lukton, *Biopolymers*, in press.
(11) J. A. Gally, Doctoral Dissertation, The Rockefeller University, New York, N.Y., p 50.
(12) S. K. Phillips and W. A. Cramer, *Biochemistry*, **12**, 1170 (1973).
(13) L. Brand, J. R. Gohlke, and D. S. Rao, *Biochemistry*, **6**, 3510 (1967).
(14) M. T. Flanagan and S. Ainsworth, *Biochim. Biophys. Acta*, **168**, 16 (1968).
(15) C. Tanford, "The Hydrophobic Effect", Wiley, New York, N.Y., 1973.
(16) M. F. Emerson and A. Moltzer, *J. Phys. Chem.*, **71**, 1898 (1967).
(17) A. B. Scott and H. V. Tarter, *J. Am. Chem. Soc.*, **65**, 692 (1943).
(18) J. N. Phillips, *Trans. Faraday Soc.*, **51**, 561 (1955).
(19) J. Steinhardt, N. Stocker, D. Carroll, and K. S. Birdi, *Biochemistry*, **13**, 4461 (1974).
(20) G. Weber, *Adv. Protein Chem.*, **8**, 415 (1953).
(21) F. Reiss-Husson and V. Luzzati, *J. Phys. Chem.*, **68**, 3504 (1964).
(22) R. W. Ricci, *J. Chem. Educ.*, **51**, 692 (1974).
(23) W. Kauzmann, *Adv. Protein Chem.*, **14**, 1 (1959).
(24) Z. N. Markina, O. P. Bovkun, and P. A. Reibinder, *Kollid Zh.*, **35**, 833 (1973).
(25) A. V. Hill, *J. Physiol. (London)*, **40**, 4 (1910).
(26) F. Wold, "Macromolecules: Structure and Function", Prentice-Hall, Englewood Cliffs, N.J., 1971.
(27) H. S. Frank and M. W. Evans, *J. Chem. Phys.*, **13**, 507 (1945).
(28) L. Stryer, *J. Mol. Biol.*, **13**, 482 (1965).
(29) A. Camerman and L. H. Jensen, *J. Am. Chem. Soc.*, **92**, 4200 (1970).
(30) W. O. McClure and G. M. Edelman, *Biochemistry*, **6**, 559 (1967).
(31) D. P. Bloxham, *Biochemistry*, **12**, 1602 (1973).
(32) S. F. Russo and W. W. C. Chen, *Biochemistry*, **13**, 5300 (1974).
(33) J. Hawiger and S. Timmons, *Biochem. Biophys. Res. Commun.*, **55**, 1278 (1973).

Adsorption of Hydrogen Peroxide on the Surface of Titanium Dioxide

A. H. Boonstra* and C. A. H. A. Mutsaers

Philips Research Laboratories, Eindhoven, The Netherlands *(Received February 20, 1975)*

Publication costs assisted by Philips Research Laboratories

Total reflection spectra of TiO_2 powder samples were measured after adsorption of different amounts of hydrogen peroxide and were compared with reflection spectra of TiO_2 samples illuminated in an oxygen atmosphere. For powders with the same specific surface area the yellow coloration observed after chemisorption of the same amounts of hydrogen peroxide was more intense for rutile than for anatase. The yellow color disappeared during uv illumination and oxygen was liberated. When TiO_2 samples, treated with H_2O_2, were heated in a vacuum system, desorption of O_2 started at 50° and the decomposition of the H_2O_2 surface compound was complete at 150°. The results were compared with those of TiO_2 samples illuminated in oxygen. It was concluded that no H_2O_2 was formed during the photoadsorption of O_2 on TiO_2 samples. The formation of hydrogen radicals is suggested as an explanation for photoactivity of TiO_2.

Introduction

The mechanism of the photoreaction of metal oxides has been the subject of numerous publications. It has been known for many years that during the illumination in the near-uv of a suspension of ZnO in water small but easily measurable amounts of hydrogen peroxide are formed.[1-5] No H_2O_2 was observed when TiO_2 was illuminated under similar conditions.[5-8]

Several studies of the photocatalytic reactions using TiO_2 have been made on the gas–solid interface. In the case of oxygen an irreversible adsorption on the surface of the TiO_2 powder has been observed during the illumination.[8-14] The amount of adsorbed O_2 depends strongly on the pretreatment of the sample. Bickley et al.[12,13] found that the adsorption of water on the TiO_2 surface was important for the photoadsorption of oxygen on rutile. Recently a relation was found between the amount of adsorbed water and the photoadsorption of oxygen on the TiO_2 surface.[14]

A decisive mechanism for the photoreaction of TiO_2 has not been reported. Some authors suggested that hydroxyl radicals were formed as a result of the illumination.[6,12,13,15-17] However, the existence of hydroxyl radicals may lead to their combination in pairs to form hydrogen peroxide. The reason why no H_2O_2 was detected after illumination of TiO_2 might be a reaction of H_2O_2, immediately after its formation, with the surface of TiO_2.

The aim of our investigations was to see if this explanation is correct. Therefore total reflection spectra of TiO_2 samples, on which different amounts of H_2O_2 had been chemisorbed, were compared with the reflection spectra of TiO_2 powders illuminated in oxygen. The influence of the increase of temperature on the properties of these powders was also investigated.

The behavior under illumination of TiO_2 samples treated with H_2O_2 was investigated and the results were compared with those of untreated TiO_2 samples.

To enhance these surface effects TiO_2 powders with large specific surface areas were used.

Experimental Section

Materials. The investigations of the reaction of hydrogen peroxide with TiO_2 powders were carried out on the following samples: (a) anatase P25 from Degussa, Frankfurt; (b) anatase MS741 from Kronos Leverkusen; and (c) a rutile laboratory sample.

The rutile sample was prepared by adding titanium tetrachloride to freezing distilled water.[18] The mixture was slowly heated to about 105° and refluxed for 60 hr. The powder was repeatedly washed with distilled water of 100° until the solution was free from Cl^- ions.

The surface areas of the samples were determined by the BET method at −195° using krypton, assuming the area of a krypton atom to be 19.5 $Å^2$. The specific surface areas of these samples are given in Table I.

Measurements on TiO_2 Samples Treated with H_2O_2. The TiO_2 samples covered with different amounts of H_2O_2 were prepared as follows.

Samples of TiO_2, 0.5–10 g, were stirred in an aqueous H_2O_2 solution and filtered after 10 min. By measuring the change in concentration of the H_2O_2 solution using a $KMnO_4$ solution the amount of adsorbed H_2O_2 could be calculated. After filtration the samples were dried under vacuum of 10 N m^{-2} for 1 hr.

Total (diffuse plus specular) reflection spectra of a number of these samples were measured by illuminating the layers with normal incident light on a Beckmann DK2A spectrophotometer with a special integrating sphere accessory.[19,20] The transmission of the TiO_2 layers with a thickness of about 5 mm was negligibly small.

To test the stability of the yellow surface compound formed by the chemisorption of H_2O_2 on the surface of TiO_2 a known amount of the sample was placed in glass bulb, which was sealed to a vacuum system[14] and evacuated at room temperature. After evacuation for 1 hr a pressure of 10^{-4} N m^{-2} was reached. Then the powder was gradually heated in a closed system to 200° for a period of 2 hr.[21] The desorbed gas was analyzed by a Perkin-Elmer Type 607-1000 partial pressure analyzer and was found to be oxygen and water. The water could be frozen out by a liquid N_2 trap. The amount of desorbed oxygen was measured by a McLeod manometer as a function of the temperature.

The influence of illumination in the near-uv on the TiO_2 samples treated with H_2O_2 was investigated at room temperature in the same vacuum system. The powder was

TABLE I: Specific Surface Area of TiO_2 Powders

Sample	Surface area, $m^2\ g^{-1}$
Degussa P25	56
Kronos MS741	110
Rutile	102

evacuated at room temperature for 1 hr. Then the system was closed and the powder was exposed to the uv light from a water-cooled Philips SP 500 W spectrum lamp. The changes in pressure were measured as a function of the illumination time. During illumination with uv light of 320–390 nm the bulb was vigorously shaken by a Wilten Holland Vortex Genie mixer to ensure that all the powder was exposed to the light. A detailed description of this method has been given elsewhere.[14]

Results

A yellow color appeared when the TiO_2 samples were treated with H_2O_2. The intensity of the coloration depended on the concentration of the H_2O_2 solution and on the specific surface area of the samples. In Figure 1 the amount of chemisorbed H_2O_2 per unit area is given as a function of the H_2O_2 concentration of the filtrate for a rutile and for an anatase sample. The yellow color was also found when the powders were exposed to the vapor of an H_2O_2 solution. Using samples with about the same specific surface area we found that the coloration of the rutile sample was more intense than that of the anatase MS741 sample at the same surface coverage. The color disappeared without desorption of H_2O_2 from the surface when a solution of NaOH was added. After acidification of the solution the same yellow color appeared again.

The adsorption of H_2O_2 on ZnO powder was also investigated. The adsorption on the ZnO sample, Analar, London (specific area 4.2 $m^2\ g^{-1}$), was found to be less than 10^{12} molecules of $H_2O_2\ cm^{-2}$ at a H_2O_2 solution concentration of 10^{-3} M. The adsorption on the TiO_2, Tiofine A10, Rotterdam, with about the same specific surface area (6.8 $m^2\ g^{-1}$) was about 4×10^{13} molecules of $H_2O_2\ cm^{-2}$. In the case of the ZnO sample supplied by the St. Joseph Lead Co. New York, no H_2O_2 adsorption was detected.

The total (diffuse + specular) reflection R of a number of TiO_2 samples covered with different amounts of H_2O_2 was then measured as a function of the wavelength of the incident light. In Figure 2 the results are given for the anatase sample MS741 and in Figure 3 for the rutile sample. In the case of anatase P25 the effect of the H_2O_2 chemisorption on the reflection is somewhat less than in the case of MS741, in agreement with the difference in specific surface areas.

We also measured the total reflection of TiO_2 samples illuminated for 3 hr in an oxygen atmosphere of about 20 N m^{-2}.[14] The amount of oxygen photoadsorbed was 8×10^{12} molecules of $O_2\ cm^{-2}$ for the anatase sample MS741 and 5×10^{12} molecules of $O_2\ cm^{-2}$ for the rutile sample. The results are given in Figure 4. Comparing these results with those given in Figures 2 and 3 we see that the spectra of the samples are the same as those of the untreated TiO_2 samples, although the amounts of adsorbed O_2 are comparable with those of adsorbed H_2O_2.

A number of the TiO_2 samples treated with H_2O_2 were evacuated at room temperature for 1 hr and then heated in a closed system. At about 50°, O_2 desorption started and at 150° the decomposition of the surface compound was complete. The original white color of TiO_2 had returned. The amount of desorbed oxygen molecules was half that of adsorbed H_2O_2 molecules. Only in the case of high surface coverages of H_2O_2 was the amount of O_2 somewhat smaller than expected which was probably due to the desorption of small amounts of H_2O_2 during the evacuation. The same heating procedure was followed with TiO_2 samples illuminated in an oxygen atmosphere and with untreated samples. The results are given in Figure 5. Up to 200° no oxygen desorption was observed on TiO_2 samples on which O_2 had been photoadsorbed to a coverage of 10^{13} molecules of $O_2\ cm^{-2}$.

Because TiO_2 samples treated with H_2O_2 slowly lose their yellow color when exposed to daylight for several hours, some samples were illuminated in the vacuum system. After evacution at room temperature for 1 hr in the dark the system was closed. No desorption took place during the following 30 min. Then the illumination in the near-uv was started and the desorption of O_2 was measured as a function of time. The results are given in Figure 6. Con-

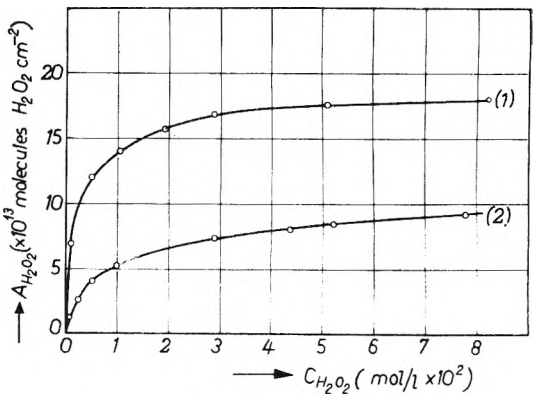

Figure 1. H_2O_2 adsorption (A) on TiO_2 as a function of the concentration of the H_2O_2 solution for (1) an anatase sample MS741 and (2) a rutile sample.

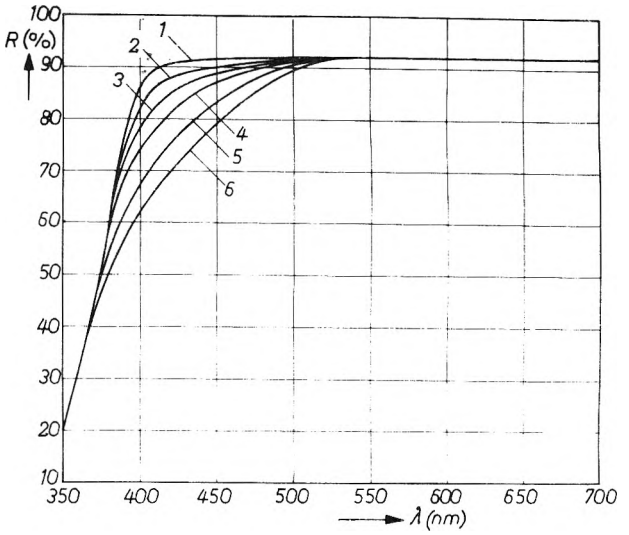

Figure 2. The total (diffuse + specular) reflection as a function of the wavelength of the incident light for the anatase samples (MS741) covered with (1) untreated, (2) 2×10^{12} molecules of $H_2O_2\ cm^{-2}$, (3) 7×10^{12} molecules of $H_2O_2\ cm^{-2}$, (4) 15×10^{12} molecules of $H_2O_2\ cm^{-2}$, (5) 36×10^{12} molecules of $H_2O_2\ cm^{-2}$, and (6) 70×10^{12} molecules of $H_2O_2\ cm^{-2}$.

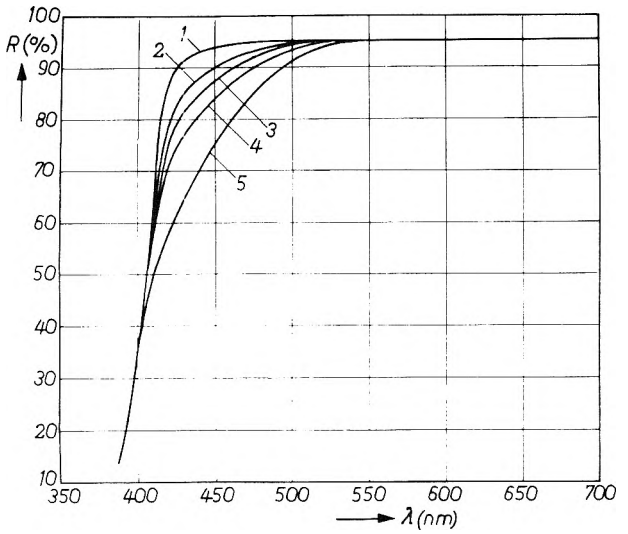

Figure 3. The total (diffuse + specular) reflection as a function of the wavelength of the incident light for the rutile sample covered with (1) untreated, (2) 10^{12} molecules of H_2O_2 cm^{-2}, (3) 2×10^{12} molecules of H_2O_2 cm^{-2}, (4) 4×10^{12} molecules of H_2O_2 cm^{-2}, and (5) 9×10^{12} molecules of H_2O_2 cm^{-2}.

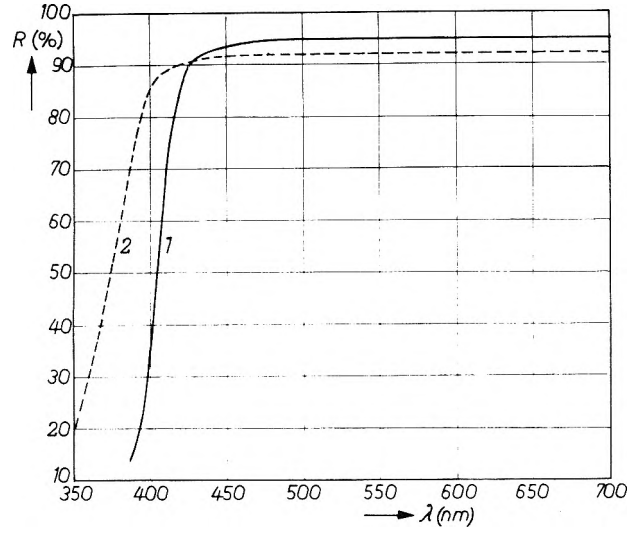

Figure 4. The total (diffuse + specular) reflection as a function of the wavelength of the incident light for (1) a rutile sample after photoadsorption of 5×10^{12} molecules of O_2 cm^{-2} and an anatase sample (MS741) after photoadsorption of 8×10^{12} molecules of O_2 cm^{-2}.

densible gases were trapped in the liquid N_2 baffle. After the illumination and after the baffle had been warmed to room temperature no H_2O_2 was detected. During illumination the yellow color of the powder slowly disappeared. The total amount of desorbed O_2 was smaller than was to be expected from the amount of chemisorbed H_2O_2. This was probably due to the normal photoadsorption of O_2 by TiO_2 which occurred simultaneously.

Discussion

From the hydrogen peroxide adsorption experiments it was found that a solution of H_2O_2 as well as an H_2O_2 vapor reacts with TiO_2 powder giving a yellow-colored surface compound. The amount of chemisorbed H_2O_2 per unit surface area depends on the concentration of the H_2O_2 solution and on the modification of TiO_2. With ZnO powders no H_2O_2 adsorption was observed.

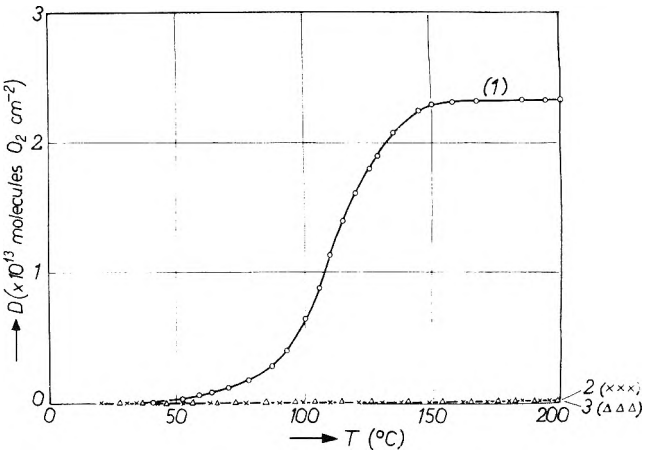

Figure 5. The amount of O_2 desorbed from an anatase sample (P25) as a function of the baking temperature for (1) a sample pretreated with 4.9×10^{13} molecules of H_2O_2 cm^{-2}, (2) a sample after photoadsorption of 1.0×10^{13} molecules of O_2 cm^{-2}, and (3) an untreated sample.

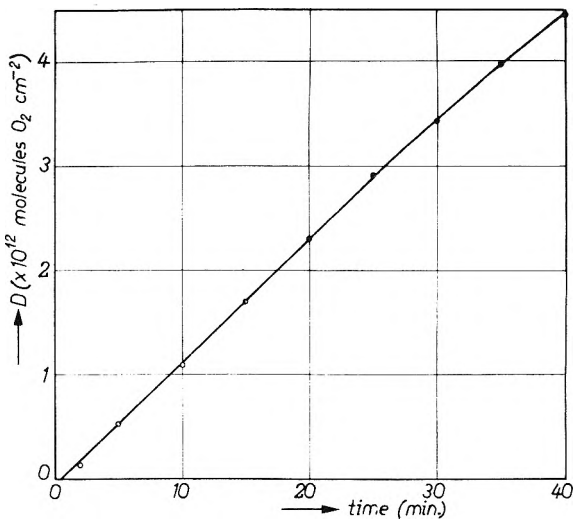

Figure 6. The oxygen photodesorption from an anatase sample (MS741) pretreated with 4.0×10^{13} molecules of H_2O_2 cm^{-2} as a function of the illumination time.

The differences between ZnO and TiO_2 with respect to the adsorption of H_2O_2 may explain why, during illumination of suspensions of ZnO in water, H_2O_2 was detected while, in the case of TiO_2 suspensions, no H_2O_2 was found. However, the total reflection measurements showed that even small amounts of chemisorbed H_2O_2 have a marked effect on the reflection of TiO_2 samples. The photoadsorption of the same amounts of oxygen does not change the reflection at all. These results agree well with those of other authors[8,16] who did not find any discoloration of TiO_2 powders after illumination in oxygen. Only Knoll et al.[22,23] reported that a yellow color was found during the illumination of TiO_2. However, the description of their experiments was not detailed. Kaluza et al.[16] reported a yellow coloration of anatase under uv illumination in the presence of Hg vapor and O_2. The same yellow color was developed when ZnO instead of TiO_2 was used. Their conclusion was that the yellow color arising during illumination was caused by the formation of HgO.

That the compound formed on the surface of TiO_2 after adsorption of H_2O_2 was different from that resulting from O_2 photoadsorption was confirmed by the thermal desorption experiments. In the case of H_2O_2 adsorption, a complete desorption of oxygen was measured, after heating the sample to 150°, whereas an O_2 photoadsorbed TiO_2 sample heated to this temperature showed no desorption of O_2. In our opinion as a result of the chemisorption of H_2O_2 the yellow color is caused by the formation of Ti_s–O–O–H groups on the surface.

It was found that illumination of TiO_2 samples treated with small amounts of H_2O_2 resulted in desorption of oxygen whereas an untreated sample did photoadsorb oxygen.

From the results mentioned it was concluded that the photoadsorption of oxygen on TiO_2 was not caused by the formation of H_2O_2. Therefore a mechanism describing the photoreaction in terms of the formation of OH radicals[12,16,17] is not probable.

Bickley[12] observed a decrease in photoreactivity of rutile after desorption of water and recently[14] we found a linear relation between the number of TiOH groups on the surface and the adsorption of oxygen under illumination. Therefore Ti_s–O–H groups must be a governing factor in the photomechanism. The photoreaction of TiO_2 can in our opinion be better described by the formation of hydrogen radicals as follows:

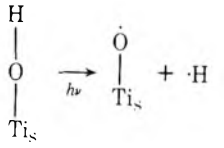

In the presence of oxygen the hydrogen radicals can react by way of intermediate radicals such as $\cdot HO_2$[6,12,13] to form water. Continuation of the illumination increases the number of Ti_s–O· radicals on the surface and consequently the probability that these radicals will trap the hydrogen radicals again. This results in a decrease in the rate of the consumption of oxygen with increasing exposure time.

Because of the acceptor-like behavior of Ti–O· radicals formed on the surface during the illumination, at least some of these are negatively charged. This trapping of electrons in the Ti–O surface states may explain the decrease in conductivity of an n-type TiO_2 sample during the illumination in oxygen.[8,11]

References and Notes

(1) E. Bauer and C. Neuweiler, *Helv. Chim. Acta*, **10**, 901 (1927).
(2) G. Winter, *Nature (London)*, **163**, 326 (1949).
(3) T. R. Rubin, J. G. Calvert, G. T. Rankin, and W. McNevin, *J. Am. Chem. Soc.*, **75**, 2850 (1953).
(4) J. G. Calvert, K. Theurer, G. T. Rankin, and W. McNevin, *J. Am. Chem. Soc.*, **76**, 2575 (1954).
(5) M. C. Markham and K. J. Laidler, *J. Phys. Chem.*, **57**, 363 (1953).
(6) G. A. Korsonovskii, *Russ. J. Phys. Chem.*, **34**, 241 (1960).
(7) G. Irick, *J. Appl. Pol. Sci.*, **16**, 2387 (1972).
(8) I. S. McLintock and M. Ritchie, *Trans. Faraday Soc.*, **61**, 1007 (1965).
(9) D. R. Kennedy, M. Ritchie, and J. Mackenzie, *Trans. Faraday Soc.*, **54**, 119 (1958).
(10) R. D. Murley, *J. Oil Colour Chem. Assoc.*, **45**, 16 (1962).
(11) G. Munuera and F. Conzalez, *Rev. Chim. Miner.*, **4**, 207 (1967).
(12) R. I. Bickley and F. S. Stone, *J. Catal.*, **31**, 389 (1973).
(13) R. I. Bickley and R. K. M. Jayanty, *Discuss. Faraday Soc.*, **58**, (1974).
(14) A. H. Boonstra and C. A. H. A. Mutsaers, *J. Phys. Chem.* **79**, 1694 (1975).
(15) W. Hughes, *FATIPEC Congr.*, **10**, 67 (1970).
(16) U. Kaluza and H. P. Boehm, *J. Catal.*, **22**, 347 (1971).
(17) H. G. Volz, G. Kampf, and H. G. Fitzky, *Farbe Lack*, **78**, 1037 (1972).
(18) Y. G. Bérubé and P. L. de Bruyn, *J. Colloid Interface Sci.*, **27**, 305 (1968).
(19) A. Netten and A. H. Boonstra, *Surface Sci.*, **27**, 77 (1971).
(20) A. H. Boonstra and R. M. A. Sidler, *J. Electrochem. Soc.*, **120**, 1078 (1973).
(21) A. H. Boonstra, *Philips Res. Rept. Suppl.*, 3 (1968).
(22) H. Knoll, R. Frydrych, and U. Kühnhold, *Naturwissenschaften*, **45**, 262 (1958).
(23) H. Knoll and U. Kühnhold, *Angew. Chem.*, 79, 998 (1967).

Hydrogenation of Di-*tert*-butyl Nitroxide Adsorbed on Supported Platinum Catalysts

Michèle M. Mestdagh,[1] George P. Lozos, and Robert L. Burwell, Jr.*

Ipatieff Laboratory, Department of Chemistry, Northwestern University, Evanston, Illinois 60201 *(Received January 13, 1975)*

Publication costs assisted by the Advanced Research Projects Agency

Di-*tert*-butyl nitroxide adsorbs on silica gel to form nitroxide strongly hydrogen bonded to silanol groups (Lozos and Hoffman). At lower coverages, adsorbed nitroxide exhibits a very low desorption pressure at 25°. The nitroxide adsorbs similarly on Pt/SiO_2 and $Pt/\gamma\text{-}Al_2O_3$ and gives ESR signals indistinguishable from nitroxide adsorbed on silica gel and on $\gamma\text{-}Al_2O_3$ alone. Exposure of the catalysts containing adsorbed nitroxide to hydrogen at 25° leads to rapid disappearance of the signal of nitroxide. Replacement of hydrogen by oxygen leads to the reappearance of a signal of nitroxide. Apparently the nitroxide is hydrogenated to di-*tert*-butylhydroxylamine which is then oxidized back to the nitroxide. The hydrogenation proceeds at −70° on Pt/SiO_2 at a wide range of coverages by nitroxide with a half-life of about 7 min. On Pt/Al_2O_3 the reaction is somewhat slower. Since the nitroxide is almost entirely on the silica portion of the catalyst surface and the desorption pressure is so low that migration of nitroxide to platinum through the vapor phase is negligible, some surface process brings together *H on platinum and nitroxide on silica. It is argued that this process is surface migration of nitroxide rather than surface migration of platinum particles or of hydrogen atoms (hydrogen spillover). The shape of the ESR signal of adsorbed nitroxide indicates that the nitroxide is reasonably uniformly distributed through the granules of the catalysts. The general procedure appears to provide a powerful method for studying surface migration.

We have studied the hydrogenation of the stable free radical di-*tert*-butyl nitroxide to di-*tert*-butylhydroxylamine

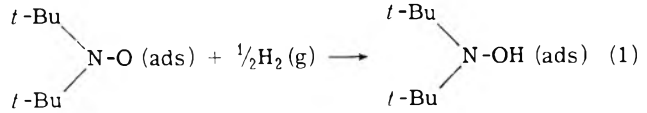

(1)

using ESR to follow the reaction. Under our conditions the nitroxide and the hydroxylamine were adsorbates on platinum/silica gel and platinum/alumina catalysts and the reaction temperatures were so low that the desorption pressures of the nitroxide and hydroxylamine were negligible. We have also observed reoxidation of the hydroxylamine to the nitroxide using oxygen and ethylene as the oxidizing agents. The occurrence of these reactions in the adsorbed phase raises interesting problems about the identity of the species whose migration transports hydrogen between platinum and species adsorbed on the surface of the silica gel.

Hoffman and Lozos have examined the ESR spectra of the nitroxide adsorbed on silica gel and on alumina.[2] Comparison of the hyperfine splitting of the signal of the nitroxide adsorbed on silica gel with that in a frozen, hydrogen-bonding solvent indicates that the nitroxide is adsorbed onto silica gel via hydrogen bonding to a hydrogen-bond donor with a pK_a near that of phenol, i.e., to a silanol group. Nitroxide on alumina exhibits a similar spectrum from nitroxide bound to surface hydroxyl groups but, in addition, it shows a spectrum split by ^{27}Al originating in nitroxide bound to the Lewis acid, Al^{3+}(cus) where (cus) means coordinatively unsaturated surface. As will appear in the present paper, deposition of particles of platinum upon silica and upon alumina has a negligible effect upon the appearance of these spectra.

Experimental Section

The reaction–ESR cell of Figure 1 contained a 5-cm length of square cross-section tubing 1.8 cm on edge. One end of this tubing was joined to a Fischer and Porter Teflon needle valve, the other to the ESR tube, a length of 4-mm o.d. tubing of fused silica. Both the lower and upper outlets terminated in short sections of 0.25-in. tubing which could be attached to Swagelock fittings using Teflon ferrules.

With the cell inverted from the position in Figure 1, about 50 mg of catalyst was inserted. It settled at position A where it was retained by a plug of glass wool. The system was attached to a gas manifold by a Swagelock connection at B. The catalyst was heated in flowing helium to 300°, and then exposed to the following gases at 300°: oxygen for 20 min, helium for 10 min, and hydrogen for 2 hr. The cell was cooled in flowing helium and then sealed off at the position marked by the arrow near B. The system was rotated 90° and the catalyst spread out upon the flat floor (area = 7 cm^2) of the tubing of square cross section to form a monolayer of granules of silica or alumina. The system was attached at C to a Nupro bellows valve behind which was a dosing bulb. The cell was evacuated, the bulb filled with vapor of di-*tert*-butyl nitroxide from another bulb containing a liquid sample held usually at 25° (vapor pressure, 1.4 Torr), and the valves between the cell and the bulb were opened for several minutes. The Teflon needle valve was closed, the system removed, rotated 90° to deliver the catalyst to the bottom of the ESR tube and the ESR spectrum was determined on a Varian E-4 spectrometer in the X-band usually at −70°. In some cases, the system was then reattached to the gas manifold and hydrogen or oxygen added followed by redetermination of the ESR spectrum. In other cases a bulb of hydrogen was attached at C and hydrogen was added while the system was at −70° in the spectrometer. The total pressure of hydrogen in the system was about 200 Torr, but the pressure was not carefully controlled.

The silica gel employed was a wide pore gel, Davison Grade 62, reported specific area 340 m^2/g, average pore diameter 14 nm, pore volume 1.15 cc/g. Details of the texture of the very similar Grade 59 are available.[3]

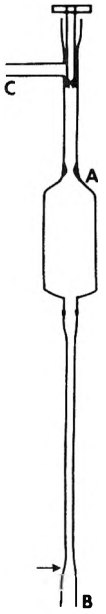

Figure 1. The reaction–ESR cell.

A 10% Pt/SiO_2 was prepared by ion exchange with a Pt(IV) ammine.[4] The 1.2% Pt/SiO_2, dispersion 22%, was prepared by Dr. Toshio Uchijima by ion exchange of $Pt(NH_3)_4^{2+}$ with Davison 62.[5] A 0.53% Pt/γ-Al_2O_3, dispersion 45%, was prepared by Dr. Harold Kung. The γ-alumina was prepared from 200–270 mesh Catapal SP (Continental Oil Co.) by calcining at 650° and rehydrating over water at 25°. Its surface area is taken as 230 m^2/g. It was impregnated with $(NH_3)_2Pt(NO_2)_{2\,aq}$, dried at 120°, calcined at 630° in oxygen, reduced at 350° in hydrogen, and rehydrated over water at 25°.

Results

The signal of nitroxide adsorbed on either Pt/SiO_2 catalyst remains unchanged for weeks if oxygen is excluded from the system, but, in the presence of oxygen, the ESR signal declines in intensity. Nitroxide adsorbed on Pt/Al_2O_3 appears to be less sensitive to oxygen.

At about −70°, hydrogenation of adsorbed nitroxide occurs rather rapidly on the 1.2% Pt/SiO_2, but at 25° hydrogen does not affect the spectrum of nitroxide adsorbed on silica gel devoid of platinum. Catalysts with several coverages of nitroxide were examined. At the conclusion of the experiments, the catalyst of highest coverage, Pt/SiO_2-I, was submitted for microanalysis. Miss H. Beck found C 1.89% and N 0.29% which corresponds to a mole ratio C/N of 7.6, about as close to 8 as one could expect. As calculated from percent C, there was 0.20 mmol of nitroxide/g of initial silica gel. The cross sectional area of di-*tert*-butyl nitroxide perpendicular to the N–O bond is about 0.7 nm^2. Thus, the total area which would be occupied by 0.20 mmol of nitroxide is 85 m^2, which corresponds to a coverage θ by nitroxide of 85/340 = 0.25. The quantity of adsorbed nitroxide on the catalysts of lower coverage was obtained from the ratio of the integrated intensity of the initial ESR signal of the sample to that of Pt/SiO_2-I. Integration was performed on an apparatus based on an operational amplifier constructed by Mr. J. R. Anderson. Pt/SiO_2-II has 0.5 the nitroxide of Pt/SiO_2-I and Pt/SiO_2-III has 0.03.

Plots of the logarithm of signal intensity vs. time of hydrogenation were linear to about 90% reacted for all samples. Beyond this, the rate of decline of the signal was smaller. The half-lives at −70° were Pt/SiO_2-I, 5 min; Pt/SiO_2-II, 10 min; Pt/SiO_2-III, 7 min.

Experiments similar to those described for Pt/SiO_2 were run with Pt/Al_2O_3. Pt/Al_2O_3-I was treated at 300° in the same way as Pt/SiO_2 and it was loaded with the nitroxide in the same way. Analysis at the end of the experiments gave C 1.57 and N 0.23 which corresponds to 0.17 mmol of nitroxide/g of Al_2O_3 or 70 m^2 of nitroxide/g of Al_2O_3 or θ = 0.30. The hydrogenation at −70° was slower than that on Pt/SiO_2 and the course of the reaction was not first order. For an initial period, the rate corresponded to a half-life of about 80 min, then the rate increased until the half-life was about 16 min. A duplicate run on Pt/Al_2O_3-II (initial coverage = 0.27) was of the same form but the hydrogenation proceeded about ⅓ faster.

As shown by Figure 2 for Pt/SiO_2-I, higher coverages by nitroxide exhibit exchange broadening of the signal. As hydrogenation proceeds, the signal approaches that of the magnetically dilute case. Similar phenomena occurred during hydrogenation of nitroxide adsorbed on Pt/Al_2O_3 as shown in Figure 3 for Pt/Al_2O_3-II. During hydrogenation of Pt/Al_2O_3-I, the initial spectrum at θ = 0.30 was of the same form as that of curve 2 in Figure 3. Structure appeared at about 60 min, θ = 0.18, and at about 90 min, θ = 0.09, the spectrum resembled that of curve 0 of Figure 2. The spectra sharpened a little until 180 min, θ = 0.03, at which time the catalyst was allowed to warm to room temperature. Two spectra were measured near the end of the warm-up at about 17°.

A cell was loaded with 25 mg each of 1.2% Pt/SiO_2 and silica gel, layered at position A of Figure 1 with the Pt/SiO_2 at the top. The sample was treated with the usual sequence of gases at 300°; the sample was transferred into the region of square cross section, mixed, and permitted to adsorb nitroxide. Analysis at the end of the experiment gave C = 1.82 and N = 0.23. This corresponds to θ = 0.24. Upon hydrogenation at −70°, one-half of the signal disappeared with an initial half-life of 8 min, a rate about that for the entire signal with Pt/SiO_2 alone. After 20 min the rate had become very slow and nearly constant in rate to 180 min after which the reaction cell was warmed to 25°. The first spectrum at 25° corresponded to a total loss of signal of 53%; after 1 hr the loss was 78% and after 18 hr, 97.5%.

The process of the previous sentence might have involved migration of nitroxide from silica to Pt/SiO_2 via the gas phase. To check on this, 43 mg of 60–70 mesh Davison Grade 62 silica gel was put in a cell and retained at A of Figure 1 by a plug of glass wool which was smaller and more open than usual. After evacuation of the silica gel at 300°, nitroxide was permitted to adsorb to a high coverage. The ESR signal was similar to that of curve 2 of Figure 3 and θ was probably about 50%. After pumping at 25° for 10 min, the signal intensity was reduced to 60–70% of the original and the spectrum was of the same form as the original except for showing on the right side a trace of the difference between curves 2 and 11 of Figure 3. Further evacuation for 4 hr at 25° had little effect. Evacuation at 60° for 4 hr altered the shape of the signal to near that of curve 0 of Figure 2, a sample with θ = 25%. Further evacuation for 4 hr at 100° gave a spectrum of the general form of curve 4 of Figure 2 corresponding to an intensity 5–10% that of the original.

After hydrogenation, Pt/Al_2O_3-II was devoid of signal. The hydrogen was pumped out after some days and about

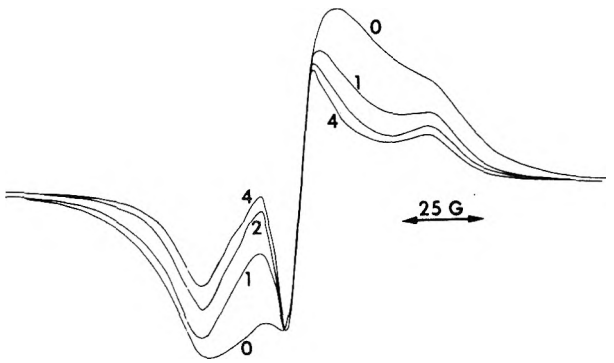

Figure 2. Hydrogenation of di-*tert*-butyl nitroxide on Pt/SiO_2-I at −70°: (curve 0) 0 min, 100% of initial signal, gain 1.0; (curve 1) 4 min, 67% of initial signal, gain 1.4; (curve 2) 7 min, 28% of initial signal, gain 2.0; (curve 4) 14 min, 7% of initial signal, gain 5.7; *x* axis, magnetic field; *y* axis, intensity.

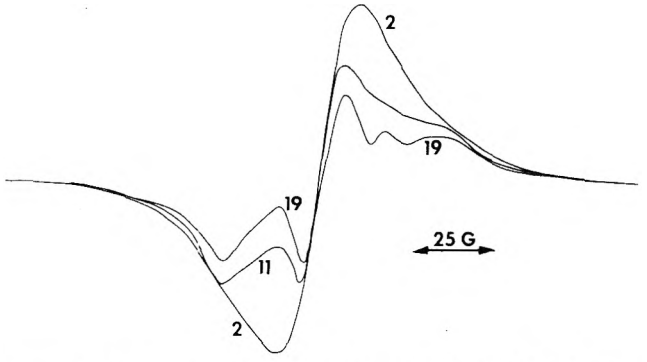

Figure 3. Hydrogenation of di-*tert*-butyl nitroxide on Pt/Al_2O_3-II at −70°: (curve 2) 8 min, 93% of initial signal, gain 10; (curve 11) 80 min, 32% of initial signal, gain 32; (curve 19) 145 min, 2.6% of initial signal, gain 200; *x* axis, magnetic field; *y* axis, intensity.

10 Torr of oxygen was added at 25°. Eight minutes after the addition, an ESR signal of nitroxide was present at 11% of its original intensity as shown by curve O_2 in Figure 4. After 2 hr the intensity had increased by a factor of 1.3. After standing under vacuum for 1 day, 10 Torr of oxygen was readded. After about 2 hr the signal intensity had reached 27% that before hydrogenation. Standing in air for 1 day had little effect upon this signal. The listed signal intensities are estimates based upon reaction with oxygen at 25° but measurement at −70° after pumping out the oxygen.

Discussion

Adsorption of Di-tert-butyl Nitroxide on Pt/SiO_2 and Pt/Al_2O_3. The texture of silica gel is something like that of a cemented gravel bed[6,7] and, in the case of the wide pore gel employed in the present work, the gravel bed analog would be a very loosely packed one. Most of our work employed a 1.2% by weight platinum on silica gel. Since the density of platinum is large, 21.4 g/cc, and that of silica about 2.2 g/cc, the volume percent is barely 0.1 the weight percent. Thus, by volume, a granule of Pt/SiO_2 is 70% void, 30% SiO_2, and 0.04% Pt.

The dispersion of the platinum as measured by hydrogen chemisorption[4,8] is 22%. To get a rough estimate of the platinum particle size, assume that the particles are identical cubes one face of which is blocked by attachment to the silica surface. For (surface Pt atoms)/(total platinum atom) = 0.22 the cube edge is 11 times the unit cell edge. Thus,

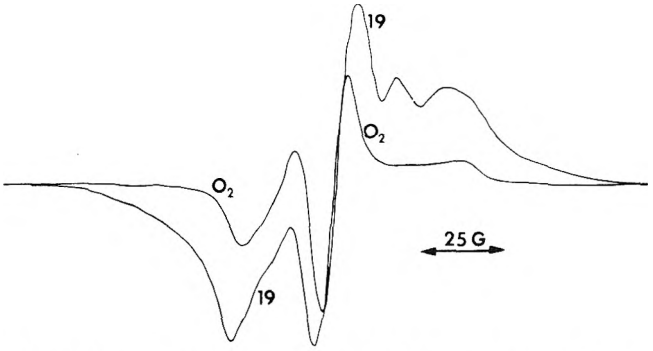

Figure 4. Hydrogenation of di-*tert*-butyl nitroxide on Pt/Al_2O_3-II at −70° and reoxidation at 25°. Curve 19 is from Figure 3. Curve O_2 is after exposure to oxygen at 25°. The gain for curve 19 is 400, for curve O_2, 50.

the particles would be about 4.3 nm on edge and contain about 5400 platinum atoms. In fact, of course, few particles would be cubes and there would be a distribution in size. The ratio of the surface area associated with platinum to that associated with silica is very small, 0.62 $m^2\ g^{-1}$/340 $m^2\ g^{-1}$.

On the simplified picture just given, there would be 6.9×10^{15} particles of platinum/g of catalyst, or one for every 4.9×10^4 nm^2 of silica surface. The platinum particles would then be 10–15 nm apart. To the degree that one can represent silica gel by cemented loosely packed spheroids about 10 nm in diameter, the number of spheroids is about 10^{17}/g of silica gel and there would be no more than one particle of platinum in each large cage in the silica gel.

As reported by Hoffman and Lozos,[2] the nitroxide is strongly adsorbed on silica gel. At very high coverages, we find that some nitroxide can be removed by pumping at 25° but at $\theta = 0.25$, the rate of desorption is very slow even at 60°. At −70°, the equilibrium pressure of nitroxide in contact with nitroxide adsorbed on silica gel is so miniscule that any transfer of nitroxide via the vapor phase is negligible. Even at 25° it appears to be slow on the time scale of minutes.

At $\theta = 0.25$ on silica gel, the area occupied by nitroxide is 85 m^2/g of catalyst. Since the platinum area of the 1.2% Pt/SiO_2 is only 0.62 $m^2\ g^{-1}$, 99+% of the nitroxide must be adsorbed on the surface of silica gel. It is not surprising that the ESR spectrum of nitroxide adsorbed on this Pt/SiO_2 is indistinguishable from that on silica gel. However, the indistinguishability also applied to Pt/SiO_2-III for which the nitroxide area is only 2.6 $m^2\ g^{-1}$ and to nitroxide adsorbed on the 10% Pt/SiO_2. Thus, either nitroxide adsorbed on platinum gives no ESR signal or adsorption of nitroxide on silica gel via hydrogen bonding to silanol groups is stronger than adsorption on platinum. We have examined Pt/Al_2O_3 less carefully, but similar conclusions appear to apply: the nitroxide is strongly adsorbed and primarily by hydrogen bonding to the surface of alumina.

Hydrogenation of Adsorbed Nitroxide. At 25° the hydrogenation of nitroxide adsorbed on Pt/SiO_2 and on Pt/Al_2O_3 is too fast to follow by our techniques, but we have been able to follow the hydrogenation at −70°. On Pt/SiO_2, with initial coverages by nitroxide of 0.25, 0.13, and 0.008, the hydrogenation is first order in nitroxide to about 90% reacted after which the rate declines. The half-lives of hydrogenation varied between 4 and 10 min, but we do not consider this variation significant. The control of temperature was not exact, the pressure of hydrogen was not care-

fully controlled, and the changing shape of the signals in the runs at higher coverages caused conversions computed from signal intensity to be inaccurate. However, integration of some of the signals indicated that results derived from signal intensity were approximately correct.

Hydrogenations of nitroxide adsorbed on Pt/Al_2O_3 were similar but the rate of hydrogenation at −70° was less than on Pt/SiO_2 and the hydrogenation was not first order in nitroxide. The reaction proceeded more slowly at the beginning of the hydrogenation and then accelerated.

At higher coverages, magnetic interactions led to the loss of hyperfine structure from the ESR spectrum. As hydrogenation proceeded, structure appeared and at high enough conversions the spectrum became that of magnetically dilute nitroxide. Although this change is a nuisance from the point of view of measuring conversions, it provides valuable information about the nature of the distribution of nitroxide in the granules of Pt/SiO_2. Thus, Figure 2 shows spectra for hydrogenation with Pt/SiO_2-I. The initial signal at a coverage of nitroxide = 0.25 is exchange broadened. Curve 4 at 93% conversion, $\theta = 0.018$, corresponds to the magnetically dilute signal and signals at higher conversions were of the same shape. Therefore, the hydrogenation proceeded throughout the catalyst granule rather than as a spherical front advancing from the outer surface of the granule to the center. Had the latter regime prevailed, the signal would have diminished in intensity without change of shape. In general, the mere shape of the ESR signal provides the basis for estimating the value of the effective θ for nitroxide.

If the top of a column of silica gel is exposed to the vapor of di-*tert*-butyl nitroxide at 25°, the nitroxide, because of its strong adsorption, is concentrated in a band at the upper end of the column. For this reason, during exposure to the vapor of nitroxide, the silica gel granules were spread as a monolayer upon a flat section of the reaction cell (Figure 1). However, even in this procedure, if the sticking coefficient is high enough, if the equilibrium pressure is low enough, and if adsorbed nitroxide is immobile, the adsorbed nitroxide would still be distributed nonuniformly. The value of θ would be large near the outer section of a granule and low or zero in the center. Had such been the case, Pt/SiO_2-II would have given initially a signal characteristic of a substantial degree of magnetic interaction. In fact, the signal was of the magnetically dilute form. Also, Pt/SiO_2-II with an initial θ of 0.13 exhibited a signal shape corresponding to that of Pt/SiO_2-I at half-hydrogenation. Since one would expect the sticking coefficient to be large here, one concludes that nitroxide is mobile within a granule of silica gel at 25°.

If one hydrogenates nitroxide adsorbed on Pt/Al_2O_3 at high coverages, one notes changes in the shape of the signal, just as with Pt/SiO_2. Figure 3 shows the evolution of the signal shape in a case in which the magnetic interactions were so severe as initially to cause complete loss in structure. Beyond $\theta = 0.01$, the signal shape is constant. The magnetically dilute signals differ between Pt/SiO_2 and Pt/Al_2O_3 as may be seen in comparing curve 4 of Figure 2 and curve 19 of Figure 3. In particular, there is an extra bump in the upper right section. The same signal appears at about −70° upon nitroxide adsorbed on alumina and has been ascribed by Hoffman and Lozos[2] to be an admixture of 90% of nitroxide hydrogen bonded to surface hydroxyl with 10% bonded to Al^{3+} (cus).

During the hydrogenation of Pt/Al_2O_3-I, we chanced to measure a spectrum at 17° in which only 0.64% of the signal intensity remained. The spectrum was almost identical with that reported at 25° by Lozos and Hoffman for the nitroxide adsorbed on alumina and silica–alumina and for the molecular complex of the nitroxide with aluminum chloride. The spectra just mentioned on Pt/Al_2O_3-I show extensive hyperfine splitting by ^{27}Al which must result from a system very heavily in the $Al^{3+}ONR_2$ form. Lozos and Hoffman had noted that nitroxide on alumina was preferably in the hydrogen-bonded form at −78° but bonded to Al^{3+} at 25°.

Oxidation of Adsorbed Di-tert-butylhydroxylamine. If Pt/Al_2O_3 containing adsorbed nitroxide is hydrogenated until the ESR signal has vanished and then exposed to oxygen at 25°, the signal of nitroxide reappears rapidly. Figure 4 shows the regenerated signal (measured at −70° after pumping out the oxygen) in comparison with the signal at a late stage in the preceding hydrogenation. The regenerated signal is characteristic of nitroxide adsorbed entirely by hydrogen bonding.[2] The absence of nitroxide bonded to Al^{3+} (cus) might result from (1) the hydroxylamine being immobile at −70° but mobile at 25° and being more strongly bonded to Al^{3+} (cus) than to σ-OH or from (2) the covering of Al^{3+} (cus) sites by water formed in the oxidation of hydroxylamine.

The maximum degree of reconversion of hydroxylamine to nitroxide in the experiments described above was 27%, but this number derives from signal intensities only and it is not very accurate. The degree of recovery of signal intensity was examined less carefully with Pt/SiO_2 but it appeared to be less than with Pt/Al_2O_3. The relative rapidity of the oxidation of the hydroxylamine particularly on Pt/Al_2O_3 suggests that catalysis by platinum is involved but we have not properly established this and uncatalyzed oxidation of the hydroxylamine is known.[9,10]

Surface Migration. The hydrogenation of nitroxides in solution has been previously reported.[9,10] The hydrogenation is unusual in that it involves the addition of just one hydrogen atom rather than two as in the case of the more common hydrogenations of olefins, ketones, etc. The mechanism of hydrogenation of nitroxides is of interest because it might involve an abstraction reaction, an elementary process for which there are few well-established examples in heterogeneous catalysis

$$R_2NO + H^* \longrightarrow R_2NOH + * \qquad (2)$$

that is, nitroxide chemisorbed at platinum does not appear as an intermediate. However, consideration of such details of mechanism can be postponed because the question of migration of reactants and products on silica and alumina is largely independent of the exact details of the processes at the surface of platinum.

Under the circumstances of the present paper, almost all of the nitroxide is adsorbed on silica or on alumina by hydrogen bonding to surface hydroxyl groups. On the average, an adsorbed molecule of nitroxide will be several nanometers from the nearest platinum crystallite. Yet it is at the platinum crystallite that hydrogen is chemisorbed and "activated." How do the nitroxide and hydrogen atom get together at −70°? We can imagine five possibilities.

(1) The metal crystallite rolls around the surface carrying H* to the nitroxide.

(2) The reaction occurs by a form of hydrogen spillover: the hydrogen atoms inately migrate from the platinum onto the silica surface, i.e., in the absence of nitroxide. In

the presence of nitroxide, the hydrogen atoms add to nitroxide molecules when they encounter them.

(3) *H decomposes into an electron and a proton at platinum and these migrate separately to adsorbed nitroxide. If the electron moves first, the reaction could be represented

$$H^* + \sigma\text{-}OH\cdots ONR_2 \longrightarrow H^{+*} + \sigma\text{-}O^- + HONR_2 \quad (3)$$

followed by

$$H^{+*} + \sigma\text{-}O^- \longrightarrow * + \sigma\text{-}OH \quad (4)$$

Or the proton might move first, but if both move together the process would be difficult to distinguish from (2).

(4a) The molecules of nitroxide are mobile on the surface even at −70 °. They migrate to the platinum crystallites and react with *H there.

(4b) The molecules of the hydroxylamine migrate to the crystallites of platinum and release an atom of hydrogen to the platinum surface during oxidation.

If (4a) is true but (4b) is false, molecules of nitroxide would diffuse to platinum crystallites, hydrogenate, and form immobile picket fences around the crystallites. The hydrogenation should grind to a halt in the systems with higher initial coverage by nitroxide. It does not. However, in solution the following homogeneous abstraction reaction

$$R_2NOH + ONR_2 \longrightarrow R_2NO + HONR_2 \quad (5)$$

is very fast on the NMR time scale at 25°, in some cases, even on the ESR time scale.[11] It seems likely that it would occur in minutes at −70°. Thus, the hydrogen exchange reaction would permit effective migration of both species over the surface even if only one was mobile. Since our data cannot rigorously distinguish between both (4a) and (4b) being true and only one being true, we will combine the two into (4).

(4) Either or both of the nitroxide and the hydroxylamine are mobile at −70°.

We doubt that we can completely rigorously eliminate any of the four mechanisms for hydrogen atom transfer, but some of the mechanisms have unattractive features which would seem to permit their classification as "improbable".

Thus, any face of the crystallite of platinum on silica is apt to contain at least 100 atoms of platinum. One would expect that the energy of physisorption of such a cluster on silica would alone generate an activation energy for migration over the surface of silica so large as to prohibit any significant degree of motion at −70°.

The driving force of reaction 3 is small. There are no chemical analogies to reaction 3 in which an electron tunnels several nanometers through an insulator under such a small driving force. Furthermore, at 25° deuterium gas does not exchange with the protons of the surface hydroxyl groups of silica and alumina containing particles of group VIII metals.[12-14] This suggests that reaction 3 must be negligibly slow at 25°.

This last observation also argues against hydrogen spillover on Pt/SiO_2. In addition, the binding energy in H* on platinum is about 65 kcal.[15] The transfer of hydrogen atoms from the surface of platinum to that of silica would require formation of some surface compound in which hydrogen *atoms* are bound with energies near 65 kcal. No form of binding which meets this requirement has been suggested. We have shown that silylation of Pt/SiO_2 with hexamethyldisilazane, which completely covers the silica with what is in effect a nearly close packed layer of methyl groups, has little effect upon the rate of hydrogenation of cyclopentene at 20°.[4] If reaction of cyclopentene with hydrogen atoms in the spillover form made any important contribution to the hydrogenation, one would expect silylation to have more effect. In sum, we consider that hydrogen spillover is unlikely to be important at 25° and even less at −70°.

Migration of nitroxide and hydroxylamine on the surfaces of silica and alumina at −70° does not appear to be implausible. If one takes desorption of nitroxide as beginning at about 60°C or 333°K, migration would begin at about 170°K if E_a for migration is one-half that for desorption. Most of the physisorption energy should remain during the act of migration and only the contribution from hydrogen bonding is lost. It seems not implausible here that the activation energy for migration should be no more than one-half that for desorption. In addition, as we showed in a previous section, there is very probably a substantial degree of surface migration at 25° over distances of about 0.1 mm within a silica gel granule. Migration over a distance of 10 nm in the same time interval at −70° does not seem unreasonable. We think it probable that both nitroxide and hydroxylamine are mobile at −70°, but for the reasons indicated we have no formal proof that this is so.

During hydrogenation at 25°, the possibility arises that migration of nitroxide via the vapor phase contributes to the overall process. However, as indicated in the first section of the Discussion, it appears unlikely that migration via the vapor phase at 25° is faster than that via the surface.

One of the definitions of spillover given by Bond[16] requires the amount of chemisorption of an appropriate gas substantially to exceed that of surface atoms of metal. Sample Pt/SiO_2-I contained 0.20 mmol of nitroxide/g and 0.014 mmol/g of surface atoms of platinum. During hydrogenation, it would have adsorbed 14 times as many hydrogen atoms as there were surface platinum atoms. One might consider this to represent a case of hydrogen spillover. However then one would have to say that oxygen spillover occurred during oxidation. There has been some tendency to restrict "spillover" of hydrogen to cases in which the nature of the bonding to the surface was mysterious. In the present situation, the hydrogen atoms are transferred to very evident acceptors, the nitroxide molecules.

The study of a catalytic reaction on a supported catalyst under such conditions that one reactant is completely adsorbed and with negligible desorption pressure appears to be a powerful method for studying surface migration of adsorbed species. One might have followed the reaction of the present paper by use of optical spectroscopy and have obtained many of our conclusions. Such use of optical spectroscopy would have eliminated the requirement that either a reactant or a product be a free radical. However, ESR has the advantage of procedural simplicity and the high sensitivity which permits work at very low coverages and, most importantly, the shape of the ESR signal provides information otherwise difficult to obtain about the uniformity of the distribution of the free radical on the surface of the support.

Acknowledgment. This work was supported through the Material Research Center of Northwestern University by the Advanced Research Projects Agency of the Department of Defense, Grant No. DAHC-15 73 G19. We are indebted to Professor Brian Hoffman for valuable counsel and to Mr. Alan Brenner for experimental assistance.

References and Notes

(1) On leave from the Université Catholique de Louvain, Louvain-la-Neuve, Belgium.
(2) G. P. Lozos and B. M. Hoffman, *J. Phys. Chem.*, **78**, 2110 (1974).
(3) K. M. Hanna, I. Odler, S. Brunauer, J. Hagymassy, Jr., and E. E. Bodor, *J. Colloid Interface Sci.*, **45**, 38 (1973).
(4) H. H. Kung, B. I. Brookes, and R. L. Burwell, Jr., *J. Phys. Chem.*, **78**, 875 (1974).
(5) H. A. Benesi, R. M. Curtis, and H. P. Struder, *J. Catal.*, **10**, 328 (1968).
(6) C. Okkerse, "Physical and Chemical Aspects of Adsorbents and Catalysts", B. G. Linsen, Ed., Academic Press, London, 1970, p 171.
(7) E. G. Acker, *J. Colloid Interface Sci.*, **32**, 41 (1970).
(8) J. Freel, *J. Catal.*, **25**, 139 (1972).
(9) A. K. Hoffman and A. T. Henderson, *J. Am. Chem. Soc.*, **83**, 4671 (1961).
(10) E. G. Rozantsev, "Free Nitroxyl Radicals", Plenum Press, New York, N.Y., 1970, Chapter IV.
(11) R. W. Kreilick and S. I. Weissman, *J. Am. Chem. Soc.*, **88**, 2645 (1966).
(12) W. K. Hall and F. E. Lutinski, *J. Catal.*, **2**, 518 (1963).
(13) J. L. Carter, P. J. Lucchesi, P. Corneil, D. J. C. Yates, and J. H. Sinfelt, *J. Phys. Chem.*, **69**, 3070 (1965).
(14) J. M. Cece and R. D. Gonzalez, *J. Catal.*, **28**, 254 (1973).
(15) G. C. Bond, "Catalysis by Metals", Academic Press, London, 1962, p 84, Table XII.
(16) P. A. Sermon and G. C. Bond, *Catal. Rev.*, **8**, 211 (1973).

Infrared Studies of Asymmetrical Dinitrogen Trioxide[1a]

Guy Martin Bradley,[1b] William Siddall, Herbert L. Strauss,* and Eduardo L. Varetti

Department of Chemistry, University of California, Berkeley, California 94720

(Received February 12, 1975)

Publication costs assisted by the National Science Foundation

We have observed bands at 76, 160, and 260 cm^{-1} in the far-infrared spectrum of liquid *as*-N_2O_3. A number of assignments and the corresponding force fields are presented which provide a reasonable fit to the vibrational data but do not give an accurate representation of the known inertial defects. We suggest that the force fields can be most easily compared to one another using a cartesian basis and suggest a definition for the "similarity" of two force fields.

Introduction

Although asymmetrical nitrogen trioxide, N_2O_3, has been studied for many years, it continues to present a number of problems. Detailed study is difficult, since high concentrations of N_2O_3 are only obtained in the presence of various other oxides of nitrogen. In spite of the difficulties, considerable information has become available. The structure and some of the parameters defining the vibrations of the molecule have been obtained from the microwave spectrum by Brittain et al.[2] The infrared spectrum has been studied a number of times and a reasonably complete analysis has been given by Hisatsune and coworkers in a number of papers.[3] Recently Bibart and Ewing[4a] have studied the infrared spectrum of the gas-phase molecule and have questioned some of Hisatsune's assignments. Varetti and Pimentel[4b] have measured the higher frequency infrared bands of many isotopic species of N_2O_3 in the matrix. In this paper, we present the results of far-infrared measurements of the liquid and attempt to describe the known frequencies and the structural information with a series of force fields.

Experimental Section

Although the phase diagram of N_2O_3 is very complicated, it has been established that the liquid phase in a mixture of oxides of nitrogen which is rich in NO consists of reasonably pure N_2O_3.[4a,5,6] Experiments were therefore done on the liquid condensed from a NO-rich mixture. The NO was at first purified by the elaborate procedure used by Nightingale et al[6b] but it was found that the same spectra resulted if the NO was used as it came from the tank (Matheson). The gaseous O_2 was taken from the house line which is supplied by boiling pure liquid O_2. The production of the N_2O_3 could be followed since the liquid is a deep blue. Cells of about 1 mm sample thickness, cooled to appropriate temperatures, were set in either a far-infrared interferometer or a Beckmann IR-11 spectrometer and were filled by condensing N_2O_3 from a sample bulb. Far-infrared spectra of the liquid are shown in Figures 1–3. Careful checks were made to make sure that none of the observed features is due to N_2O_4.

Assignments

The frequencies of the various normal modes are summarized in Table I. For the most part, they follow earlier assignments. There is little question of the proper assignment of the higher frequency modes as they occur at approximately the frequencies of the vibrations of the separate NO and NO_2 molecules. The recent work of Bibart and Ewing[4a] has provided further evidence for these assignments by providing band contours for gaseous N_2O_3 and illustrating the similarities to the N_2O_4 spectrum. A number of the assignments are not straightforward, however, and require discussion. Figure 1 shows a strong band at 76 cm^{-1}, and there is little question that this is the torsional vibration. A similar frequency of 63 cm^{-1} is assigned by Bibart and Ewing to the torsional frequency in the ν_5 excited state (gas phase) and their data also suggest that the ground state torsional frequency is about 7 cm^{-1} higher than 63-cm^{-1} band. The remaining difference between the 76-cm^{-1} band and the approximately 70-cm^{-1} band implied by Bibart and Ewings' data may be due to condensed

TABLE I: N_2O_3 Frequencies

	Obsd frequency, cm^{-1}	Ref	Approx description	Simple molecule frequencies,[d] cm^{-1}
ν_1	1839.7	*a*	Nitroso stretch	N–O stretch 1904
ν_2	1630.4	*a*	Asym nitro stretch	NO_2 stretch 1618
ν_3	1302.5	*a*	Sym nitro stretch	NO_2 stretch 1320
ν_4	775.7	*a*	Nitro scissors	NO_2 bend 750
ν_5	420.5	*a*	Nitro rock	
ν_6	260	*b*	Nitroso rock[e]	
ν_7	160	*b*	N–N stretch[e]	
ν_8	624	*c*	Nitro out-of-plane wag[f]	
ν_9	76	*b*	Torsion	

[a] Reference 4b. [b] This work. [c] Reference 3. [d] Frequencies of the separate NO_2 and NO molecules from ref 7. [e] Assignment reversed in ref 4a (modes mixed). [f] 337 cm^{-1} suggested in ref 4a, see text.

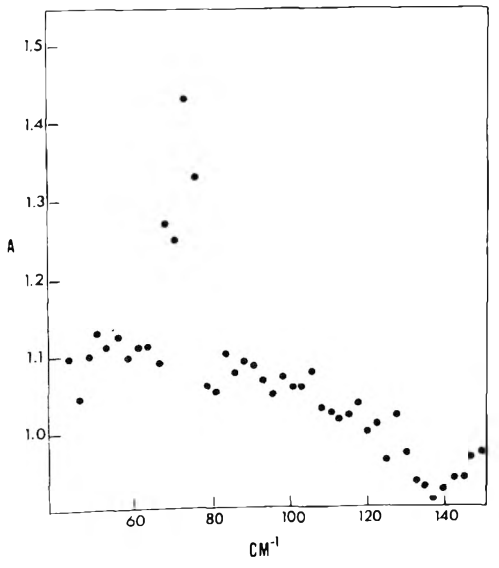

Figure 1. Interferometer spectrum of N_2O_3. Four sets of spectra were averaged to obtain this diagram. The spectra were taken at −50°.

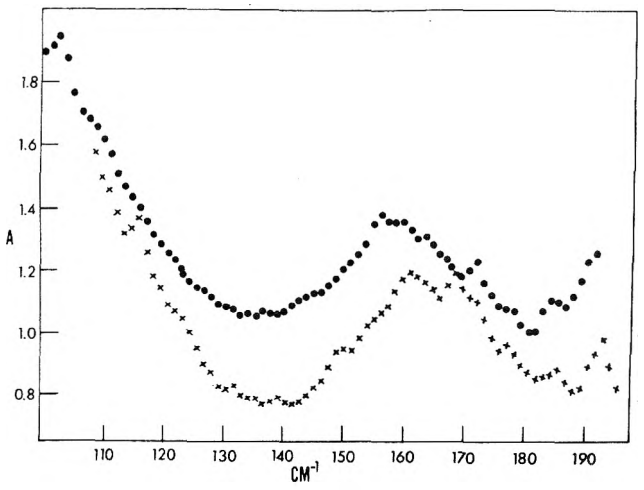

Figure 2. Interferometer spectrum of N_2O_3. The upper spectrum was taken at −10°, the lower one at −35°.

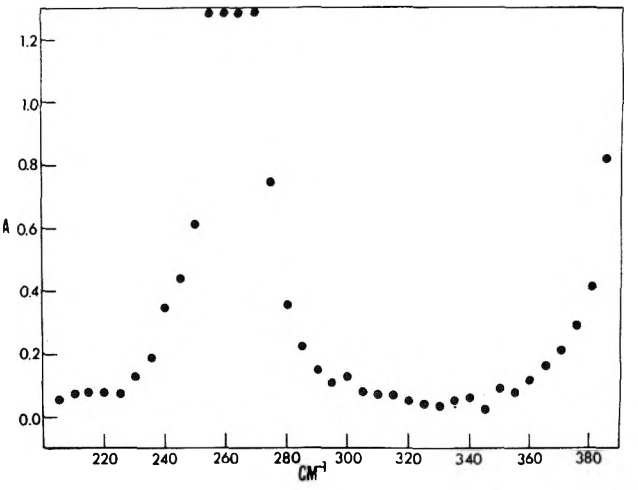

Figure 3. IR-11 spectrum of N_2O_3 taken at −35°.

phase effects. Assuming a cosine shaped potential, we obtain a torsional barrier of about 1.6 kcal/mol or 580 cm^{-1}.

The next higher frequency band observed by us is a weak band at 160 cm^{-1}. It is broad as distinguished from the sharp torsional band. In the gas phase, the out-of-plane bands should show a structure with a sharp Q branch while the in-plane modes are expected to have a hybrid structure ($\kappa = -0.77$). This suggests that in the liquid, out-of-plane modes should have the narrower band profile, and this is what we observe. A number of different in-plane motions could give rise to the 160-cm^{-1} band, and we consider this question further below.

The next lowest in-plane mode we assign to the broad band at 260 cm^{-1}, which corresponds to a band seen in the Raman spectrum by Hisatsune et al[3] at 253 cm^{-1}. The next higher band is seen by many workers at about 420 cm^{-1} and the band contour in the gas phase definitely assigns this as an in-plane mode. The higher frequency in-plane modes are all close enough to the frequencies of the individual NO and NO_2 molecules to leave no question as to their assignment. This leaves one frequency, the higher out-of-plane frequency, unaccounted for. Hisatsune et al. assign this mode to a band seen at about 624 cm^{-1}, but Bibart and Ewing suggest a band about 337 cm^{-1} instead, since the weak features they see around 600 cm^{-1} do not have the correct band shape. Hisatsune et al. see a weak feature at 313 cm^{-1} but assign it to ν_7. If a frequency of about 600 cm^{-1} is indeed the out-of-plane motion, the 313-cm^{-1} band could be the overtone of the 160-cm^{-1} mode we observe. If a band appears at all near 300–350 cm^{-1} in the liquid, it is very weak (Figure 3). We tentatively assign ν_8 as 624 cm^{-1}.

Numerous vibrational satellites were observed in the microwave spectrum.[2] Vibrational information can be derived from these satellites in two ways: directly from their intensity, or more indirectly from their inertial defects. Intensity measurements suggest frequencies of 125, 200, and 260 cm^{-1} with the last two assigned as in-plane modes by virtue of their inertial defects. This fits relatively well with our assignment, but the calculated values of the inertial defects are not in good agreement with experiment and will be discussed further after we consider the potential functions.

Normal Coordinate Analysis and Force Constants

The results of the various force fields tried are summarized in Table II. We started from the force field given by

TABLE II: In-Plane Force Fields for N_2O_3

	Hisatsune et al.[a]	I	II	III[b]	σ[c]	IV[d]	V[e]
K_{12}[f]	15.12	14.69	14.69	14.74	0.01	14.81	15.9
K_{23}	0.66	0.156	0.156	0.233	0.22	0.399	
K_{34}	7.93	8.378	8.38	10.09	0.075	10.15	11.043
K_{35}	7.93	8.378	8.38	10.09	0.075	10.15	11.043
H_{123}[f]	0.40			0.653	0.047	0.619	
H_{234}	1.15	0.956	0.942	0.432	0.051	0.085	
H_{235}	1.15	0.956	0.942	0.432	0.051	0.085	
H_{435}	0.17	0.254	0.274	1.547	0.055	1.68	1.60
F_{15}	3.05	2.528	2.599			0.24	
F_{13}	0.29						
F_{14}	0.10	0.41	0.409	0.042	0.14		
I NO_2 stretch stretch				1.599	0.074	1.53	0.481
I NO_2 stretch bend				0.673	0.060	0.672	2.56
Accuracy, σ in frequency[c]		1.6×10^{-3}		1.03×10^{-3}		1.06×10^{-3}	

[a] Reference 3. [b] Best force field. Note large errors in K_{23} and F_{14}, see text. [c] Standard error in III. [d] With assignment of ref 4a. [e] Individual NO and NO_2 molecules, ref 7 and 8. [f] Stretching constants in mdyn/Å, bending constants in (mdyn/Å)/(square radian). See Figure 4.

TABLE III: Observed Frequencies and Agreement with the Calculations Using Force Field III

	$^{14}N_2{}^{16}O_3$ obsd[a]	Error	$^{16}O^{15}N$-$^{14}N^{16}O_2$[b]	Error	$^{16}O^{14}N$-$^{15}N^{16}O_2$	Error	$^{15}N_2{}^{16}O_3$	Error	$^{18}O^{14}N$-$^{14}N^{16}O_2$	Error	^{16}O-$^{14}N^{14}N$-$^{18}O^{16}O$	Error	$^{16}O^{14}N$-$^{14}N^{18}O_2$	Error
ν_1	1839.7	−0.5	32.3	1.1	−0.6	0.8	32.4	1.2	46.7	0.5	0.0	0.0[c]	0.0	0.1
ν_2	1630.4	−0.8	0	0.1	35.6	1.1	35.8	1.0	0.0	0.4	11.7	2.3	30.9	−0.9
ν_3	1302.4	−0.5	0	0.0	14.7	0.3	15.7	−0.7	0.0	0.0	23.9	0.9	45.1	2.3
ν_4	775.7	−0.4	0.6	−0.6	10.5	−0.8	10.8	−1.1	0.0	0.0	12.8	1.6	26.3	2.8
ν_5	420.5	−1.5	1.6	6.7			10.9	−2.2						
ν_6	253	−0.3												
ν_7	160	2.4												

[a] Absolute frequency in cm^{-1}. [b] Frequency shift from $^{14}N_2{}^{16}O_3$ isomer. A positive shift is to *lower* frequency. Errors are given for the shifts. [c] The calculated values for the two possible isomers differ by small amounts.

Hisatsune et al.[3] and found that we could achieve just as good results using a force field which left out the bending constant H_{123} and the similar Urey–Bradley force constant F_{13} (see Figure 4 for the numbering of the atoms). In these first attempts, we used only some of the isotopic data available and attempted to fit the inertial defect (see below). This resulted in force field I. When all of the isotopic data were added, providing 38 frequencies and shifts in all, we obtained force field II (ignoring the inertial defects). Adding two more force constants, we obtained our best fit, III. All of these fits are such that ν_7 is primarily the N–N stretch according to our assignment. Force field IV results from forcing ν_6 to be primarily the stretch as suggested by Bibart and Ewing.[4a] The fit in this case is slightly worse. In either case, the N–N stretching coordinate is heavily involved in the coordinates of ν_3, ν_4, and ν_5 as well. Finally we give the force fields for the separate NO_2 and NO molecules (V). Table III lists the observed frequencies and shifts, and the errors in the corresponding calculated quantities. We used one shift that does not appear in the table derived from the observed frequencies 313 and 308 cm^{-1} for the solids of $^{14}N_2O_3$ and $^{15}N_2O_3$, respectively.[3] We assign these as $2\nu_7$ giving a $\Delta\nu$ of 2.5 cm^{-1} and calculated shift of 1.9 cm^{-1}.

The standard errors in the fit to the frequencies and the calculated expected standard deviations in the force constants are given in Table II. The errors were calculated using the standard choice of weights, $1/\lambda$ ($\lambda = 4\pi^2c^2\tilde{\nu}^2$). The

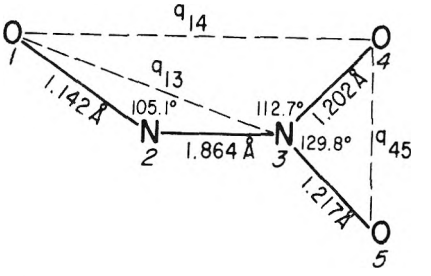

Figure 4. Structure of N_2O_3 from ref 2 and numbering of the atoms.

weight for the frequency shifts are likewise taken as $1/4\pi^2c^2(\Delta\tilde{\nu})^2$. Examination of the weights shows that the expected standard deviation in what is perhaps the most interesting force constant, K_{23}, the N–N stretching force constant, is almost the same size as the force constant. The value calculated for this force constant is, of course, heavily dependent on what assumptions are made about the force field and this shows up in the large variation in K_{23} among the various force fields of Table II. Also noteworthy is the estimated error in the Urey–Bradley constant F_{14}. The error is much larger than the constant and so it is reasonable to take F_{14} as zero in force field III. The standard errors for this force field were calculated for nine constants and would be a bit smaller if the force field were considered to have only eight adjustable constants.

It is difficult to compare the various force fields of Table

II, especially since they differ in form. In order to provide a quantitative measure of the similarity of two force fields, it is necessary to transform them into a common coordinate system. We have chosen the cartesian coordinates as such a system. The force constant matrix can be transformed into cartesian coordinates by the transformation

$$\mathbf{F}_c = \mathbf{B}'\mathbf{F}\mathbf{B} \quad (1)$$

where **F** is the usual force constant matrix expressed in any convenient basis, $\mathbf{F}_c$ is the force constant matrix in cartesian coordinates, and **B** is the usual transformation between internal and cartesian coordinates, with **B**′ as its transpose. This quantity is easy to calculate as **B** is generated by most normal coordinate computer programs. We then define the measure of the similarity of two force fields, s^2, as

$$s^2 = \frac{1}{3N-6}\sum_i^{3N}\sum_j^{3N}(F_{cij}^{\,1} - F_{cij}^{\,2})^2 = \frac{1}{3N-6}\,\mathrm{Tr}\,[(\Delta\mathbf{F}_c)^2] \quad (2)$$

In eq 2, $\mathbf{F}^1$ and $\mathbf{F}^2$ are the matrices of the two force fields to be compared. The factor of $3N - 6$ (for nonlinear molecules) is a factor which should make the s^2 approximately comparable for molecules of different size. The similarity, s^2, is invariant to the choice of orientation of the cartesian axes, since it is in the form of the trace of a matrix and thus is invariant to rotations of the coordinate axes.[9] The values of s^2 for a number of pairs of force fields are compared in Table IV. Comparison with force field V is made using just the NO_2 part of the N_2O_3 molecule and, of course, a factor of $N = 3$ in eq 2. The values behave as expected and show that the various force fields attempted for N_2O_3 are much closer to one another than they are to the force field of NO_2. It is perhaps surprising that the "'best" force fields based on different suggested assignments of the N–N stretching frequency, force fields III and IV, are closer than any of the other pairs listed in Table IV.

In principle, the inertial defects contain considerable detailed information on the form of the normal modes. Unfortunately, we have not been able to reproduce the measured inertial defects satisfactorily. Our calculations are compared to the measurements of Brittain et al. in Table V. The different force fields produce different inertial defects but none are particularly close to experiment. For example, all of the force fields give a difference between the ground state and the first torsional excited state which is considerably too large although force field III is the best in this respect. The different assignment of the in-plane modes of force field IV together with the different values of the higher out-of-plane frequency gives inertial defects which are about the same as force field I. Our force fields give about the correct changes of the ground state inertial defects on isotopic substitution (Table V).

Thermodynamic measurements of N_2O_3 have been made a number of times. From these measurements we have estimated $S°_{298}$ and obtained 74.25, 72.26, and 70.90 eu from the data in ref 10, 11, and 12, respectively. Using our frequencies we calculate 73.79 eu using a harmonic oscillator torsional potential and 74.24 using a cosine torsional potential.

TABLE IV: Similarity[a] Among the Force Fields of Table II

	I	III	IV	V
I		0.89	0.99	4.0
III			0.26	2.0
IV				1.8

[a] See text for definition, eq 2.

TABLE V: Inertial Defects

	Obsd[a]	I[b]	III	IV[c]
Ground state	0.1283[d]	0.0439	0.0384[d]	−0.0189[d]
First excited torsion	−0.9126	−1.2233	−0.9710	−1.2150
Second excited torsion	−1.8279	−2.4904	−1.9804	−2.4111
Excited planar modes	1.1669 0.1805	0.8741[e] 0.3546[e]	0.4256[e]	0.8330[e]

[a] Reference 2. [b] Labeled as in Table II. [c] The out-of-plane frequencies are taken as 337 and 62 cm^{-1} from ref 4a for this calculation. [d] For $ON^{15}NO_2$, the observed interval defect is 0.1340 and the calculated one is −0.0108 for force field IV, for $ON_2O^{18}O$ observed 0.1432, calculated 0.0010 (IV), 0.0470 (III), for $O^{15}NNO_2$ observed 0.1297, calculated 0.0361 (III). [e] For the first two in-plane excited states for I and for the 160-cm^{-1} state for III and IV.

Conclusions

In this paper we reported the observation of two new bands of N_2O_3, the bands at 160 and 76 cm^{-1} and the first infrared observation of the 260-cm^{-1} band. We considered a number of alternate proposals for the assignment of the normal modes. Both our assignment with the 160-cm^{-1} band assigned to the N–N stretch and the assignment of Bibart and Ewing yield reasonable force fields that fit most of the data and indeed do not differ much from each other. It is suggested that force fields expressed in a cartesian basis are useful for such comparisons. The force fields we have tried do not provide a particularly convincing fit to the inertial defects with either set of assignments. This is probably due to the presence of a number of large amplitude vibrations in the molecule, which leads to rotation–vibration interactions we have not taken into account. The value of the entropy calculated from the frequencies is within the range estimated from thermodynamic measurements, but this range is too large to provide definitive information.

It is particularly unfortunate that the evidence does not discriminate between the two values suggested for ν_8, the nitro out-of-plane way. In the spectra of Bibart and Ewing the band at 340 cm^{-1} assinged as ν_8 is reasonably strong and certainly stronger than the weak feature at ~600 cm^{-1} and this is perhaps the best evidence for the assignment of ν_8 as 337 cm^{-1}. Further work will have to be done to explain the existing data on this intriguing but elusive molecule.

Acknowledgments. It is a pleasure to acknowledge helpful discussions with Professors R. L. Kuczkowski, G. E. Ewing, and G. C. Pimentel. We wish to thank Professors Kuczkowski and Ewing for sending us their data before publication.

References and Notes

(1) (a) Supported in part by the National Science Foundation. (b) National Science Foundation Predoctoral Fellow.
(2) A. H. Brittain, A. P. Cox, and R. L. Kuczkowski, *Trans. Faraday Soc.*, 65, 1963 (1969), and private communication with R. L. Kuczkowski.

(3) J. P. Devlin and I. C. Hisatsune, *Spectrochim. Acta*, **17**, 218 (1961); I. C. Hisatsune and J. P. Devlin, *ibid.*, **16**, 401 (1960); I. C. Hisatsune, J. P. Devlin, and Y. Wada, *J. Chem. Phys.*, **33**, 714 (1960).
(4) (a) C. H. Bibart and G. E. Ewing, *J. Chem. Phys.*, **61**, 1293 (1974); (b) E. L. Varetti and G. C. Pimentel, *ibid.*, **55**, 3813 (1971).
(5) A. J. Vosper, *J. Chem. Soc. A*, 1795 (1966).
(6) (a) G. M. Bradley, Ph.D. Dissertation, University of California, Berkeley, 1971. (b) R. E. Nightingale, A. R. Dowle, D. L. Rotenberg, B. Crawford, Jr., and R. A. Ogg, Jr., *J. Phys. Chem.*, **58**, 1047 (1954).
(7) G. Herzberg, "Molecular Spectra and Molecular Structure", Van Nostrand, New York, N.Y. Vol. I, 1945; Vol. III, 1966.
(8) G. R. Bird, J. C. Baird, A. W. Jache, J. A. Hodgeson, R. F. Curl, Jr., A. C. Kunkle, J. W. Bransford, J. Rastrup-Andersen, and J. Rosenthal, *J. Chem. Phys.*, **40**, 3378 (1964).
(9) A number of suggestions of the utility of a cartesian force field appear in the literature. For example, W. T. King and A. J. Zelano, *J. Chem. Phys.*, **47**, 3197 (1962).
(10) I. R. Beattie and S. W. Bell, *J. Chem. Soc.*, 1681 (1957).
(11) F. H. Verhock and F. Daniels, *J. Am. Chem. Soc.*, **53**, 1250 (1931).
(12) M. Sole and V. Pour, *Collect. Czech. Chem. Commun.*, **32**, 3031 (1967).

Infrared Studies of Nitrosobenzene[1a]

Guy Martin Bradley[1b] and Herbert L. Strauss*

Department of Chemistry, University of California, Berkeley, California 94720 *(Received March 17, 1975)*

Publication costs assisted by the National Science Foundation

The infrared spectrum of nitrosobenzene vapor from 50 to 3500 cm^{-1} is presented. The result of investigation of nitrosobenzene solutions is listed together with an approximate assignment and normal coordinate analysis. The nitroso torsional frequency is found to be about 101 cm^{-1} and the band which contains most of the CNO bend is found to be at about 200 cm^{-1}.

Introduction

There has been considerable spectral work done on nitrosobenzene in an attempt to define the effect of the interaction of the nitroso group with the benzene ring and considerable infrared work has been done on nitroso compounds in general.[2] However, only a few of the characteristic vibrational bands have been assigned. The microwave spectrum of nitrosobenzene has been studied and information obtained about both the ground and the excited vibrational states.[3,4] In addition, studies of the electronic spectrum have been made at a resolution sufficient to obtain some vibrational information.[5] In this report, we present the results of a complete study of the infrared spectrum including the far-infrared and of an approximate assignment and normal coordinate analysis.

Experimental Section

Some care must be taken in handling nitrosobenzene since it undergoes decomposition rapidly under some conditions and can also form a dimer.[2b] The sample as obtained from Aldrich Chemical Co. was yellow-brown and was purified by sublimation. The monomer is a characteristic green, and this color was observed on rapidly condensing the nitrosobenzene on a cold finger. However, the color rapidly changed to the off-white of the dimer on warming. Both the vapor and the dissolved compound formed from the dimerized solid are monomeric. However, the solid did turn brown slowly and we had to use freshly sublimed compound for each set of experiments.

The vapor pressure of nitrosobenzene is only about 0.6 Torr at room temperature[6] which proved sufficient for the observation of the gas-phase infrared spectrum in a 10-m pathlength cell on a Beckmann IR-12 spectrometer in the region of about 300 to 3200 cm^{-1}. Similar spectra were taken on an IR-11 spectrometer in the region of 40 to 650 cm^{-1} but with the cell heated to obtain sufficient vapor pressure. Unfortunately, the polyethylene windows of the cell could not be heated evenly and the nitrosobenzene condensed in the center of the windows. Satisfactory results were obtained using our interferometer equipped with a new long pathlength cell.[7] This cell has a pathlength of 39 m and was run at about 50°. At this temperature, nitrosobenzene has about 10 Torr pressure and gave satisfactory spectra.

Figure 1 shows representative vapor phase spectra taken on the IR-12. Figures 2 and 3 show the far-infrared spectra taken on the interferometer. The frequencies observed in the various vapor phase and solution spectra are listed in Tables II and III.

Assignment and Discussion

The vibrational spectrum of benzene is understood in detail, and the spectra of the various benzene derivatives can be correlated with that of benzene and with the spectra of other derivatives. Comprehensive reviews exist such as the short review of Dollish et al[8] and the long review by Varsányi.[9] Inevitably there exists a number of common systems of notation for the normal modes. Following Dollish et al., we will use the "Wilson notation".[10] Table I lists the normal coordinates (except for the CH stretches) according to their calculated frequencies, the Wilson notation and the Whiffen notation,[11] and a very qualitative description of the normal mode.

Table II lists the calculated frequencies of the normal modes (omitting the C–H stretching modes) together with the observations in both the gas phase and solution. Table III lists the observed gas-phase frequencies together with the assignments. These follow the assignments of the other

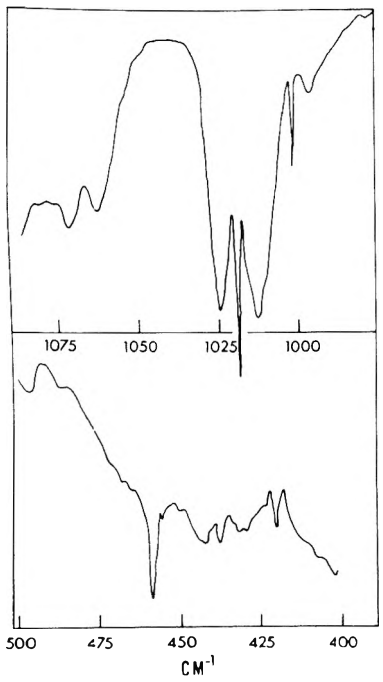

Figure 1. Representative spectra of nitrosobenzene taken on a Beckmann IR-12 spectrometer in a 10-m pathlength cell at room temperature. Transmittance is plotted vs. frequency.

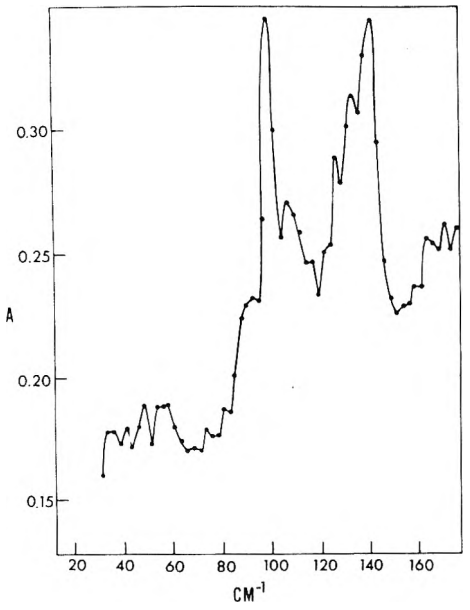

Figure 2. Spectrum of nitrosobenzene from 20 to 170 cm^{-1} taken on an interferometer in a 39-m pathlength cell at 50°. The figure is the average of 17 sample and 11 background spectra. Absorbance is plotted vs. frequency. Polypropylene was used for the cell windows.

known monosubstituted benzenes. To emphasize this, we have listed the frequencies of the comparable normal modes for the similar molecules nitrobenzene[12] and anisole[13] in Table II. We also have listed the gas-phase band shape when this could be determined from the spectrum and also the relative strength of the bands. The strength of the normal modes in nitrosobenzene correlates well with those of benzene. Table II shows that the modes allowed in benzene are also strong in nitrosobenzene, with the exception of the bands we have assigned as 19a and 17a.

TABLE I: Notation and Frequencies for the Fundamentals of Nitrosobenzene In-Plane Vibrations

Approx Frequency[a]	Very approx description[b]	Notation	
		Wiffen[c]	Wilson[d]
1672	Ring stretch	k	8a
1661	Ring stretch	l	8b
1513	Ring stretch and deformation	m	19a
1448	NO stretch		
1481	Ring str and deformation	n	19b
1344	Ring stretch	o	14
1275	CH def	e	3
1179	CH def	a	9a
1172	CH def	c	15
1199	C-N str*	q	13
1093	CH def	d	18b
1042	CH def	b	18a
995	Ring def	p	12
801	Ring breath and C-N str*	r	1
588	Ring def	s	6b
522	Ring def and CNO bend*	t	6a
377	CNO bend*	u	9b
170	CNO bend*		
	Out-of-Plane Vibrations		
991	CH def	j	5
970	CH def	h	17a
907	CH def	i	10b
836	CH def	g	10a
744	CH def	f	11
661	Ring def	v	4
499	Ring def + CNO def*	y	17b
361	Ring def	w	16a
297	Ring def + CNO def*	x	16b
108	torsion*		

[a] Calculated frequency. [b] The descriptions are approximate. The descriptions labeled with an asterisk indicate normal modes strongly affected by the substituent. [c] Reference 11. [d] Reference 10.

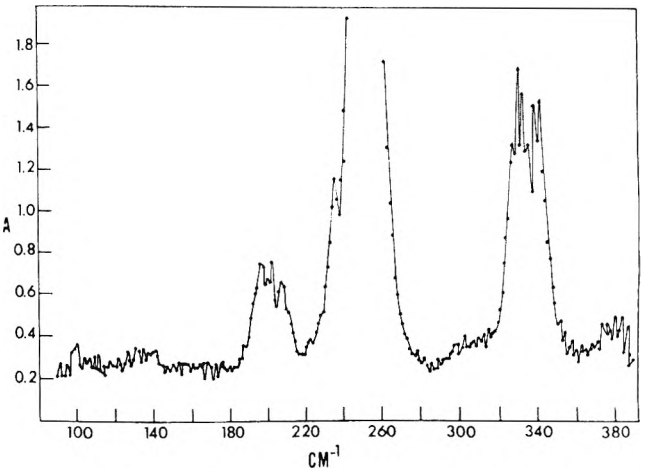

Figure 3. Spectrum of nitrosobenzene from 90 to 390 cm^{-1} taken on an interferometer in a 39-m pathlength cell at 50°. The figure is the average of 20 sample and 20 background spectra. Absorbance is plotted vs. frequency. Polyethylene windows were used. The bands shown are stronger than those of Figure 2 as can be seen by comparing the 100–140-cm^{-1} region.

TABLE II: Observation and Assignment of the Lower Frequency Fundamentals

	Calcd frequency[a]		Wilson	Gas obsd	Solution obsd	Band	Nitro-		
	A	B	notation	frequency	frequency	shape[b]	benzene[c]	Anisole[d]	Benzene[e]
				In-Plane Vibrations					
1	1672	1635	8a	~1615?			1610	1603	R
2	1661	1587	8b	~1615?			1585	1593	R
3	1513	1481	19a	1477			1486	1497	Ir
4	1448	1450	N–O str	1523		in, s			
5	1481	1459	19b	1455		in, s	1412	1443	Ir
6	1344	1323	14	1314		in, s	1316	1338	
7	1275	1286	3	1291		in	1309	1296	
8	1179	1161	9a	1176		in, s	1176	1182	R
9	1172	1151	15	1159			1160	1153	R
10	1199	1106	13	1112		in, s	1112	1248	Ir
11	1093	1073	18b	1067		in	1069	1076	
12	1042	1032	18a	1018		in, s	1020	1019	Ir
13	995	1004	12	997		in	1002	995	
14	801	810	1	812		in, s	682	783	R
15	588	592	6b				591	613	R
16	522	436	6a	437	440	in	397	444	R
17	377	253	9b	254	~260	in, s	252	258	Ir
18	170	198	CNO bend	200					
				Out-of-Plane Vibrations					
1	991	1007	5	1002		out	900	975	
2	970	971	17a	(970)[f]			977	957	Ir
3	907	930	10b	933		out, s	935	882	R
4	836	838	10a	850		s	837	819	R
5	744	746	11	750		out, s	792	754	Ir
6	661	680	4	682		out, s	677	692	
7	499	466	17b	458	460	out	420	511	
8	361	381	16a	384	380				
9	297	330	16b	337	354		176	209	
10	108	98		101		out			

[a] Calculation A uses the first set of force constants (Table IV) and calculation B uses the second set, see text. [b] The band shape, if it can be determined. Strong bands are designated by s. "in" means an in-plane mode, "out", an out of plane mode. [c] Reference 12. [d] Reference 13. [e] Selection rules for benzene. [f] Derived from combination bands.

We have carried out an approximate normal coordinate analysis to help with the assignment and to give a qualitative idea of the magnitude of the force constants and the nature of the normal coordinates. A more detailed analysis would require using information from isotopic substitution or other sources. The analysis we have carried out follows the work of Scherer closely. Values of the force constants for the benzene ring were taken from Scherer's 23 parameter out-of-plane force field for the chlorobenzenes[14] and from his 26 parameter in-plane force field.[15] Values for the nitroso group were estimated from the known constants for nitrosomethane[16] and the various interaction constants were guessed at. This first set of force constants produced the calculated frequencies listed as *A* in Table II. The force constants were then changed in an attempt to improve the fit and finally resulted in the somewhat better fit, *B*. The two sets of forces constants are shown in Figures 4 and 5 and Table IV using the diagrams suggested by Scherer.[14,15] Diagrams illustrating the details of the normal modes and tables of the potential energy distribution may be found in ref 17. The designation of the normal modes and even the identification of the fundamental bands is difficult in the absence of accurate force field models for the compound involved. The mixing of the simple internal coordinates in the normal modes has been discussed in great detail for the chlorobenzenes by Scherer.[18] His work emphasizes that the simple descriptions of the normal modes such as those in Table I can only be taken as a very rough guide.

One of the most interesting frequencies of nitrosobenzene is the frequency of the NO torsion. The microwave intensity measurements of Hanyu et al.[3] give a value of 80 or 93 cm^{-1} for the energy of the first excited torsional state, depending on how the numerical analysis is done. The values of the inertial defect suggest a value of about 100 cm^{-1}. The analysis of the electronic spectrum[5] suggests a value of about 86 cm^{-1}. In our spectra, bands of appreciable intensity appear at 101 and 140 cm^{-1}. The lower of these is within the range suggested for the torsional frequency and we assign it as such. The 140-cm^{-1} band is then assigned as a difference band. The frequency of 101-cm^{-1} band leads to a barrier to internal rotation of the nitroso group of about 3.7 kcal/mol.

The bands in the 200–400-cm^{-1} region are often quite sensitive to the nature of the substituent. However, many of the bands do not seem to shift much from their position in nitrobenzene or anisole. The normal coordinate calculations also reproduce these frequencies fairly well since the force constants have been transferred from similar molecules. The designation of the normal modes by the simple descriptions is rather misleading as the simple motions are

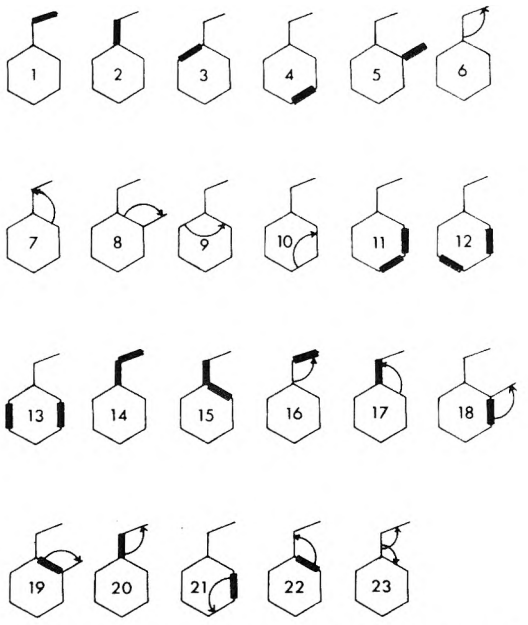

Figure 4. Diagram showing the in-plane force field. The values of the force constants are listed in Table IV.

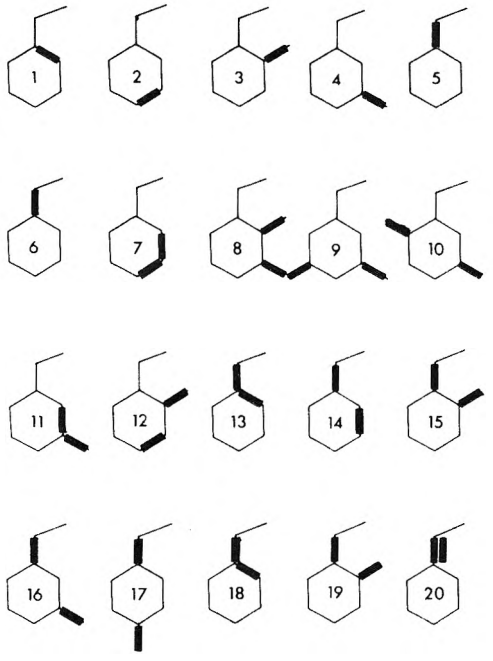

Figure 5. Diagram showing the out-of-plane force field. The values of the force constants are shown in Table IV. Table IV also indicates whether the C–N–O motion illustrated is the torsion (τ) or the out-of-plane bend of the NO(δ).

substantially mixed. For example, the CNO bending coordinate contributes significantly to the normal modes at 254 and 437 cm^{-1} as well as being the major constituent of the 200-cm^{-1} normal mode. Similarly the "X-bend" (the bend of the nitroso group about carbon 1) contributes to the mode at 437 cm^{-1} although its major contribution is to the mode at 254 cm^{-1}. Obviously, a number of alternate assignments are possible and could be fit with reasonable force fields. The in-plane mode for which a frequency of about 220 cm^{-1} has been derived from the microwave measurements of Hanyu et al.[3] is presumably the bending mode at 200 cm^{-1}. A similar frequency is prominent in the spec-

TABLE III: Observed Frequencies and Assignments

Frequency, cm^{-1}	Rel intensity[a]	Assignment
3080	s	CH str
3052	vw	CH str
2919	w	CH str
2912	vw	2(19b) = 2910
2769	vw	14 + 19b = 2769
2703	vw	NO str + 9a = 2699
2324	vw	5 + 14 = 2316
2218	w	2(13) = 2224
1970	w	5 + 17a = 1972
1915	w	10b + 17a = 1903
1811	w	10a + 17a = 1820
1772	vw	10a + 10b = 1780
1690	vw	11 + 10b = 1683
1615	w, broad	8a and 8b?
1554		6a + 13 = 1549
1528 P, 1523 Q, 1517 R	vs	NO str
1477	w	19a
1462 P, 1455 Q, 1450 R	s	19b
1389	vw	16a + 5 = 1386
1348	vw	?
1314	s	14
1295 P, 1286 R	vw	3
1261 P, 1255 Q, 1249 R	vw	1 + 6a = 1249
1181 P, 1176 Q, 1170 R	s	9a
1160 Q, 1155 R	vw	15
1112	vs	13
1071 P, 1063 R	vw	18b
1024 P, 1018 Q, 1012 R	s	18a
1002	w, sharp	5
997	vw	12
933	s, sharp	10b
856 P, 844 R	s	10a
812	vs	1
750	vs, sharp	11
682	vs, sharp	4
458	w, sharp	17b
443 P, 438 Q, 431 R	vw	6a
420	vw	?
384	vw	16a
337	m	16b
260 P, 248 R	s	9b
200	w	CNO bend
140	vw	16b − CNO bend = 137
101	vw	torsion

[a] s, strong; w, weak; vw, very weak.

TABLE IV: Force Constants

	In-plane[a]				Out-of-plane[b]	
	I	II			I	II
1	9.0	9.0	1		0.27	0.27
2	5.2	4.51	2		0.26	0.26
3	6.76	7.11	3		0.43	0.43
4	6.73	6.39	4		0.45	0.45
5	5.12	5.12	5	δ	0.58	0.82
6	0.38	0.43	6	τ	0.7	0.16
7	0.83	0.60	7		−0.07	−0.07
8	0.51	0.50	8		−0.07	−0.07
9	0.87	0.27	9		0.003	0.003
10	0.99	0.96	10		−0.01	−0.01
11	0.83	0.93	11		0.15	0.15
12	−0.47	−0.27	12		−0.04	−0.04
13	0.28	0.44	13	δ	0.18	0.30
14	0.50	0.16	14	δ	−0.05	0.00
15	0.40	1.36	15	δ	−0.09	0.13
16	0.06	0.40	16	δ	0.006	0.04
17	0.65	0.0	17	δ	−0.02	−0.03
18	0.09	0.08	18	τ	−0.07	−0.14
19	0.10	0.10	19	τ	−0.01	−0.09
20	0.14	0.14	20	$\tau - \delta$	−0.005	−0.005
21	0.29	0.0158				
22	0.20	0.0				
23	0.06	−0.19				

[a] Force constants in 10^5 erg/cm^2, 10^{-3} erg/cm radian or 10^{-11} erg/radian^2. The in-plane force constants 1-5 are stretching constants, 6-10 bending, 11-15 stretch-stretch interaction, 16-22 stretch-bend interaction, and 23 bend-bend interaction. [b] Force constants in 10^{-11} erg/radian^2. The designation δ represents the out-of-plane deformation coordinate of the nitroso, τ represents the nitroso torsional coordinate. The out-of-plane force constants 1 and 2 are torsions; 3 and 4 C-H out-of-plane deformations; 7 is a torsion-torsion interaction; 8, 9, and 10 are deformation interactions; 11 and 12 torsion deformation interactions; 13, 14, and 18 are interactions of the NO group with the C-C torsions, 15, 16, 17, and 19 with the C-H deformations.

trum of the electronically excited C_6H_5NO.[5] Force field *B* uses a CNO bending constant of 0.43×10^{-11} ergs/radian^2 which is a bit smaller than the bending frequency of nitrosomethane,[16] 0.69×10^{-11} erg/radian^2. A possible alternate assignment would use a CNO force constant of about this latter value and assign the 254-cm^{-1} band as the primary CNO bending mode. Both of these possibilities are still very much lower than the assignment of the CNO bend at 457 cm^{-1} given by Luttke.[1] Our assignment with the CNO band at 200 cm^{-1} explains qualitatively why the 200-cm^{-1} frequency appears with such prominence in the electronic absorption spectrum of the 7500-Å transition which involves the nonbonding nitroso electrons.

The out-of-plane substituent modes are also badly mixed. Our assignment of the mode approximately described as 16b is at a considerably higher frequency than in nitrobenzene or anisole, and this apparent discrepancy is due to the different amounts of mixing of the simple motions in these different compounds.

The next set of frequencies for which we have other information is the set which appears in the electronic spectrum, frequencies at 568, 791, and 1134 cm^{-1} in the excited state.[5] The 791- and the 1134-cm^{-1} mode correlate nicely our observed modes 1 and 13 at 812 and 1112 cm^{-1} both of which contain appreciable contributions from the CN stretching coordinate in agreement with the Luttke's assignment.[2a] The remaining frequency of 568 cm^{-1} probably correlates with the mode 6b which we calculate to be at about 590 cm^{-1} and which appears to be a rather pure ring bending mode. We have no reason to expect this particular mode to be prominent in the electronic spectrum.

The assignment of the modes at a bit higher frequency can be checked by using the characteristic sum bands with which appear in the spectrum between 1700 and 2700 cm^{-1}. These sum bands let us derive the value of mode 17a with considerable confidence. Modes 19a, 19b, and the NO stretch are badly mixed in our calculation and can be shifted about by relatively small variations in the force field. The positions of these bands correlates well with similar bands in related compounds[2a,12,13] making the assignment relatively straightforward. However, force fields *A* and *B* do not properly model the interactions between the nitroso and the ring motions in this frequency region.

Acknowledgments. We wish to thank Dr. J. R. Scherer for his advice on the normal mode analysis and Professor C. N. R. Rao for communicating his results prior to publication.

References and Notes

(1) (a) Supported in part by the National Science Foundation. (b) National Science Foundation Predoctoral Fellow.
(2) (a) W. Luttke, *Z. Elektrochem.*, **61**, 302 (1957); (b) B. G. Gowenlock and W. Luttke, *Quant. Rev.*, **12**, 321 (1958).
(3) Y. Hanyu, C. O. Britt, and J. E. Boggs, *J. Chem. Phys.*, **45**, 4725 (1966).
(4) Y. Hanyu and J. E. Boggs, *J. Chem. Phys.*, **43**, 3454 (1965).
(5) V. V. Bhujle, C. N. R. Rao, and U. P. Wild, *J. Chem. Soc., Faraday Trans. 2*, **70**, 1761 (1974).
(6) C. Drucker and T. Flade, *Z. Wiss. Photogr.*, **29**, 29 (1930).
(7) H. M. Pickett, G. M. Bradley, and H. L. Strauss, *J. Appl. Opt.*, **9**, 2397 (1970).
(8) F. R. Dollish, W. G. Fateley, and F. G. Bentley, "Characteristic Raman Frequencies of Organic Compounds", Wiley, New York, N.Y., 1974, Chapter 13.
(9) G. Varsányi, "Vibrational Spectra of Benzene Derivatives", Academic Press, New York, N.Y., 1969.
(10) E. B. Wilson, Jr., *Phys. Rev.*, **45**, 706 (1974), see also ref 8.
(11) D. H. Wiffen, *J. Chem. Soc.*, 1350 (1956), see also ref 8.
(12) J. H. S. Green, *Spectrochim. Acta*, **18**, 39 (1962).
(13) J. H. S. Green and D. J. Harrison, *Spectrochim. Acta, Part A*, **26**, 1925 (1970).
(14) J. R. Scherer, *Spectrochim. Acta, Part A*, **23**, 1489 (1962).
(15) J. R. Scherer, *Spectrochim. Acta*, **20**, 345 (1964).
(16) R. N. Dixon and H. W. Kroto, *Proc. R. Soc., Ser. A*, **283**, 423 (1965).
(17) G. M. Bradley, Ph.D. Dissertation, University of California, Berkeley, Calif. 1971.
(18) J. R. Scherer, *Spectrochim. Acta*, **19**, 601 (1963); **21**, 321 (1965); *ibid., Part A*, **24**, 747 (1968).

Molecular Motion in Supercooled Liquids. I. Pulsed Nuclear Magnetic Resonance of Lithium-7 in 11 *M* Aqueous Lithium Chloride

E. J. Sutter and J. F. Harmon*

Departments of Chemistry and Physics, Idaho State University, Pocatello, Idaho 83209 *(Received February 14, 1975)*

Publication costs assisted by Idaho State University

The temperature dependence of the spin–lattice relaxation time (T_1) has been measured with pulsed NMR for ^{7}Li in 11 *M* (18 mol %) LiCl solution in H_2O and in D_2O. The temperature range (170–298°K) over which the measurements were made includes the T_1 minimum. The diffusion constants, at 293°K, of Li in H_2O, of Li in D_2O, and of the H_2O in these solutions have been measured using pulsed NMR. A model based upon spin–lattice relaxation by translational diffusion is employed as a best explanation for the relaxation behavior. From this model the temperature dependence of the mean time between diffusive jumps for H_2O is found to be $\tau = 3.0 \times 10^{-15} \exp(3.1 \times 10^3/T)$. A structural model of this sytem is discussed.

Introduction

It has become increasingly clear that much important information can be obtained from the study of supercooled and glassy liquids. Indeed Angell[1] has remarked that the supercooled state may play the role in liquid-state theory analogous to that of the Einstein–Debye region in solid-state theory. Aside from theoretical advantages, an important experimental consequence of the study of liquids in the supercooled region is that molecular motions are sufficiently slow so that probes such as nuclear magnetic resonance can yield specific information concerning structure and dynamics. For instance, in the application of high-resolution NMR to aqueous solutions of Al, Ga, Be, and In salts at sufficiently low temperatures (−50°), Fratiello et al.[2,3] have shown that the proton line may be resolved into two components, one resulting from the water of hydration and the other from bulk water. From the relative areas of these peaks, hydration numbers can be obtained. As is well known, nuclear magnetic spin–lattice relaxation time measurements (T_1) bear directly upon the nature of molecular motions. Because molecular motions in liquids are generally far more rapid than the time scale of this type of probe, the information contained in relaxation measurements is limited in the sense that the T_1 values will reflect a time average of a number of different motions. Much more detailed inferences may be made about the motions in a given system if their time scale is of the order of the Larmor period of the nucleus under investigation (i.e., the condition for a T_1 minimum), a circumstance which will prevail in liquids which can be coerced into supercooling down to the glassy state. For example, NMR relaxation studies conducted on glycerol as a supercooled liquid[4-7] have produced much information concerning rotational and translational motions of this molecule.

Though there have been many magnetic resonance investigations of ionic aqueous solutions[8] (see also the excellent reviews by Deverell[9] and Hertz[10]), these studies have generally been restricted to low ionic stengths and limited temperature ranges—the former circumstance presumably because of the assumed complicated nature of concentrated electrolyte solutions and the latter because dilute solutions cannot be supercooled to the glassy state. Highly concentrated ionic solutions can, in many cases, be made to vitrify[11] thus extending the liquid range to the region of "slow" molecular motions. Aqueous and D_2O solutions of LiCl offer a number of advantages as a representative system. In addition to three nuclei easily observable by NMR, ^{7}Li, ^{1}H, and ^{2}H, there is a relatively wide range of concentrations that will supercool to the glassy state.[11]

In the particular system under consideration in this paper (aqueous 18.04 mol % (11 *M*) lithium chloride) we demonstrate the temperature dependence of T_1 through the minimum for the relaxation of the Li nucleus. The diffusion constants, at a single temperature, of Li in H_2O and Li in D_2O have been measured and compared with the diffusion constant of H_2O in these solutions. A model based upon spin–lattice relaxation by translational diffusion has been employed as a best explanation for the relaxation behavior. From the theory and the experimental results we can extract estimates of the relative diffusion constants between lithium and water and lithium and D_2O down to the temperature at which the supercooled solution becomes a glass.

Experimental Section

The lithium T_1 values were determined by measuring the magnetization following the last pulse in 180°–*t*–90° or 90°–*t*–90° sequences at a Larmor frequency of 14 MHz. The magnetization vs. *t* data fitted a simple exponential decay with a single time constant within experimental error. The decay of the magnetization was followed over at least one decade of the exponential. The spectrometer used was of conventional design, with the exception of the linear detector which is built around a Model 9004 Optical Electronics Absolute Value Module.[20] A simple detection system based upon this device has been developed by Burnett.[12] Data were accumulated with a boxcar integrator and chart recorder. Integration times sufficient to improve the signal:noise ratio by a factor of 3 or 4 were used. Temperatures in the cryostat, a blowing gas type, were electronically controlled and measured by a copper–constantan thermocouple. The temperatures were controlled to within 1°K and measured to within 2°K. T_1 data were reproducible to between 5% and 10%, depending upon the temperature, the

* To whom correspondence should be addressed at the Department of Physics, Idaho State University.

10% figure obtaining at the highest and lowest temperatures.

Diffusion constants were determined using a steady linear magnetic field gradient and observing the decay of a 90°–t–180° spin echo of Li or a proton as a function of pulse spacing, t. The field gradient was calibrated using the value of the self-diffusion constant of water as reported by Trappeniers et al.[13] Rather large gradients of several gauss per centimeter were necessary for the small diffusion constants encountered in our system.

Baker Analyzed reagent grade lithium chloride was dried at 130° for several days and was used without further purification (99.2% pure). Distilled water and 99.7% D_2O (BDH Chemicals, Ltd.) were used for the solvents. Approximately 100 g of solution was prepared by weighing the reagents. Aliquots (2 ml) of these solutions were placed in 10-mm o.d. Pyrex tubing with a thermocouple well fused into one side. Dissolved gases were removed by repeated freeze–thaw–pump cycles, and the tubes were sealed off under vacuum. The densities of the solutions were determined at 20° using standard pycnometer techniques. Glass transition temperatures were measured using the differential temperature technique reported previously[11] with a warm-up rate of 9°/min. This method measures the increase in heat capacity as the system moves from the disordered solid (glass) state to the supercooled liquid state.

Relaxation Model

In this section we develop a model of the molecular motion in the LiCl–H_2O system that accounts for the observed relaxation of the Li nucleus. In general nuclear relaxation takes place when the couplings of a nucleus with its surroundings are modulated, usually by molecular motions. Since Li has both dipole and quadrupole moments, one might expect that the Li nucleus can be relaxed by both dipolar interactions and processes that modulate the electric field gradient at the site of the nucleus. Order of magnitude calculations indicate that only the quadrupolar mechanism is significant. Thus it is expected that the solvent molecules, and perhaps ions, making up the solution give rise to electric field gradients that couple with the quadrupole moment of the Li nucleus. Random thermal motions of the entities producing the gradients cause fluctuating electric fields at the Li nuclear site and thus relaxation of the Li spin. The behavior of the nuclear magnetization in a pulsed NMR experiment will depend upon the type of random thermal motion that dominates the modulation of the coupling between the Li nucleus and the fluctuating electric field gradient. Hubbard[14] has shown that the magnetization decays as a sum of exponentials for nuclei with $I > 1$ and with the quadrupolar interaction modulated by rotational motion. This means that there is not a unique T_1 for such systems. On the other hand if the primary modulation is caused by translational diffusive motion, a simple exponential decay of the magnetization and a single T_1 is predicted. Guided by the observed simple exponential behavior of the Li magnetization even at the T_1 minimum where the Hubbard effect is predicted to be the largest, we assume that the primary motion is translational rather than rotational. A simple model[15] for relative translation between the Li nuclei and entities causing the electric field gradient is the following. The entity and nucleus for a time τ are at their respective sites a distance ξ apart. They then jump apart suddenly a distance comparable to ξ. Thus τ is the mean time between diffusive jumps and is related to the diffusion constant for this process by the usual relation

$$\tau = \xi^2/6D \tag{1}$$

That is, D is the relative diffusion constant between Li and the entity causing the field gradient. Using this model and the standard theory[21] for calculating relaxation rates gives the result

$$T_1^{-1} = \frac{A\tau/2}{1 + \omega^2\tau^2/4} \tag{2}$$

While eq 2 has a familiar form, it should be emphasized that the τ represents the mean time between diffusive jumps rather than the usual vaguely defined correlation time. That is, the form of the relaxation equation is a consequence of the translational model chosen and as such, the model can be tested with T_1 and diffusion data. In eq 2, A contains quantities which cannot be evaluated from the properties of our system such as the magnitude of the field gradient (for a discussion of this quantity in aqueous alkali halide systems, see ref 9). Thus A becomes an adjustable parameter in this case. Further, as can be seen from eq 2, T_1^{-1} will have a maximum (T_1 minimum) when $\tau = 2/\omega$, where ω is the Larmor frequency, in our case $2\pi \times 14$ MHz. Thus $\tau(\text{min}) = 2.3 \times 10^{-8}$ sec. This circumstance and the experimental value of T_1 at the minimum can be used to evaluate A.

Results and Discussion

The results of the self-diffusion constant measurements are displayed in Table I. We assume no better than 10% accuracy in the data with the possibility of a 10% systematic error due to the uncertainty of the literature values for the diffusion constant of pure water.[13,16] However, our value for the self-diffusion constant of water at this concentration of lithium chloride is in accord with that reported by McCall and Douglass.[17] Diffusion constants of the magnitude reported here (10^{-6} cm^2/sec) represent about the lower limit for the steady-gradient technique, so that data at lower temperatures and higher concentrations were not pursued. Perhaps pulse-gradient methods[18] could extend these measurements to an order of magnitude smaller values.

Displayed in Figure 1 are the T_1 data as a function of inverse temperature for Li relaxation in H_2O and in D_2O at 18 mol % LiCl. The data from the D_2O and H_2O systems can be compared by noting from eq 1 and 2 that, if relaxed by a common mechanism, at a given temperature we should expect

$$T_1(\text{Li–}D_2O)/T_1(\text{Li–}H_2O) = \text{constant}$$

above the T_1 minimum such that $\omega^2\tau^2/4 \ll 1$ and

$$T_1(\text{Li–}D_2O)/T_1(\text{Li–}H_2O) = \text{constant}^{-1}$$

below the T_1 minimum such that $\omega^2\tau^2/4 \gg 1$. The above constant will, to a good approximation, be given by the ratio of the self-diffusion constant of Li in D_2O to that of Li in H_2O (from Table I). The above ratios are obeyed, within experimental error; thus we conclude that if the Li–H_2O system has an additional mechanism of relaxation, it is less than our experimental error, so that lithium–proton coupling does not contribute significantly to the total relaxation of the lithium nucleus. We conclude then that the primary relaxation mechanism is quadrupolar in both cases

TABLE I: Diffusion, Density, and Glass Transition Temperature Data for LiCl in H_2O and D_2O

Solvent	[LiCl], mol %	Temp, °C	Self-diffusion const × 10^6, cm^2 sec^{-1}		Density, g cm^{-3}	T_g, °C
			Li	H_2O		
H_2O	18	20 ± 1	3.0 ± 0.3	5.2 ± 0.5[a]	1.21 ± 0.01	−135[b]
D_2O	18	20 ± 1	2.1 ± 0.2		1.26 ± 0.01	−122

[a] Compared to 5.4 × 10^{-6} estimated from data in ref 17 at 25°. [b] Compared to −130° in ref 11.

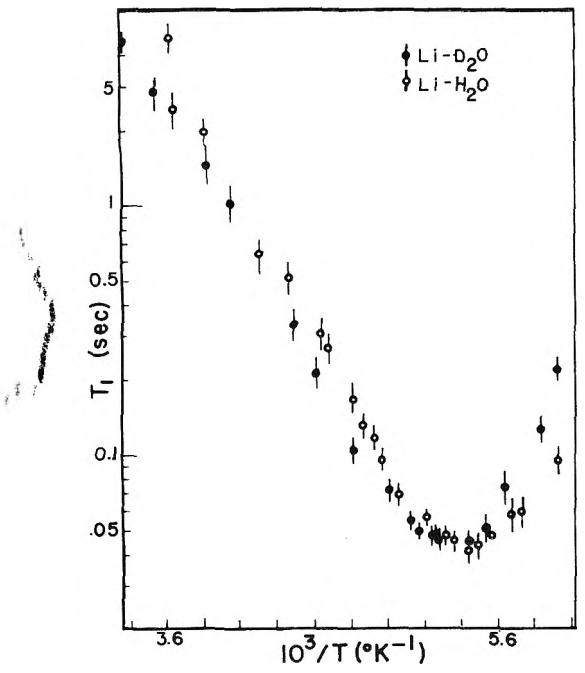

Figure 1. Logarithm of spin–lattice relaxation time in seconds plotted against inverse temperature: open circles, 18 mol % of LiCl in H_2O; closed circles, 18 mol % of LiCl in D_2O.

(confirming our order of magnitude calculations referred to previously) and henceforth will discuss only the Li–D_2O system.

Assuming that a lithium nucleus is wholly relaxed by the interaction of its quadrupole moment with fluctuating electric field gradients, one asks: "What is the agent responsible for these gradients?" A simple calculation shows that the electric field gradient produced by the chloride ion at the lithium site (assuming that it is outside the hydration sphere of the lithium ion) is at least a factor of 10 less than the field due to the electric dipole moment of a molecule of water of hydration. We assume therefore that it is the dipole moment of the water of hydration which is the agent responsible for the gradients at the site of the Li nuclei.

How well does eq 2 describe the relaxation data? A in eq 2 cannot be evaluated from first principles, but it is conveniently calculated from the value of T_1 at the minimum at which point $\tau = 2.3 \times 10^{-8}$ sec. Thus $A = 1.90 \times 10^9$ sec^{-2} and the equation for T_1 for Li in D_2O becomes, from eq 2

$$T_1 = (1.00 + 1.93 \times 10^{15}\tau^2)/(1.90 \times 10^9\tau) \quad (3)$$

If one inverts eq 3, then the relaxation data can be used to establish the temperature dependence of τ. This result is displayed in Figure 2. The solid line, a least-squares fit, is given by

$$\tau = 3.0 \times 10^{-15} \exp(3.1 \times 10^3/T) \quad (4)$$

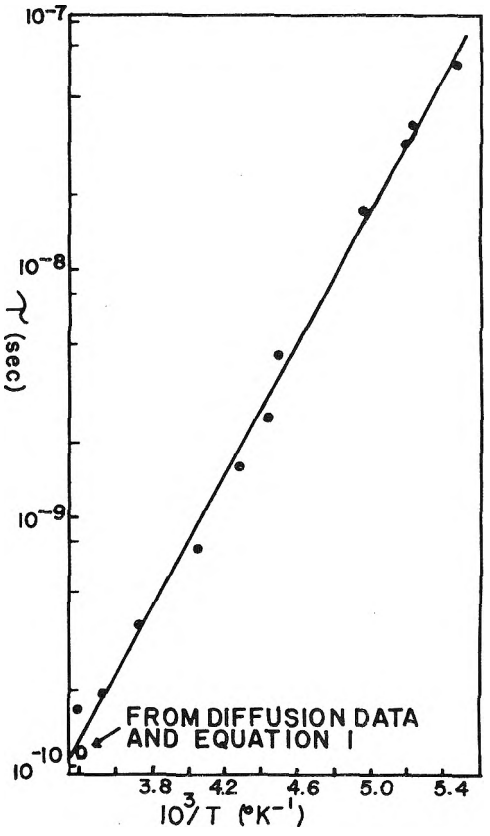

Figure 2. Logarithm of τ (seconds) plotted against inverse temperature: solid line, least-squares fit of the data; open circle, independent calculation of τ as discussed in the text.

τ may be determined independently from the T_1 data, by using the measured diffusion constants at 20° and eq 1. The appropriate diffusion constant to be used in eq 1 is the relative diffusion constant between lithium and its solvent

$$D = (D_{Li} + D_{solvent})/2 \quad (5)$$

Finally a value for the root-mean-square distance of a relative diffusive jump between Li and D_2O must be adduced. An estimate of this quantity can be made based upon consequences of the following model for the local structure of the liquid. The Li ions and their water of hydration are in chains, several hydrated ions long. The chains are stabilized and are separated by Cl^- ions. We imagine that the diffusive process involves, primarily, jump motions of water along the chains. For a given hydration sphere, the removal of a water will cause a readjustment of the remaining waters and a consequent displacement of the Li ion. This latter motion implies that the mean time between a diffusive displacement for a water and for a Li ion are the same. Thus it follows from a relation like eq 1 for each diffusing species that

$$D_{solvent}/D_{Li} = (\xi_{solvent})^2/(\xi_{Li})^2$$

where $\xi_{solvent}$ and ξ_{Li} are the mean diffusive jump distances of water and the Li ion, respectively. Using the data from Table I and the above equation results in

$$\xi_{Li} = \xi_{solvent}/1.32$$

Now if we assume that the water jumps a distance comparable to its diameter (2.8 Å), then the mean relative diffusive jump distance that the T_1 experiment is sensitive to is

$$\xi = \xi_{solvent} + \xi_{Li} \simeq 5 \text{ Å} \quad (6)$$

We now have D from eq 5 and ξ from eq 6. Putting these two values into eq 1 gives a τ of 1.1×10^{-10} sec at 20° (on Figure 2) in good agreement with the τ derived from the T_1 data (1.3×10^{-10} sec at 20°). The simple model seems to account for the data adequately. From eq 1 and 4 with the assumption of $\xi = 5$ Å one can deduce the diffusion constant as a function of temperature

$$D = 0.13 \exp(-3.1 \times 10^3/T)$$

The corresponding equation for the Li–H_2O diffusion constant is

$$D = 0.18 \exp(-3.1 \times 10^3/T)$$

from which the activation energy is 6.2 kcal/mol for the diffusive process. From the magnitude of this energy one might conclude that in the diffusive process two hydrogen bonds are broken since one expects energy for this process to be about 3 kcal/mol per bond. Extrapolation of the relative diffusion constant to the glass transition temperature yields a value of approximately 7×10^{-11} cm^2/sec. From the data in ref 6 it is possible to estimate that the self-diffusion constant of glycerol is $<10^{-16}$ cm^2/sec (this is consistent with the commonly held notion that in the glass a molecule jumps about once/sec). Clearly the water in our system is still quite free at the glass transition temperature. Further the Arrhenius behavior of this diffusive process implies that it is not a property of the liquid exclusively; that is, there is no loss of configurational entropy for the water on going through the glass transition. Thus we must conclude that the change in heat capacity observed during the glass transition temperature experiments must be governed by the change in the motions of the lithium and chloride ions. We therefore expect that the transport properties dependent primarily on the motion of these ions would follow a non-Arrhenius temperature dependence of the form $A \exp[-\text{constant}/(T - T_g)]$, a view that is consistent with measurements of viscosity and conductance.[19]

Conclusion

We have been able to describe the T_1 of Li in supercooled LiCl solutions by a simple model based upon relaxation by translation modulation of the electric field gradient produced at the Li nucleus by its water of hydration. The resulting theory allows the mean time between diffusive jumps to be displayed and, with an estimate of the root mean-square jump distance, the relative diffusion constant to be calculated. It is argued that the configuration of the water molecules is unaffected by the glass transition and would be the same in the hypothetical solid state of this system.

Acknowledgments. We wish to thank Mr. Dana Updegrove for making the density measurements and Dr. L. J. Burnett of the Physics Department at San Diego State University for providing us with the details of the linear detector circuit prior to publication.

References and Notes

(1) C. A. Angell, *J. Chem. Phys.*, **46**, 4673 (1967).
(2) R. E. Fratiello, et al., *J. Chem. Phys.*, **48**, 3705 (1968).
(3) R. Schuster and A. Fratiello, *J. Chem. Phys.*, **47**, 1554 (1967).
(4) F. Noack and G. Preissing, *Proc. Colloq. AMPERE*, **14**, 104 (1967).
(5) J. F. Harmon and L. J. Burnett, *Z. Phys.*, **253**, 183 (1972).
(6) L. J. Burnett and J. F. Harmon, *J. Chem. Phys.*, **57**, 1293 (1972).
(7) L. J. Burnett and S. B. W. Roeder, *J. Chem. Phys.*, **60**, 2420 (1974).
(8) R. G. Bryant, *J. Phys. Chem.*, **73**, 1153 (1969).
(9) C. Deverell, *Prog. Nucl. Magn. Reson. Spectrosc.*, **4**, 235 (1969).
(10) F. Franks, "Water—A Comprehensive Treatise", Vol. 3. Plenum Press, New York, N.Y., 1973, Chapter 7.
(11) C. A. Angell and E. J. Sare, *J. Chem. Phys.*, **52**, 1058 (1970).
(12) L. J. Burnett and C. R. Winther, *J. Magn. Reson.*, **17**, 344 (1975).
(13) N. J. Trappeniers, C. J. Gerristsima, and P. H. Oosting, *Phys. Lett.*, **18**, 256 (1965).
(14) P. S. Hubbard, *J. Chem. Phys.*, **53**, 985 (1970).
(15) M. Bloom, *Proc. Int. Conf. Low Temp. Phys.*, **7** (1961).
(16) K. T. Gillen, D. C. Douglass, and M. S. R. Hoch, *J. Chem. Phys.*, **57**, 5117 (1972).
(17) D. W. McCall and D. C. Douglass, *J. Phys. Chem.*, **69**, 2001 (1965).
(18) E. O. Stejskal and J. E. Tanner, *J. Chem. Phys.*, **42**, 288 (1965).
(19) C. A. Angell, *J. Am. Ceram. Soc.*, **51**, 117 (1968).
(20) Available from Optical Electronics, P.O. Box 11140, Tucson, Ariz. 85734; $33.00 plus socket.
(21) The spectral density was calculated using a probability function that describes the simple jump model as described by Bloom in ref 15. The starting point for the calculation is most conveniently taken to be an equation for T_1^{-1} such as found in M. Eisenstadt and H. L. Friedman, *J. Chem. Phys.*, **44**, 1407 (1966).

Intramolecular Interactions.[1] XXIV. Conformations of Benzylic Compounds. Molecular Optical Anisotropies, Dipole Moments, and Kerr Constants

Michel Camail,* Alain Proutiere, and Patrick Verlaque

Laboratoire de Chimie Organique Structurale (Associé au CNRS No. 109), Université de Provence, Centre de Saint-Jérôme, 13397 Marseille Cedex 4, France *(Received September 24, 1974; Revised Manuscript Received March 3, 1975)*

Publication costs assisted by the University of Niamey (Niger)

For the series C_6H_5–CH_2Z (Z = Me, Cl, Br, or CN), p-BrC_6H_4–CH_2Br, and m-ClC_6H_4–CH_2Z (Z = Cl or Br), from bond parameters, the molecular optical polarizabilities are calculated as a function of the rotational angle ϕ. They are used for relating γ^2, μ^2, and S_k to $\cos^2(\phi)$. For the hypothesis of "locked" conformations, the experimental values are in agreement with a C_1 symmetry. Comparison of the dihedral angles shows clear relationships with the steric hindrance of the Z substituents and with the electron withdrawing abilities of the p-Br and m-Cl substituents.

Introduction

Following the tuning of a Kerr effect apparatus (static electric field) and a critical examination of the Kerr constant expression,[2] we have established an empirical correlation between the Kerr constant (S_k) and molecular optical anisotropy (γ^2) for an important series of apolar compounds (linear saturated and aromatic hydrocarbons).

$$S_{k(\mu=0)} = \frac{2\pi N}{9M}\left(f\frac{2\gamma^2}{45kT} + 10\bar{\Gamma}\right) \quad (1)$$

Thus, for aromatic compounds, the f coefficient has been evaluated (0.644). Related to the hyperpolarizability tensor, the term $\bar{\Gamma}$ can be neglected for compounds having $\gamma^2 > 5$ Å.[6] This correlation being established, the principal optical polarizabilities (α_{11}, α_{22}, α_{33}) of polar molecules may be calculated, in the optical valence hypothesis, from the three self-reliant equations

$$\frac{9M}{4\pi Nd}\frac{n^2-1}{n^2+2} = \alpha_{11} + \alpha_{22} + \alpha_{33} = 3\bar{\alpha} \quad (2)$$

$$2\gamma^2 = (\alpha_{11} - \alpha_{22})^2 + (\alpha_{22} - \alpha_{33})^2 + (\alpha_{33} - \alpha_{11})^2 \quad (3)$$

$$S_k = \frac{2\pi N}{9M}\left\{f\frac{2\gamma^2}{45\,kT} + \frac{1}{45k^2T^2}\sum_{i\neq j}(\alpha_{ii} - \alpha_{jj}) \times (\mu_i^2 - \mu_j^2)\right\} \qquad i, j = 1, 2, 3 \quad (4)$$

Only two of these equations have been used in earlier research:[3] (2) and (3)[4] or (2) and (4).[5] To obtain the polarizability tensor $\{\alpha\}$, we now need less hypothesis.

As a first step,[6] we have evaluated the principal molecular optical polarizabilities of monosubstituted benzenes (C_6H_5–R; R = CH_3, Cl, or Br) and calculated the associated principal bond polarizabilities (Table I).

The self-consistency of the model and the validity of the parameters have been shown by comparison of $\bar{\alpha}$, γ^2, and S_k calculated and experimental values of a series of di- and trisubstituted benzenes.

Now, in a second step, this method can be used for studying conformational problems of polar molecules. Experimental[7,8] and theoretical[9,10] research on internal rotation (around C_{Ar}–C bond) of benzylic compounds have led to conflicting conclusions about the symmetry of these molecules.

Important and significant modifications of γ^2 and S_k with dihedral angle ϕ ($\phi = 0°$ for Z in the ring plane) are expected for largely anisotropic substituents Z = Cl, Br, CN; this has induced our choice of molecules (compounds **1**–**7**). Experimental data are listed in Table II.

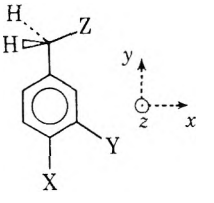

	1	2	3	4	5	6	7
Z =	CH_3	Cl	Br	CN	Br	Cl	Br
X =	H	H	H	H	Br	H	H
Y =	H	H	H	H	H	Cl	Cl

To deal with the internal rotation problem, the optical polarizability tensor of each molecule has to be calculated from the principal bond optical polarizabilities; the dipole moment components have to be evaluated. Then, γ^2 and S_k are calculated (eq 3 and 4 as a function of ϕ and compared with experimental values (Table II).

Dipole Moment Components Calculation

The vectorial addition method has been used including bond dipole moments and induced moments $\Delta\vec{\mu}$. These correspond to the interaction of polar bonds on the $(i-1)$ bonds (A–B), such as, for a molecule R–Z

$$\vec{\mu}_{R\text{-}Z} = \vec{\mu}_{R\text{-}H} + \vec{\mu}_{C\text{-}Z} + \sum_{i-1}\Delta\vec{\mu}_{C\text{-}Z;A\text{-}B} - \vec{\mu}_{C\text{-}H} - \sum_{i-1}\Delta\vec{\mu}_{C\text{-}H;A\text{-}B} \quad (5)$$

From this equation and the experimental dipole moment of R–Z = CH_3–CH_2–Z, the bond dipole moment $\vec{\mu}_{C\text{-}Z}$ is calculated (Table IV) $\Delta\vec{\mu}_{C\text{-}Z;A\text{-}B}$ being estimated with an approximate value of $\vec{\mu}_{C\text{-}Z} = \vec{\mu}_{CH_3\text{-}Z} + \vec{\mu}_{C\text{-}H}$. Then for R = Ar–$CH_2$, the same equation leads to $\vec{\mu}_{R\text{-}Z}$, the modulus of which is compared to the experimental value (Table II). Moreover, for benzyl chloride **2**, the comparison is extended to the dipole moment components, these being evaluated from the experimental dipole moment (2.22 D) of p-bis(chloromethyl)benzene (cf. Appendix I).

The results of these calculations are listed in Table III.

TABLE I: Bonds Optical Polarizabilities (in $Å^3 = 10^{-24}$ esu)

	C_{ar}–C_{ar}	C_{ar}–C	C_{ar}–Cl	C_{ar}–Br	C_{ar}–H[b]
$\alpha_{\parallel}$[a]	2.71	1.06	4.80	6.99	0.82
$\alpha_{\perp}$[a]		0.62	1.92	2.06	0.60
$\alpha_{\perp}$[a]	0.46	0.07	1.21	2.18	0.60

[a] $\alpha_{\perp}$ in the ring plane; $\alpha_{\parallel}$ perpendicular to the ring plane. [b] The values of C–H bond polarizabilities of normal alkanes have been used.

Molecular Optical Anisotropy and Kerr Constant Calculations

The polarizability tensor $\{\alpha\}$ of a molecule is calculated as a sum of bond polarizability tensors. Nevertheless, Caristan and Bothorel[11] have shown the importance of bonds "mutual perturbations", the induced dipole moment in a bond inducing in its turn moments in other bonds. This being so, the apparent molecular polarizability α^* is the sum of perturbated bond polarizabilities α_i^*:

$$\alpha^* = \sum_i \alpha_i^* = \sum_i \left(\alpha_i + \sum_{i \neq j} \alpha_i \cdot T_{ij} \cdot \alpha_j \right) \qquad (6)$$

where $T_{ij} = (3/r^5)\cdot(r^{\mu}r^{\nu}) - (\delta^{\mu\nu}/r^3)$,[12] r^{μ} is the r vector component on u axis, the r vector bonding dipole i (origin) to dipole j.[12]

This method needs the estimation of the nondisturbed bonds polarizabilities α_i. However, the α_i values are actually those of perturbated bonds in reference molecules where mutual perturbations occur. Therefore, only the interactions absent in reference molecules are taken into account. In order to simplify the corresponding corrective terms calculations, we look at the aromatic ring as a unique polarizable group, the induced moment being located at the ring baricenter (Table IV).

Calculated in this way, the molecular optical polarizabilities (Table V) are used to obtain γ^2 and S_k values as a function of the internal rotation angle ϕ, and for $\phi = 0$, 90, and 180° (Table VI). If $\vec{\mu}$ is independent of ϕ (except for **6** and **7**), γ^2 is moderately and S_k largely dependent on ϕ values (except for **1**).

Conformations

In a first approach to the internal rotation problem of this type of molecules, the hypothesis of "locked" conformations may be considered. Molecules **1–5** are characterized by dihedral angles ϕ_0 and molecules **6** and **7** involve two conformers (syn and anti) in equilibrium with angles $\phi_0(\text{anti}) = 180° - \phi_0(\text{syn})$.

For each compound **1–5**, each of the equations (Table VI) $\gamma^2 = a + b\cos^2(\phi)$; $S_k = a' + b'\cos^2(\phi)$ gives a $\cos^2(\phi_0)$ value. The mean of these is calculated by taking into account the a, b, a' and b' uncertainties (Table VII).

$$\cos^2(\phi_0) = \left(\frac{(\cos^2(\phi_0))_1}{A_1} + \frac{(\cos^2(\phi_0))_2}{A_2} \right)(A_1 A_2)$$

with $A_i = \epsilon_i / \Sigma\epsilon_i$ and

$$\epsilon_i = \Delta(\cos^2(\phi_0))/(\cos^2(\phi_0)) \qquad (7)$$

For **6** and **7**, experimental values of G ($= \gamma^2$, S_k, μ^2) are related to specific G values (eq 6), these being expressed in terms of cos (ϕ_0)(syn) $\{= -\cos(\phi_0)(\text{anti})\}$. The two unknowns (angle ϕ_0 and molar fraction n_{syn}) are calculated by solving the system of three equations with the same errors minimization procedure as for **1–5** (Table VII).

For the set of compounds, the mean discrepancy between experimental and calculated values for $\phi = \phi_0$ (Table VII) is about 7% for γ^2 and 10% for S_k. This gives a good idea of the precision of polarizability tensors and dipole moments calculations in agreement with previous estimations.[6] For the present time, this semiempirical method of calculation seems to be still the better one; indeed, for molecules as large as those considered, quantum mechanics calculations involve numerous approximations and the electronic excited states descriptions are difficult.

All the ϕ_0 values being very different from $\phi = 0$ or 90° (Table VII), our results are in agreement with Verdonck et al.'s conclusions[7] based on Raman spectroscopic observations. The comparison of ϕ_0 values (Table VII) sets up the order: **4** (Z = CN) < **2** (Z = Cl) < **1** (Z = CH_3) < **3** (Z = Br) which corresponds to an increase of ortho-hydrogen–Z distance, in accordance with steric hindrance of Z substituents.

For molecules **5–7**, the ϕ_0 values are smaller than expected; the electron withdrawing ability of the ring substituents may be the factor responsible of this fact.

For **6** and **7**, the greater stability of the anti conformer is easily explained in terms of dipole–dipole repulsions between C–Z and C–Y bonds; the corresponding calculated[12] value of the energy difference between conformers is in agreement with the experimental value (0.3 kcal mol^{-1}).

The hypothesis of low internal rotation barriers is considered in the following paper.[13]

Conclusion

In preceding papers,[2,6] we have shown the possibilities and the interest of a conjoint use of the experimental quantities γ^2, μ^2, and S_k; this object has been carried on in this paper by the study of a conformational problem.

The semiempirical method of $\{\alpha\}$ and μ^2 calculations has been improved by rationalization of the calculation of bonds mutual perturbations.

To check the method, we have studied rather simple molecules involving a very polarizable group and substituents chosen on a wide range of polarizabilities and dipole moments. For the "locked" conformations hypothesis, this study has shown up the autocoherency of the methods in the limits of the experimental data reliability.

Appendix I. Dipole Moment Calculation

Benzyl chloride **2** is taken as an example. The ethyl chloride dipole moment can be expressed as eq 5

$$\vec{\mu}_{Et\text{-}Cl} = \vec{\mu}_{Et\text{-}H} - \vec{\mu}_{C\text{-}H} - \Sigma\Delta\vec{\mu}_{CH;Et} + \vec{\mu}_{C\text{-}Cl} + \Sigma\Delta\vec{\mu}_{CCl;Et}$$

$\Sigma\Delta\vec{\mu}_{CX;Et}$ (X = Cl or H) corresponds to the dipoles induced by C–X dipole moment on all the other bonds of ethyl group and reciprocally

$$\Sigma\Delta\vec{\mu}_{CX;Et} = \sum_i \alpha_i \cdot T_i \cdot \vec{\mu}_{C\text{-}X} + \sum_i \alpha_{C\text{-}X} \cdot T_i \cdot \vec{\mu}_i \qquad i = 1, 2, \ldots, 6$$

where the indexes 1, 2, 3 correspond to the three methyl group C–H bonds, 4 to the C–C bond, and 5 and 6 to the last two C–H bonds. T is a geometric matrix.[11] Expanding

$$\Sigma\Delta\vec{\mu}_{CH;Et} = (\alpha_1 \cdot T_1 + \alpha_2 \cdot T_2 + \alpha_3 \cdot T_3 + \alpha_4 \cdot T_4 + \alpha_5 \cdot T_5 + \alpha_6 \cdot T_6) \cdot \vec{\mu}_{C\text{-}H} + \alpha_{C\text{-}H}(T_1 \cdot \vec{\mu}_1 + T_2 \cdot \vec{\mu}_2 + T_3 \cdot \vec{\mu}_3 + T_4 \cdot \vec{\mu}_4 + T_5 \cdot \vec{\mu}_5 + T_6 \cdot \vec{\mu}_6)$$

TABLE II: Experimental Data

Compd	$a_{(n^2)}$[a]	$a_{(\epsilon_r)}$[a]	$a_{(\rho)}$[a]	$10^{14}\, a_{(s_k)}$[a]	$a_{(y)}$[b]	$10^{14} S_k$	$10^{18}\mu$	$10^{48}\gamma^2$
1	0.21	0.379	−1.254	14.4		15.7	0.54	45.0[c]
2	0.20	5.59	−0.705	10.1		11.4	1.85	49.7[c]
3	0.43	4.21	−0.199	35.2		36.5	1.83	57.0[c]
4	0.34	20.5	−0.781	193.6	1.360	195.5	3.45	62.1
5	0.45	2.65	0.307	−64.4	1.387	−62.8	1.67	135.3
6	0.38	5.26	−0.365	−18.0	1.200	−16.6	1.99	75.4
7	0.43	4.20	0.038	−25.7	1.071	−26.4	1.98	85.9

[a] $a_{(X)} = (\delta X/\delta t)_{t \to 0}$; n is the refractive index of a CCl_4 solution; ϵ_r, the relative dielectric constant of the solution; ρ, the density of the solution; t, the concentration of the solution expressed in g g^{-1}. [b] $y = (i/i_0)(n^2/n_0^2)(n^2+2)^{-2} - (c_0/\rho_0)(n_0^2+2)^{-2}$; i_0 is the depolarized light intensity scattered by the solvent; c_0, the concentration of the solvent (g ml^{-1}). [c] Reference 14.

TABLE III: Calculated Dipole Moments (in D = 10^{-18} esu)

	μ_x	μ_y	μ_z	$\lvert\mu\rvert$[a]
1	−0.096 cos ϕ	−0.266	−0.122 sin ϕ	0.29
2	1.665 cos ϕ	0.843	1.648 sin ϕ	1.86
3	1.685 cos ϕ	0.988	1.708 sin ϕ	1.96
4	3.076 cos ϕ	1.769	3.221 sin ϕ	3.61
5	1.685 cos ϕ	−0.532	1.708 sin ϕ	1.78
6	1.647 cos ϕ + 1.342	0.120	1.648 sin ϕ	
7	1.667 cos ϕ + 1.342	0.265	1.708 sin ϕ	

[a] $\lvert\vec{\mu}\rvert \simeq \{[(\mu_x + \mu_z)/2]^2 + \mu_y^2\}^{1/2}$.

TABLE IV: Bond Parameters Used for Molecular Polarizabilities Calculations (cf. also Table I)

Bond $C^{\delta+}$–$Z^{\delta-}$	$\alpha_\parallel$, Å^3	$\alpha_\perp$, Å^3	$\alpha_\perp$, Å^3	μ,[a] D	d,[b] Å
C–Cl[c]	4.23	1.78	1.78	2.12	1.72[e]
C–Br[c]	5.84	2.69	2.69	2.10	1.50[e]
C–CN[d]	4.45	1.28	1.28	3.73	1.47
C–Ar[d]	13.71	11.31	5.85	0.62	2.93
C–H[c]	0.82	0.60	0.60	0.30	0.77

[a] From μ_{CH_2Cl}.[16] [b] Length between carbon and bond dipole. [c] Reference 15. [d] This work. [e] Reference 11.

$\Sigma\Delta\vec{\mu}_{CCl;Et}$ has a similar form. The difference between these two equations is

$$\Sigma\Delta\vec{\mu}_{CCl;Et} - \Sigma\Delta\vec{\mu}_{CH;Et} = \sum_i (\alpha_i \cdot T_i' \cdot \vec{\mu}_{C\text{-}Cl} - \alpha_i \cdot T_i \cdot \vec{\mu}_{C\text{-}H} + \alpha_{C\text{-}Cl} \cdot T_i' \cdot \vec{\mu}_i - \alpha_{C\text{-}H} \cdot T_i \cdot \vec{\mu}_i)$$

For benzyl chloride, a similar treatment leads to (7 being the phenyl group)

$$\Sigma\Delta\vec{\mu}_{CH;C_6H_6\text{-}CH_2\text{-}} = (\alpha_4 \cdot T_4 + \alpha_5 \cdot T_5 + \alpha_6 \cdot T_6 + \alpha_7 \cdot T_7) \cdot \vec{\mu}_{C\text{-}H} + \alpha_{C\text{-}H} \cdot (T_4 \cdot \vec{\mu}_4 + T_5 \cdot \vec{\mu}_5 + T_6 \cdot \vec{\mu}_6 + T_7 \cdot \vec{\mu}_7)$$

hence

$$\Sigma\Delta\vec{\mu}_{CCl;C_6H_5\text{-}CH_2\text{-}} - \Sigma\Delta\vec{\mu}_{CH;C_6H_5\text{-}CH_2\text{-}} - \Sigma\Delta\vec{\mu}_{CCl;Et} + \Sigma\Delta\vec{\mu}_{CH;Et} = (\alpha_7 \cdot T_7' - \alpha_1 \cdot T_1' - \alpha_2 \cdot T_2' - \alpha_3 \cdot T_3') \cdot \vec{\mu}_{C\text{-}Cl} + \alpha_{C\text{-}Cl} \cdot (T_7' \cdot \vec{\mu}_7 - T_1' \cdot \vec{\mu}_1 - T_2' \cdot \vec{\mu}_2 - T_3' \cdot \vec{\mu}_3) - (\alpha_7 \cdot T_7 - \alpha_1 \cdot T_1 - \alpha_2 \cdot T_2 - \alpha_3 \cdot T_3) \cdot \mu_{C\text{-}H} - \alpha_{C\text{-}H} \cdot (T_7 \cdot \vec{\mu}_7 - T_1 \cdot \vec{\mu}_1 - T_2 \cdot \vec{\mu}_2 - T_3 \cdot \vec{\mu}_3)$$

The different parameters of this equation are listed in Table IV. The permanent dipole moment of the benzylic group is located on carbon 1. The expression

$$\vec{\mu}_{C_6H_5\text{-}CH_2\text{-}Cl} = \vec{\mu}_{C_6H_5\text{-}CH_3} + \vec{\mu}_{Et\text{-}Cl} + \Sigma\Delta\vec{\mu}$$

becomes, after numerical application

$$\mu_{C_6H_5\text{-}CH_2\text{-}Cl} = \begin{Bmatrix} 0 \\ -0.32 \\ 0 \end{Bmatrix} + \begin{Bmatrix} 1.89\cos\phi \\ 0.67 \\ 1.89\sin\phi \end{Bmatrix} + \begin{Bmatrix} -0.23\cos\phi \\ 0.50 \\ -0.25\sin\phi \end{Bmatrix} = \begin{Bmatrix} 1.66\cos\phi \\ 0.85 \\ 1.64\sin\phi \end{Bmatrix}$$

The dipole moment mean value (1.85 D) is calculated as the μ_x and μ_y average.

The μ_x component may be compared to experience. θ and θ' being the internal rotation dihedral angle of *p*-bis(chloromethyl)benzene, its total dipole moment is

$$\vec{\mu} = \begin{Bmatrix} \mu_x(\cos\theta + \cos\theta') \\ 0 \\ \mu_x(\sin\theta + \sin\theta') \end{Bmatrix}$$

and, as a consequence, the modulus

$$\mu^2 = 2\mu_x^2(1 + \cos(\theta - \theta'))$$

For each CH_2–Cl group, the internal rotation potential varies with θ, hence for the molecule $V = V(\theta) + V(\theta')$. Owing to symmetry $V(\theta) = V(-\theta) = V(180° - \theta) = V(\theta - 180°)$. Then, each rotational energy state being 16-fold degenerated, the average of the molecular square dipole moments in this state

$$\mu^2 = \frac{1}{16}\sum_{i,j} 2\mu^2(1 + \cos(\beta_i - \beta_j')) \qquad i, j = 1, \ldots, 4$$

where $\beta_1 = \theta$, $\beta_2 = -\theta$, $\beta_3 = 180 - \theta$, $\beta_4 = \theta - 180$; $\beta_1' = \theta'$, $\beta_2' = -\theta'$, $\beta_3' = 180 - \theta'$, $\beta_4' = \theta' - 180$, is $\mu^2 = 2\mu_x^2$, hence, the mean dipole moment: $\langle\mu\rangle = \mu_x \cdot \sqrt{2} = 2.32$ D.

The discrepancy with the experimental value (2.22 D) is very small; nevertheless, it may be explained by a slight orientational correlation, the electrostatic energy difference for the two conformations $\Phi = 0°$ and $\Phi = 180°$ ($\Phi = \theta - \theta'$) being 0.2 kcal mol^{-1}.

Appendix II. Molecular Optical Polarizabilities Calculations

Benzyl chloride **2** is taken as an example. The ethyl chloride optical polarizability is considered as the sum of bond

TABLE V: Calculated Molecular Optical Polarizabilities (in Å^3)

Compd	α_{xx}	α_{yy}	α_{zz}	α_{xy}	α_{xz}	α_{yz}
1	15.36 + 1.44 $\cos^2\phi$	17.04	10.04 − 1.23 $\cos^2\phi$	1.45 $\cos\phi$	1.33 $\sin\phi\cos\phi$	1.25 $\sin\phi$
2	15.41 + 1.91 $\cos^2\phi$	16.69	10.79 − 1.72 $\cos^2\phi$	1.75 $\cos\phi$	1.81 $\sin\phi\cos\phi$	1.59 $\sin\phi$
3	15.73 + 2.59 $\cos^2\phi$	18.66	12.10 − 2.41 $\cos^2\phi$	2.73 $\cos\phi$	2.50 $\sin\phi\cos\phi$	2.45 $\sin\phi$
4	15.69 + 1.82 $\cos^2\phi$	18.37	11.11 − 1.73 $\cos^2\phi$	2.41 $\cos\phi$	1.77 $\sin\phi\cos\phi$	2.06 $\sin\phi$
5	17.19 + 2.59 $\cos^2\phi$	24.83	13.68 − 2.41 $\cos^2\phi$	2.73 $\cos\phi$	2.50 $\sin\phi\cos\phi$	2.45 $\sin\phi$
6	18.81 + 1.91 $\cos^2\phi$	18.79	11.43 − 1.72 $\cos^2\phi$	−1.19 + 1.75 $\cos\phi$	1.81 $\sin\phi\cos\phi$	1.59 $\sin\phi$
7	19.13 + 2.59 $\cos^2\phi$	20.76	12.73 − 2.41 $\cos^2\phi$	−1.19 + 2.73 $\cos\phi$	2.50 $\sin\phi\cos\phi$	2.45 $\sin\phi$

TABLE VI: Molecular Optical Anisotropies, Specific Kerr Constants, and Dipole Moments

		$\phi = 0°$	$\phi = 80°$	$\phi = 180°$	Exptl
1	$\gamma^2 = 40.5 + 25.9\cos^2\phi$	66.4	40.5	66.4	45.0
	$\mu^2 = 0.08$				0.12
	$S_k = 14.6 + 8.2\cos^2\phi$	22.8	14.6	22.8	15.8
2	$\gamma^2 = 36.4 + 35.9\cos^2\phi$	72.3	36.4	72.3	49.7[a]
	$\mu^2 = 3.46$				3.42
	$S_k = -36.2 + 246\cos^2\phi$	210	−36.2	210	11.4
3	$\gamma^2 = 50.5 + 47.8\cos^2\phi$	98.3	50.5	98.3	57.0[a]
	$\mu^2 = 3.85$				3.35
	$S_k = 22.3 + 187\cos^2\phi$	209	22.3	209	36.5
4	$\gamma^2 = 53.2 + 38.0\cos^2\phi$	91.2	53.2	91.2	62.1
	$\mu^2 = 13.0$				11.9
	$S_k = -206 + 1167\cos^2\phi$	961	−206	861	196
5	$\gamma^2 = 116 + 47.7\cos^2\phi$	163	116	163	135
	$\mu^2 = 3.16$				2.79
	$S_k = -98.8 + 119\cos^2\phi$	20.1	−98.8	20.1	−62.8
6	$\gamma^2 = 66.2 - 12.5\cos\phi + 50.0\cos^2$	104	66.2	129	75.4
	$\mu^2 = 4.53 + 4.42\cos$	8.95	4.53	0.11	3.96
	$S_k = -73.3 + 195\cos\phi + 298\cos^2\phi$	420	−73.3	30.1	−16.6
7	$\gamma^2 = 75.7 - 19.5\cos\phi + 70.9\cos^2\phi$	127	75.7	166	85.9
	$\mu^2 = 4.72 + 4.47\cos\phi$	9.19	4.72	0.25	3.92
	$S_k = -66.5 + 153\cos\phi + 254\cos^2\phi$	340	−66.5	34.4	−26.4

[a] Reference 14.

TABLE VII: Calculated Values of Dihedral Angles ϕ_0 and of Corresponding γ^2, μ^2, and S_K[a]

		1	2	3	4	5	6	7
ϕ_0, deg		66	63	73	55	55	59	60
$n_{(5\,Y\,a)}$							0.380	0.311
$G(\phi_0)$	γ^2	44.7 (45.0)	43.7 (49.7)	54.8 (57.0)	66.0 (62.1)	131 (135)	81.1 (75.4)	97.2 (85.9)
	μ^2						3.98 (3.96)	3.87 (3.92)
	S_k	15.9 (15.8)	14.0 (11.4)	39.1 (36.5)	187 (196)	−60.1 (−62.8)	−18.0 (−16.6)	−31.8 (−26.4)

[a] Experimental values are in parentheses.

polarizabilities and of mutual perturbations of all the bonds (eq 5):

$$\alpha_{Et\text{-}Cl} = \alpha_{Et\text{-}H} - \alpha_{C\text{-}H} - \Delta\alpha_{CH;Et} + \alpha_{C\text{-}Cl} + \Delta\alpha_{CCl;Et}$$

The same indexes as in Appendix I are used

$$\Delta\alpha_{CCl;Et} = \alpha_{C\text{-}Cl}\cdot(T_1'\cdot\alpha_1 + T_2'\cdot\alpha_2 + T_3'\cdot\alpha_3 + T_4'\cdot\alpha_4 + T_5'\cdot\alpha_5 + T_6'\cdot\alpha_6) + (\alpha_1\cdot T_1' + \alpha_2\cdot T_2' + \alpha_3\cdot T_3' + \alpha_4\cdot T_4' + \alpha_5\cdot T_5' + \alpha_6\cdot T_6')\cdot\alpha_{C\text{-}Cl}$$

A similar expression is obtained for $\Delta\alpha_{CH;Et}$. For benzyl chloride, eq 5 gives

$$\alpha_{C_6H_5CH_2Cl} = \alpha_{C_6H_5CH_3} - \alpha_{C\text{-}H} - \Delta\alpha_{CH;C_6H_5CH_2} + \alpha_{C\text{-}Cl} + \Delta\alpha_{CCl;C_6H_5CH_2}$$

$\alpha_{C\text{-}Cl}$ obtained from the first equation, yielded

$$\alpha_{C_6H_5CH_2Cl} = \alpha_{C_6H_5CH_3} + \alpha_{Et\text{-}Cl} - \alpha_{Et\text{-}H} + \Delta\alpha$$

where

$$\Delta\alpha = \alpha_{C\text{-}Cl}\cdot(T_7'\cdot\alpha_7 - T_1'\cdot\alpha_1 - T_2'\cdot\alpha_2 - T_3'\cdot\alpha_3) - \alpha_{C\text{-}H}\cdot(T_7\cdot\alpha_7 - T_1\cdot\alpha_1 - T_2\cdot\alpha_2 - T_3\cdot\alpha_3) + (\alpha_7\cdot T_7' - \alpha_1\cdot T_1' - \alpha_2\cdot T_2' - \alpha_3\cdot T_3')\cdot\alpha_{C\text{-}Cl} - (\alpha_7\cdot T_7 - \alpha_1\cdot T_1 - \alpha_2\cdot T_2 - \alpha_3\cdot T_3)\cdot\alpha_{C\text{-}H}$$

The different parameters of this equation are listed in Table IV; conventional geometries are assumed. The results are listed in Table V.

References and Notes

(1) (a) Preceding paper in this series: R. Lafrance, J. P. Aycard, J. Berger, and H. Bodot, *Org. Magn. Resonance*, in press. (b) This paper is a part of the "Doctorat ès-Sciences Physiques" to be presented to the "Université de Provence" by M. Camail.
(2) A. Proutiere and J. G. R. Baudet, *C. R. Acad. Sci., Paris, Ser. C*, **267**, 682 (1968).
(3) B. A. Arbuzov and co-workers (cf., for instance, C. G. Vulfson, R. A. Emagulov, and A. N. Vereshchagin, *Izv. Akad. Nauk SSR, Ser. Khim.*, **4**, 927 (1973)) use the three equations, but with an arbitrary value of the *f* coefficient. We thank Miss M. Deneux for the translation of the russian papers.
(4) P. Bothorel, *Ann. Chim. (Paris)*, 669 (1959), and following papers.
(5) R. J. W. Lefevre, *Adv. Phys. Org. Chem.*, **3**, 90 (1965).
(6) A. Proutiere and M. Camail, *Mol. Phys.*, **29**, 1473 (1975).
(7) L. Verdonck and G. P. Van Der Kelen, *Spectrochim. Acta, Part A*, **28**, 51 (1972); L. Verdonck, G. P. Van Der Kelen, and Z. Eckhaut, *ibid.*, **29**, 813 (1973).
(8) F. G. Brickwedde, M. Moskow, and R. B. Scott *J. Chem. Phys.*, **13**, 547 (1945).
(9) M. Simonetta, B. Calcagno, R. Santi, and P. Schwartz, *Chim. Ind.*, **55**, 222 (1973).
(10) W. H. Hehre, L. Radom, and J. A. Pople, *J. Am. Chem. Soc.*, **94**, 1496 (1972).
(11) A. Caristan and P. Bothorel, *J. Chim. Phys.*, **66**, 740 (1969).
(12) E. Durand, "Electrostatique", Vol. 1, Masson, Paris, 1964.
(13) M. Camail, A. Proutiere, and H. Bodot, *J. Phys. Chem.*, following paper in this issue.
(14) A. Unanue and P. Bothorel, *Bull. Soc. Chim. Fr.*, 573 (1964).
(15) C. Clement and P. Bothorel, *C. R. Acad. Sci., Paris, Ser. C*, **251**, 2323 (1960).
(16) "Mc Clellan Tables of Experimental Dipole Moments", W. H. Freeman, San Francisco, Calif., 1963.

Intramolecular Interactions. XXV.[1] Internal Rotation Barriers of Benzylic Compounds. Molecular Optical Anisotropies, Dipole Moments, and Kerr Constants

Michel Camail,* Alain Proutiere, and Hubert Bodot

Laboratoire de Chimie Organique Structurale (Associé au CNRS No. 109), Université de Provence, Centre de Saint-Jérôme, 13397 Marseille Cedex 4, France

(Received September 24, 1974; Revised Manuscript Received March 3, 1975)

Publication costs assisted by the Université de Niamey (Niger)

For the series C_6H_5–CH_2Z (Z = Me, Cl, Br, or CN), *p*-BrC_6H_4–CH_2Br, the internal rotation problem is considered on the basis of V_2 and V_4 terms of the Fourier series, connected to $\langle\cos^2(\phi)\rangle$ (mean value of square cosine of torsional angle ϕ). $\langle\cos^2(\phi)\rangle$ values are obtained from experimental molecular optical anisotropies and Kerr constants. The internal rotation barriers are estimated and discussed as a function of spectroscopic data and in terms of molecular mechanics. For *m*-ClC_6H_4–CH_2Z (Z = Cl or Br), the V_1 term is also evaluated.

Introduction

In the preceding paper,[1] we have calculated the expressions of the molecular optical anisotropy γ^2, of the dipole moment μ, and of the specific Kerr constant S_k as a function of torsional angle ϕ ($\phi = 0°$ when Z is in the ring plane) for each of the compounds of the series: C_6H_5–CH_2Z; Z = Me (**1**), Cl (**2**), Br (**3**), CN (**4**); p-BrC_6H_4–CH_2 Br (**5**); *m*-ClC_6H_4–CH_2Z Z = Cl (**6**), Br (**7**).

Bringing the experimental values of γ^2, μ^2, and S_k into these expressions, conformational information has been obtained, in a first approach, on the basis of the "locked" conformation hypothesis.

As more crowded similar molecules[2] involve internal rotation barriers of approximately 15 kcal mol^{-1}, our molecules may present rather lower barriers; for **1**,[3] it has been estimated[4] to 1.3 kcal $mole^{-1}$. We must show how it is possible to determine these barriers from our experimental results.

Two hypothesis about the potential energy curve have to be considered: (1) it presents two maxima (for a 360° rotation) of equal energy for **1** to **5**, and *a priori* different for **6** and **7** (Figure 1); (2) it presents four maxima for a 360° rotation (Figure 2).

First Hypothesis

Owing to symmetry, the maxima are located either at $\phi = 0$ and 180° or at $\phi = 90$ and 270°. The simplest expression for the potential energy is

$$V(\phi) = \sum_k V_k(1 + \alpha_k \cos(k\phi))/2 \quad \alpha_k = \pm 1 \quad (1)$$

As in similar studies,[5] this expansion has been limited to potentials V_1 to V_4 ($V_k = 0$ when $k > 4$). Owing to symmetry, $V_1 = V_3 = 0$ for molecules **1**–**5**. With **6** and **7**, the potential function dissymmetry mainly results from electrostatic interaction[6] betweeen dipoles C–Z and *m*-Cl, hence, V_3 is neglected. To have only two maxima, the analytical condition is $V_4 \leq V_2/4$ (when α_2 and α_4 have the same sign). For a progressive investigation of V_2 and V_4, we will first postulate $V_4 = 0$.

Taking all the possible conformations (defined by ϕ_i angles) into account, their populations (molar fractions n_i) can be evaluated on the basis of a Boltzmann distribution (nonquantic treatment). Owing to the additivity of molecular G values ($G = \gamma^2$, μ^2, and S_k), the experimental data may be compared with calculated mean values $\langle G\rangle$.

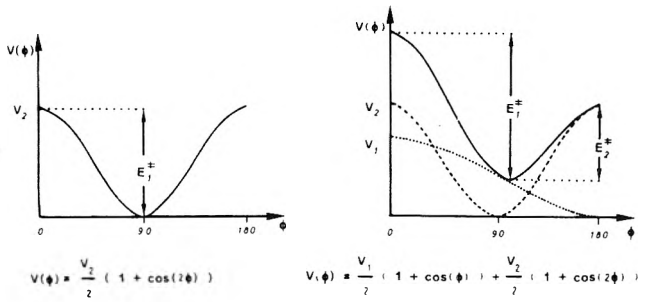

Figure 1. Potential energy curves (hypothesis 1).

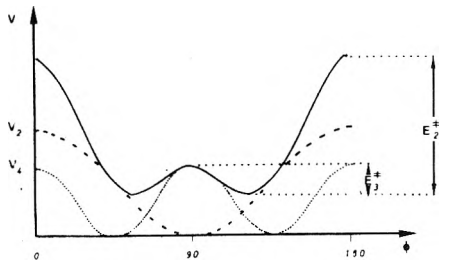

Figure 2. Potential energy curve (second hypothesis, $V_1 = 0$).

$$\langle G \rangle = \sum_i n_i G_i \text{ with } n_i = \frac{N_i}{N} = \frac{\exp(-V(\phi_i)/RT)}{\sum_i \exp(-V(\phi_i)/RT)} \quad (2)$$

In Table VI of the preceding paper,[1] our calculations have led to expressions such as

$$G = \sum_n a_n \cos^n(\phi) \qquad n = 0, 1, 2 \quad (3)$$

Correlating eq 1–3

$$\langle G \rangle = \sum_n a_n \frac{\sum_{\phi=0}^{\phi=180^\circ} \cos^n(\phi_i) \exp\left(-\sum_k V_k(1 + \alpha_k \cos(k\phi))/2RT\right)}{\sum_{\phi=0}^{\phi=180^\circ} \exp\left(-\sum_k V_k(1 + \alpha_k \cos(k\phi)/2RT\right)} \quad (4)$$

Equation 4 has the form

$$\langle G \rangle = \sum_n a_n \langle \cos^n(\phi) \rangle \qquad n = 0, 1, 2 \quad (5)$$

For molecules **1–5**, eq 5 becomes

$$\langle G \rangle = a_0 + a_2 \langle \cos^2(\phi) \rangle = a_0 + a_2 f\left(\frac{\alpha_2 V_2}{RT}\right) \quad (6)$$

$\langle \cos^2 \phi \rangle$ have been calculated for different values of $(\alpha_2 V_2/RT)$ (Table I) by two different ways: (1) $\int_0^{\pi/2} \cos(nm\phi) \exp(-z \cos(m\phi)) = I_n(z)\pi/2m(-1)^n$ for $m = 2$, $n = 0$ and $m = 2$, $n = 1$; (2) numerical integration between 0 and $\pi/2$ of $\cos^p(\phi) \exp(-z \cos 2\phi)$ for $p = 0$ and $p = 2$, with 0.01 radian-step. The two methods give the same results but the second one is faster and is used in all our calculations.

Now, it is possible to determine the sign of α_2 and to obtain an estimation of V_2 for molecules **1–5** (Table II, $V_4 = 0$).

For **6** and **7**, eq 6 involves a supplementary term

$$\langle G \rangle = a_0 + a_1 \langle \cos \phi \rangle + a_2 \langle \cos^2 \phi \rangle \quad (7)$$

$\langle \cos \phi \rangle$ and $\langle \cos^2 \phi \rangle$ are both dependent of $(\alpha_1 V_1/RT)$ and $(\alpha_2 V_2/RT)$. The two unknowns $\langle \cos \phi \rangle$ and $\langle \cos^2 \phi \rangle$ (only the last one for **1–5**) are determined by solving equations (**1–5**) or couples of equations (**6** and **7**) of Table VI of the preceding paper.[1] For each unknown, two or three solutions are obtained, and the corresponding weighted mean value is calculated by the procedure previously described.[1]

For molecules **1–5**, $\langle \cos^2 \phi \rangle$ being less than 0.5 (Table II), the coefficient α_2 is positive (Table I); this corresponds to energy maxima located at $\phi = 0$ and 180° (C–Z bond in the ring plane). Hence, for **6** and **7**, $\alpha_2 = +1$ is assumed; $\langle \cos \phi \rangle$ being negative, $\alpha_1 = +1$ and the highest barrier is located at $\phi = 0°$. The two equations ($\langle \cos \phi \rangle$ and $\langle \cos^2 \phi \rangle$) with the two unknowns (V_1/RT and V_2/RT) are numerically solved (Table II, $V_4 = 0$). In Table II, the maximal values of V_2 are reported; they correspond to hypothesis $V_4 = V_2/2$. Except for **3**, the height of potential barrier ($E_1^\ddagger$) is slightly changed.

Second Hypothesis

The observation of depolarization ratio of Raman bands has led Verdonck et al.[7] to exclude C_s symmetry for this kind of molecules. Therefore, the potential energy curve needs four maxima located at $\phi = 0$, 90, 180, and 270°, corresponding to eq 1 with $V_1 = 0$ for **1–5**, $V_3 = 0$ and $V_4 > V_2/4$. Correlating this equation with eq 2 and 3, we get an expression similar to eq 4 where $\langle \cos \phi \rangle$ and $\langle \cos^2 \phi \rangle$ are both functions of (V_1/RT), (V_2/RT), and (V_4/RT).

For molecules **1–5**, derivation of eq 1 leads to the smallest barrier height $E_3^\ddagger$ and to the angle ϕ_m for the minimum potential energy

$$E_3^\ddagger = \frac{(4V_4 - V_2)^2}{16V_4} \quad (8)$$

$$\cos^2(\phi_m) = \frac{4V_4 - V_2}{8V_4} \quad (9)$$

Owing to the magnitude of experimental torsional frequencies,[7] the barrier height $E_3^\ddagger$ cannot be less than 0.25 kcal mol^{-1}; minimal values of V_2 can be infered (Table III). For increasing values of V_2, $\cos^2(\phi_m)$ steeply reach a limit, and a narrow range of ϕ_m may be deduced (Table III).

For molecules **6** and **7**, the numerical solving of the system of two equations ($\langle \cos \phi \rangle$ and $\langle \cos^2 \phi \rangle$) with three unknowns ($V_1$, V_2, V_4) leads to a family of solutions (Figure 3). In each case, V_1 value is nearly independent of V_2 and V_4 values; so, it is well defined: 0.7 and 1.3 kcal mol^{-1} for **6** and **7**, respectively. Then again, it is possible to get V_2 and V_4 minimal values corresponding to the appearance of two energy minima (two conformers). For **6**, these values are 5.7 and 2.4 kcal mol^{-1} respectively when the smallest barrier between conformers is 0.25 kcal mol^{-1}. Any conformer mixture having not been set up by vibrational study,[7] our results give informations about the maximal values (kcal mol^{-1}) of V_2 (5.7) and V_4 (2.4) and of the 0 and 180° barriers (6.6 and 5.9).

Discussion

The accuracies of γ^2, μ^2, and S_k measurements and calculations methods have been discussed in the preceding paper.[1] Another factor able to affect the structural conclusions is the nonquantic treatment of the molecules distribution worked up for lack of spectroscopic data.

TABLE I: $\langle\cos^2\phi\rangle$ Calculated for Different Values of $(\alpha_2 V_2/RT)$

V_2/RT		0.0	0.2	0.5	1.0	1.5	2.0	3.0	4.0	5.0	7.0
$\langle\cos^2\phi\rangle$	$\alpha_2 = +1$	0.5	0.475	0.437	0.378	0.323	0.276	0.201	0.150	0.116	0.078
	$\alpha_2 = -1$	0.5	0.525	0.563	0.622	0.677	0.724	0.799	0.850	0.884	0.922

TABLE II: Barriers to Internal Rotation (kcal mol^{-1}, T = 298 K)

		1	2	3	4	5	6	7
$\langle\cos\phi\rangle$		0[a]	0[a]	0[a]	0[a]	0[a]	−0.117	−0.153
$\langle\cos^2\phi\rangle$		0.162	0.204	0.090	0.337	0.325	0.195	0.164
$V_4 = 0$	V_1	0[a]	0[a]	0[a]	0[a]	0[a]	0.7	1.3
	V_2	2.3	1.8	3.5	0.8	0.9	2.0	2.5
	$E_1^{\ddagger}$ $(E_2^{\ddagger})$	2.3	1.8	3.5	0.8	0.9	2.4 (1.6)[b]	3.2 (1.9)[c]
$0 \le V_4 \le \frac{V_2}{4}$	$V_2 \le$	3.5	2.4	8.0	0.9	1.1		
	$E_1^{\ddagger} \le$	2.6	1.8	6.0	0.8	0.9		

[a] Due to symmetry. [b] ϕ_m = 95°. [c] ϕ_m = 97°.

TABLE III: Minimal Values of V_2 and V_4 Corresponding to $E_3^{\ddagger} \ge 0.25$ kcal mole^{-1} and the Range of the Angle ϕ Corresponding to Energy Minimum (ϕ_m): $\phi_1 \le \phi_m \le \phi_2$

Compd	V_2 (min)	V_4 (min)	$E_2^{\ddagger}$	ϕ_1, deg	ϕ_2, deg
1	6.6	2.4	6.9	65	66
2	3.9	1.6	4.2	61	63
3	>12				
4	1.2	0.8	1.5	53	57
5	1.3	0.8	1.5	54	57

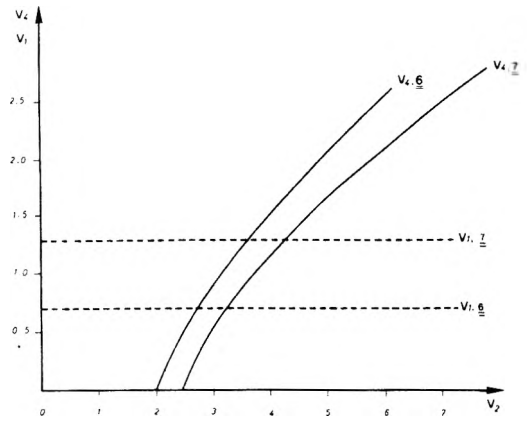

Figure 3. For compounds **6** and **7**, V_1 and V_4 values as a function of V_2 values which obtain the experimental $\langle\cos\phi\rangle$ and $\langle\cos^2\phi\rangle$.

It is clear that the "locked" conformation hypothesis (preceding paper) is only (a) a first approach to the problem raised in the second hypothesis of the present paper (very large V_2 and V_4 values); (b) an autocoherence test of the method as above recalled.

As a matter of fact the observed rotational frequencies[7] correspond to rather low internal rotation barriers, which allows us to consider the two hypothesis brought up in this paper.

As shown in Table I, the barriers heights are slightly modified (except for 3) when the V_4 term is taken into account. Therefore we may now compare these barriers.

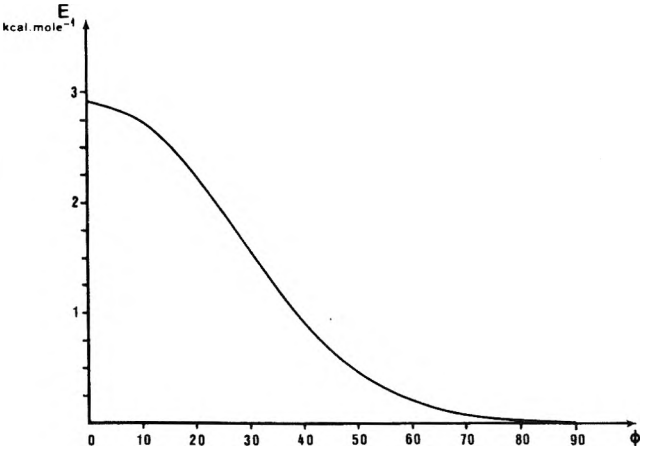

Figure 4. Calculated potential energy of C_6H_5–CH_2Cl as a function of the torsional angle ϕ.

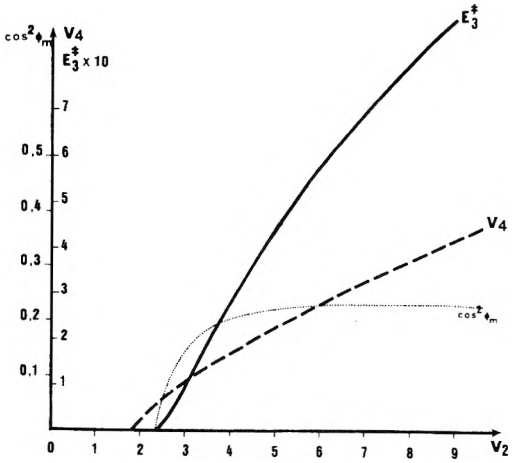

Figure 5. V_4, $E_3^{\ddagger}$, and $\cos^2\phi_m$ as a function of V_2; ϕ_m is the angle of minimal potential energy.

For compound 3, the relatively low value of $\langle\cos^2\phi\rangle$ leads to a potential barrier higher than the others and also, to a greater inaccuracy; this one may be responsible of $V_4 > V_2/4$ for a fair value of V_2.

A tight correlation raises between the barrier height $E_1^{\ddagger}$ and the Z group size for molecules **1–4**, **6**, and **7** (Table I). The $E_1^{\ddagger}$ relatively low value for **1** is related to the methyl rotation gear effect. The $E_1^{\ddagger}$ value of **5** and the $E_2^{\ddagger}$ value of **7** are quite smaller than the corresponding barriers of the nonsubstituted molecule **3**; this shows the part of the electron-withdrawing ring substituent. A similar observation about the neopentyl group rotation has been reported by Carter et al.[8]

Lastly, the experimental differences $E_1^{\ddagger} - E_2^{\ddagger}$ V_1 for **6** (0.7 kcal mol^{-1}) and for **7** (1.3 kcal mol^{-1}) are larger than the electrostatic energy (between C–Z and *m*-C–Cl dipoles) difference calculated (0.5 kcal mol^{-1}) for the two corresponding conformations ($\phi = 0°$ and $\phi = 180°$). These discrepancies, clearly show that other factors must be taken into account. For $\phi = 0°$ and $\phi = 180°$ at the energy barrier tops, a geometry modification (o-C–H bond in plane bending) may occur; it would be more difficult when a meta substituent is present ($\phi = 0°$); this buttressing effect would be very sensitive to the Z substituent size.

To agree with the spectroscopic study of Verdonck et al.[7] led us to the second hypothesis involving a secondary energy maximum for $\phi = 90°$. Our experimental results are consistent with this hypothesis as with the first one, *viz.* that they cannot lead to a choice between them. Nevertheless, for the second hypothesis, the corresponding energy barriers are rather high ($E^{\ddagger} > 4.2$ kcal mol^{-1} for **2**).

Molecular mechanics calculations are able to obtain an insight into the origin of the secondary energy barrier ($\phi = 90°$). For benzyl chloride **2**, the nonbonding interactions have been calculated as a function of ϕ. The chosen potential functions are those of a preceding paper in this series;[9] the atoms involved in the calculation are the carbons and hydrogens in the ortho positions and the chlorine and hydrogens in the benzylic position. The corresponding strain energy has been minimized with respect to the C_{Ar}–C–Cl angle. Other bonds angles and lengths are not allowed to change, so that the calculated energies are slightly overestimated. The calculated potential energy curve (Figure 4) has been expanded as a Fourier series limited to terms V_2 (2.9 kcal mol^{-1}) and V_4 (0.8 kcal mol^{-1}). These values lead to $\langle\cos^2\phi\rangle = 0.188$ in agreement with the experimental value (0.204). However the calculated potential energy curve does not show any maximum for $\phi = 90°$. So, the secondary energy barrier must be due to a factor neglected in the molecular mechanics calculations, as an electronic delocalization stabilizing the planar conformation ($\phi = 0°$) of the molecule.

Conclusion

This study has unambiguously shown that the main potential barrier corresponds to a coplanarity of the C–Z bond with the ring. For the series of molecules, significant changes of barrier heights have been observed and analyzed in terms of steric, electrostatic, and electronic effects.

Appendix I. Calculation of V_2(min) and $E_1^{\ddagger}$(min) Values and of the ϕ_m Range

Benzyl chloride **2** for which $\langle\cos^2\phi\rangle = 0.204$ is taken as an example. We have compiled a table of $\langle\cos^2\phi\rangle$ values for different V_2/RT and V_4/RT values (from 0 to 8). All the couples of these values leading to $\langle\cos^2\phi\rangle = 0.204$ are listed (Figure 5). From the corresponding graph of $E_3^{\ddagger} = f(V_2)$ (Figure 5), we obtain the minimal value of V_2 (3.9 kcal mol^{-1}) for the condition $E_3^{\ddagger} \geq 0.25$ kcal mol^{-1} which corresponds to $\cos^2(\phi_m) \geq 0.20$. As, for large values of V_2, $\cos^2(\phi_m) = 0.23$, we may deduce $0.20 \leq \cos^2(\phi_m) \leq 0.23$.

References and Notes

(1) Preceding paper in the series: M. Camail, A. Proutiere, and P. Verlaque, *J. Phys. Chem.*, preceding paper in this issue.
(2) J. B. Rowbotham, A. F. Janzen, J. Peeling, and T. Schaefer, *Can. J. Chem.*, **52**, 481 (1974).
(3) F. G. Brickwedde, M. Moskow, and R. B. Scott, *J. Chem. Phys.*, **13**, 547 (1945).
(4) This value may be underestimated as the rotational energy barrier of CH_3–CCl_3: 2.7 kcal mol^{-1} from thermodynamic studies against 5.7 kcal mol^{-1} from different more recent studies (cf. J. R. Durig, W. E. Bucy, and C. J. Wurrey, *J. Chem. Phys.*, **60**, 3293 (1974)).
(5) A. V. Cunliffe in "Internal Rotation in Molecules", W. J. Orville Thomas, Ed., Wiley, London, 1974.
(6) E. Durand, "Electrostatique", Vol. 1, Masson, Paris, 1964.
(7) L. Verdonck and G. P. Van Der Kelen, *Spectrochim. Acta Part A*, **28**, 51 (1972); L. Verdonck, G. P. Van Der Kelen, and Z. Eeckhaut, *ibid.*, **29**, 813 (1973).
(8) B. Nilson, P. Martinson, K. Olsson, and R. E. Carter, *J. Am. Chem. Soc.*, **95**, 5615 (1973).
(9) A. Goursot-Leray and H. Bodot, *Tetrahedron*, **27**, 2133 (1971).

Viscosities of Mixtures of Branched and Normal Alkanes with Tetrabutyltin. Effect of the Orientational Order of Long-Chain Alkanes on the Entropy of Mixing

Genevieve Delmas,* Patricia Purves, Pierre de Saint-Romain

Departement de chimie, Université du Quebec à Montréal, Montréal, Québec, Canada H36 3P8 *(Received August 1, 1974; Revised Manuscript Received April 11, 1975)*

Solution viscosities have been measured for the following systems: a spherical molecule liquid, $Sn(Bu)_4$, with 10 normal alkanes and 3 branched alkanes, 2,2,4-trimethylpentane (br-C_8), 2,2,4,4,6,6-pentamethylheptane (br-C_{12}), and 2,2,4,4,6,8,8-heptamethylnonane (br-C_{16}) at 25°; br-C_{12} + n-C_{12} at 25°; br-C_{16} + n-C_{16} at 18.5, 25, 35, 55, and 80°. The effect of orientational order of the long-chain alkanes on solution viscosities is investigated as well as the adequacy of free volume theories used to predict solution viscosities. $\Delta \ln \eta$ i.e., $\ln \eta_s - (x_1 \ln \eta_1 + x_2 \ln \eta_2)$ and $\delta = \Delta \ln \eta_{expt} - \Delta \ln \eta_{th}$ have been obtained. $\Delta \ln \eta_{th}$ is calculated from free volume theories and experimental heats of mixing. For systems with large differences of free volume, the prediction is correct to within 20–30%. For long linear alkanes of free volume similar to $Sn(Bu)_4$, δ is positive and large and is associated with ΔS for the disordering of the long-chain alkane. For branched alkanes, δ is negative and smaller than for the normal alkanes. For the br-C_{16} + n-C_{16} system, δ diminishes rapidly with increasing temperature as does the orientational order of n-C_{16} as shown from the heats of mixing.

Normal alkane mixtures seem to be suitable systems with which to test theories of nonpolar mixtures and their thermodynamic properties have been studied extensively for 40 years. Branched and normal alkanes might be expected to have similar thermodynamic behavior. However, recent work[1] on the heats of mixing of a globular molecule with a linear alkane and with its branched isomer has shown that these heats are very different (ΔH_M, $SnBu_4$ + n-C_{16} = 360 J mol^{-1}, ΔH_M, $SnBu_4$ + heptamethylnonane = −40.1 J mol^{-1}). These and other results involving similar systems[2] cannot be explained by recent theories of nonpolar solutions (Prigogine,[3] Patterson,[4] Flory[5]) which introduce a contribution to the excess thermodynamic properties arising from a difference in free volume between the composents. The new results may be explained if the liquid state of a long-chain normal alkane retains some of the orientational order characteristic of the solid state. On the other hand, little orientational order is found in a short-chain alkane or a liquid composed of globular molecules such as a branched alkane. When a long-normal alkane is mixed with a globular molecule liquid, its orientational order is destroyed, hence the relatively large endothermic heat. This hypothesis also explains the fact that the heats of mixing of a short and a long linear alkane are positive although the free volume theory predicts negative heats.[2]

Depolarized Rayleigh scattering results are in agreement with the presence of orientational order in higher n-alkanes. Bothorel and coworkers[6] find that if the alkane is long, the apparent optical anisotropy γ^2 is smaller in solution than in the pure state, and this difference defines a parameter, J, characterizing the orientational order:

$$J = \frac{\gamma^2(\text{pure})}{\gamma^2(\text{solution})} - 1$$

The disordering process of a long-chain alkane liquid by a spherical molecule must involve two terms, an enthalpy change and an increase in entropy. The aim of this work was to measure the viscosities of mixtures of molecules which had been studied by calorimetry and had shown a heat of disordering, and then to find indirectly a term corresponding to the entropy of disorder. This contribution to the viscosities due to the entropy of disorder should therefore be present for linear alkanes and absent for branched alkanes. This term was calculated by comparing the predicted and experimental viscosities of linear and branched alkanes.

Experimental results are given for the viscosities of 15 mixtures: tetrabutyltin ($SnBu_4$) in 10 normal alkanes (C_5 to C_{17}, except C_{11}, C_{13}, C_{15}) and in three branched alkanes: 2,2,4-trimethylpentane (br-C_8), 2,2,4,6,6-pentamethylheptane (br-C_{12}), 2,2,4,6,6,8,8-heptamethylnonane (br-C_{16}) at 25°. The following alkane systems were also studied: br-C_{12} + n-C_{12} at 25° and br-C_{16} + n-C_{16} at 18.5, 25, 35, 55, and 80°.

Experimental Section

Materials. These were of the same origin and purity as in ref 1.

Viscosities. The measurements were made in an Ubbelohde viscometer in a bath controlled to +0.008°. The temperature was measured by a Hewlett-Packard precision quartz thermometer.

The viscometers were calibrated and two constants C and B obtained using three reference liquids bought at the Cannon Instrument Co. (State College, Pa.). The dynamic viscosities in centipoise were obtained from the flow time t by the relation $\eta = (d_l - d_v)[Ct - (B/t)]$ where d_l and d_v are the densities of, respectively, the liquid and the vapor. However d_v could be neglected for all systems except those containing pentane and hexane. Depending on the concentration range, the solutions were made either by volumetric dilution in the viscometer or by weighing the two components separately.

The viscosities found for the alkane compared well with those in the literature. For n-C_{16} Heric and Brewer[7] quote a range of literature values between 3.03 and 3.10, their

own value being 3.062 while ours is 3.067 cP. For $SnBu_4$ and br-C_{16}, the viscosities and densities are found to be, respectively, 2.315 cP, 1.0408 g cm^{-3}; 3.333 cP, 0.7819 g cm^{-3} at 25°.

Excess Volumes. The densities of mixtures necessary to obtain the dynamic viscosities were measured with an Anton Paar precision density meter (Fisher Co.). They are published separately.[8]

Theory

Comparison of Calculated and Experimental Excess Viscosities. Theories establish a relation between the solution viscosity and either the activation energy required for the molecule to overcome the attractive forces of its neighbors and flow to a new position (absolute reaction rate theory) or the probability that an empty site exists near a molecule (free volume theory). Recent work has combined the absolute reaction rate and free volume theories. For comparison with experimental results, the activation energy is usually related to the more accessible free energy of mixing. The new theories of solutions[3-5] that take into account free volume give an expression for the free energy of mixing and the free volume contribution to the excess viscosity. The equation developed recently by Bloomfield and Dewan[9] is used:

$$\ln \eta - (x_1 \ln \eta_1 + x_2 \ln \eta_2) = -\frac{\Delta G_R}{RT} + \frac{1}{\tilde{v} - 1} - \left(\frac{x_1}{\tilde{v}_1 - 1} + \frac{x_2}{\tilde{v}_2 - 1}\right) \quad (1)$$

The left-hand side of eq 1 represents the excess viscosity, i.e., the viscosity of the solution minus an "ideal" viscosity. The right-hand side shows the two contributions to the excess viscosity, the residual free energy of mixing ΔG_R and the free volume contribution. Here $\tilde{v}$, $\tilde{v}_1$, and $\tilde{v}_2$ are, respectively, the reduced volume of the solution and of the two pure solvents; ΔG_R is the sum of ΔH_M, the heat of mixing, and of $T\Delta S_R$, the residual or noncombinatorial entropy. The experimental heats of mixing will be used for ΔH_M. $T\Delta S_R$, using the van der Waals model for the energy, is found to be[5,10]

$$\frac{\Delta S_R}{R} = 3c_1x_1 \ln \frac{\tilde{v}_1^{1/3} - 1}{\tilde{v}^{1/3} - 1} - 3c_2x_2 \ln \frac{\tilde{v}_2^{1/3} - 1}{\tilde{v}^{1/3} - 1} \quad (2)$$

where $c_i = \frac{1}{3}P_i^*V_i^*/RT_i^*$. P_i^*, V_i^*, and T_i^* are the pressure, volume, and temperature reducing parameters. The solution reduced volume is obtained according to a good approximation:

$$\tilde{v}^{-1} = x_1\tilde{v}_1^{-1}(U_1^*/U_m^*) + x_2\tilde{v}_2^{-1}(U_2^*/U_m^*) \quad (3)$$

details of which can be found in ref 10; $U^* = P^*V^*$, and $U_m^* = x_2U_2^* + x_2U_2^*$.

Equation 1 can be written

$$\Delta \ln \eta_{th} = -\frac{\Delta H_M}{RT} + \frac{\Delta S_R}{R} + f(\tilde{v}) = \ln \eta_H + \ln \eta_s + \ln \eta_v \quad (4)$$

where $\ln \eta_H$, $\ln \eta_s$, and $\ln \eta_v$ correspond, respectively, to $-\Delta H_M/RT$, $\Delta S_R/R$, and $f(\tilde{v})$. Comparison of eq 4 is made with the experimental quantity

$$\Delta \ln \eta_{expt} = \ln \eta - (x_1 \ln \eta_1 + x_2 \ln \eta_2) \quad (5)$$

Equation 5 defines an experimental value $\Delta \ln \eta_{expt}$ since η, η_1, and η_2 can be measured. The quantity $\Delta \ln \eta_{expt} - \Delta \ln \eta_{th}$ will be used to analyze the quality of the predictions of the theory and the possibility of a contribution of orientational disorder to the viscosity of the solutions.

Parameters for the Pure Components. P^*, V^*, and T^* can be obtained from α, the expansion coefficient, and γ, the thermal pressure coefficient of the pure components. The sources of these data are given in ref 1 and 2.

Results

Figure 1 shows $\Delta \ln \eta_{expt}$ for $SnBu_4$ with linear and branched alkanes at 25°, and Figure 2 uses the same expression for br-C_{12} + n-C_{12} at 25° and br-C_{16} + n-C_{16} at 18.5, 25, 35, 55, and 80°. $\Delta \ln \eta_{expt}$ has been fitted with the equation

$$\Delta \ln \eta_{expt} = x_1x_2[A_0 + A_1(x_1 - x_2) + A_2(x_1 - x_2)^2] \quad (6)$$

The first six columns of Table I give the three coefficients of eq 6, the standard deviation, the concentration of the maximum, and $\Delta \ln \eta_{expt}$ at that concentration. The next four columns show the different contributions in eq 4 and their sum, $\Delta \ln \eta_{th}$. The last column gives $\Delta \ln \eta_{expt} - \Delta \ln \eta_{th}$.

Discussion

Comparison of the different contributions to $\Delta \ln \eta_{th}$ in Table I shows that the systems can be classified in two different ways.

Systems with a Large Free Volume Difference. In the series from C_5 to C_{17}, the free volume difference changes from large to negligible as seen from $\ln \eta_v$ which goes from 0.362 to 0.0. The main contribution to $\Delta \ln \eta_{th}$ for alkanes up to C_9 results from the contraction on mixing which increases the solution viscosity. Since for these systems ΔH_M is small, one obtains

$$\Delta \ln \eta_{th} \simeq \Delta \ln \eta_v = \left[\frac{1}{\tilde{v}} - \left(\frac{x_1}{\tilde{v}_1} + \frac{x_2}{\tilde{v}_2}\right)\right] \quad (7)$$

The agreement is reasonably good for the lower alkanes since the predicted value is within 30% of the experimental value. The agreement of $\Delta \ln \eta_{expt}$ with eq 7 indicates that the solution free volume as expressed by eq 3 is reasonable as also shown by the good agreement between calculated and experimental V_E.[8] Since Bloomfield and Dewan analyzed systems with very small free volume differences ($\Delta \ln \eta_{expt} < 0.05$) it is not too surprising that their agreement between calculated and experimental values is very good. However, the systems $SnBu_4$ with the lower alkanes, involving liquids with large free volume differences, constitute a more severe test of the theory which appears to give quite reasonable results. It is also worth noticing that for large free volume differences, $\Delta \ln \eta_v$ and $\Delta \ln \eta_s$ do not cancel each other as was the case for systems of ref 9. $\Delta \ln \eta_v$ is always much larger in absolute value than $\Delta \ln \eta_s$. Br-C_8 + $SnBu_4$ is another system for which the prediction is within 30% of the experimental value even when using eq 7. It is perhaps surprising to find that the predicted values of $\Delta \ln \eta_{th}$ are too low, since previous work on free volume contributions to the heats of mixing of the same systems showed an overestimation of the free volume contribution to the heat for large free volume differences. It is also possible that the entropy contribution is overestimated by eq 2. Indeed one can see on the middle columns of Table I that the sum of $\ln \eta_H$ and $\ln \eta_v$ only is in better agreement with $\Delta \ln \eta_{expt}$, within 5%, than is the complete $\Delta \ln \eta_{th}$.

TABLE I: Experimental and Calculated Parameters Related to the Viscosities of the Four Series of Solutions: (I) $SnBu_4$ + Linear and Branched Alkanes, (II) br-C_{12} + n-C_{12}, (III) br-C_{16} + n-C_{16}, (IV) Literature Values

Systems (1) (2)	T, °C	A_0	A_1	A_2	σ,[d] $\times 10^3$	x_2	$\Delta \ln \eta_{expt}$ max	$\ln \eta_H$	$\ln \eta_v$	$\ln \eta_s$	$\Delta \ln \eta_{th}$	$\Delta \ln \eta_{expt} - \Delta \ln \eta_{th}$
n-C_5 + $SnBu_4$	25	1.61	−0.57	0.25	18	0.415	0.42	0.017	0.399	−0.092	0.323	0.097
n-C_6 + $SnBu_4$	25	1.15	0.30	−0.001	20	0.44	0.29	0.007	0.287	−0.065	0.229	0.061
n-C_7 + $SnBu_4$	25	0.831	−0.167	0.116	6	0.45	0.210	−0.004	0.212	−0.047	0.161	0.051
n-C_8 + $SnBu_4$	25	0.650	−0.113	−0.078	7	0.44	0.162	−0.018	0.159	−0.035	0.106	0.056
n-C_9 + $SnBu_4$	25	0.458	−0.096	−0.062	3.2	0.46	0.115	−0.033	0.116	−0.025	0.058	0.057
n-C_{10} + $SnBu_4$	25	0.358	0.003	0.030	2.3	0.52	0.09	−0.040	0.085	−0.020	0.025	0.065
n-C_{12} + $SnBu_4$	25	0.097	−0.025	−0.049	0.8	0.50	0.025	−0.075	0.038	−0.012	−0.049	0.074
n-C_{14} + $SnBu_4$	25	0.005	0.049	0.040	1.9	—	$\pm < 0.01$	−0.109	0.014	−0.008	−0.102	0.102
n-C_{16} + $SnBu_4$	25	−0.082	0.028	0.040	2.3	0.55	−0.022	−0.143	0.0006	−0.004	−0.146	0.124
n-C_{17} + $SnBu_4$	25	−0.073	0.004	0.008	0.7	0.61	−0.017	−0.158	−0.003	−0.003	−0.164	0.147
br-C_8 + $SnBu_4$	25	0.827	−0.203	0.123	6	0.45	0.210	0.012	0.195	−0.033	0.174	0.036
br-C_{12} + $SnBu_4$	25	0.212	0.009	0.027	1.6	0.52	0.052	0.012	0.060	−0.010	0.062	−0.010
br-C_{16} + $SnBu_4$	25	−0.245	0.039	0.013	1.3	0.47	−0.061	0.016	0.008	−0.0008	0.024	−0.088
n-C_{12} + br-C_{12}	25	−0.067	0.010	−0.06	2.1	0.50	−0.017	−0.053	−0.003	−0.0001	−0.056	0.039
n-C_{16} + br-C_{16}	18.5	−0.194	0.039	0.005	0.7	0.45	−0.049	−0.130	−0.010	−0.001	−0.141	0.092
n-C_{16} + br-C_{16}	25	−0.184	0.032	−0.004	1.0	0.45	−0.047	−0.109	−0.009	−0.001	−0.119	0.072
n-C_{16} + br-C_{16}	35	−0.151	−0.012	0.092	0.4	0.52	−0.044	−0.086	−0.009	−0.001	−0.096	0.052
n-C_{16} + br-C_{16}	55.4	−0.136	0.031	−0.013	0.8	0.45	−0.034	−0.052	−0.009	−0.001	−0.062	0.030
	80	−0.115	0.018	0.0007	3.7	0.53	−0.029	−0.026	−0.008	−0.0009	−0.035	0.006
n-C_{12} + n-C_6[a]	25					0.54	0.139	−0.015	0.116	−0.024	0.076	0.081
n-C_{14} + n-C_6[b]	25					0.56	0.196	−0.030	0.166	−0.032	0.101	0.095
n-C_{16} + n-C_6[b]	25					0.58	0.281	−0.042	0.223	−0.042	0.138	0.142
n-C_{16} + n-C_7[c]	25					0.51	0.234	−0.039	0.153	−0.026	0.088	0.146
n-C_{16} + CCl_4[b]	25					0.58	0.212	−0.238	0.177	−0.023	0.084	0.128
n-C_{16} + benzene[b]	25					0.54	0.153	−0.445	0.176	−0.021	−0.291	0.444

[a] Reference 11. [b] Reference 7. [c] Reference 12. [d] Standard deviation on experimental $\Delta \ln \eta$.

The fact that $\Delta \ln \eta_{expt} - \Delta \ln \eta_{th}$ goes through a minimum for C_8–C_9 is indicative of another effect for longer alkanes which we believe is associated with the orientational order in the normal alkanes.

Systems with a Small Free Volume Difference. For $SnBu_4$ with the longer normal alkanes or the branched alkanes, the main contribution to $\Delta \ln \eta$ comes from $\ln \eta_H$ since $\ln \eta_v$ and $\ln \eta_s$ are negligible, and therefore we obtain

$$\Delta \ln \eta_{th} \simeq -\Delta H_M/RT \qquad (8)$$

Linear Alkanes. For the systems with $SnBu_4$ + n-C_{12} to n-C_{17}, the excess viscosities are much less negative than calculated by eq 8. The difference between the experimental and calculated values increases regularly with the chain length, as seen in Figure 3, and could correspond to an inadequate calculation of the entropy of mixing. The theory in fact expresses only the change of entropy due to the free volume difference between the components. We associate $\Delta \ln \eta_{expt} - \Delta \ln \eta_{th}$ with an entropic effect $\Delta S(\text{disorder})/R$ arising from the break up of orientational order in the normal alkane in the mixing process. It would be interesting to see if other order breakers would give similar $\Delta S(\text{disorder})/R$ values as measured by excess viscosities. Therefore on the same graph, this difference for literature[11,12] systems is given where the order breaker is CCl_4, n-C_6, or n-C_7 instead of $SnBu_4$. One sees that the general trend of $\Delta S(\text{disorder})/R$ is the same whatever order breaker is used. For n-C_{16}, for instance, one finds $\Delta S(\text{disorder})/R$ equal to 0.144, 0.147, and 0.115 with n-C_6, n-C_7, and $SnBu_4$, respectively, as order breakers. With CCl_4 and benzene one finds much larger values 0.290 and 0.430 (not in Figure 3) which can come from CCl_4 being a better order breaker or from the disorientation of benzene itself.

$\Delta S(\text{Disorder})/R$ and the Correlation of Molecular Orientation Parameter J. According to Bothorel,[6] the correlation of molecular orientation parameter J for the normal alkanes is related to carbon atom number by the relation

$$J = 0.106n - 0.448 \qquad (9)$$

Figure 4 shows the relationship between J and $\Delta \ln \eta_{expt} - \Delta \ln \eta_{th} = \Delta S/R$. As the length of the alkane increases, the orientational order becomes larger as shown by the variation of J. Consequently, the mixing process gives a ΔS disorder which increases with the length of the alkane. It is possible that the high values of $\Delta \ln \eta_{expt} - \Delta \ln \eta_{th}$ found for the lower alkanes are due to an overestimation of the free volume term.

Hydrodynamic Contributions to $\Delta \ln \eta$. Dewan et al.[9b] have analyzed the results on intrinsic viscosities of the normal alkanes in benzene. They can predict intrinsic viscosities either from equations similar to eq 5 (I) or from continuum hydrodynamic calculation (II). They found that method II is adequate for chains longer than C_{25} while method I is good for alkanes shorter than C_{15}. For intermediate chain lengths a combination of the two methods gives good results. It is necessary to ask if in the present experiments, hydrodynamic effects could contribute to the increase of $\Delta \ln \eta_{expt} - \Delta \ln \eta_{th}$ with chain length. We think it is possible that part of the difference may be due to this contribution not accounted for by thermodynamic effects. However, this

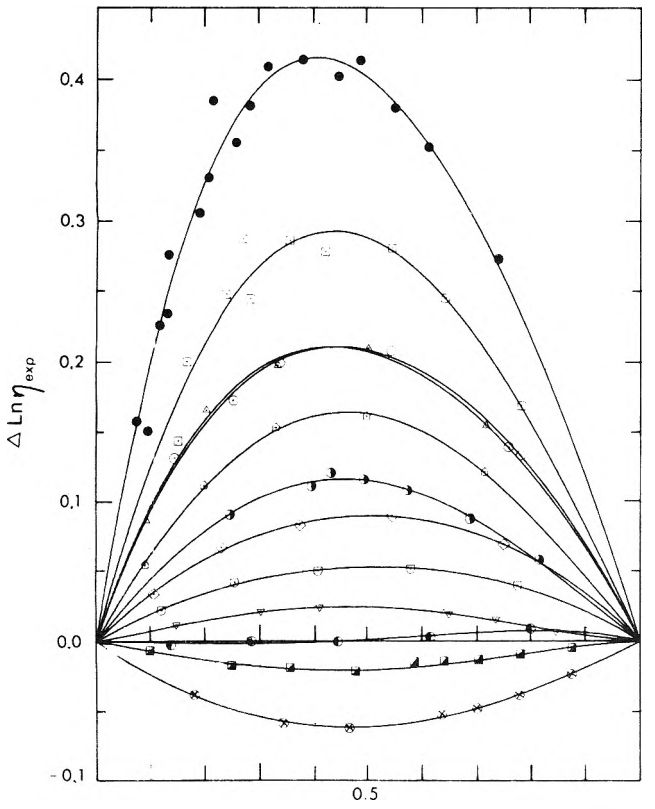

Figure 1. Δ ln η_{expt} for $SnBu_4$ with nine linear alkanes and three branched alkanes vs. the mole fraction of $SnBu_4$. The symbols are as follows; (●) n-C_5, (□) n-C_6, (⊙) n-C_7, (△) n-C_8, (◑) n-C_9, (◈) n-C_{10}, (▽) n-C_{12}, (◐) n-C_{14}, (◪) n-C_{16}, (▲) br-C_8, (⊡) br-C_{12}, (⊗) br-C_{16}.

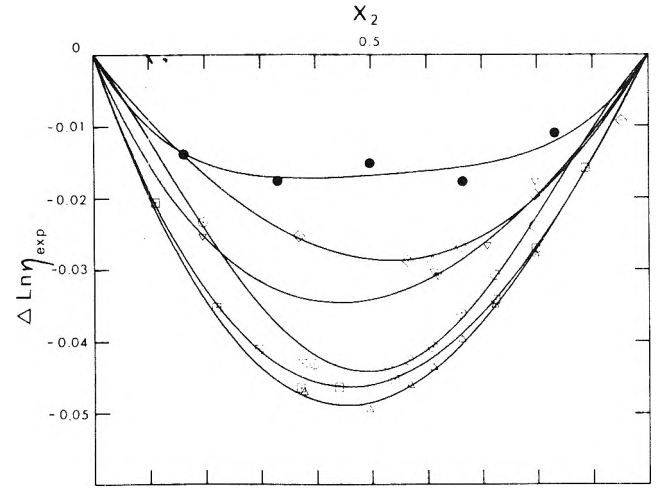

Figure 2. Δ ln η_{expt} vs. the mole fraction of the branched alkane, for branched and linear alkanes: (●) n-C_{12}–br-C_{12}, n-C_{16}–br-C_{16} at (△) 18.5, (□) 25, (⊙) 35, (▽) 55.4, (◈) 80°.

contribution should not be dominant since Δ ln η_{expt} − Δ ln η_{th} is of the other sign and smaller for an isomer of C_{16}, br-C_{16} for which one would expect hydrodynamic effects similar to those of n-C_{16}. It is perhaps not safe either to draw conclusions for solutions from results at an extremity of the concentration range as it is the case for $[\eta]$. Intrinsic viscosities must be a more severe test for the theory than solution viscosities. On the other hand, it is possible that somewhat different results for $[\eta]_{th}$ could be found from taking the experimental ΔH_M rather than a constant X_{12} parameter

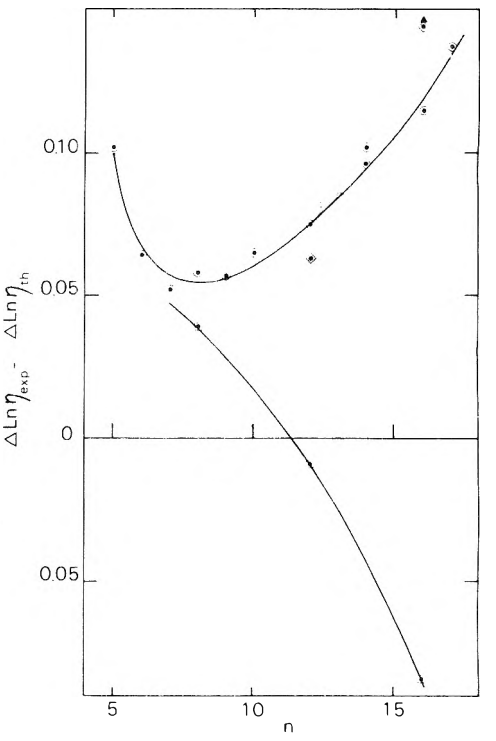

Figure 3. Δ ln η_{expt} − Δ ln η_{th} vs. the carbon number of the alkane for linear alkanes: (⊙) with $SnBu_4$ (this work), (◈) with C_6, (▲) with C_7 (literature values); for branched alkanes: (⊡) with $SnBu_4$.

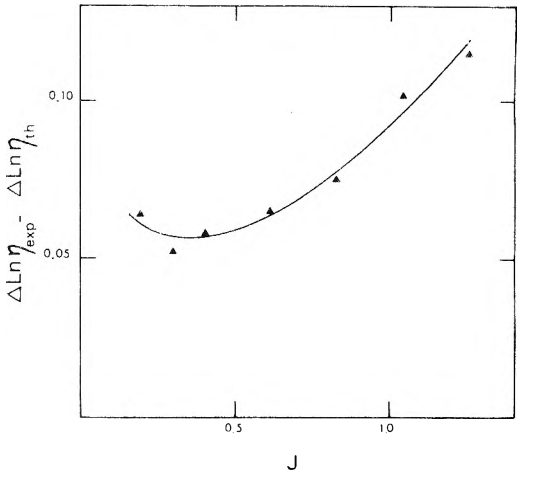

Figure 4. Δ ln η_{expt} − Δ ln η_{th} vs. J, the molecular orientation parameter of the normal alkanes (eq 9), for $SnBu_4$ in the alkanes.

for the series as was done in ref 9b. One can see in ref 1 and 2 that for rather similar systems X_{12} increases by a factor of 3 from C_6 to C_{16}.

Branched Alkanes + $SnBu_4$. Branched-C_8 and br-C_{12} correspond to the case where ln η_v is the main contributor, and the prediction relatively good. The system br-C_{16} + $SnBu_4$ should be a good test of eq 8 since the free volume effects are very small. The lower curves of Figure 3 show Δ ln η_{expt} − Δ ln η_{th} for the branched alkanes. One sees that for branched alkanes the trend of Δ ln η_{expt} − Δ ln η_{th} is reversed; it is diminishing with chain length instead of increasing as for linear alkanes. The same results have been found on the X_{12} parameter for the same two series (Figure 4 of ref 2). X_{12} was obtained from calorimetry and associ-

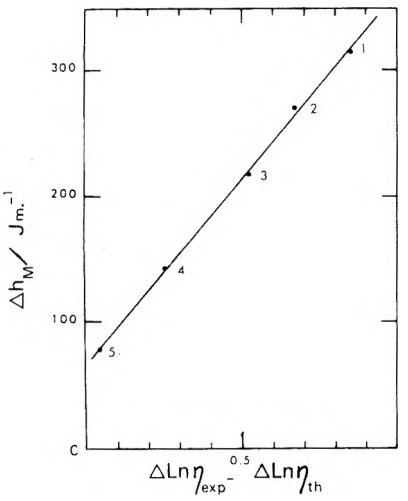

Figure 5. ΔH_M for the system br-C_{16} + n-C_{16} at different temperatures vs. $\Delta \ln \eta_{expt} - \Delta \ln \eta_{th}$: (1) 18.5, (2) 25, (3) 35, (4) 55.4, and (5) 80°.

ated with orientational order. The comparison of the viscosities of branched and linear alkane solutions seems to verify well the hypothesis of orientational order: [$\Delta \ln \eta_{expt} - \Delta \ln \eta_{th}$] is not very different, 0.058 and 0.039, for the two octanes because orientational order is not large for the linear octane. For the hexadecane, the two values of $\Delta \ln \eta_{expt} - \Delta \ln \eta_{th}$ are much more apart, 0.115 and −0.088, as the orientational order of the n-C_{16} has increased.

In the preceding discussion ΔS(disorder)/R was associated with $\Delta \ln \eta_{expt} - \Delta \ln \eta_{th}$ and was found to be 0.124 for n-C_{16}. It is possible that an equally valid choice for ΔS-(disorder) is the difference between $\Delta \ln \eta_{expt} - \Delta \ln \eta_{th}$ for the branched and the linear isomers. In this case, ΔS(disorder) is larger and equal to 0.124 + 0.0888 = 0.21. However, the heats and the volumes of mixing of the $SnBu_4$ + br-C_{16} are both more negative[1,8] than expected from the free volume differences. Thus it seems very likely that there is a specific effect of contraction or of good packing for the systems $SnBu_4$ + br-C_{16}. In this case 0.124 would be more reasonable for ΔS(disorder)/R. One would have expected the contraction for the system $SnBu_4$ + br-C_{16} to increase the viscosity although it appears to have reduced it.

The effect of branching and of packing in the liquid state on the pure liquid viscosity is not clear. Recent work[13] on the viscosity of pure isomers of hexane has shown that increased branching may increase the viscosity as well as diminish the density. Measurements of the viscosities and the densities made in this laboratory on seven C_8 isomers do not give a monotonous correlation between densities and viscosities. For this reason, one cannot be expected to predict the excess viscosities only from considerations of packing and changes of density. If the mixing process has changed the packing that one of the pure components had in the pure liquid state, the effect of this change on the solution viscosity is at present unpredictable.

One could speculate on the effect of flexibility on the packing in solution: due to the many side groups, br-C_{16} is a rigid molecule. When mixed with the more flexible molecule $SnBu_4$, it has the effect of diminishing the flexibility of $SnBu_4$, i.e., of diminishing the viscosity. For this reason, one finds that the values of V^E, ΔH_M, and $\Delta \ln \eta_{expt}$ are too negative. The reduction of free volume of the solution of $SnBu_4$ + br-C_{16} is not due only to the difference of expansion coefficients which is small but also to a specific effect of the shape of the molecules.

br-C_{16} + n-C_{16} System at Different Temperatures. This system is rather similar to the $SnBu_4$ + n-C_{16} system, with negligible difference in free volumes while $\ln \eta_H$ is the main contribution to $\Delta \ln \eta$; br-C_{16} acts as a order breaker for the n-C_{16}. In this system, there is also a positive contribution not accounted for by the theory which increases the viscosity and is associated with the orientational order in n-C_{16}. For this system ΔS(disorder)/R is 0.072 at 25° compared to 0.124 for $SnBu_4$ + n-C_{16}. The smaller value for br-C_{16} could be explained by the fact that br-C_{16} is not as good an order breaker as the spherical $SnBu_4$. When the temperature increases, the orientational order in n-C_{16} diminishes due to the thermal agitation. The fact that $\Delta \ln \eta_{expt} - \Delta \ln \eta_{th}$ diminishes from 0.092 to 0.00 between 18.5 and 80° seems to be adequate evidence that this difference is related to the entropy of disordering. Figure 5 shows the correlation of ΔH_M[14] with $\Delta \ln \eta_{expt} - \Delta \ln \eta_{th}$ at different temperatures. It is interesting to note that $\Delta \ln \eta_{expt} - \Delta \ln \eta_{th}$ diminishes quickly between 25 and 55° and more slowly at higher temperature in a manner similar to ΔH_M.

Acknowledgments. This work was made possible through the France Québec collaboration, the Ministère de l'Education, and the National Research Council of Canada.

References and Notes

(1) G. Delmas and S. Turrell, *J. Chem. Soc., Faraday Trans. 1*, **70**, 572 (1974).
(2) P. Tancrede, L. V. Lam, P. Picker, and D. Patterson, *J. Chem. Soc., Faraday Trans. 1*, **70**, 1465 (1974).
(3) I. Prigogine with A. Bellemans and V. Mathot, "The Molecular Theory of Solutions", North Holland, Amsterdam, and Interscience, New York, N.Y., 1957.
(4) D. Patterson, *Rubber Rev.*, **4**, 1 (1967).
(5) P. J. Flory and A. Abe, *J. Am. Chem. Soc.*, **86**, 3563 (1964).
(6) (a) P. Bothorel, *J. Colloid Sci.*, **27**, 529 (1968); (b) P. Bothorel, C. Clement, and P. Maraval, *C. R. Acad. Sci.*, **264**, 568 (1967); (c) P. Bothorel and G. Fourche, *J. Chem. Soc., Faraday Trans. 2*, **69**, 411 (1973); (d) P. Bothorel, C. Such, and C. Clement, *J. Chim. Phys.*, **10**, 516 (1972); (e) H. Quinones and P. Bothorel, *C. R. Acad. Sci.*, **277**, 133 (1973).
(7) E. L. Heric and J. G. Brewer, *J. Chem. Eng. Data*, **12**, 4, 574 (1967).
(8) G. Delmas, P. de St-Romain, and P. Purves, *J. Chem. Soc., Faraday Trans. 1*, **71**, 1181 (1975).
(9) (a) V. A. Bloomfield and R. K. Dewan, *J. Phys. Chem.*, **75**, 3113 (1971); (b) R. K. Dewan, V. A. Bloomfield, and P. B. Berget, *ibid.*, **75**, 3120 (1971).
(10) G. Delmas and D. Patterson, *Discuss. Faraday Soc.*, **49**, 98 (1970).
(11) E. Meeussen, C. Debeuf, and P. Huyskens, *Bull. Soc. Chim. Belg.*, **76**, 147 (1967).
(12) T. A. Bak and K. Anderson, *Acta Chem. Scand.*, **12**, 1367 (1958).
(13) L. D. Eicher and B. J. Zwolinski, *J. Phys. Chem.*, **76**, 3295 (1972).
(14) M. Croucher and D. Patterson, *J. Chem. Soc., Faraday Trans. 2*, **70**, 1479 (1974).

Low Temperature Chemisorption of Molecular Nitrogen on Platinum

E. F. Rissmann* and J. M. Parry

Tyco Laboratories Incorporated, Waltham, Massachusetts 02154 *(Received March 17, 1975)*

The low temperature chemisorption of nitrogen on high surface area platinum samples was investigated by volumetric gas adsorption methods. The extent of this phenomenon was found to depend sensitively on the sample preparation procedures. Chemisorption of nitrogen, apparently, only occurs on clean platinum surfaces. The heat of adsorption was found to be 4.3 kcal/mol. The results have been compared with data from various infrared spectroscopic studies of this system. Good agreement was found.

Introduction

A number of years ago, in a short publication we presented some preliminary evidence for the low temperature chemisorption of molecular nitrogen on high surface area unsupported platinum samples.[1] We shall now discuss this phenomenon in more detail.

At the time of our original publication, the only work reported on the nitrogen–platinum system was an infrared study by Van Hardeveld and Van Montfoort[2] in which a band, observed at 2230 cm^{-1}, for nitrogen adsorbed on alumina supported samples was attributed to a physical adsorption effect occurring only on certain sites. Recently, Egerton and Sheppard[3] have performed a similar study with silica supported samples and have presented a considerable amount of evidence favoring weak chemisorption of nitrogen on sites which are sensitive to contamination and possibly also to thermal effects. We now present our study to show agreement between two different methods of investigation.

Our method is based on the fact that if physical adsorption of nitrogen alone occurs, once correct molecular areas have been chosen, there should be no consistent differences between BET surface area measurements obtained with either argon or nitrogen on clean platinum. If chemisorption is occurring, however, the obtaining of both argon and nitrogen isotherm data should reveal the presence of excess nitrogen to variable extents. The amount of this excess material should be sensitive to sample preparation methods and the excess gas should be more strongly held to the surface than the physically adsorbed species.

Also, if the same species are present at low and at near ambient temperatures, the heats of adsorption from our data and the infrared work should agree.

Experimental Section

A volumetric gas adsorption apparatus with a two stage mercury diffusion pump was used. The system could be readily evacuated at 10^{-6} to 10^{-7} Torr and had a working volume of about 130 cc.[4] Pressures were measured with a manometer constructed of precision bore tubing and read with a cathetometer to 0.01 mm. Liquid nitrogen and gold foil traps in series served to protect the samples and working volume of the apparatus from contamination with mercury vapors from the manometer.

The nitrogen, hydrogen, helium, and argon used were obtained in 1-l. Pyrex flasks from Airco. The nitrogen contained between 3 and 10 ppm argon; the hydrogen contained a few ppm nitrogen; the helium contained similar small amounts of neon; and the argon contained about 10 ppm nitrogen. Both commercial platinum black (Englehard) and samples produced by reaction of chloroplatinic acid with formaldehyde[5] were studied. In the latter case, samples were dried and stored in air for several days prior to use to remove any carbon monoxide present.

The pretreatment procedure for the platinum samples involved several critical steps. The platinum blacks were first outgassed in vacuo at 80° for several hours to remove weakly adsorbed materials. They were then cooled to either 0 or −80°, and treated with hydrogen. Here, the samples were first exposed to ca. 10 Torr of gas and the gas pressure slowly increased stepwise until a final pressure of ca. 200 Torr was obtained. The blacks were left at temperature for several hours, with a few replacements of hydrogen, and were then warmed over a few hours to room temperature in hydrogen to complete the reaction. The samples were then heated to a temperature in the 70–125° range and outgassed prior to commencement of measurements.

In determining the outgassing times to be used, preliminary experiments were run to examine the effect of such times on the extents of nitrogen chemisorption observed for several individual samples. At 70°, the amount of nitrogen chemisorption was found to level off with outgassing time after about 12 hr. Accordingly, a 16-hr time generally was employed. At 125°, no further increases were seen after 2 hr. Hence, a 3-hr time was selected.

In these experiments, the samples were all of the commercial material. They were hydrogen treated at −80° as described earlier and then outgassed for fixed periods at the temperature under study. At intervals, the outgassing was interrupted and nitrogen and argon isotherms were run at −195°. The outgassing was then resumed. At 70° little sintering was encountered, but at 125° some was seen. Also, for samples fully outgassed at 70°, subsequent 125° outgassing produced no additional nitrogen sites. In this work, the cross sectional areas used for nitrogen and argon were 16.2 and 14.6 $Å^2$, respectively.

Results

A. Comparative Nitrogen and Argon BET Measurements. The accuracy and reliability of the measurements were first established by replicate measurements with nitrogen and argon of the surface areas of commercial silica, titania, and untreated platinum black. The results are listed in Table I.

As can be seen, the same nitrogen to argon ratios of the

* Address correspondence to this author at 54 Parker St., Watertown, Mass. 02172.

TABLE I: Nitrogen Chemisorption on Platinum

Sample	Surface area,[a] m^2/g		Ratio N_2/Ar	Corr ratio[b]	Ratio surface area after cleaning to initial surface area
	N_2	Ar			
TiO_2	5.28	4.83	1.076	1.00	
	5.28	4.83			
	5.27	4.85			
SiO_2	24.4	22.6	1.074	1.00	
	24.3	22.6			
Pt black oxygenated	29.66	27.83	1.067	1.00	
Pt black commercial clean no. 1	30.1	21.0	1.43	1.34	0.81
73-48	29.0	26.2	1.11	1.045	0.89
73-51	21.0	14.9	1.39	1.30	0.75
73-45	32.7	25.0	1.28	1.19	0.93
73-57	20.8	14.9	1.38	1.28	0.70
73-57	21.1	15.0	1.39	1.29	0.70
Pt black commercial clean no. 2	10.21	7.68	1.32	1.23	0.29
73-99	20.61	18.19	1.14	1.07	0.68

[a] Cross sectional areas used for N_2 and Ar were 16.2 and 14.6 $Å^2$, respectively. [b] Assuming ratio for TiO_2 and SiO_2 should be 1.00.

TABLE II: Preparation Conditions for Platinum Samples[a]

Sample	
Pt black commercial no. 1	H_2 treatment at −80°, then at 20°, evacuation at 70° for 16 hr
73-48	H_2 treatment at −80°, then at 20°, evacuation at 70° for 16 hr
73-51	H_2 treatment at −80°, then at 20°, evacuation at 80° for 16 hr
73-45	H_2 treatment at −80°, then at 20°, evacuation at 70° for 16 hr
73-57	H_2 treatment at −80°, then at 20°, evacuation at 80° for 16 hr
Pt black commercial no. 2	H_2 treatment at 0°, then at 20°, evacuation at 125° for 3 hr
73-99	H_2 treatment at 0°, then at 20°, evacuation at 125° for 3 hr

[a] The general preparative procedure for these samples is presented in J. Giner, J. M. Parry, and S. M. Smith, *Adv. Chem. Ser.*, No. 90, pp 151-161 (1969). The specific differences between our samples was that for samples 73-45, 73-99, 73-51, and 73-57 decreasing percentages of the total solutions were used in the prenucleation step. Sample 73-48 was produced under the same conditions as 73-45 using a lower chloroplatinic acid concentration. All samples were washed, dried, and air stored prior to use. For more details see ref 5.

surface areas were obtained for these materials. Therefore, the amount of chemisorption may be expressed in terms of the ratios of the differences between the N_2 and Ar values to the Ar values of the surface areas. Here, a small correction must first be made so that the N_2 to Ar ratios of the surface areas of silica, titania, and untreated platinum black are unity. This correction compensates for a poor initial choice of the argon molecular area.

B. Sintering and Surface Cleanliness Considerations. The extents of nitrogen chemisorption on several of the cleaned platinum blacks are also listed in Table I. The detailed preparation and pretreatment conditions for these cleaned samples are given in Table II. Comparison of the data in these two tables suggested that the nitrogen sites may be fairly sensitive to sintering.

To prove this point, a series of samples was prepared from the commercial material using a variety of hydrogen treatments at lower temperatures and followed in all cases by outgassing at 70°. The results are given in Table III. As can be seen, there is apparently a preferential sintering of the nitrogen active sites. For the other cleaned blacks, more drastic hydrogen treatment and outgassing conditions also led to increased sintering and lower concentrations of nitrogen active sites.

Studies were also made of the thermal sintering of the blacks to elucidate differences between surface area losses occurring in the presence of reacting adsorbates and those taking place at higher temperatures on clean surfaces. For this series of experiments, a number of samples were prepared from the commercial material by hydrogen treatment at −80°. Care was taken in each case to minimize sintering by slowly raising the sample temperature in the presence of hydrogen to 0° over a 16-hr interval. The results are listed in Table IV.

Comparison of the data for the samples outgassed at 155° shows that, while the surfaces are rapidly activated for nitrogen adsorption at this temperature, there is also significant sintering and subsequent loss of the nitrogen sites. Examination of the data for samples 1 and 6 reveals that, at 70°, long outgassing periods are required to obtain maximum nitrogen coverages and that, for fully outgassed samples, further evacuation at higher temperatures does not lead to increased nitrogen coverages.

All of the data in Table IV suggest that the nitrogen sites are sensitive to sintering and that the appearance of the nitrogen sites as a function of outgassing times is related to the desorption of some species (hydrogen or water vapor).

Also, in further studies, reexposure to oxygen after the nitrogen experiments did not result in any measurable loss of surface area. This indicated that little, if any, hydrogen remained on the samples. On the oxygen covered blacks, the nitrogen and corrected argon BET values agreed.

C. Characterization of the Adsorbed Nitrogen. On some of the samples studied, determinations were made of the

TABLE III: Effect of Sintering on N_2 Chemisorption on Platinum (Commercial)

Ratio surface area (clean sample) to initial surface area	Corrected ratio[a] N_2/Ar
0.86	1.34
0.81	1.34
0.70	1.27
0.46	1.22
0.29	1.23
0.19	1.02
0.18	1.08

[a] Same definition as used in Table I.

TABLE IV: Effects of Vacuum Sintering On Nitrogen Chemisorption

Sample	Pretreatment conditions (temp time)	Surface area (Ar), m^2/g	Ratio of initial surface area to surface area after cleaning and outgassing	Nitrogen coverage [$\theta = (N_2/Ar) - 1$]
1	70°, 1 hr	25.3	0.96	0.03
	70°, 16 hr	25.25	0.96	0.38
	70°, 18 hr	25.3	0.96	0.38
2	155°, 0.5 hr	17.80	0.68	0.13
3	155°, 1.5 hr	10.96	0.42	0.05
4	155°, 3 hr	7.14	0.27	0.02
5	125°, 1 hr	20.1	0.77	0.13
	3 hr	19.50	0.75	0.25
	5 hr	19.10	0.73	0.23
6	70°, 16 hr	22.4	0.86	0.34
	plus 2 hr at 125°	21.6	0.83	0.32

[a] Corrected argon values were used here.

amounts of nitrogen and argon adsorbed at −80°. In no case was any uptake of argon observed. From the results at −195 and −80° calculations of the heat of adsorption were made. A value of 4.3 kcal/mol was obtained.

One further series of experiments was performed on a few of the blacks studied. In these runs, the argon surface area was first measured. An initial nitrogen determination was then made and the samples were then evacuated at 10^{-6} Torr and −195° for 30 min. A second nitrogen run was then conducted. In all cases, the surface area obtained on the second nitrogen run agreed well with the corrected argon value.

The more tightly held nitrogen is removable by evacuation at higher temperatures (−80 and 0°).

In a rigorous sense, this direct approach taken with the above data is expected to be valid only if nitrogen physically adsorbs on both platinum and on chemisorbed nitrogen with approximately the same heat of adsorption. An a posteriori justification for this approach is the strict linearities of the N_2 BET plots obtained.

Discussion

A. Comparison of Results. Our results can now be compared with the work of Egerton and Sheppard.[3] In that work, the infrared active adsorbed nitrogen was found to have a heat of adsorption of 3.6 kcal/mol and to be very sensitive to pretreatment conditions. Nitrogen adsorption, it was also found, could be prevented by preadsorption of either oxygen, carbon monoxide, or hydrogen. Our results, which show a heat of adsorption of 4.3 kcal/mol and a similar sensitivity to pretreatment and to preadsorbed hydrogen and oxygen are in close agreement. Also, our data indicate that at least part of the problems encountered by these workers can be traced to preferential sintering effects.

Egerton and Sheppard, in an analysis of a variety of infrared data on nitrogen adsorption on platinum, iridium, palladium, and nickel, found that all of the results obtained are consistent with weak chemisorption but not with interpretations favoring selective physical adsorption. Indeed, our results are exactly what is to be expected if weak chemisorption is occurring.

Another comparison may be made with the infrared studies of Harrod, Roberts, and Rissmann[6] of oxidation of carbon monoxide on evaporated platinum films. In that work, it was found that samples exhibiting extensive ir bands for adsorbed CO at frequencies below 1800 cm^{-1} were more reactive toward oxygen than those without such bands in this region. It was concluded that the more reactive sites, which were present on the less stable crystal planes, were either sintered or were irreversibly poisoned by oxygen. The fact that our nitrogen sites are preferentially sintered and can be cleaned of adsorbed oxygen at lower temperatures suggests that our sites are the same as those responsible for the infrared bands with adsorbed CO in the 1800-cm^{-1} region. Such a correlation already exists in the case of nickel.[7,8]

Also, Somorjai and coworkers[9] have found that the high index planes of platinum are more reactive than either the 100 or 111 planes for a variety of adsorption processes and simple reactions including the dissociation of oxygen, hydrogen, and several hydrocarbon species.

B. Surface Cleanliness Considerations. Recently, field emission studies by Nieuwenhuys and Sachtler[10] have shown that nitrogen is adsorbed at very low pressures on clean platinum at 80°K. These authors also observed a heat of adsorption of ca. 5 kcal/mol and, in some evaporated film work, noted preferential sintering effects similar to those reported here.

Norton and Richards,[11] using flash desorption methods, have shown that hydrogen rapidly desorbs from platinum at about 150°. The 110 and higher index planes were found to be responsible for most of the desorption at this temperature. Our results showed a rapid desorption of some species covering the nitrogen active sites at 155°. Taken together, these two sets of data suggest that hydrogen desorption was being directly determined in some of our nitrogen coverage vs. outgassing time studies.

This suggests that our platinum surfaces were substantially clean. Indeed, in this study and in the work of Egerton and Sheppard,[3] hydrogen has been found to poison the sites responsible for the nitrogen adsorption.

Several of our samples were prepared from reaction of formaldehyde with chloroplatinic acid and then air stored for several days. Data available on carbon monoxide oxidation[6] strongly indicates that this procedure should have been effective for removal of any carbon monoxide initially present.

The thermal desorption of hydrogen from platinum in

the 70–155° range requires some further discussion. From infrared data[12] two forms are known. One, H_α, desorbs rapidly above ca. 50°. The other, H_B, is apparently that corresponding to the 150° flash desorption peaks.[11] In our case, hydrogen desorbed rapidly at 155° and slowly at 70–150° (or rather the nitrogen sites appeared as a function of desorption temperature in that manner). The times in our experiments increased with falling temperature in a manner too slow to suggest a direct desorption process (a rate difference of ca. 10^2/50° in that range would be expected.) This suggests that, at these temperatures, the following occurs:

$$H_\alpha \rightarrow H_2 \text{ gas} \quad \text{fast } (T > 50°) \tag{1}$$

$$H_B \rightarrow H_\alpha \quad \text{slow} \tag{2}$$

$$H_\alpha \rightarrow H_2 \text{ gas} \quad \text{fast} \tag{3}$$

From our data, an activation energy of <10 kcal/mol is seen, which is in the range expected for a surface diffusion process.

One further point may be made with regard to our sample pretreatment procedures. One might question whether evacuation at ca. 10^{-6} Torr was sufficient to remove all of the adsorbed hydrogen prior to the nitrogen measurements. Here, our findings that, for fully outgassed samples, there were no surface area losses on reexposure to oxygen at room temperature and that, for similar samples, further evacuation at higher temperatures produced no additional nitrogen sites strongly suggest that most, if not all, of the hydrogen was removed by our outgassing procedures. Recent studies of the hydrogen–platinum system[11,13] support our contentions that the nitrogen active sites should have been free of hydrogen under our experimental conditions. Indeed, the hypothesis of clean nitrogen adsorption sites is probably the only simple self-consistent explanation for the observed effects of outgassing conditions on nitrogen coverages obtained.

C. Nature of the Nitrogen Sites. Egerton and Sheppard[3] observed two infrared bands for the platinum–nitrogen system. The first, at 2230 cm^{-1}, appeared on all samples, while the second, at 2242 cm^{-1}, was present only as a weak shoulder in certain cases. This implies that the sites responsible for the latter band are the less stable. If one assumes that nitrogen chemisorbs on the 110 and high index planes of platinum, then the 2230-cm^{-1} band should be due to sites on $1\bar{1}0$. The 2242-cm^{-1} band should be due to high index plane sites, which are also responsible for infrared bands for adsorbed CO at frequencies below 1800 cm^{-1}.

Here, examination of published spectra[6,14] of adsorbed CO on platinum in the 1800-cm^{-1} region shows that the broad band in this region is assymetric, tailing off less sharply toward lower frequencies. This may be interpreted in terms of two heavily overlapping bands, one with a maximum at ca. 1800 cm^{-1}, and the other with a weaker maximum at somewhat lower frequencies.

If the above argument is valid, one would expect, from the work of Somorjai et al.,[9] to find evidence of more extensive dissociation of hydrocarbons on preparations which produced the 2242-cm^{-1} band in the work of Egerton and Sheppard.[3] This has been observed.[15]

The preceding arguments have made extensive use of the known thermal stabilities of different crystal plane surfaces. A mathematical model treating these matters already exists.[16]

Conclusions

Using the volumetric method, evidence has been obtained favoring the chemisorption of molecular nitrogen on platinum. The data obtained agree well with that developed by other methods.

Acknowledgments. This work was supported by the U.S. Army Engineer Research and Development Laboratories, Fort Belvoir, Va., under Contract No. DAAE 15-67-C-0048 and by the Air Force Cambridge Research Laboratories, Office of Aerospace Research, Bedford, Mass., under Contract No. AF 19(628)-5549. We also wish to extend our appreciation to Professor N. Sheppard, F.R.S., for many fruitful discussions of these matters.

References and Notes

(1) J. M. Parry and E. F. Rissmann, *J. Phys. Chem.*, **71**, 3362 (1967).
(2) R. Van Hardeveld and A. Van Montfoort, *Surface Sci.*, **4**, 396 (1966).
(3) T. A. Egerton and N. Sheppard, *J. Chem. Soc., Faraday Trans. 1*, **70**, 1357 (1974).
(4) J. Giner and E. Rissmann, *J. Catal.*, **9**, 115 (1967).
(5) J. Giner, J. M. Parry, and S. M. Smith, ECS Meeting, Dallas, Tex., May 1967, Extended Abstracts, Vol. 3, p 40.
(6) J. F. Harrod, R. W. Roberts, and E. F. Rissmann, *J. Phys. Chem.*, **71**, 343 (1967).
(7) R. Van Hardeveld and F. Hartog, *Proc. Int. Cong. Catal., 4th*, **No. 70** (1968).
(8) A. M. Bradshaw and J. Pritchard, *Surface Sci.*, **19**, 198 (1970).
(9) G. A. Somorjai, R. W. Joyner, and B. Lang, *Proc. R. Soc., Ser. A*, **331**, 335 (1972).
(10) B. E. Nieuwenhuys and W. M. H. Sachtler, *Surface Sci.*, **34**, 317 (1973).
(11) P. R. Norton and P. J. Richards, *Surface Sci.*, **44**, 129 (1974).
(12) L. H. Little, "Infrared Spectra of Adsorbed Species", Academic Press, London, 1966, p 90.
(13) L. T. Dixon, R. Barth, and J. W. Gryder, *J. Catal.*, **37**, 368, 376 (1975).
(14) R. P. Eischens and W. A. Pliskin, *Adv. Catal.*, **10**, 1 (1958).
(15) T. A. Egerton and N. Sheppard, private communication.
(16) L. D. Landau and E. M. Lifshitz, "Statistical Physics", Pergamon Press, London, 1958, p 460.

On the Intercalation of Ammonia into Tantalum Disulfide[1]

Martin Dines* and Ricardo Levy

Exxon Research and Engineering Company, Linden, New Jersey 07036 *(Received June 4, 1975)*

Publication costs assisted by Exxon Research and Engineering Company

In an effort directed toward a more thorough comprehension of the process of intercalation of Lewis-base guests into the layered transition metal dichalcogenides, we studied the gas–solid reaction of ammonia and tantalum disulfide. The uptake and desorption were followed gravimetrically. Isotherms for $(NH_3)_xTaS_2$ between 308 and 353°K and $0.65 < x < 0.85$ did not show hysteresis. In this concentration range, the variation of composition with temperature at constant NH_3 pressure (1 atm) shows the presence of a simple homogeneous phase. This is confirmed by X-ray diffraction. Deintercalation below $x \sim 0.65$ leads to the formation of a second-stage compound. In the single phase region, the isosteric enthalpy of intercalation increases with increasing ammonia content. This suggests strong interaction between intercalated molecules and a structure having the C_3 axis of the guest parallel to the layer planes.

Introduction

Intercalation refers to the process of two-dimensional inclusion of a guest species between the composite sheets of a lamellar host. Generally, the driving force for such a reaction is attributed to the interaction between guest and host, which overcomes the relatively weak interlayer forces of the host. The nature of this bonding may be covalent, ionic, or even van der Waals. Graphite is often cited as an example of an "amphoteric" host capable of interaction with a broad spectrum of electron donors or acceptors. This interaction may be viewed as a localized phenomenon or as involving the energy bands of the host, but in either case, the results are the same—namely, that in the product, both guest and host experience some degree of perturbation of their geometrical and electronic structure to minimize energy.

Many of the transition metal dichalcogenides belong to a class of lamellar hosts capable of intercalating only Lewis base or electron-donating species (such as alkali metals). This behavior is attributed to the population and energy of the bands of the solid.[2a] Despite the substantial attention recently paid to these compounds and the materials resulting from their intercalation, there is a lack of information on the details of the intercalation process itself.

We have investigated as a prototypical case the system ammonia–tantalum disulfide, and examined in some detail the pattern of their interaction. We chose this particular system because the starting materials are relatively simple, well characterized, and they react under ambient conditions at rates which are easily followed by conventional vacuum system techniques. Furthermore, the product has been examined in parallel investigations using solid-state NMR[2b] and X-ray and neutron diffraction.[3]

In this study we looked at the kinetics and thermodynamics of intercalation by gravimetric absorption, thermal gravimetric analysis, differential scanning calorimetry, and X-ray diffraction. Particular emphasis was placed on the phase behavior of $(NH_3)_x$–TaS_2 in the regime $0.5 < x < 1.0$.

Experimental Section

2H-Tantalum disulfide was prepared from the elements by a slow cooling technique from 1173°K.[4] The samples were sieved through a 100 mesh screen, and had a BET surface area of 0.1 to 0.2 $m^2\ g^{-1}$. The ammonia was obtained from Matheson Corp. (Anhydrous) and was of 99.99% purity. Prior to use, it was distilled from sodium.

The NH_3 uptake was followed gravimetrically using a Cahn microbalance enclosed in a glass vacuum manifold connected to mechanical and oil diffusion pumps. Pressure was read by a calibrated Baratron gauge.

Thermogravimetry and differential scanning calorimetry were performed on a Dupont 900 instrument. Heating rates of 10°/min were employed, and argon or ammonia was the carrier gas, run at atmospheric pressure.

X-Ray patterns were obtained on a Phillips powder diffractometer using Ni-filtered Cu Kα radiation.

Results and Discussion

A. Uptake and Deintercalation Experiments. The uptake of ammonia at 298°K and 1 atm is shown in Figure 1. Fresh TaS_2 exhibits a sigmoidal uptake curve with no observable breaks. However, a threshold pressure of ca. 700 Torr was found, below which intercalation could not be detected. This observation, coupled with the relatively slow initial rate seen in the uptake suggests a nucleation process. The NH_3 uptake of previously deintercalated tantalum disulfide, on the other hand, does not show either a slow initial rate or threshold pressure. The nucleation is, therefore, related to the initial cleaving of the tantalum disulfide planes. In either case, absorption of ammonia proceeds until approximately one molecule of guest is included per formula unit of host. At 1 atm ammonia pressure and room temperature, this saturation value actually occurs at about 0.95 ammonias per tantalum disulfide.

Pumping on the fully intercalated product at room temperature resulted in rapid loss in weight, which soon levels (although never truly asymptotically) at a value of composition of nearly one-half the initial total weight gain (Figure 1). This composition, $(NH_3)_{\sim 0.5}TaS_2$, was shown via X-ray powder diffraction (Figure 2) to be a second-stage compound. In such a compound the intercalated ammonia occupies every other van der Waals space in the layered structure. Although not previously seen in the case of TaS_2–NH_3, such second-staged compounds are well known in the chemistry of graphite, and have also been reported in the

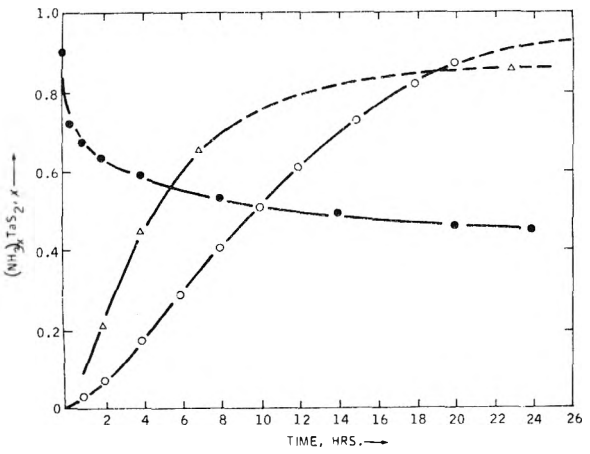

Figure 1. Uptake and deintercalation of ammonia by tantalum disulfide at STP. Open circles are initial uptake, closed circles are deintercalation at ca. 10^{-4} Torr. Triangles refer to the uptake of a previously deintercalated sample.

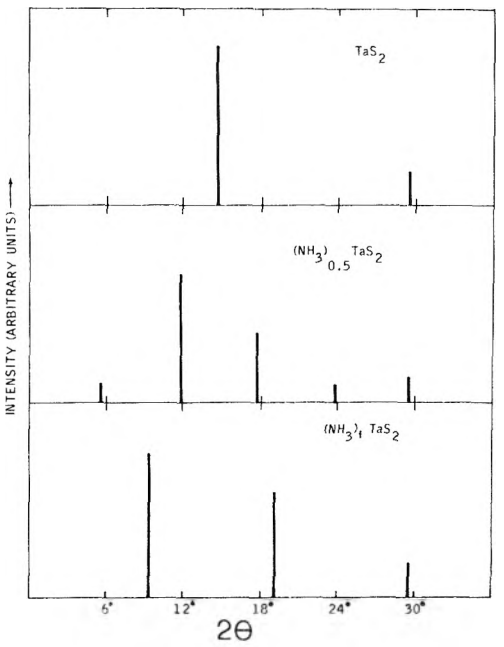

Figure 2. X-Ray powder diffraction results on the starting material, second-stage product, and fully intercalated product (only the 00*l* reflections are shown).

case of tantalum disulfide–pyridine and titanium disulfide–ammonia.[5]

Although the density of the ammonia within the layers of the second-stage compound is nearly the same as the first stage (indicated by the composition) it is apparent that its vapor pressure is much lower. The same second-stage compound is obtained if tantalum disulfide is allowed to absorb 0.5 equiv of ammonia and the product subsequently equilibrated several days at 373°K in a sealed tube.

The process of intercalation can be completely reversed by pumping on the product at elevated temperatures ($T >$ 423°K). However, the tantalum disulfide thus recovered shows significant loss of crystal perfection.

B. Thermal Analysis. The thermogravimetric behavior of the nominally 1:1 ammonia–tantalum disulfide product (Figure 3) had the following salient features: (1) the weight loss commenced immediately, indicating a high vapor pressure for the saturated product; (2) no discernable steps

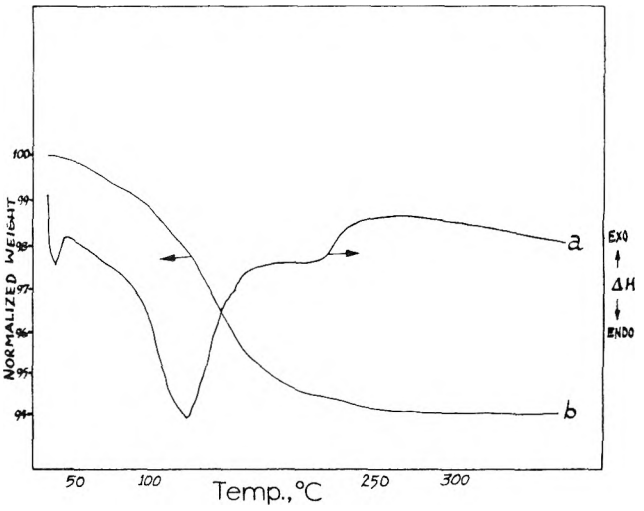

Figure 3. (a) Differential scanning calorimetric curve for $(NH_3)_{0.95}TaS_2$. The endothermic heat is measured to be ca. 8.5 kcal/mol referenced to indium melting. (b) Thermogravimetric curve for the same compound. Weight loss corresponds to 6.06%.

were seen in the deammoniation; (3) the overall weight loss corresponds to 6.06% of the initial weight. The weight loss is consistent with the formulation of the starting composition of $(NH_3)_{0.93}TaS_2$. Diffraction patterns of the product of the TGA experiment were typical of pure tantalum disulfide, although with broadened 001 reflections indicative of disorder in the *c*-axis lattice direction. If ammonia was the carrier gas, essentially the same results were found.

Differential scanning calorimetry using indium as a standard indicated a broad endothermic process for the deammoniation, with an enthalpy for the overall reaction of ca. 8–9 kcal/mol (Figure 3). This value is probably good to only about ±20% due to the large error in the method and the fact that the process occurred over such a broad range of temperature. This overall enthalpy has two main components, the endothermic heat necessary to overcome whatever forces keep the ammonia in the lattice, and an exothermic term regained when the layered tantalum disulfide lattice is recovered on evacuation by the guest.

The value of this interlayer enthalpy is not known, but probably is less than about 4 kcal/mol and nearer to 1 kcal/mol. This estimation is based on phase transformation studies conducted by Huismann,[6] and the heat of condensation of sulfur (2.5 kcal/g atom).[7]

In layered tantalum disulfide the chalcogen bears a partial negative charge. Therefore, it is argued that due to mutual repulsions, the molar interlayer enthalpy should be lower than the heat of condensation of sulfur. Thus, the overall value for the heat of intercalation from the DSC experiment of ca. 8 kcal/mol can be considered to be a lower limit to the overall average bonding energy of the complex.

C. Intercalation Isotherms. Between 310 and 353°K, the uptake and desorption isotherms of the NH_3–TaS_2 system show no hysteresis. As shown in Figure 4, the composition at these temperatures varies between $0.65 < x < 0.85$ for variations in NH_3 pressure from 10 to 700 Torr. At lower and higher temperatures, on the other hand, strong hysteresis is observed. The high-temperature hysteresis is probably due to the phase change which occurs near $x = 0.5$. This has limited the thermodynamic study to the 310–353°K temperature range. In this range, and for $0.65 < x < 0.85$, $(NH_3)_xTaS_2$ is a homogeneous solid phase. This is con-

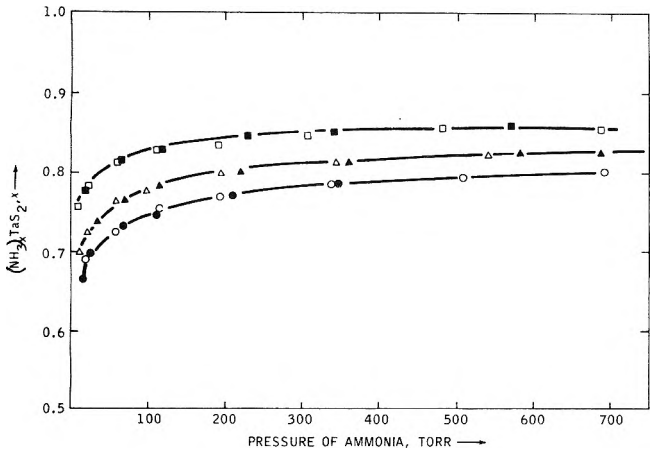

Figure 4. Intercalation isotherms for TaS_2–NH_3. Circles refer to a run conducted at 346°K, triangles at 331°K, and squares at 311°K. Closed data points are for the forward (intercalation) direction and open points are the reverse.

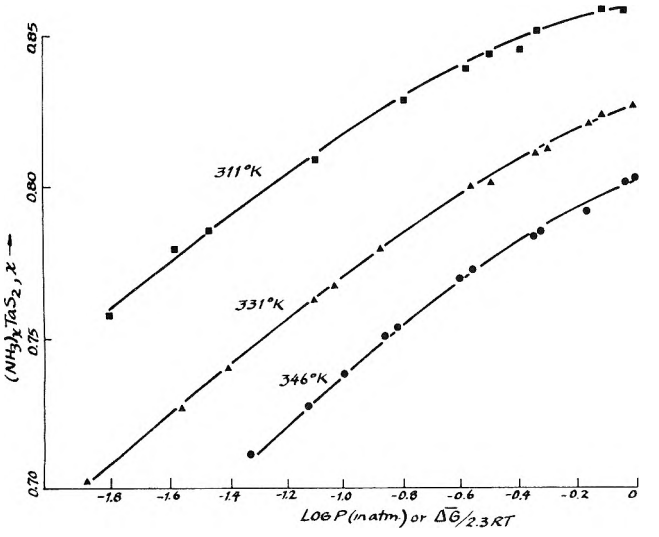

Figure 5. Semilog plot of Figure 4, indicating the dependence of the partial molal free energy on filling of the lattice by ammonia.

firmed by the pressure–composition behavior and the presence of one single phase in the X-ray powder pattern.

D. Interaction Enthalpy. This enthalpy represents the heat of interaction of the NH_3 with the layer. The removal or addition of NH_3 in the homogeneous phase region of $(NH_3)_xTaS_2$ is accomplished without expenditure of work to separate the TaS_2 layers. The phase is, in effect, a solid solution of NH_3 in partially intercalated TaS_2. Application of the Clausius–Clapeyron relationship to the data of Figure 4 therefore results in an isosteric enthalpy involving only two contributions: (1) the bonding energy between guest and host, and (2) any existing guest–guest interactions.

Figure 6 shows a plot of ln p vs. $1/T$ for several compositions in the $0.65 < x < 0.85$ region. As expected from the Clausius–Clapeyron equation, a straight line behavior is observed. The slopes of the lines correspond to $\overline{\Delta H}/R$, the partial molal enthalpy of the interaction for the incremental compositions $(NH_3)_{x+dx}TaS_2$.[8] These enthalpies are plotted in Figure 7 as a function of NH_3 composition. It can be seen that the negative enthalpy *increases* linearly with increasing NH_3 occupation of the host. Such behavior is not usually observed in surface adsorption, where due to

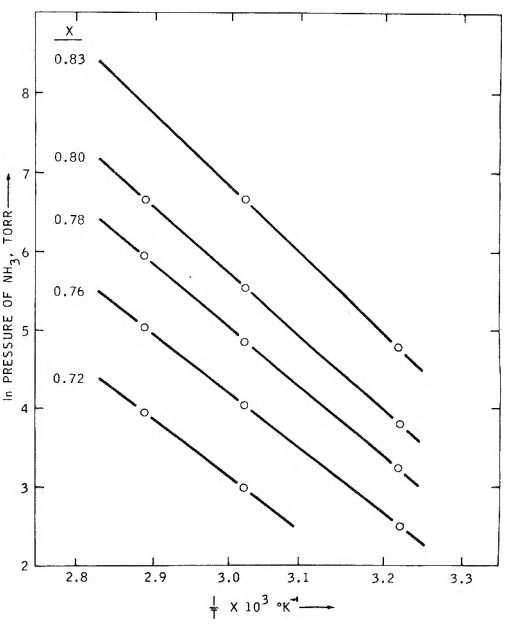

Figure 6. Clausius–Clapeyron plots at various stoichiometries.

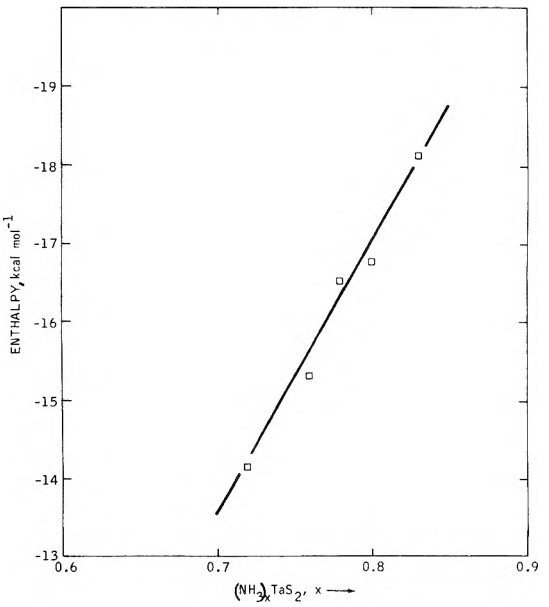

Figure 7. Partial molal enthalpies (derived from the slopes of Figure 6) found as a function of composition.

the heterogeneity of the energy of surface sites, the most active ones are occupied first, resulting in a decrease in heat of interaction with increasing coverage. However, in cases where there are strong interactions between molecules or atoms in the adsorbed layer, an increase is observed with coverage.[9] This same effect is seen for the α phase of the hydrogen–palladium system, where the heat of absorption increases linearly with increasing hydrogen concentration.[10] However, in that case, the effect is probably due to the expansion of the lattice, an effect that in the $(NH_3)_xTaS_2$ case can only account for a small fraction of the observed increase, since no change in the c-lattice parameter is observed.

The increase in the heat of ammonia intercalation with occupation can be accounted for by an increase in the guest–guest interaction. This behavior can be most simply

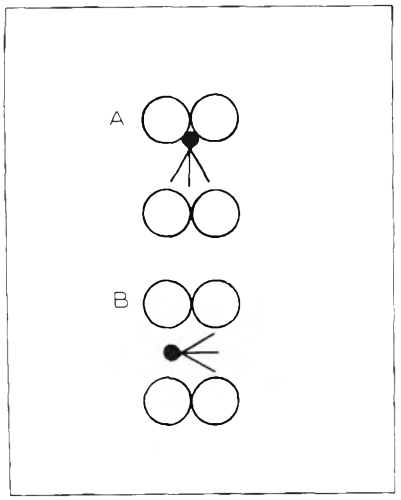

Figure 8. Two generalized models of alternative configurations of the intercalate: (A) threefold axis of guest parallel to the c direction of host lattice; (B) threefold axis perpendicular to the c direction.

rationalized by invoking significant hydrogen bonding between ammonias. The geometry of the intercalated ammonia, therefore, must allow for strong intermolecular hydrogen bonding. Two models of the configuration of NH_3 in TaS_2 can be postulated. They differ in the orientation of the ammonia C_3 axis with respect to the planes, as shown in Figure 8. In structure A the ammonia is "plugged into" the surface of the layer in a configuration similar to the one expected for surface adsorption. In this case, the nonbonding electrons of the nitrogen are directed toward the layer, and are unavailable for hydrogen bonding with neighboring guest molecules. In structure B, on the other hand, hydrogen bonding can occur. In this case, the nitrogen is bonded to the hybridized sp^3 orbitals of sulfur in a three-center S–N–S bonding. This is consistent with the observed trigonal prismatic coordination of the sulfur about the NH_3. Recent NMR studies of the anisotropy of the intercalated ammonia also strongly indicates such a placement of the molecule.[11]

Conclusions

We have shown that the intercalation of ammonia into tantalum disulfide is a nucleated process with a threshold pressure. A second-stage compound is intermediate to the formation of the nominally 1:1 saturated first-stage product. In the second-stage compound the density of guests in every other interlayer region is approximately the same as the 1:1 compound as shown by its stoichiometry of ca. $\frac{1}{2}$:1. In the phase region in which the ratio of ammonia to tantalum disulfide is >0.5 a solid solution occurs with a vapor pressure dependence on composition which varies such as to indicate rising negative enthalpy with increasing occupation by the guest. This observation is most simply explained by invoking significant interguest hydrogen bonding, which in turn implies that the ammonias are not "plugged in" to the layers as might be expected on conventional coordination chemistry grounds, but rather they lie with their C_3 axes parallel to the TaS_2 layers. Bonding to the layers thus involves a sulfur–nitrogen–sulfur three-center interaction.

Acknowledgment. The authors are grateful to several colleagues, in particular to M. S. Whittingham and J. P. deNuefville for their helpful comments and discussion. In addition, we are thankful to R. Kelly and J. Picone for their able assistance.

References and Notes

(1) Presented in part at the 168th National Meeting of the American Chemical Society, Atlantic City, N.J., Sept. 1974.
(2) (a) For a comprehensive review, see A. D. Yoffe, *Annu. Rev. Mater. Sci.*, **3** (1973); (b) B. G. Silbernagel and F. R. Gamble, *Phys. Rev. Lett.*, **32**, 1436 (1974).
(3) R. R. Chianelli, J. C. Scanlon, M. S. Whittingham and F. R. Gamble, *Inorg. Chem.*, **14**, 1691 (1975).
(4) F. R. Gamble and T. H. Geballe in "Treatise on Solid State Chemistry", Vol. 2, N. B. Hannay, Ed., Pergammon Press, New York, N.Y., 1974.
(5) F. R. Gamble, J. H. Osiecki, M. Cais, R. Pisharody, F. J. DiSalvo, and T. H. Geballe, *Science*, **174**, 493 (1971).
(6) R. Huismann, Dissertation, Groningen, 1969.
(7) B. Mayer, "Elemental Sulfur", Interscience, New York, N.Y., 1965, p 87.
(8) The overall or integrated enthalpy (equivalent to $\int_{x1}^{x2} \overline{\Delta H}\, dx$) can be calculated from the straight line equation: $\overline{\Delta H} = -35x + 11$ (see Figure 7). In the region $0.65 < x < 0.85$ this integrated enthalpy increases by about −3 kcal/mol, about half the value found for the partial molal counterpart.
(9) G. M. Holmes in "The Solid-Gas Interphase", Vol. I, E. Alison Flood, Ed., Marcel Decker, New York, N.Y., 1966, p 133.
(10) E. Wicke and G. H. Nernst, *Ber. Bunsenges. Phys. Chem.*, **68**, 224 (1964).
(11) B. G. Silbernagel and F. R. Gamble, *J. Chem. Phys.*, in press.

COMMUNICATIONS TO THE EDITOR

Corrections to "Conductance–Concentration Function for Associated Symmetrical Electrolytes"

Publication costs assisted by the Office of Water Research and Technology

Sir: The writer is grateful to Dr. Alan D. Pethybridge (University of Reading, U.K.) for calling attention to errors in the text of the above paper.[1] In the original manuscript, the symbol $c_i = c\gamma$ was used for ionic concentration; the subscript i was inadvertently omitted in the text. In accordance with the definition of κ by (1.8), the factor $\gamma^{1/2}$ should be inserted after $c^{1/2}$ in the following places: eq 3.23, 3.24, 3.25, 3.28, 3.29, 3.44, 3.47, and 4.5; p 536, column 1, line 10; p 536, column 2, line above (3.44); p 537, column 1, lines 8 and 10 below (3.50). This factor was, of course, included in the computer programs (ref 16) and in the preliminary announcement[2] of the conductance function.

Several other corrections are: (1) delete the zero subscripts on X in the denominators on the right-hand side of (2.116) and (2.117); (2) insert a minus sign before $\Delta X/X$ on the left-hand side in (2.116); replace the plus sign by an equality before 5.854 in (4.5); replace $(\tau^2/3)$ by $(\tau^2/3\mu^2)$ in (2.116) and (2.117). In line above (2.114), change {2.41} to {2.74} and insert $[-\exp(-qt)][\ln (2 + q)/(2 - q)]$ in (2.114). To the Supplementary Material, add after (2.110) the definition: $M_0 = 2(1 + qt + t^2/6) \exp(-qt) - (1 + t + t^2/3) \exp(-t)$.

References and Notes

(1) R. M. Fuoss, *J. Phys. Chem.*, **79**, 525 (1975).
(2) R. M. Fuoss, *Proc. Natl. Acad. Sci. U.S.*, **71**, 4491 (1974); eq A15, A16, A20.

Sterling Chemistry Laboratory
Yale University
New Haven, Connecticut 06520
Raymond M. Fuoss

Received June 23, 1975

Rate Constants for the Hydrogen Atom Abstraction by Phenyl Radical from Methanol, Ethanol, and 2-Propanol as Studied by Electron Spin Resonance Spin Trapping Techniques

Sir: Recently we have reported some estimates of the absolute rate constants for trapping *tert*-butoxy,[1] phenyl,[2] and benzoyloxy[2,3] radicals by certain nitroso and nitrone compounds. The rate constants are obtained from competition reactions which give a ratio of rate constants based on the ratio of the initial buildup of two spin adducts. Thus for phenyl radical in methanol the appearance of the phenyl and hydroxymethyl spin adducts of phenyl *tert*-butyl nitrone (PBN) is monitored at room temperature as a function of time. The source of phenyl radicals is the thermal decomposition of phenylazotriphenylmethane (PAT). The following mechanism is assumed.

$$\text{PAT} \longrightarrow \text{Ph}\cdot + \text{N}_2 + \underset{\text{not trapped}}{\text{Ph}_3\text{C}\cdot} \quad (1)$$

$$\underset{\text{PBN}}{\text{Ph}\cdot + \text{PhCH}{=}\text{N(O)CMe}_3} \longrightarrow \underset{\text{Ph-SA}}{\text{Ph}_2\text{CHN(O}\cdot\text{)CMe}_3} \quad (2)$$

$$\text{Ph}\cdot + \text{CH}_3\text{OH} \longrightarrow \cdot\text{CH}_2\text{OH} + \text{PhH} \quad (3a)$$

$$\cdot\text{CH}_2\text{OH} + \text{PBN} \longrightarrow \underset{\underset{\text{HM-SA}}{\text{CH}_2\text{OH}}}{\text{PhCHN(O}\cdot\text{)CMe}_3} \quad (4a)$$

Then

$$\frac{\text{d(Ph-SA)}/dt}{\text{d(HM-SA)}/dt} = \frac{k_2[\text{PBN}]}{k_{3a}[\text{CH}_3\text{OH}]}$$

In accordance with this expression a plot of the initial rate ratio is found to be linear with PBN within the range [PBN] = 0.01–0.1 M. From the slope of this plot k_2/k_{3a} = 130.

The absolute rate constant for hydrogen atom abstraction from methanol by *p*-methylphenyl radicals has been estimated from a pulse radiolysis study of the *p*-tolyldiazonium cation in methanol to be "at least" 1.4×10^5 M^{-1} sec^{-1}.[4]

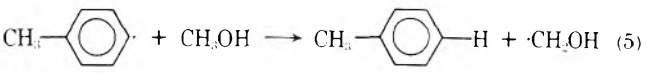

(5)

If we make the assumption $k_5 \simeq k_{3a}$[5,6] then $k_2 = 1.8 \times 10^7$ M^{-1} sec^{-1}.

A recent paper by Bhatia and Schuler[7] prompted us to determine the rate constant for hydrogen abstraction by phenyl radicals from ethanol and isopropyl alcohol based on the rate constant obtained for the trapping of phenyl radicals in methanol. The following mechanism is assumed with steps 1 and 2 as before:

$$\text{Ph}\cdot + \text{MeCH}_2\text{OH} \longrightarrow \text{MeC}\dot{\text{H}}\text{OH} + \text{PhH} \quad (3b)$$

$$\text{MeC}\dot{\text{H}}\text{OH} + \text{PBN} \longrightarrow \underset{\underset{\text{MeCHOH}}{|}}{\text{PhCHN(O}\cdot\text{)CMe}_3} \quad (4b)$$

$$\text{Ph}\cdot + \text{Me}_2\text{CHOH} \longrightarrow \text{Me}_2\dot{\text{C}}\text{OH} + \text{PhH} \quad (3c)$$

$$\text{Me}_2\dot{\text{C}}\text{OH} + \text{PBN} \longrightarrow \underset{\underset{\text{Me}_2\text{COH}}{|}}{\text{PhCHN(O}\cdot\text{)CMe}_3} \quad (4c)$$

The hyperfine splitting constants for phenyl and hydroxyalkyl spin adducts are given in Table I. The structures of these nitroxides have been verified by preparing the spin adducts by alternate methods. Slight overlap in the phenyl and hydroxyalkyl spin adduct spectra necessitated analyzing the results by computer simulation of partly overlapped peaks. From ratios of initial rates of formation of spin adducts as a function of PBN concentration we find k_2/k_{3b} = 78 and k_2/k_{3c} = 44. If the rate constant for trapping phenyl radicals by PBN is taken as $1.8 \pm 0.1 \times 10^7$ M^{-1} sec^{-1} in all alcohols, $k_{3b} = 2.3 \pm 0.1 \times 10^5$ M^{-1} sec^{-1} and $k_{3c} = 4.1 \pm 0.1 \times 10^5$ M^{-1} sec^{-1} where the error indicated is the deviation obtained depending on the choice of simulation used. Thus the relative reactivities toward phenyl radical for

TABLE I: Hyperfine Coupling Constants of Phenyl and Hydroxyalkyl Spin Adducts of PBN[a] $C_6H_5CH(R)N(O\cdot)C(CH_3)_3$

Solvent	R	a_N	a_β^H
CH_3OH	C_6H_5	15.25	3.14
CH_3CH_2OH	C_6H_5	15.06	2.99
$(CH_3)_2CHOH$	C_6H_5	14.93	2.91
$(CH_3)_3COH$	C_6H_5	14.89	2.79
CH_3OH	CH_2OH	15.19	3.76
CH_3CH_2OH	$CH(CH_3)OH$	15.25	3.63
$(CH_3)_2CHOH$	$C(CH_3)_2OH$	15.31	3.61

[a] In gauss in the solvent indicated at room temperature.

methanol:ethanol:isopropyl alcohol are 1.0:2.4:8.8 per hydrogen atom. Data for this series have not been reported by Russell[8] in an extensive study of the relative reactivity of phenyl radical toward hydrogen donating compounds. However the methyl radical shows similar reactivities toward these alcohols in the gas phase 1.0:2.6:9.2 per hydrogen atom at room temperature.[9]

Bhatia and Schuler's paper[7] describes a product study of the γ radiolysis of aqueous solutions of *p*-bromophenol. From the amount of phenol produced in the presence of isopropyl alcohol a ratio of the rate constants for the addition of *p*-hydroxyphenyl radicals to *p*-bromophenol and abstraction from isopropyl alcohol was calculated. Using the value of $7 \times 10^7\ M^{-1}\ \text{sec}^{-1}$ reported by Cercek and Kongshaug[10] for *p*-hydroxyphenylation of bromophenol, Bhatia and Schuler obtain $3 \times 10^7\ M^{-1}\ \text{sec}^{-1}$ for the rate constant for hydrogen abstraction by *p*-hydroxyphenyl from isopropyl alcohol. This value would seem to be at least a factor of 20 and possibly as much as a factor of 75 too large if compared directly with our results on phenyl radicals. Moreover electron-donating substituents are expected to *decrease* not increase the reactivity of the phenyl radical.[5] This large difference in estimated rate constants would appear to come from the unusually large rate constant of $7 \times 10^7\ M^{-1}\ \text{sec}^{-1}$ assigned by Cercek and Kongshaug to the addition of *p*-hydroxyphenyl radical to *p*-bromophenol. For the addition of phenyl radicals to benzene in benzene we obtain a rate constant of $1.2 \times 10^5\ M^{-1}\ \text{sec}^{-1}$ based on the results of Packer et al.[4] and Levy et al.[11] estimate a rate constant of $\sim 5 \times 10^5\ M^{-1}\ \text{sec}^{-1}$ in methylcyclohexane based on the assumption that the rate of reaction of phenyl radicals with I_2 is diffusion controlled. Since it is apparent from the work of Levy et al.[11] that electron-donating substituents deactivate and electron-withdrawing substituents activate the ring toward phenyl radical addition one would predict that if phenyl radicals add to *p*-bromophenol in the usual way the rate constant for this reaction should be about the same as the rate constant for the addition to benzene, i.e., $\sim 10^5\ M^{-1}\ \text{sec}^{-1}$.

References and Notes

(1) E. G. Janzen and C. A. Evans, *J. Am. Chem. Soc.*, **95**, 8205 (1973).
(2) E. G. Janzen and C. A. Evans, *J. Am. Chem. Soc.*, **97**, 205 (1975).
(3) E. G. Janzen, C. A. Evans, and Y. Nishi, *J. Am. Chem. Soc.*, **94**, 8236 (1972).
(4) J. E. Packer, D. B. House, and E. J. Rasburn, *J. Chem. Soc. B*, 1574 (1971).
(5) Inspection of the literature indicates that electron-donating substituents in the para position have little if any effect on the reactivity of phenyl radicals; see, e.g., W. A. Pryor, J. T. Echols, Jr., and K. Smith, *J. Am. Chem. Soc.*, **88**, 1189 (1966).
(6) In agreement with a reviewer's comment we note that the lack of a sizable hyperfine splitting from the para proton in the ESR spectrum of phenyl radicals (J. E. Bennett and B. Mile, *J. Phys. Chem.*, **75**, 3432 (1971), and references therein) can also be used to support the assumption that the reactivity of the *p*-methylphenyl radical will be essentially the same as that of the phenyl radical.
(7) K. Bhatia and R. H. Schuler, *J. Phys. Chem.*, **77**, 1356 (1973).
(8) G. A. Russell in "Free Radicals", Vol. 1, J. K. Kochi, Ed., Wiley, New York, N.Y., 1973, Chapter 7, p 299.
(9) S. W. Benson, "The Foundations of Chemical Kinetics", McGraw-Hill, New York, N.Y., 1960, p 297.
(10) B. Cercek and M. Kongshaug, *J. Phys. Chem.*, **74**, 4319 (1970).
(11) A. Levy, D. Meyerstein, and M. Ottolenghi, *J. Phys. Chem.*, **77**, 3044 (1973).

Department of Chemistry
The University of Georgia
Athens, Georgia 30602

Edward G. Janzen*
Dale E. Nutter, Jr.
C. Anderson Evans

Received September 9, 1974; Revised Manuscript Received February 20, 1975

PHYSICAL PHENOMENA

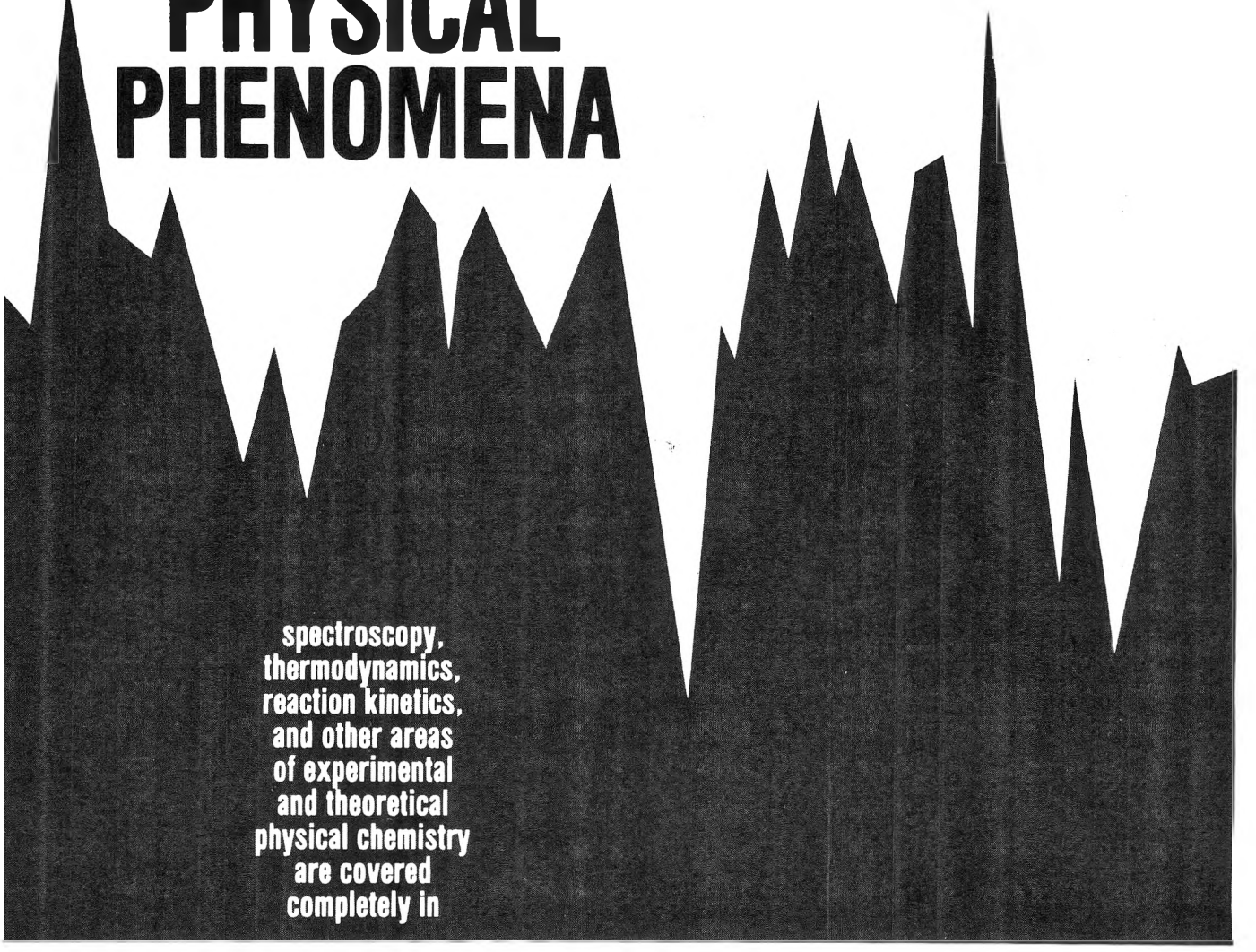

THE JOURNAL OF PHYSICAL CHEMISTRY

The biweekly JOURNAL OF PHYSICAL CHEMISTRY includes over 25 papers an issue of original research by many of the world's leading physical chemists. Articles, communications, and symposia cover new concepts, techniques, and interpretations. A "must" for those working in the field or interested in it, the JOURNAL OF PHYSICAL CHEMISTRY is essential for keeping current on this fast moving discipline. Complete and mail the coupon now to start your subscription to this important publication.

The Journal of Physical Chemistry
American Chemical Society
1155 Sixteenth Street, N.W.
Washington, D.C. 20036

1975

Yes I would like to receive the JOURNAL OF PHYSICAL CHEMISTRY at the one-year rate checked below:

	U.S.	*Canada***	*Latin America***	*Other Nations***
ACS Member One-Year Rate*	☐ $20.00	☐ $24.50	☐ $24.50	☐ $25.00
Nonmember	☐ $80.00	☐ $84.50	☐ $84.50	☐ $85.00

Bill me ☐ Bill company ☐ Payment enclosed ☐

Air freight rates available on request

Name _____

Street _____ Home ☐ Business ☐

City _____ State _____ Zip _____

Journal subscriptions start on January '75

*NOTE: Subscriptions at ACS member rates are for personal use only. **Payment must be made in U.S. currency, by international money order, UNESCO coupons, U.S. bank draft, or order through your book dealer.

RADIONUCLIDES IN THE ENVIRONMENT

ADVANCES IN CHEMISTRY SERIES NO. 93

Twenty-eight papers from a symposium sponsored by the Division of Nuclear Chemistry and Technology, chaired by E. C. Freiling.

Pollution . . . a growing concern . . . a concept not generally associated with radionuclides. The successful control of this hazardous waste product of nuclear energy is essential to the continued use and development of nuclear power. Critical to this problem is an understanding of the processes by which radionuclides are produced, dispersed, and retained in the environment.

The papers in this volume discuss and evaluate the properties and problems relating to radionuclides, including

- mechanisms of release, absorption, uptake, transport
- behavior, measurement and characterization, specific weapons tests
- specific activity, public health aspects, fallout
- new methods and equipment

522 pages with index Clothbound (1968) $15.00
Set of L.C. cards with library orders upon request.

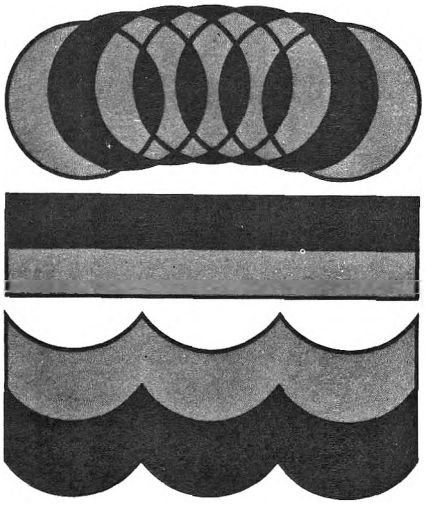

Other books in the ADVANCES IN CHEMISTRY SERIES OF related interest include:

No. 89 Isotope Effects in Chemical Processes. Methods of separating isotopes and labeled molecules—chemical exchange, electromigration, photochemical processes, and distillation—are examined, along with factors that suit a process to isotope separation—single stage fractionation, exchange rate, and reflux.
278 pages cloth (1969) $13.00

No. 82 Radiation Chemistry—II. Thirty-six papers and 17 abstracts on radiation chemistry in gases, solids, and organic liquids. Includes three plenary lectures. 558 pages cloth (1968) $16.00

No. 81 Radiation Chemistry—I. Forty-one papers and 17 abstracts on radiation chemistry in aqueous media, biology, and dosimetry. From the international conference at Argonne National Laboratory. 616 pages cloth (1968) $16.00. No. 81 and 82 ordered together $30.00

No. 72 Mass Spectrometry in Inorganic Chemistry. A basic tool for chemical manipulations, the mass spectrometer is a conventional monitor for any stage in a research problem to help establish what is going on. 21 Research reports. 329 pages cloth (1968) $12.00

No. 68 The Mössbauer Effect and Its Application in Chemistry. Ten papers that will familiarize chemists with Mössbauer spectroscopy as an analytical tool for studying chemical bonding, crystal structure, electron density, magnetism, and other properties.
178 pages cloth (1967) $8.00

No. 66 Irradiation of Polymers. Eighteen papers survey radiation mechanics in polymers, the chemical nature of reactive species produced, crosslinking and scission, homopolymerization, graft copolymerization, and the effects of ultraviolet light radiation.
275 pages cloth (1967) $10.00

No. 58 Ion–Molecule Reactions in the Gas Phase. Eighteen papers survey spectrometric and other methods for producing and studying ion–molecule reactions such as pulsed sources for studying thermal ions, reactions in flames and electrical discharges.
336 pages cloth (1966) $10.50

No. 50 Solvated Electron. Reviews of theory, structure, reactions of solvated and hydrated electrons; detailed papers on electrical transport properties, photochemistry, theory of electron transfer reactions, structure of solvated electrons, hydrated electron research. 304 pages cloth (1965) $10.50

Postpaid in U. S. and Canada; plus 30 cents elsewhere.
Order from:

SPECIAL ISSUES SALES
AMERICAN CHEMICAL SOCIETY
1155 SIXTEENTH ST., N.W.
WASHINGTON, D. C. 20036